# CHARACTERIZATION OF THE THERMAL HYDRAULIC BEHAVIOR OF AN EXPERIMENTAL REACTOR CAVITY COOLING SYSTEM WITH WATER

A Thesis

by

MICHAEL JOSEPH GORMAN

Submitted to the Office of Graduate and Professional Studies of
Texas A&M University
in partial fulfillment of the requirements for the degree of

MASTER OF SCIENCE

| | |
|---|---|
| Chair of Committee, | Yassin Hassan |
| Committee Members, | Maria King |
| | William Marlow |
| Head of Department, | Yassin Hassan |

August 2015

Major Subject: Nuclear Engineering

# ABSTRACT

An existing experimental Reactor Cavity Cooling System using water as the coolant received extensive instrumentation and control upgrades to allow for a thorough investigation into the single-phase flow behavior of the system under a variety of experimental conditions. Base level conditions used a uniform heat flux at a power level appropriately scaled from a benchmark computer simulation of the Gas Turbine Modular Helium Reactor (GT-MHR) using scaling relationships derived by Argonne National Laboratory. Experiments were setup to gauge the effects of flow throttling, non-uniform heat flux profiles, alternate power levels and alternate coolant inventory levels on the flow distribution in the Cooling Panel, and to investigate the relationships between system variables of applied power, the temperature difference across the Cooling Panel ($\Delta T$) and flowrate. In addition, a single scoping experiment was executed to observe system performance with coolant at the saturation temperature.

The system variables proved to have highly linear relationships amongst each other under all experimental conditions. Flow instabilities were observed in the form of counter-phase sinusoidal oscillations of flowrate and $\Delta T$, the frequency thereof showed a roughly linear relationship with power. Ultrasonic Velocity Profiling (UVP) was used to determine the flow distribution, which increased at the outlet side of the panel with either increased system flowrate or higher heat flux applied to the outlet side, and vice-versa. The effect caused by flowrate changes was the same whether due to a change in power level or throttling, indicating the fluid's momentum is the driving factor.

The phenomenon of sudden, high velocity, short duration flow excursions, called geysering, was observed as the system coolant was brought to saturation. This was caused by the trapping of non-condensable gases in the top horizontal section of the flow loop, which in turn brought the flowrate down considerably, increasing residence time and temperature of the coolant in the Cooling Panel. Subsequent rise of saturated coolant to a higher elevation in the hot leg resulted in flashing of the coolant to steam, whose sudden expansion drove the flow excursion.

# DEDICATION

Like any thesis, this report contains a detailed account of all of the experiments conducted by the author to characterize the behavior of the experimental Reactor Cavity Cooling System at Texas A&M University, along with procedures, results, analysis, conclusions, and other relevant information. In addition, it will provide an account summarizing the history of the experimental facility, from the objectives of the original proposal, to all of the instrumentation and control system upgrades along with the underlying motivations, and the challenges faced, overcome, and those that are still lurking. This thesis is intended to both be a stand-alone and closed account of the work conducted by the author, and yet also give understanding of where this endeavor fits in the 'big picture' of research conducted by other scientists at the University of Wisconsin, University of Idaho, Argonne National Laboratory, and previous activity at Texas A&M.

The hope therein is to provide the future researcher with insight and perspective that will allow him or her to quickly and efficiently formulate a plan to keep moving forward with research related to this facility, be it using the experimental data to validate computer codes, further research into the two-phase behavior, or simply to construct similar facilities for thermal hydraulic research. The knowledge that mankind has acquired at any point in history is the sum of the collective efforts of all the scientists and researchers who had come before, and accordingly this thesis is dedicated to the future scientists who will continue to expand our knowledge of the universe, one step at a time.

ACKNOWLEDGEMENTS

I would like to thank the following peers, student workers, and visiting students who helped me conduct the system modifications and research presented in this report: Michael Mariano, Colton Hermes and Eden Marroquin of the Nuclear Engineering Department, Texas A&M University, Hristo Goumnerov and John Budd of the Mechanical Engineering Department, Texas A&M University, and Anqi Xu and Chengqi Wang of Harbin Engineering University.

I would also like to thank the following Texas A&M University staff members for helping with making the extensive modifications to the glass manifolds required to seal the system of leaks and install the UVP transducers, and other modifications: Bill Merka of the Department of Chemistry's Glass Shop, Will Seward of the Department of Chemistry's Machine Shop, and Troy Stepfan and student workers of the Department of Nuclear Engineering's Machine Shop.

Special thanks to Darius Lisowski of the University of Wisconsin, Madison for providing inspiration for the test plan and providing tips on equipment setup and experimental procedures used in this research.

Special thanks to Dr. Akira Tokuhiro of the University of Idaho for graciously loaning the Ultrasonic Velocity Profiling equipment used to ascertain the flow distribution in the Cooling Panel.

Special thanks to Dr. Qingzong Tseng for graciously updating the PIV plugin he wrote for ImageJ so I could more readily analyze the large data sets generated for this thesis.

Thanks also go to my friends and colleagues and the department faculty and staff for making my time at Texas A&M University a great experience.

## NOMENCLATURE

| | |
|---|---|
| ANL | Argonne National Laboratory |
| CAD | Computer Aided Drafting |
| DAQ | Data Acquisition |
| DOE | Department of Energy |
| FFT | Fast Fourier Transform |
| GT-MHR | Gas Turbine Modular Helium Reactor |
| H2O | Water |
| HVAC | Heating, Ventilation, and Air-Conditioning |
| I&C | Instrumentation and Control |
| IAEA | International Atomic Energy Agency |
| ID | Inside Diameter |
| LOCA | Loss of Coolant Accident |
| NCG | Non-Condensable Gas |
| NEUP | Nuclear Energy University Program |
| NGNP | Next Generation Nuclear Plant |
| NMT | Normalized Mean Test |
| OD | Outside Diameter |
| PFC | Phase Fired Controller |
| PIV | Particle Image Velocimetry |
| PRF | Pulse Repetition Frequency |
| RCCS | Reactor Cavity Cooling System |
| RMS | Root-Mean-Square |
| RPV | Reactor Pressure Vessel |
| SS | Stainless Steel |
| TAMU | Texas A&M University |
| T/C | Thermocouple |
| UI | University of Idaho |
| US | Ultrasonic |

| | |
|---|---|
| USB | University Science Building |
| UVP | Ultrasonic Velocity Profiling |
| UW | University of Wisconsin, Madison |
| VHTR | Very High Temperature Gas-Cooled Reactor |
| Chimney | The vertical 4” pipe section of the hot leg |
| Cooling Panel | The nine riser tubes and interconnecting fins that the coolant passes through while in the Heated Cavity |
| Downcomer | The vertical 4” pipe section of the cold leg |
| Heated Cavity | The insulated space containing the heaters and Cooling Panel |
| Magmeter | Electromagnetic flowmeter |
| Manifolds | The glasswork that splits the main flow into 9 separate pipes of the Cooling Panel or collects the flow back into one single pipe |
| Riser | The vertical 2” pipes that comprise the Cooling Panel |
| Tank Return Line | The horizontal 4” pipe section of the hot leg at the top of the loop |
| Test Section | The Heated Cavity and the upper and lower manifolds collectively |
| $c_p$ | Specific heat capacity under constant pressure |
| E | Energy |
| E.T. | Elapsed Time |
| $\rho$ | Density |
| P | Power |
| Q | Volumetric Flowrate |
| T | Temperature |
| t | Time |
| V | Volume |
| $\Delta T$ | Temperature difference across inlet and outlet of Test Section |
| °C | Degree Celsius |
| cm | Centimeter |
| hrs | Hours |
| Hz | Hertz |

| | | |
|---|---|---|
| kJ | Kilojoule | |
| kW | Kilowatt | |
| LPM | Liter per minute | |
| m | Meter | |
| mA | Milli-Ampere | |
| mbar | Millibar | |
| min | Minute | |
| mm | Millimeter | |
| MW | Megawatt | |
| sec | Second | |
| μm | Micrometer | |
| abs | Absorbed | (as subscript) |
| avg | Average | (as subscript) |
| in | Inlet | (as subscript) |
| mag | Electromagnetic flowmeter | (as subscript) |
| out | Outlet | (as subscript) |
| req | Required | (as subscript) |
| sat | Saturation | (as subscript) |
| th | Thermal | (as subscript) |

TABLE OF CONTENTS

LIST OF FIGURES

LIST OF TABLES

# CHAPTER I
# INTRODUCTION

## I.1 Purpose of the RCCS and General Information

It is a commonly held belief today that there is going to be a need in the near future for a more abundant, sustainable, environmentally friendly, safe, and economical energy source to replace dwindling fossil fuel supplies and meet the ever increasing global demand. Advocates for nuclear power have proposed several advanced reactor designs to act as such a source, one example being the Very High Temperature Gas-Cooled Reactor (VHTR). This reactor uses a gas coolant to transfer heat from the core to a steam generator for use in a traditional Rankine cycle; alternatively the gas can be used to directly power a turbine-generator via the Brayton cycle. Purported advantages of this Next Generation reactor over traditional light-water pressurized reactors are increased safety, decreased risk of proliferation of nuclear materials, and increased efficiency, especially considering applications requiring high temperature heat for industrial processes [1]. New technologies, however, come with new challenges that must be overcome in order for them to be implemented successfully.

As its name implies, the gas coolant used in such a reactor is expected to reach very high temperatures, approaching 1000 °C in some designs, and the outside wall of the reactor pressure vessel (RPV) containing the coolant could reach temperatures as high as 440 °C during normal operation [2]. As the RPV is enclosed in a concrete containment structure, there exists a need to remove the heat radiated by the RPV which becomes trapped in the *cavity* or void space that lays between the RPV and the containment in order to prevent thermal damage to the concrete, hence the need for a Reactor Cavity Cooling System (RCCS). An illustration of a typical VHTR reactor cavity is shown in Figure 1 below [3].

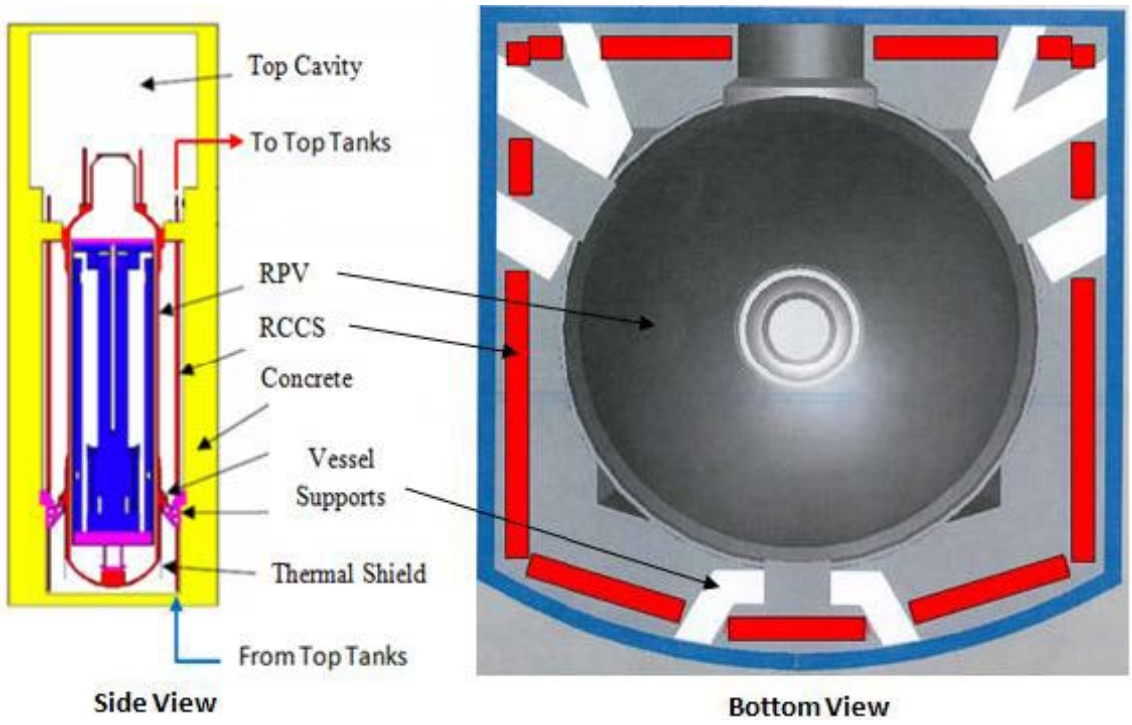


**Figure 1.** Reactor Cavity around a VHTR (RCCS Cooling Panels in Red) [3]

In the bottom view of Figure 1, note the vertical cooling panels of the RCCS shown in red in the reactor cavity between the cylindrical RPV in dark grey and the concrete containment walls in blue. These panels are hollow pipes or ducts that carry water or air, respectively, to large tanks or reservoirs wherein the heat can be removed via either a heat exchanger into a secondary coolant loop or naturally released to the surrounding environment before being returned to the reactor cavity. In terms of the RCCS itself, Figure 1 is incomplete as the tanks and supplying pipework is not shown; it only shows the cooling panels which exists in the reactor cavity itself. A more complete concept of the RCCS is shown in Figure 2, below [4]. This illustration depicts an RCCS with a secondary cooling loop, powered by a pump. Note that the containment structure is not shown in this figure and that the cooling fluid used in the RCCS flows under the force of natural convection.

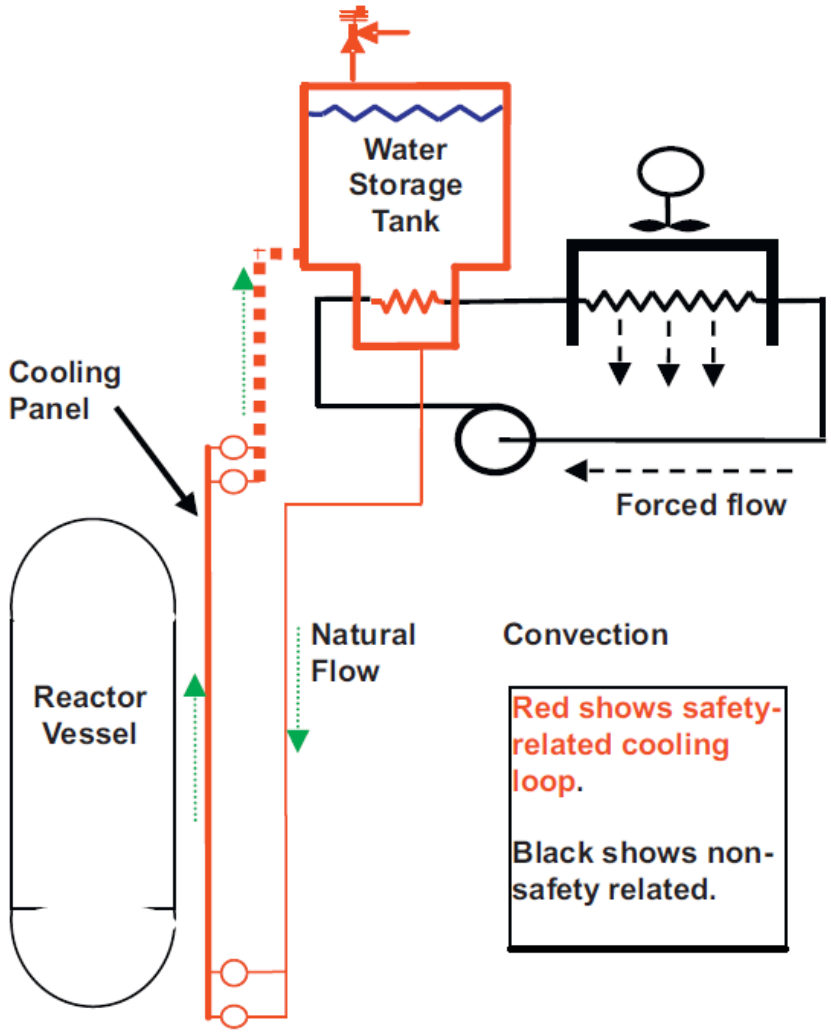


**Figure 2.** RCCS Concept with Secondary Cooling Loop [4]

Since the cooling fluid will flow via natural convection whether the secondary loop is active or not, the RCCS can be designed with enough heat capacity to absorb all the decay heat emitted by a scrammed reactor for a desired period of time, limited by the physical size of the system. This would provide emergency cooling to the reactor core itself in the event of an accident in which all electrical power is lost. *It is exactly this scenario of using the RCCS as a completely passive heat removal system powered by natural convection alone which is of interest for study in this thesis*. An illustration of this concept is provided in Figure 3 below [5].

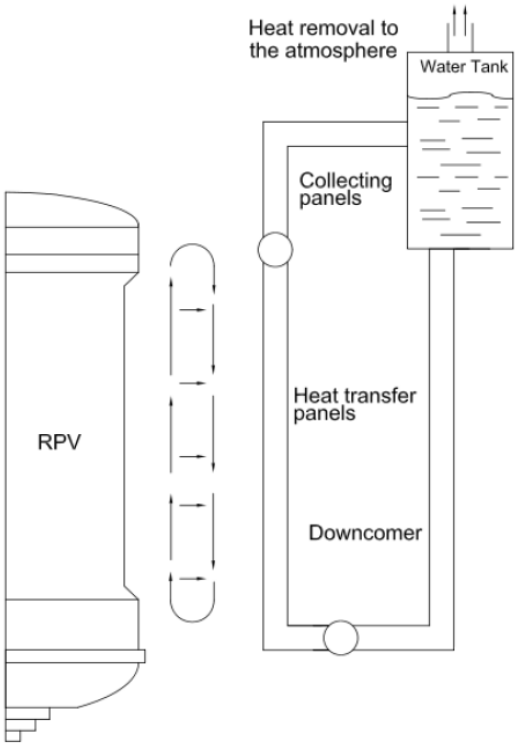


**Figure 3.** Water filled RCCS Concept Operating in the Passive Cooling Mode [5]

Proposed heat transfer or cooling panels for a water cooled RCCS consist of a series of pipes, referred to as risers, lined up side by side in a straight line, with flat metal plates welded between adjacent pipes along a common diameter line, which are called fins, as shown in Figure 4 [6].

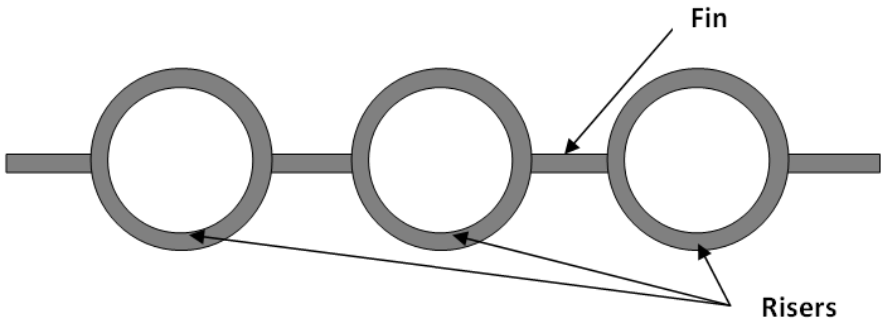


**Figure 4.** Fin style Cooling Panel design for a Water-cooled RCCS [6]

The flow from all the pipes in a single panel is merged together via manifolds into single large diameter pipes that carry the water between the tank and the reactor cavity. Thus, the RCCS would consists of several independent flow loops, each with its own storage tank and manifolds to store coolant and distribute the flow throughout the reactor cavity. An illustration of a single flow loop is in Figure 5 on the next page.

### I.2 Description of the Water-Cooled RCCS Facility at Texas A&M University

The RCCS built at Texas A&M University is the same as shown in Figure 5 below and as mentioned represents one of the independent flow loops of a complete system, with a cooling panel consisting of nine individual risers. The design shown in the figure is generic and was conceived and by Rodolfo Vaghetto at Texas A&M University [6]. There have been a couple of moderate changes to the original design shown in [6], these will be discussed in Chapter II in detail, but the basic concept is the same.

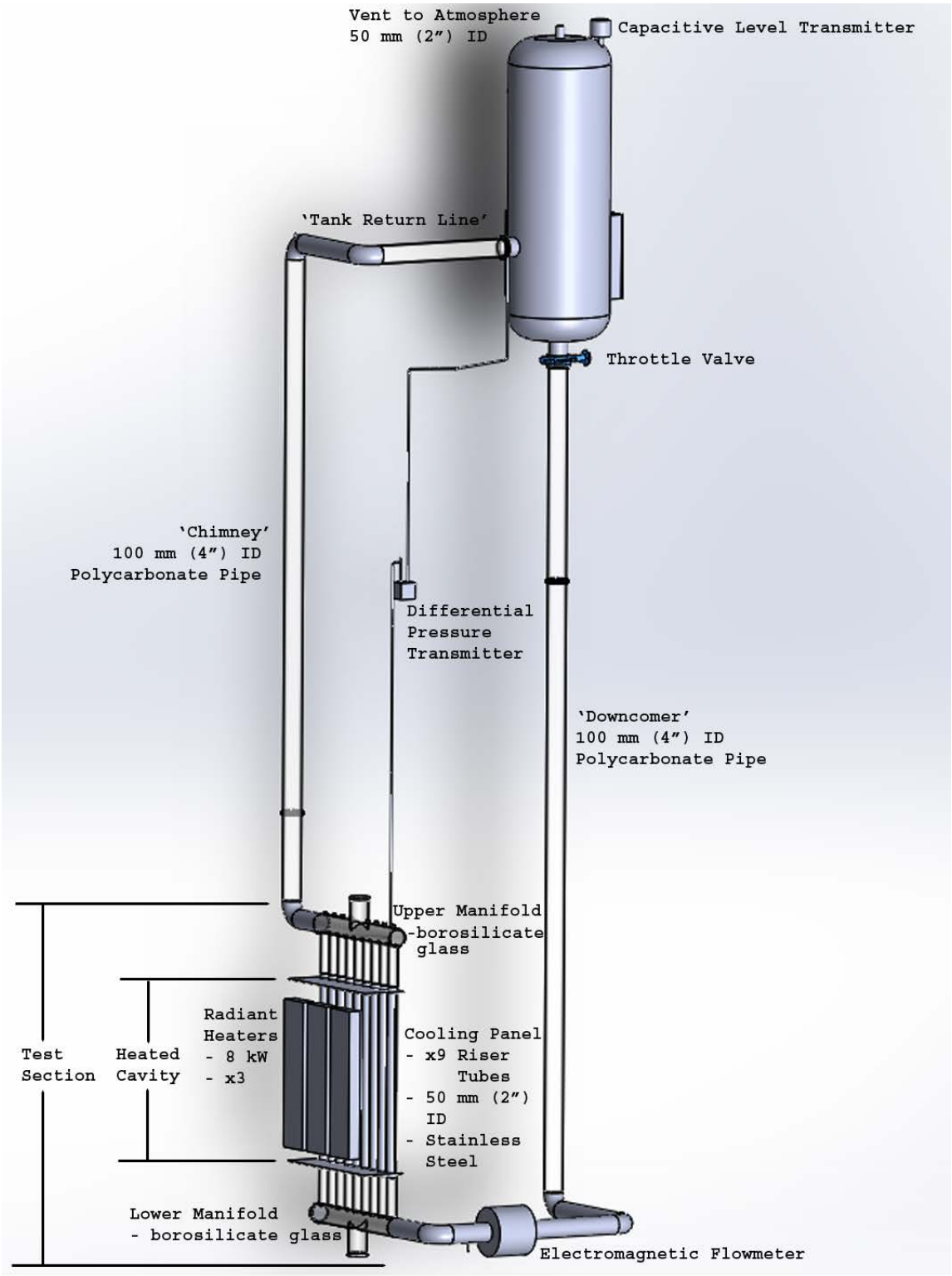


**Figure 5.** Single RCCS Flow Loop. Design of System at Texas A&M University

Referring to Figure 5, the flow runs in a clockwise direction, entering the Test Section through the Lower Manifold and exiting the Upper Manifold into the Chimney, through the Return Line into the Coolant Storage Tank, and finally down the Downcomer to go back to the Test Section. Before entering the Test Section the flow goes through an electromagnetic flowmeter to measure the system flowrate. The Downcomer, Chimney, and Return Line are all 4" (100 mm) inside diameter polycarbonate pipes with a 4.5" (114 mm) outside diameter. The use of polycarbonate allows for flow visualization. The Downcomer will sometimes be referred to as the 'cold leg' and the Chimney and Return Line as the 'hot leg'.

The cavity of the VHTR is simulated by the 'Heated Cavity' shown in Figure 5, and uses three 8 kW radiant heaters to provide the heat that would be emitted by the RPV. The Cooling Panel is constructed of nine 2" (50 mm) inside diameter stainless steel (SS) pipes, spaced 4" (100 mm) apart with fins welded between the risers as shown in Figure 4 earlier. There are 45 thermocouples arranged into 5 rows on each of the 9 risers to read the water temperatures. The Cooling Panel and heaters are enclosed in a cube shaped enclosure made of 1" (25 mm) thick Microtherm insulation panels, which have a thermal conductivity of 0.03 watts per meter per degree Kelvin at 500 °C. The height of the heated section is 1.1 meters, which represents approximately a 1:21 scale to the prototype system.

The manifolds that bring the flow into and out of the Cooling Panel are made of borosilicate glass to allow for flow visualization and have the same inside diameters as the connecting pipes in the system. The upper manifold has 8 mm diameter holes bored above the centerlines of the 2" (50 mm) riser connectors, except for on the center riser, that allow for the insertion of measurement probes. There are also threaded glass mounts glued to the manifold. The assembly of the Heated Cavity and the upper and lower manifolds will be referred to as the Test Section in this thesis. There are single thermocouples (t/c) at the inlet and outlet of the Test Section in the stainless steel elbows directing the flow into the manifolds to read the coolant temperatures before and after being heated in the cavity.

The coolant storage tank is made of carbon steel and is vented to atmosphere via a 2” (50 mm) diameter port at the top dead center of the tank, with thermocouples at the inlet and outlet of the tank. A capacitive level sensor is used to measure the coolant level, and there are two windows on adjacent quadrants on the sides of the tank to provide flow visualization. A 4” (100 mm) butterfly valve is located at the outlet of the tank to provide flow throttling capabilities.

The entire model is approximately 7 meters in height and is surrounded and supported by a three story steel structure. At the time of writing of this report, it is located in Room 127M of the University Science Building off of Old TI Road in College Station, TX.

A detailed description and analysis of all aspects of the design and construction of the original RCCS at Texas A&M University, including scaling to find the appropriate power levels for the heaters and other variables can be found in Dr. Vaghetto’s doctoral dissertation [6] and will not be repeated here. Dr. Vaghetto’s work with the experimental facility essentially ended with the completion of its construction. As such, the research activities in this thesis and purposes behind them will now be referenced back to the original request for proposal for the Department of Energy’s (DOE) Next Generation Nuclear Power Plant (NGNP) Project Number 09-202.

### I.3. Objectives and Tasks of NEUP Project #09-202

This research was initiated as part of the DOE’s Next Generation Nuclear Plant project, formally established by the Energy Policy Act of 2005, with the ultimate goal to design and build an advanced VHTR demonstration plant [1]. Some of the money appropriated for the NGNP project went to university research and development (R&D) programs under the Nuclear Energy University Programs (NEUP) initiative, which was intended to consolidate university support under one enterprise and better integrate university research within the DOE’s nuclear technical programs [7]. As noted in the abstract for project #09-202, the University of Idaho (UI), University of Wisconsin (UW), and Texas A&M University (TAMU) were charged with the following tasks [8]:

1. Conduct separate-effects, single phase flow experiments, in order to
    A. Develop scaling analyses for comparison to system-level computational modeling for the RCCS standpipe design
    B. Measure global flow behavior
    C. Measure local flow velocities and distribution in the Test Section
    D. Develop instrumentation for use in larger scale tests
2. Conduct separate-effects, two-phase flow experiments, in order to
    A. Develop a phenomenological model that will describe the Flashing and Flow Stability phenomena
    B. Determine the Efficiency of Phase Separation in the Storage Tank
3. Develop a System Level Computational Model that will describe the overall RCCS behavior

Originally, UW was to build an experimental facility to conduct the single-phase and two-phase testing, and UI was to primarily aid in developing instrumentation and other support functions. TAMU was tasked with developing the computational model in the form of RELAP5-3D computer codes. Ultimately, Texas A&M decided to build their own experimental facility as well, the main differences being the number of risers in the panel and their pitch to diameter ratio, the scaled height of the Test Section (and subsequently the power level for the heaters), and the materials used for construction. Due to the differences in system geometry and other considerations, the primary focus of this thesis will not be to make comparisons to the UW facility, but nonetheless a few evaluations of the TAMU system against the UW system will be made in Chapter VI.

Referring back to these original objectives, the research presented in this report was motivated by the desire to directly address tasks 1.B., 1.C, and 2.A. An attempt to validate the scaling laws (task 1.A above) developed by Argonne National Labs in their feasibility study to use the Natural Convection Shutdown Heat Removal Test Facility (NSTF) as an RCCS was not conducted in this report [3]. Likewise, task 2.B is beyond the scope of this research and will be left for future study. Task 3, the development of

system level computational models, has already been undertaken by researchers at TAMU, further information can be found in R. Vaghetto's doctoral dissertation [6]. Results of the experiments conducted for this thesis may, however, be used by a future researcher to validate and further refine these computational models.

### I.4 Summary of Conducted Research

The tasks outlined in NUEP Project #09-202 are somewhat vague and would need further refinement before meaningful research could begin. It was decided that the primary objective would be to measure the flow distribution in the Test Section, and to see how this distribution changes under different experimental conditions. This objective is in line with task 1.C above. While conducting the experiments to measure the flow distribution, system parameters such as power applied from the heaters, the temperature difference developed in the coolant across the Test Section, system flowrate, and the amount of power absorbed by the coolant could be measured and/or calculated. This would allow for characterization of the system flow behavior as charged by task 1.B.

As mentioned in the background section earlier, the RCCS is to be operated in a completely passive mode with no secondary cooling loop in operation. This will result in the coolant temperature continuing to rise, eventually reaching two-phase conditions, and this provides for the opportunity to observe how the flow distribution changes over time as the fluid continues to increase in temperature and the system flow rate stabilizes during each experiment. Another result of the passive cooling mode of operation is a minor flow instability in the form of small amplitude sinusoidal oscillations. These instabilities are characterized for each experiment type as well.

The experimental variables of the most interest to system behavior are the heat flux profiles and power levels being applied to the Cooling Panel within the Heated Cavity. As noted in Figure 1, the distance and viewing angle from the RPV wall to each individual pipe in a Cooling Panel can vary significantly, therefore it is pertinent to observe the effect of varying these parameters. In addition, some of the work conducted previously at Argonne and the University of Wisconsin on the RCCS concept was

referenced to a 10 °C temperature difference between the coolant entering and leaving the Test Section [3], and preliminary experiments showed that the TAMU_RCCS only produces a 2 °C temperature difference as designed. Therefore, it was desired to be able to throttle the flow and allow the fluid to remain in the Test Section for a longer period of time to achieve higher temperature differences, and to subsequently observe the effects on the flow distribution. With this information one could gain a better understanding of the separate effects of incoming fluid momentum and heat flux to the flow distribution in the Cooling Panel. Finally, the effect of tank water level on system behavior could also be explored relatively easily, so it was added to the list of experimental conditions. Descriptions of the single phase experiments conducted and the results therefrom are detailed in Chapter IV of this report.

In addition, it was desired to conduct at least one experiment wherein the system would reach two-phase operation. This was successfully performed with some rather spectacular results in the form of violent geysering phenomena, and this is documented in Chapter V. Video of the geysering phenomena is available and can be provided on request by contacting the author via email.[1]

Unfortunately, at the beginning of the research endeavors it was evident that the RCCS was suffering from three problems requiring immediate attention. First, the system leaked at essentially all of the interfaces where the pipes were joined to other pipes, the tank, and to the manifolds. There were also many leaks in the connections of the glass risers of the manifolds to the stainless steel pipes of the Test Section. Second, there was a general lack of instrumentation and controls available to alter system parameters and record the results to the extent that was desired. Finally, the thermocouples attached to the outside face of the pipes and fins of the riser panel in the Test Section were continually falling off the surface, giving erroneous results.

The first two issues were resolved successfully. Chapter II details how the leaks were fixed and lists all of the instrumentation and control (I&C) upgrades made to the system. Unfortunately, the Cooling Panel surface thermocouple bonding issue was not

[1] mjgorman21@gmail.com

addressed successfully, leaving a gap in the logical progression of events that will also be discussed in Chapter II. Suggestions as to how to resolve this issue will be discussed in Chapter VII.

The task of adding instrumentation to measure the local flow velocity of the coolant in each individual riser in the Cooling Panel was no small one, primarily because of the extremely low flow velocities typically found in systems powered by natural convection. Turbine and paddle meters, variable-area vane style meters, rotameters, and positive-displacement type meters all rely on the fluid physically moving objects in its flow path, and it is unlikely that the fluid in the RCCS would have enough momentum to do so. A Coriolis effect based flowmeter or a differential pressure based meter would require either a split path for the fluid to travel in or a pressure drop inducing constriction such as an orifice plate or venturi in order to operate, and again the fluid does not have enough energy to spare. Electromagnetic, Karman vortex shedding, and transit-time based ultrasonic flowmeters all require a certain minimum fluid flow velocity to operate, preliminary estimates of the velocities showed that the fluid was less than that minimum value. Thermal dispersion type meters were not investigated.

Thankfully, two solutions presented themselves. First, the fact that the upper and lower manifolds are made of clear borosilicate glass allows for the introduction of seed particles and Particle Image Velocimetry (PIV) techniques to be used to measure the flow. Second, it came to the author's attention that the University of Wisconsin had successfully used a novel instrument that they borrowed from the University of Idaho called on Ultrasonic Velocity Profiler (UVP) which uses pulse-Doppler techniques to determine the fluid velocity, similar to SONAR and RADAR. The same UVP instrument as used at UW was acquired from UI, courtesy of Dr. Akira Tokuhiro. Both of these measurement techniques require seeding the coolant with small, neutrally buoyant particles and then extensive calibration and post-processing to obtain meaningful results. Chapter III is devoted to detailing these issues for both PIV and UVP.

A summary of the work performed, along with conclusions arrived from the data is presented in Chapter VI. This also includes some comparisons to results from the University of Wisconsin's RCCS system. Chapter VII, already referred to several times thus far, contains suggestions for future research in thermal hydraulics using the RCCS at Texas A&M, along with a list of further modifications suggested for the system and the underlying motivations as to why.

# CHAPTER II
# SYSTEM UPGRADES AND UNDERLYING MOTIVATIONS

## II.1 Summary of Changes and Additions

As mentioned in the Introduction, the RCCS needed to have the leaks fixed and needed Instrumentation and Control upgrades to facilitate a higher variety of experimental conditions and ability to record the resulting data. The most significant change to the original design was to remove the stainless steel plate that simulated the RPV, which was previously in the Heated Cavity, and to re-orient the heaters to a vertical configuration as opposed to a horizontal layout which they had originally. This will be discussed further later in this chapter. Most other changes were the installation of new measurement equipment. Illustrations of the original and current (at the time of this writing) systems are shown side by side for comparison in Figure 6 below, with changes annotated within the text in the figure. Please note that the Solidworks model used to represent the old system was off in scale for the horizontal piping by a factor of approximately 2, the relative lengths of the piping is more accurately represented by the updated model on the right of Figure 6 and have not actually physically changed.

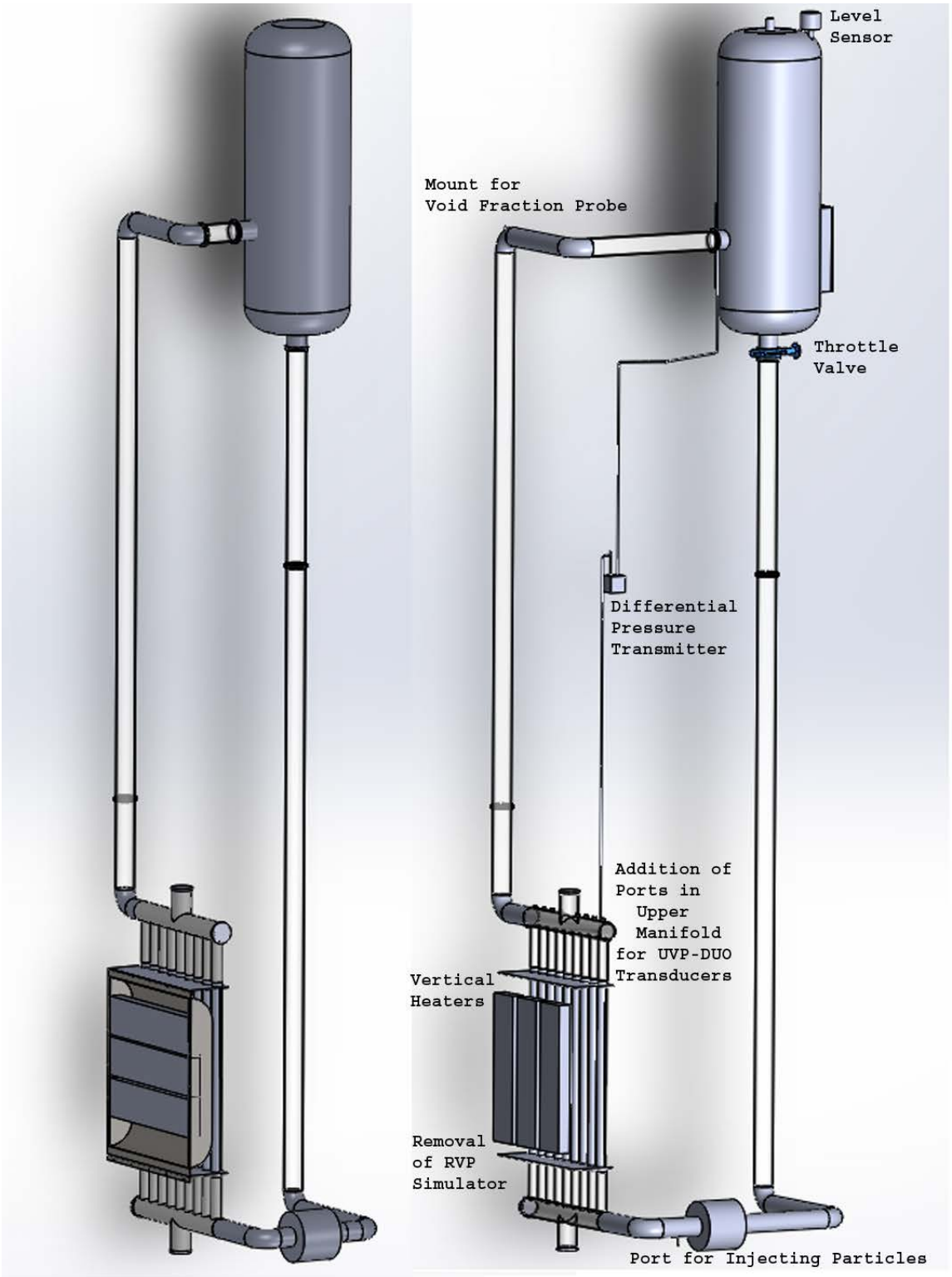


**Figure 6.** Original (left) and Current (right) Designs of the RCCS at Texas A&M

From the figure above, note the heaters are now vertically mounted, and the RPV simulator has been removed. A capacitance based level transmitter has been added to measure the water level in the tank. A differential pressure transmitter was installed with impulse lines from the upper manifold outlet to the inlet of the water storage tank. An injection port has been added just past the magmeter for introducing the microspheres which are used as reflectors of the acoustic signal for UVP measurements and fluorescent reflectors of light for PIV measurements. To further facilitate the UVP measurements, the Upper Manifold has had 8 ports added to allow for mounting the ultrasonic transducers; each pointing straight down into every riser tube of the Cooling Panel except for the one at the center. A port and mount for an optical probe used to measure void fraction during two-phase experiments has been installed at the stainless steel (SS) elbow on top of the Chimney. Finally, a 4” (100 mm) butterfly valve used to throttle the flow has been added just below the Coolant Tank outlet.

A couple of additions not shown in the figure were that a single thermocouple was added to the system at the top of the Chimney, in close proximity to where the void fraction probe port was installed, analog outputs were added to the temperature controllers for the radiant heaters, and the demand signals from the controllers to the heaters were ran through the Data Acquisition system (DAQ) as well in order to record the power sent to the Heated Cavity. Finally, the data acquisition system itself had to be rewired for the additional measurements and the software updated accordingly. The rest of this chapter will detail all changes mentioned for documentation purposes.

## II.2 Resolution of System-wide Coolant Leaks

Problematic water leaks were experienced at almost every joint in the entire RCCS system and were caused primarily by two sources. First, piping made from different types of materials which have different dimensional standards and temperature and pressure ratings was used in construction, so there was no standard method of connecting them together. Second, during the layout phase of construction the pipes were not cut to the proper lengths to allow the ends of the loop to come together in perfect alignment. Since the axial centerlines of the pipes did not line up properly, small angles and stresses were placed at the joints upon connection, exacerbating the first problem. The problems and solutions are divided into 3 separate categories.

### II.2.1 Leaks at the Joints of the 4” Diameter Polycarbonate Pipes

The 4” polycarbonate pipes were connected to the inlet and outlet flanges of the storage tank, to the stainless steel pipe elbows between the Chimney and Tank Return Line, and to each other in the Downcomer and Chimney via flange connectors made of plastic. An example of a connection using these plastic flanges is shown at the top of Figure 7 on the next page. Eventually, the bending stress brought about by trying to bring the misaligned pipes together caused cracks to develop at the joint of the polycarbonate pipe and its flange, subsequently causing leaks. Large amounts of silicon caulking, UV activated epoxies, and other materials were used in an attempt to deal with the leaks, to no avail.

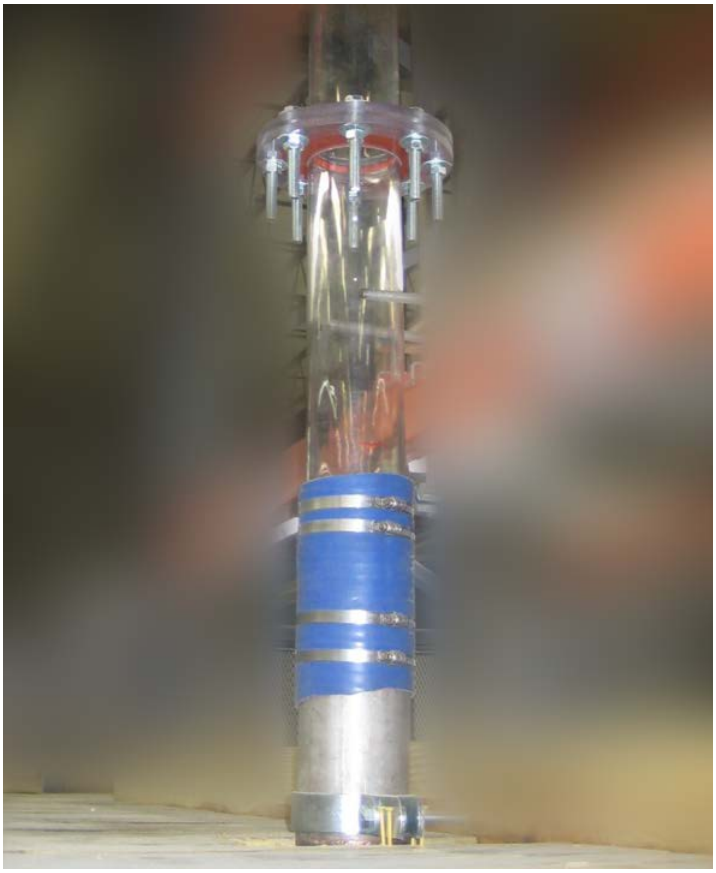

**Figure 7.** Plastic Flange and Hose-Style Connections used in the Original Design

The solution came from observing that two particular joints never leaked, both made the steel to polycarbonate connection using a silicon rubber hose that fits over each end and is secured with hose clamps. One was at the bottom of the Downcomer where it fed into the stainless steel elbow before the magmeter, and the other was at the beginning of the Chimney as it left from the SS elbow connected to the upper manifold. The hose-style Chimney connection is pictured at the bottom of Figure 7 above.

The hose-style connection originally had a 1/8” (3 mm) thick black rubber insert between the hose and the polycarbonate pipe. This is because 4” (100 mm) stainless pipe has an outside diameter (OD) of 4.5” (114 mm), and the polycarbonate pipe’s diameter is only 4.25” (108 mm). The hose has an inside diameter (ID) of 4.5” (114 mm) which matches the steel, so the rubber insert makes up the difference on the polycarbonate side.

It was decided to replace all of the 4.25” (108 mm) OD polycarbonate pipes with thicker wall 4.5” (114 mm) pipes to negate the need for rubber inserts, and to replace all joints using plastic flanges with the hose-style connection. An example of this for polycarbonate to polycarbonate connections is shown in Figure 8 below.

**Figure 8.** Replacement of Plastic Flanges with Hose Connections for Pipe-to-Pipe Joints

In order to make a hose type connection against the steel flanges of the storage tank and the SS elbows between the Chimney and Tank Return Line, a short section of steel pipe with a flange on one end and a smooth cutoff at the other had to be installed. This was done at all such connection points; a typical result is shown in Figure 9 below. This immediately stopped all these types of leaks as the flexible rubber hoses could make up for the misalignments in the pipe network.

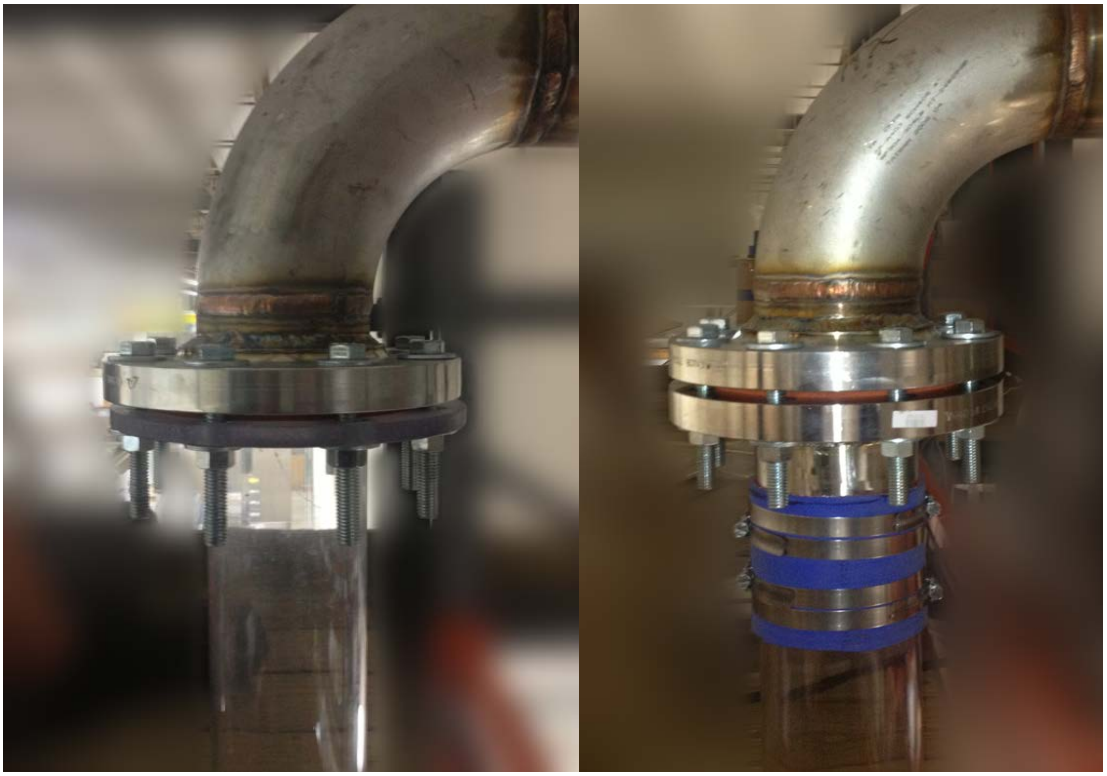

**Figure 9.** Replacement of Plastic Flanges with Hose Connections for Pipe-to-Steel Joints

II.2.2 Leaks at the Joints of the 4" Diameter Glass Manifold

The second category of leaks arise from where the SS elbows mate to the 4" (100 mm) ends of the glass manifold, and from the end caps used to seal the unused outlets of the manifolds. The glass tubing used to construct the manifolds is typically used and marketed for drainage and ventilation systems in laboratories, so the connectors are not designed to hold back any significant positive pressure [9]. A picture of the connectors originally used for both the end caps and SS elbow is in Figure 10 below.

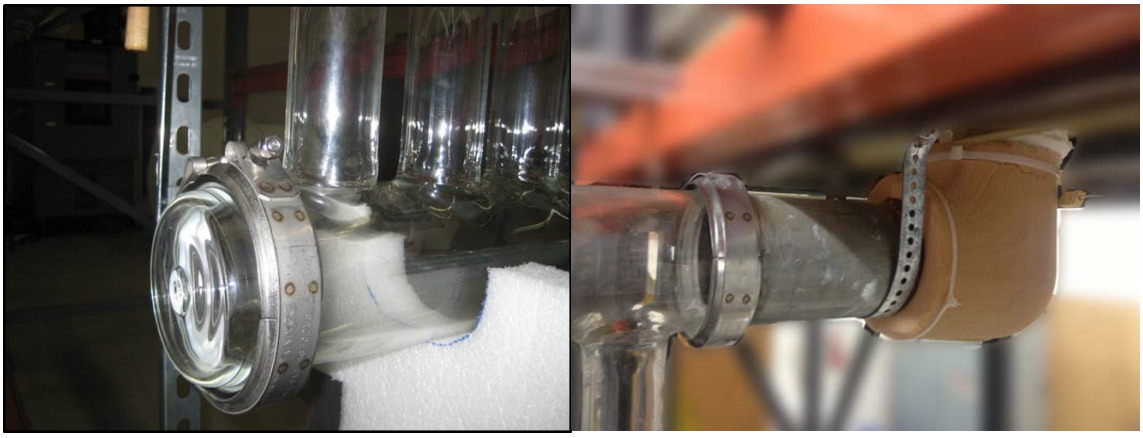

**Figure 10.** Glass Manifold Connections – to End Cap (left) – to SS Elbow (right)

The bead-to-bead compression couplings shown in Figure 10 are designed to join similar glass ends together. In an attempt to make this coupling work for the SS to glass transition, the SS elbows were modified by having a strip of steel welded onto the end to form a raised bead similar to what is seen at the end of the glass tube, as shown in Figure 11 below.

**Figure 11.** Detail of Bead on the Glass Manifold (left) and SS Elbow (right)

Unfortunately this coupling only applies force in the direction from the point of contact at the circumference of the bead towards the axial centerline of the pipe as it is tightened (hence the term *compression* coupling); it does not apply a strong direct force to push the pipes together. Subsequently, as the pressure of the water from 5 to 7 meters of head pushed on the piping, it would physically separate the pipes and/or end caps from one another, causing a full scale LOCA (loss of coolant accident). This presented a serious safety hazard should it occur during a two-phase experiment. Alternative measures to connect the glass manifolds had to be explored.

Realizing that the beads on the glass and the SS provided a surface wherein a force could be applied to push the pipes together, a custom coupling system was designed with the help of the TAMU Department of Chemistry's Glass Shop and Machine Shop. A simplified Solidworks CAD drawing is provided in Figure 12 below.

**Figure 12.** CAD Drawing of Custom Manifold Couplings (not complete)

Note the coupling is essentially a doughnut shaped aluminum plate with a recessed bore machined halfway through the total thickness of the plate. This forms a step or ledge that matches up to the side of the bead on the 4" (100 mm) glass tube, SS elbow, or glass end cap. When one of these plates is installed on each side of the joint

with the step pressing against the bead, 4 bolts are then used to bring the two pipes together. Note that the metal step does not touch the pipe bead or cap directly, a soft rubber O-ring lays in the step to prevent metal to glass contact and to take up any tolerances present. The profiles of the glass pipe bead and the glass end caps are not square, so the O-ring can deform to fit the profile tightly and take up the slack of any tolerances present. A gasket is placed between the faces of the pipes and/or end caps for complete sealing. Photograph examples of the final results are shown in Figures 13 and 14 below.

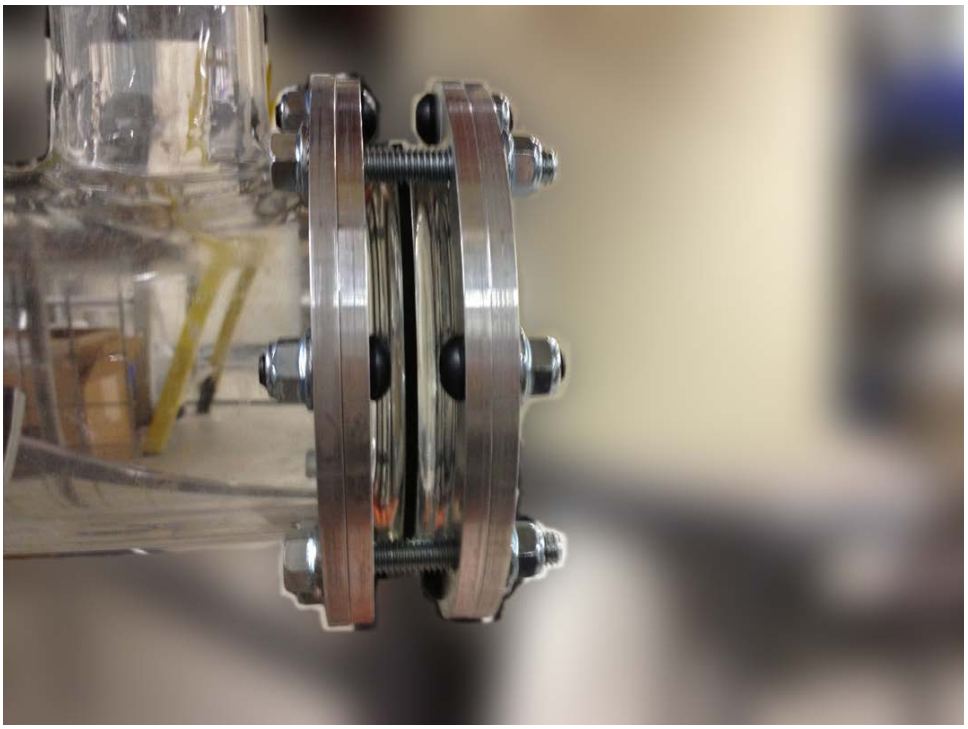

**Figure 13.** Detail of Custom Manifold Coupling on End Cap

**Figure 14.** Custom Manifold Couplings installed on the Lower Manifold

II.2.3 Leaks at the Joints of the 2” Diameter Tubes of the Glass Manifold

The last category of leaks that had to be resolved were where the 2” (50 mm) SS risers of the Cooling Panel had to mate to the 2” (50 mm) glass tubes of the upper and lower manifolds. In the original construction, silicon rubber hoses of the same type as mentioned earlier were used with hose clamps to connect the pipes, as shown in Figure 15 below. Unlike the hose connections used previously on the polycarbonate, however, these joints leaked profusely, necessitating an investigation as to why this was occurring.

**Figure 15.** Hose-Style Connections of the Cooling Panel to the Upper Manifold

The source of the problem was that the glass tubes had a nominal OD of 2.325” (59 mm), while the schedule 40 SS pipes have an OD of 2.375” (60.3 mm). Since the silicon hose also has an ID of 2.375” (60.3 mm) the glass tube does not make a full interference fit all the way across its circumference. This is obviously a source of leaks, and initial efforts to fix this consisted of silicon caulking, multiple layers of Teflon tape, and new ‘constant-tension’ hose clamps, but all these solutions proved to be unsatisfactory.

Unlike the 4” (100 mm) glass pipe shown previously in Figure 11, the 2” (50 mm) glass tubes did not have a bead at the end, keeping the same OD all the way to the end of the tube. It was decided that the simplest solution would be to take the manifolds to the Glass Shop and have the ends heated up and ‘rolled out’ in order to create a makeshift bead. This would provide a full interference fit with the hose and would hopefully stop the leaks. A detail of one of the modified glass tubes and how it fits with the hose is shown in Figure 16 below. A bulge in the hose where the bead is located can be seen clearly in the figure, indicating that there is contact around the full 360° circumference of tube. All 9 riser tubes on both manifolds were modified in this fashion.

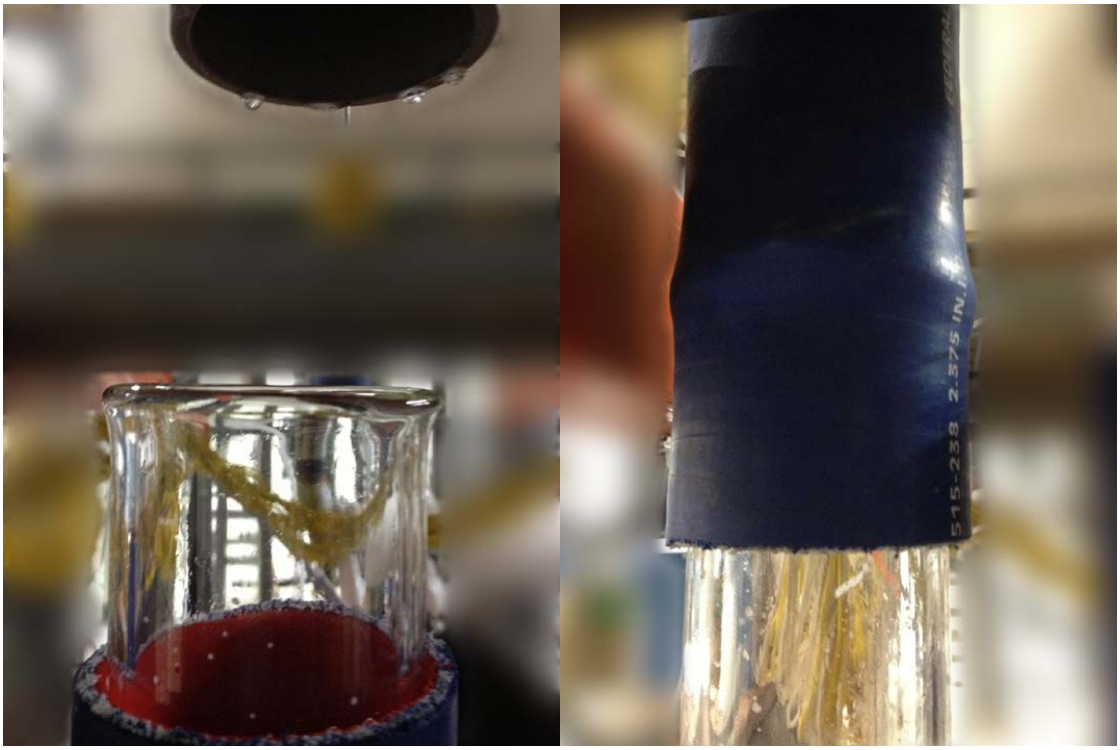


**Figure 16.** Modified Glass Manifold to Steel Riser Connection

At this point it should also be mentioned that the construction of the glass manifold, specifically the spacing of the 2” (50 mm) tubes and the angle at which they exit the 4” (100 mm) header, is not exact and the glass tubes do not line up perfectly with the SS risers. This can be noted by observation in Figure 16 above. This may have some negative consequences for UVP measurements, noted in Chapter III. It also required the application of silicon caulking inside the hose before the bead to ensure a leak free seal as the rubber hoses were bent significantly in some cases. Nonetheless, the solution worked satisfactorily, even providing leak-free service during the steam generation and geysering events seen during the two-phase experiment detailed in Chapter V.

### II.3 Addition of Throttle Valve

As mentioned in the Introduction, it was desired to conduct some of the experiments under the condition that the difference in temperatures of the fluid entering and leaving the Test Section, hereinafter referred to as the Test Section ΔT or simply ΔT, would be 10 °C. Both the TAMU and UW RCCS systems operated with a 2 °C ΔT when the appropriately scaled power levels were applied. Preliminary estimates showed that the temperature limits of the heaters would be exceeded if the power were raised to a level that could induce a 10 °C ΔT, in either system. The only other way to achieve this set of boundary conditions at the Test Section is to restrict or throttle the flow through the system. An orifice plate at the inlet of the Test Section was used at the UW-RCCS system to do this, but for the TAMU system it was decided to use a butterfly valve (McMaster Carr part #4850K33) to be able to vary the amount of throttling and hence the ΔT, adding versatility to the system. The butterfly valve has the same bore diameter as the piping, so that when fully open it would present essentially zero obstruction to the flow. It was decided to place it at the outlet of the storage tank in order to minimize its effects on the flow distribution in the Test Section. A photograph of the valve as installed in the system is in Figure 17 below.

**Figure 17.** Throttle Valve under the Coolant Storage Tank

## II.4 Changes to the Heated Cavity

### II.4.1 Removal of the Reactor Pressure Vessel Simulator

The 2000 IAEA study mentioned previously [2] predicted that for the 600 $MW_{th}$ modular high temperature reactor designed by General Atomics (the GT-MHR), the RCCS system would absorb a total of 0.74 MW of energy during normal operation. After scaling for RPV height (i.e. the 1.1 meter height of the Heated Cavity) and the fraction of the reactor cavity perimeter covered by the TAMU-RCCS Cooling Panel (9 out of 227 risers) using the scaling laws developed by Argonne, it was previously determined that the power level in the Heated Cavity should be 6 kW [6].

Initial runs of the RCCS using the scaled power output of 6 kW showed that the temperature of the heaters reached approximately 700 °C, which is only 60 °C away from the point beyond which damage would likely occur. As a result, it would not be possible to perform experiments at significantly higher power levels, reducing the range of experiments that could be done. It can be noted in Figure 18 below that the heaters were placed essentially inside the RPV Simulator, and then sealed in the back with insulation, making them completely encased in the Heated Cavity.

**Figure 18.** Horizontal Heaters laid inside the RPV Simulator (left) and enclosed in the Heated Cavity (right)

The heaters are a radiant type heater designed to project 78.5% of the energy in the direction the heater is facing [10], so it is not absolutely required that they be encased in the cavity. Theoretically, by flush mounting the heaters with the insulation, leaving the body of the heater exposed to the ambient environment, the temperature felt by the internal components could be reduced. This would be difficult to do with the heaters placed inside the RPV as shown in Figure 18, and at that point the questions arose as to what the effect of the RPV itself was and whether or not it was truly beneficial to keep it.

The alternative to having the RPV simulator was to simply remove it and have the heaters point directly at the Cooling Panel in the same manner that the UW-RCCS was constructed. The heaters could then be spaced apart vertically as desired within the limits of the cavity, and custom insulation panels with holes for flush mounting could be fabricated and installed for a clean installation. Potential benefits from doing so included:

- an increase in the percentage of the power emitted by the heaters being absorbed by the water in the Cooling Panel
- a greater range of heater powers could be used in experiments
- the heaters could be turned vertically to allow for a changing heat flux profile from the inlet to the outlet
- increased heater life due to lower internal component temperatures

The stated purpose of the RPV Simulator was to provide a more uniform heat flux across a 2-D surface [6]. In the end, this hypothesis was never tested vigorously, but there were a few tests ran that indicated with the RPV Simulator removed much higher surface temperatures would be generated on the Cooling Panel and the heaters would run much cooler at the same power levels. In addition, removing the RPV Simulator would make the TAMU system more similar to Wisconsin's. For these reasons it was decided by the RCCS committee to remove the RPV Simulator.

### II.4.2 Heater Orientation

After removing the RPV Simulator, the heaters were initially left horizontal and spaced apart so that there was equal spacing between the heaters themselves and from the edges of the heaters to the bottom and top of the Heated Cavity. See the left side of Figure 19 for a photograph of the arrangement of the heaters in the cavity in this configuration.

It was soon after decided, however, that investigating the effect of azimuthally varying heat flux profiles would be more important than investigating profiles that vary in elevation. Previous results from D. Lisowski at the UW RCCS [5] show that there is little difference between a uniform and a more realistic 'cosine' shaped heat flux profile in elevation to system behavior, but changing the heat flux profile azimuthally does have a significant impact on the flow distribution in the Cooling Panel. For this reason, the heaters were turned vertical as shown in the right side of Figure 19, and all experiments and results presented in this report are resultant from this configuration.

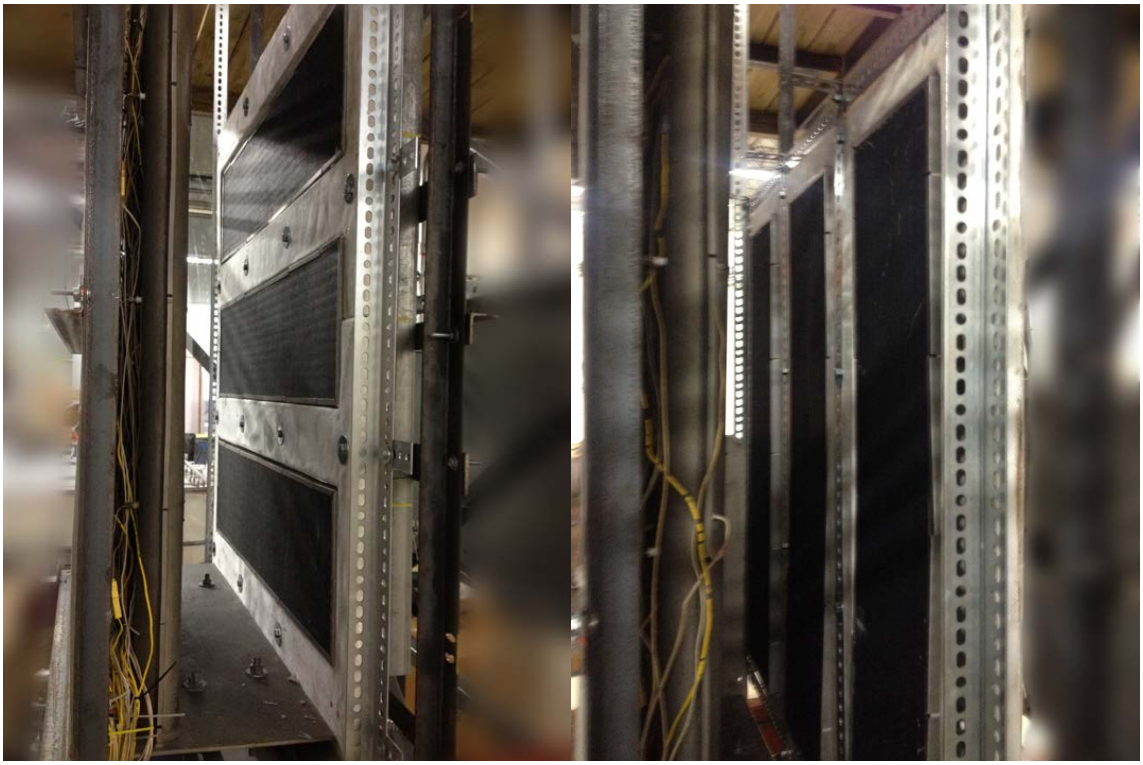

**Figure 19.** Horizontal and Vertical Heater Configurations w/o the RPV Simulator

II.4.3 Custom Insulation Panels

It can be noted that some of the insulation panels in Figures 18 and 19 are different. The new panels are still composed primarily of Microtherm insulation as before (25 mm thick Promalight Board), but in addition they are wrapped in a high temperature pre-shrunk silica material that provides more structural integrity to the panels. This enables them to be constructed with tight fitting holes to provide for flush-mounting the heaters, and helps to prevent the panels from crumbling apart as they are handled during configuration changes and repairs or modifications to the instrumentation in the Test Section. In Figure 19, the wrapped panels have a bright white appearance and are between the heaters, the regular panels, one being shown on the side obscuring the view of the vertically mounted heaters, are a gray earth tone color. It is suggested that all panels be replaced with the wrapped ones for future experiments as they are not very expensive.

II.4.4 Instrumenting Heater Power and Surface Temperature

The FUZYPRO model 6100 temperature controllers had 4-20 mA retransmit cards installed so that the heater surface temperatures could be relayed to the LabVIEW data acquisition system for recording. Also, the demand signal sent to the phase-fired controllers (PFC) was routed in series through the DAQ so that the amount of power sent to the heaters could be recorded at all times during the course of an experiment. It should be noted that for all of the experiments presented in this report the power was applied as a step input and was not time-varying. Nonetheless, this upgrade will ensure that the power applied can be known accurately for any future experiments that utilize a time varying profile, especially one under automatic control to maintain a static or time-varying temperature setpoint.

## II.5 Temperature Measurement Changes and Additions

II.5.1 Surface Thermocouples

For the experiments presented in this report, the Cooling Panel surface temperatures were not recorded using the K type thermocouples bonded via metallic adhesive to the panel. The reason for this is that the thermocouples would periodically detach from the panel. This caused the thermocouples to report the air temperatures instead, which were much higher than the Cooling Panel surface. An example of a detached thermocouple is in Figure 20 below.

**Figure 20.** Detached Thermocouple on the Coolant Panel Surface

This problem was present ever since the original construction was completed. The two main problems were that the adhesive, Durabond™ 954 from Cotronics, was neither mixed nor cured properly during application. The adhesive is an epoxy type and consist of a dry powder and a liquid hardener which must be mixed together in a certain ratio to form a strong bond. This was not done because the thermocouples were installed after the Cooling Panel was installed in its current vertical orientation, and the viscosity of the fluid was too low to be applied to a vertical surface when mixed in the proper proportions. After application of a mixture with too little hardener, the Cooling Panel was never placed in an oven for proper curing per the manufacturer's directions. At best, once all thermocouples that detached were repaired (again without the proper mix ratio or proper curing) more would begin to fall off within a few days. Correspondence with technical personnel in charge of the UW-RCCS facility indicated that the t/c should be reattached via direct fusion into the metal risers and fins using a TIG welder.

Successfully carrying out this repair is the single most important modification that needs to be made to the TAMU RCCS for future experiments, since the temperature measurements are necessary to more accurately determine the heat flux across the Cooling Panel and represents the most critical piece of missing information in these experiments. More information on this topic is in Chapter VII.

## II.5.2 Wetted Thermocouples

### *II.5.2.1 Physical Calibration of Insertion Depth*

During system modifications it was discovered that the insertion depths of the wetted thermocouples in the coolant panel were not uniform; in some instances the thermocouples were inserted so far as to actually be in contact with the heated wall (see Figure 21).

**Figure 21.** Inconsistent Thermocouple Insertion Depths in the Coolant Panel

To remedy this, the pressed-on ferrule inserts were removed from the t/c probes and replaced with new ones at locations that would allow them to all to be inserted to the same depth, which is 13 mm away from the interior surface of the heated wall. This is about 75% of the way into the ID of the pipe. This was done because this was the distance at which the smallest fraction of the 45 wetted thermocouples in the coolant panel that would have to be modified, and in the process of removing the ferrules sometimes the probes would be destroyed and have to be replaced entirely.

*II.5.2.2 Software Calibration*

A two-point calibration in the LABVIEW SignalExpress software was performed using an ice bath and a pot of boiling water, for 0 and 100 °C, respectively, on all 45 thermocouples in the Cooling Panel and the other 5 wetted thermocouples in the system.

*II.5.2.3 Thermocouple Additions*

It was suspected by D. Lisowski in his dissertation that the location of the 'boiling boundary' or the exact point in the hot leg at which boiling occurs can be located by looking at the 'phase difference' between the thermocouples located throughout the hot leg [5]. As there were only 2 thermocouples in the hot leg, one at the Test Section outlet and the second at the Storage Tank inlet, it was decided to place one more thermocouple in the hot leg at the top of the Chimney to better test this possibility. This is assuming the technique is valid and a similar boiling phenomenon would be encountered in the TAMU system. Its insertion depth is only about ¼ of the way into the pipe so that the probe tip will not directly interfere with the RBI optical void fraction probe, which can be inserted above it.

**II.6 Addition of the Level Sensor**

A capacitance based level transmitter, Dwyer Instruments model CRF2, was installed in the North-East corner of the Coolant Storage Tank. As installed it has the capability of reading the water level from the beginning of the cylindrical tank section to the top of the tank, but is scaled to show high level at the upper port of the secondary

cooling loop (not used), as shown in Figure 22 below. It transmits a 4-20 mA signal to the LABVIEW data acquisition system where it is converted to a voltage signal by a 200 Ω resistor. The volumes listed beside the levels in the figure are for the entire system.

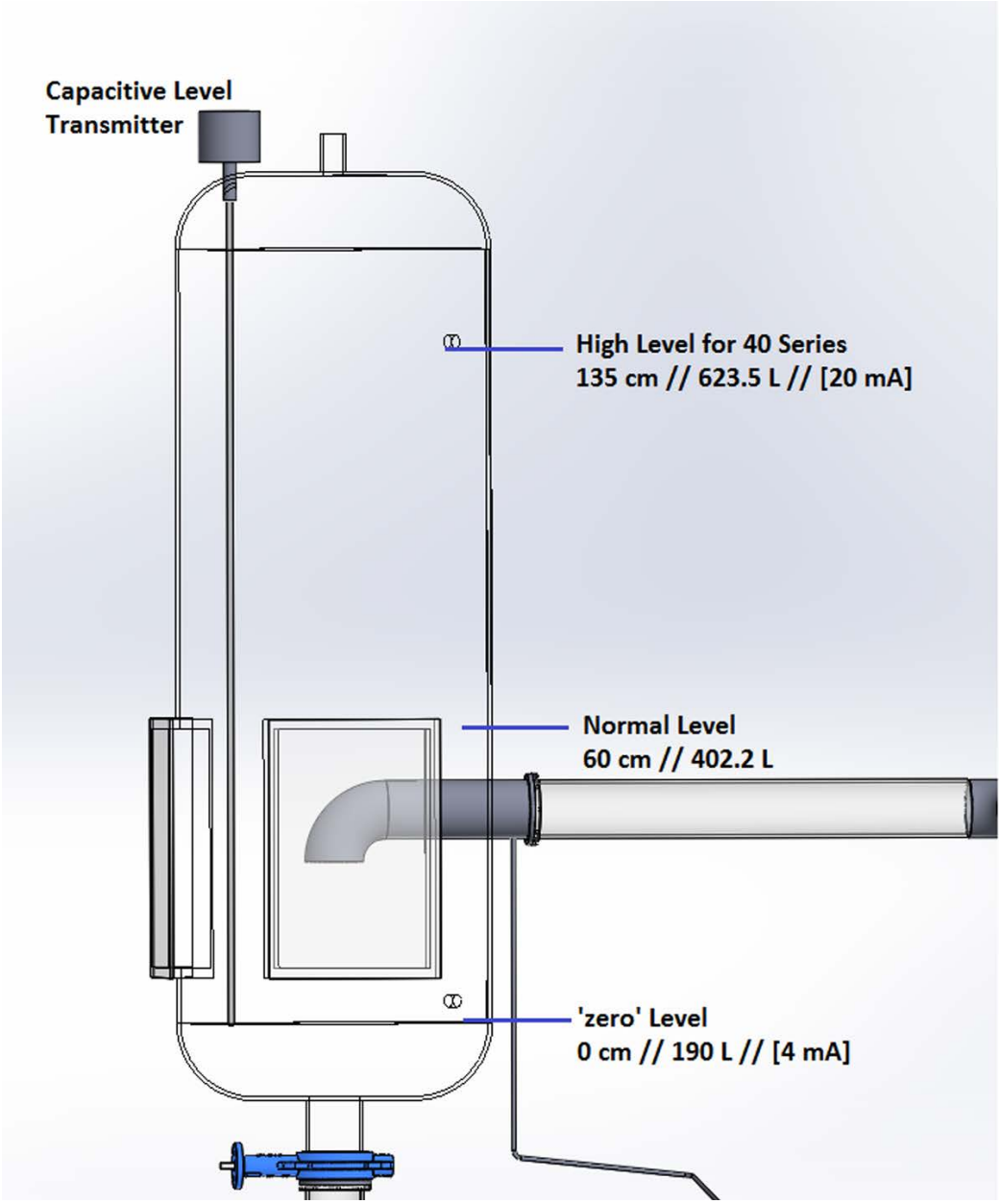


**Figure 22**. Setup of Level Transmitter in the Coolant Storage Tank

### II.7 Addition of Differential Pressure Sensor

An Azbil model AT9000 differential pressure sensor was installed in the system at the second floor of the RCCS support structure. It is connected to the RCCS via taps at the bottom of the steel pipes at the Test Section outlet and Tank inlet, as shown in Figure 23 below. The impulse lines are seamless stainless steel with a 3/8" (9.5 mm) OD and 0.035" (1 mm) wall thickness. A 3-way manifold (Dwyer BBV-1) at the transmitter inlets, tee connections at the top and bottom of the high pressure leg, and a gentle slope of the horizontal sections of the low pressure leg are all used to ensure the lines can be bled of any entrained air and flushed of any trapped particles or sediment.

It was attempted to locate the transmitter approximately half-way between the elevations of the taps of the impulse lines in order to keep the lines as equal in length as possible. In addition, due to the elevation difference in the taps a significant static pressure difference exists at the transmitter. The only methods to compensate are to form the lower impulse line to the same peak height as the upper line, and then come down into the transmitter, or to simply ‘zero’ the device out electronically. A combination of the two methods was used in this installation.

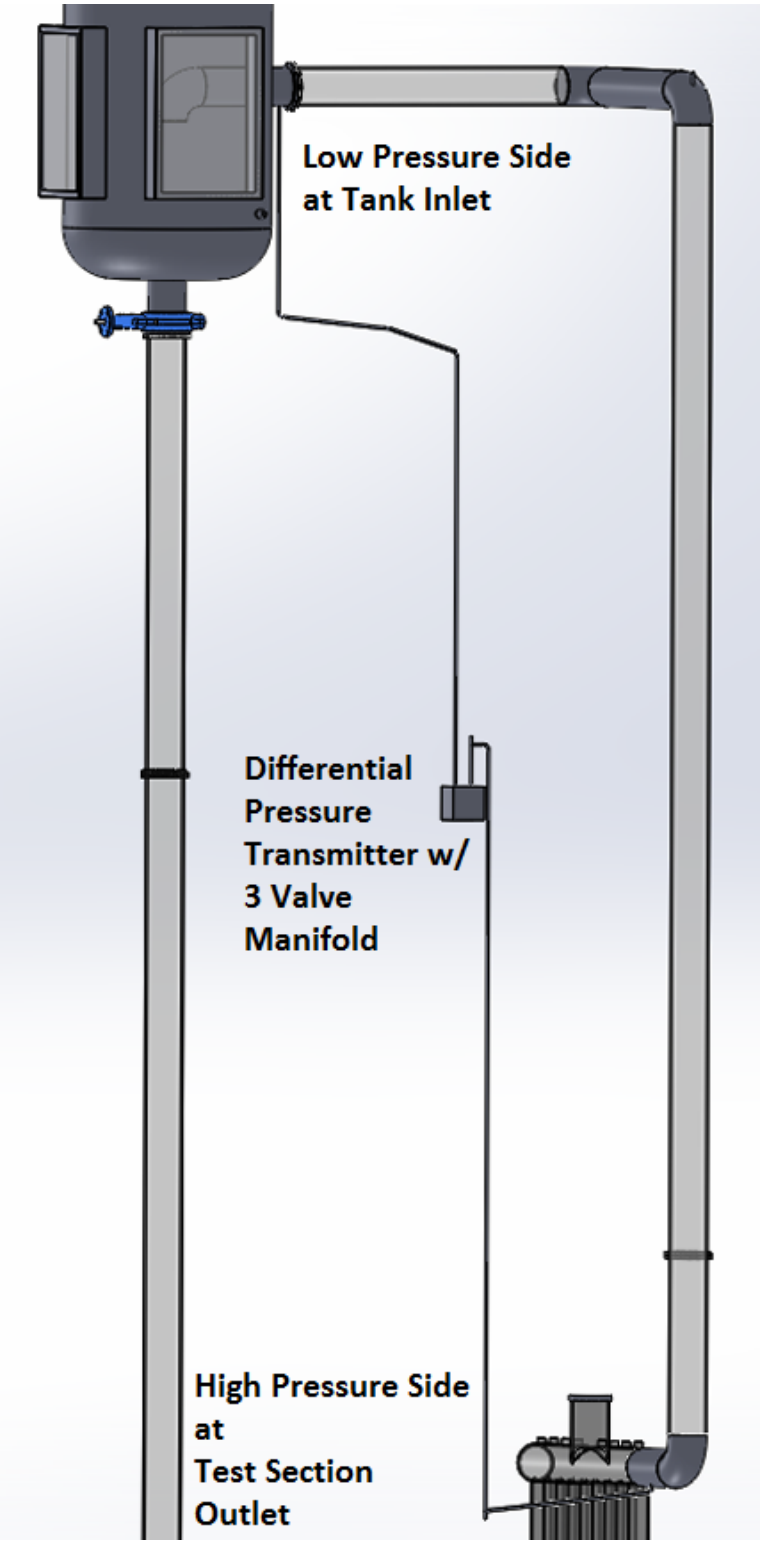


**Figure 23**. Differential Pressure Sensor with Impulse Lines

**II.8 Data Acquisition System Upgrades**

The LABVIEW Signal Express software of the data acquisition system was modified to include the measurements of the level and pressure transmitters and the extra thermocouple in the Chimney, plus the heaters' PFC demand signals and retransmitted heater surface temperature signals. The sampling frequency was increased to 1 Hz from $0.0\overline{6}$ Hz in order to better capture the oscillation phenomena. Finally, the wiring was redone in order to accommodate the new measurements, and to clean up the thermocouple wiring around the Cooling Panel, as seen in Figure 24 below.

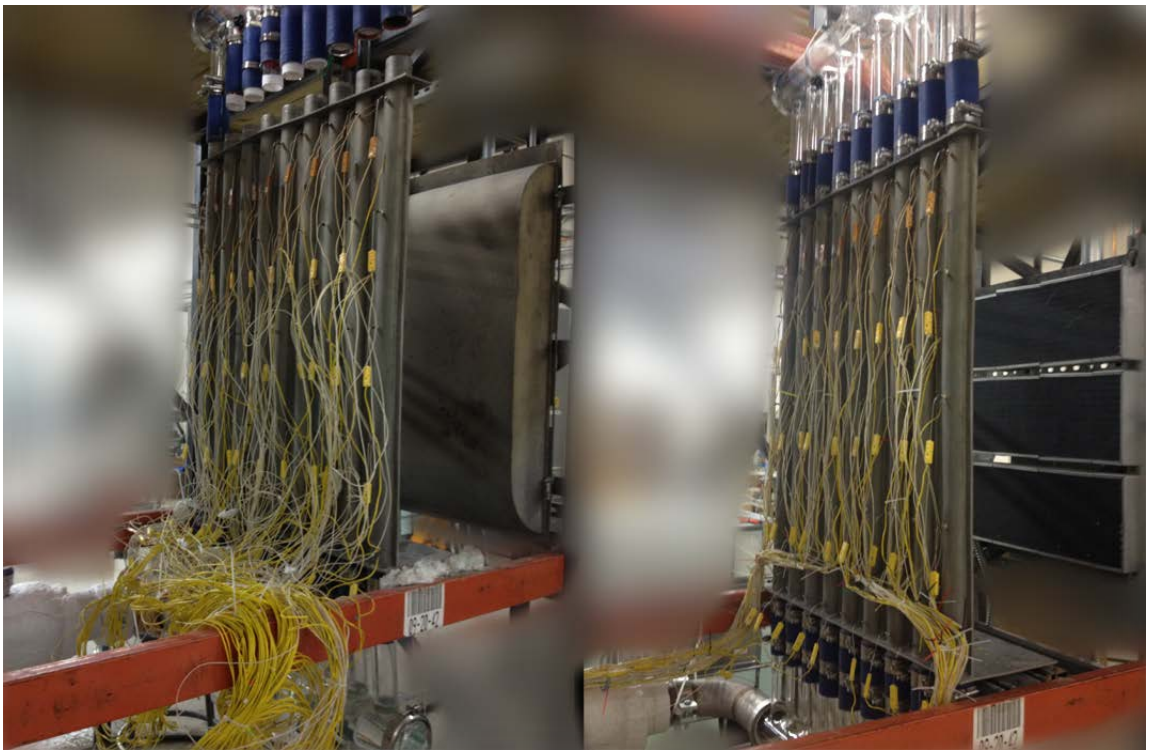

**Figure 24.** Before and After Rewiring the Cooling Panel Thermocouples

### II.9 Addition of Void Fraction Probe

In preparation for two-phase operations, an 8 mm swaged mount (Swagelok part# SS-8M0-1-4W) was welded into the SS elbow at the top of the Chimney, as shown in Figure 25 below. The mount was sized for a dual-tip optical probe from RBI, a French instrumentation company, and was on loan from the University of Idaho, courtesy of Dr. Akira Tokuhiro. With this device, the local bubble velocity and void fraction over time at that particular point in the flowstream could be ascertained. Unfortunately, due to time constraints the system was never setup and calibrated for the TAMU RCCS and no results from the device are present in this report.

**Figure 25.** Swagelok Mount for the RBI Optical Void Fraction Probe

## II.10 Additions and Upgrades Related to Flow Measurement

### II.10.1 Addition of Grounding Rings for the Electromagnetic Flowmeter

Stainless steel grounding rings were added to either side of the magmeter and connected to the ground reference wires supplied on its flowtube. This was necessary because the flowtube selected for the system did not include internal grounding electrodes, nor had the ground wires been attached to the steel piping. The flange bolts do not provide a good electrical connection to the piping unless the protective coating of paint on the outside of the flowtube is scraped off, which is not recommended for corrosion resistance. It was noted that after this fewer instances of the flow measurement intermittently dropping out at the DAQ were encountered.

### II.10.2 Addition of UVP Transducer Mounts in the Upper Manifold

In order to mount the ultrasonic (US) transducers in the system for flow velocity measurements in the individual riser tubes of the Cooling Panel using UVP, the upper glass manifold had to be modified as follows:

1. Holes were made in the 4” glass tube in line with the central axis of each riser tube.
2. Internally threaded glass connectors from Ace-Threds (Ordering Code #7644-10) were custom fitted to the manifold by forming a ‘saddle’ that could straddle the hole
3. The connectors were glued on using Nano50 glass-to-glass adhesive

These modifications were done by the Department of Chemistry’s Glass Shop. Detail photos of the fittings can be seen in Figure 26 below. It can be noted in the figure that the threaded glass connectors have a nylon bushing that presses against a rubber O-ring, which itself acts as a compression fitting against the US transducer, holding it securely in place.

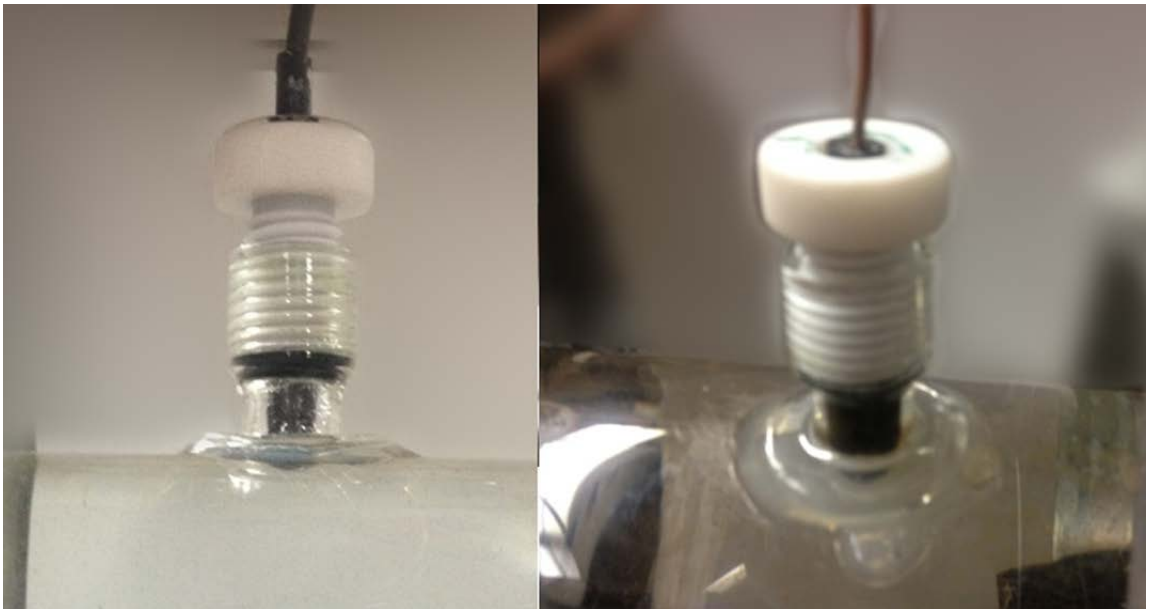

**Figure 26.** Detail of US Transducer Mount installed on the Upper Manifold

It was found over the course of several experiments that the glue used to bond the threaded connector to the manifold eventually weakens due to constant contact with the hot water. This caused the connector to separate from the manifold on one occasion, so in order to mitigate any possible damage from this event thick nylon zip-ties were used to ensure the connectors would not fly off suddenly during an experiment (see Figure 27 below). Unfortunately, it must be stated here that, after a thorough and exhaustive search, no adhesive solution could be found that can withstand constant contact with boiling hot water. A future mechanical solution could possibly be 'glass welding' the saddle of the connector to the manifold, which carries some risk of cracking the manifold.

**Figure 27.** Nylon Safety Straps on Upper Manifold

II.10.3 Addition of Acoustic Reflector Particle Injection Port

The principle of operation of UVP calls for seeding the fluid under flow with small solid particles or gas bubbles that will act as reflectors of the acoustic energy. In a similar way, PIV requires small particles that are simply visible enough to be captured with a camera; typically particles that will fluoresce under the light emitted by a laser are used for maximum clarity. In either case a system must be in place to introduce these particles to the fluid in a manner that provides a consistent concentration in the flow stream.

It was decided to inject the particles into the system after the system was filled with water and the onset of flow had begun from natural circulation. They would be injected at a rate that would match the rate of coolant flow in such a way that the injection of particles would stop as soon as the coolant inventory had turned over one time past the injection point. To that end, an injection port was drilled and tapped into the SS elbow between the lower manifold and the Magmeter. Into this hole a small SS tube with a 90° bend was installed via a compression fitting. A quarter turn ball valve was then attached to the tubing on the other side of the fitting. This tube is centered on the main flow axis and points in the direction of flow (see Figure 28 below).

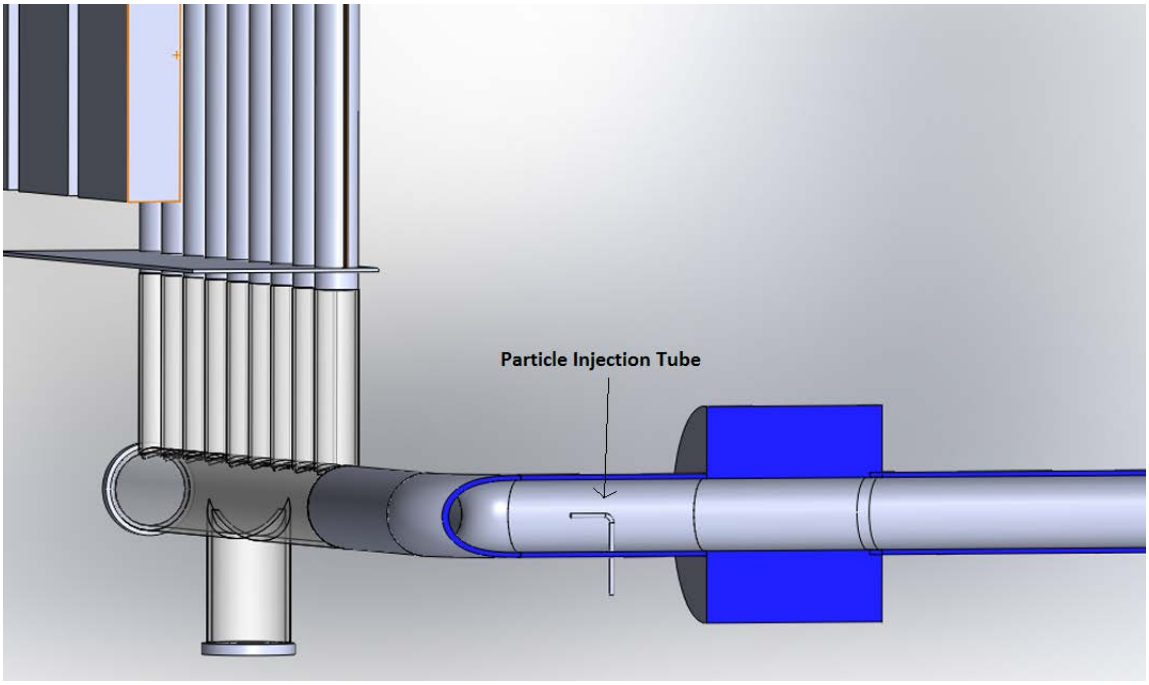


**Figure 28.** Particle Injection Port before the Test Section Inlet

Once the injection port was in place, an injection system had to devised, and consists of the following. An injection device using syringes, known as the Harvard Apparatus, was found at the University Science Building (USB). It has a plate attached to a threaded rod. When the rod is spun by a gear drive attached to a small electric motor, the plate moves and pushes simultaneously on as many as nine syringes of 60 mL capacity, which are full a solution containing the particles. The outputs of each syringe were initially merged together using a cascading series of 3-way plastic fittings, ultimately bringing 8 syringes down to a single output that goes the injection port via a ¼" (6 mm) plastic tube (see Figure 29 next page).

It was found over time that this was unnecessarily complex and subject to plugging, so eventually the cascading series of 3-way splitters was replaced with a single brass manifold for pneumatic systems (Clippard model MAN-12), and a total of 3 syringes were used instead of 8 (see Figure 30 next page).

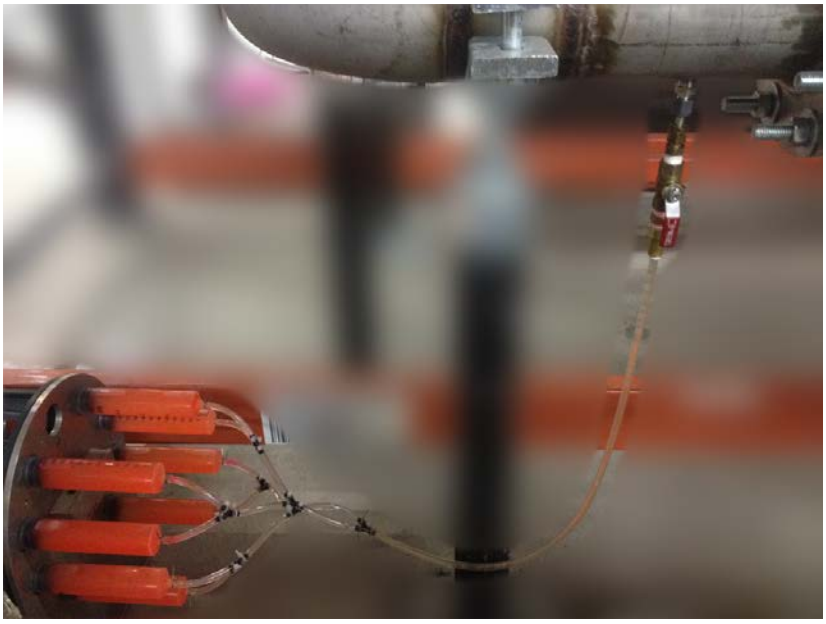

**Figure 29.** Original Setup of Particle Injection System w/ Cascading Outputs

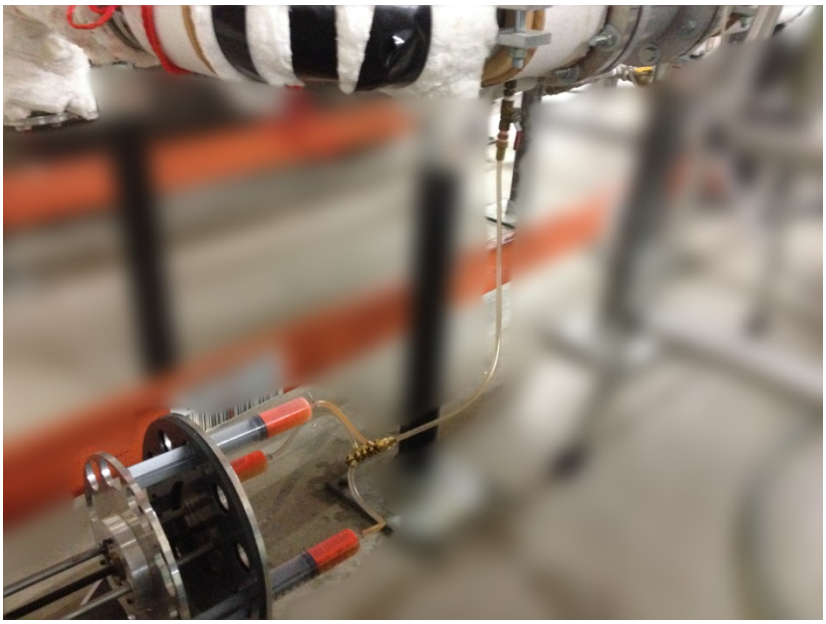

**Figure 30.** Final Setup of Particle Injection System w/ Brass Manifold

Details on the selection criteria for the particles themselves and procedures of the injection process are covered in the next Chapter.

# CHAPTER III
# OPTIMIZATION AND POST PROCESSING OF MEASUREMENT TECHNIQUES USED TO ANAYLYZE THE FLOW DISTRIBUTION

It was decided that the primary method to determine the flow distribution in the Cooling Panel would be to use an Ultrasonic Velocity Profiler on loan from the University of Idaho to determine the flow velocity along the centerline in each riser. The flow distribution would then be known if it is assumed that the cross sectional profiles are similar enough to where the relative velocities would be the same as the relative flowrates. UVP is a relatively obscure measurement technique, not widely used outside of specialized applications with liquid metals, opaque substances etc. in laboratories, so some effort has to be made in adapting it to each particular application.

In addition, it was noted that the opportunity existed to incorporate a few PIV type measurements as well, though these were not done in the traditional process using a laser and high speed cameras, but rather with blacklights and camcorders. The author did not intend to do a thorough survey using PIV, so those results are rather a supplement to the primary data which is from the UVP.

In both cases, proper setup, measurement technique, and post-processing are key, and it would be very difficult for other researchers to evaluate the validity of the results presented in the next chapter without knowing the details of how were obtained. To that end, the rest of this chapter is dedicated to chronicling all of these details.

## III.1 Ultrasonic Velocity Profiling

### III.1.1 UVP Principle of Operation

Courtesy of Dr. Akira Tokuhiro of UI, Texas A&M University received a Met-Flow UVP-DUO measurement system, along with 6 High Temperature US transducers rated for 150 °C and 2 standard transducers rated for 60 °C (see Figure 31 below [11]).

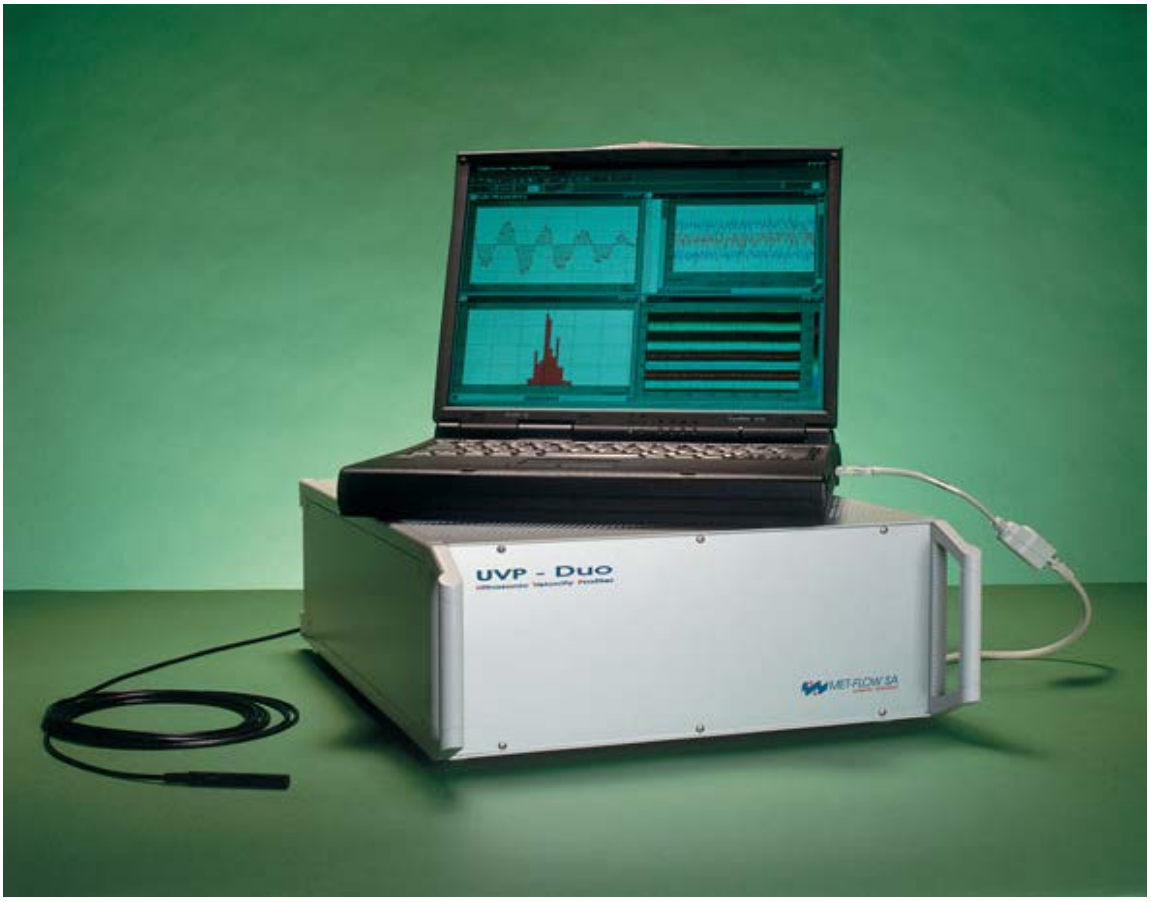

**Figure 31.** UVP-DUO System from Met-Flow SA [11]

UVP works off of the principle of Pulse-Doppler: the DUO emits an US wave via the transducer (the Pulse) then the wave reflects off of a moving object and returns to the transducer with a slightly different frequency caused by the Doppler shift. The distance between the object and the transducer can be calculated from the time between emission and return of the wave, if the wave speed of propagation in the medium is known. The moving object's velocity is given from the Doppler induced frequency shift. Typically not the entire wave is reflected by a single object, some of it continues to travel further and can hit other objects; separate echoes are received from each one of them. In this way, the velocity and distance information of several objects along the line of sight of the transducer can be measured [11].

It should now be noted that UVP does not work by reading the fluid velocity directly, rather it reads the velocity of solid particles or tiny gas bubbles entrained in the fluid stream and moving along with it. For this reason, it is absolutely critical to select these acoustic reflector particles with a proper size and density so that they faithfully follow the movement of the fluid itself. At the same time, it is equally critical that their size, sonic impedance (affected by density) and concentration in the fluid is large enough to get a strong signal to noise ratio. Effectively particle size and material, along with how many are injected and in what manner they are injected, will have a profound effect on how effective the system is.

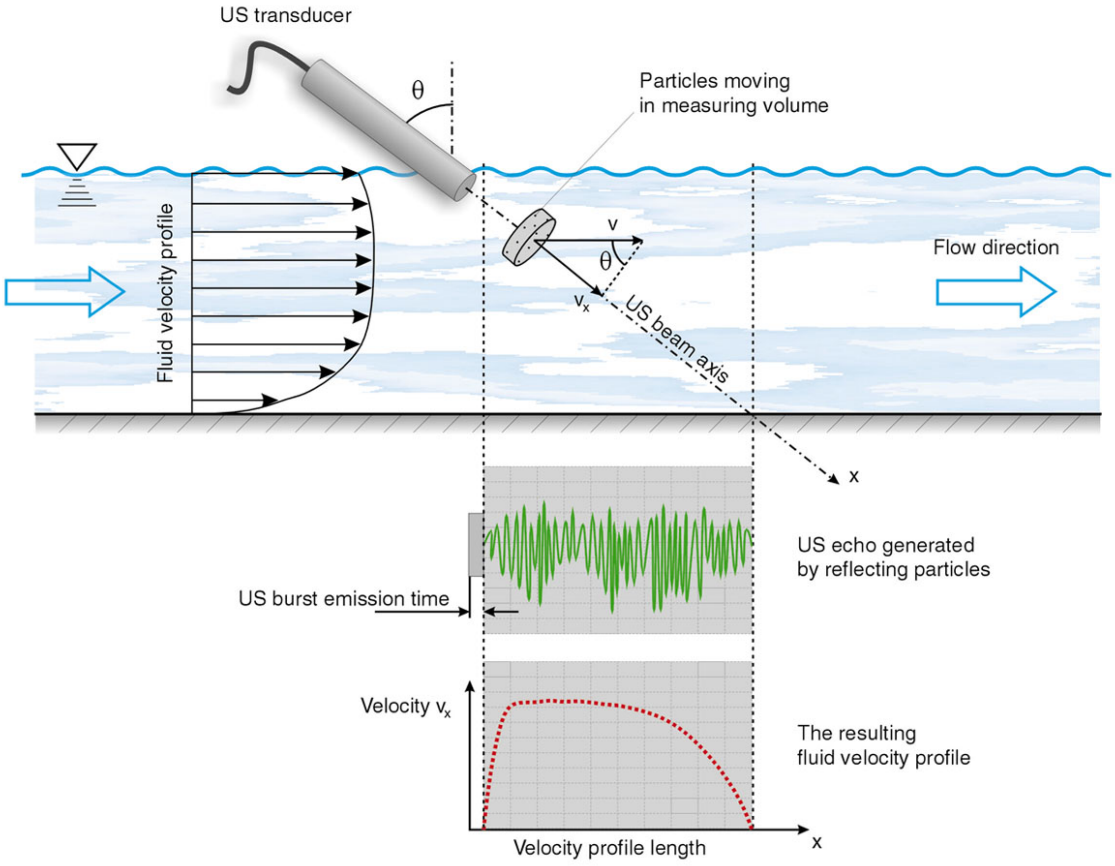


**Figure 32.** UVP Principle of Operation and Typical Application [11]

## III.1.2 Application of UVP to Measuring Relative Flowrates in the Cooling Panel

### *III.1.2.1 Physical Orientation in the Cooling Panel*

As noted in Figure 32 on the previous page [11], the intended or at least typical purpose of UVP is to obtain a Velocity Profile of the fluid, or how the velocity magnitude varies along a line normal to the flow. The purpose for this research is different; namely to determine the flowrate in the riser. Taking a profile across a line normal to the flow path could suit this purpose, but unfortunately a provision to mount the transducers in the glass riser tubes of the manifolds or in the steel risers of the Cooling Panel did not exist in the original RCCS design. After considering how difficult it would be to create transducer mounts in these areas, because of excessive heat, available space, and the level of craftsmanship and expense that would be required, no pursuit was made to mount the transducers in such a way.

As previously mentioned, it was decided to emulate what had previously been done at UW; to mount the transducer probe facing down the centerline of the riser, essentially reading the peak velocity of the flow (assuming a normal fully developed profile). This velocity should theoretically be constant down the centerline, based on the conservation of mass of an incompressible fluid and again assuming a fully developed flow profile. As mentioned in the previous chapter, mounts for the transducers were attached to the manifold as shown in the Figure 33 below.

**Figure 33**. Mounting of the US Transducers in the Upper Manifold – Pointing Down the Axial Centerlines of the Cooling Panel Risers

Preliminary results did not yield the expected profile shape mentioned in the previous paragraph and illustrated in Figure 34 below; rather the velocity profiles looked extremely jagged once the signal was in the 2” (50 mm) riser tube. There appeared to be locations where the velocity went to an extremely low value; even down to zero in some places for some profiles. From continuity this is obviously an incorrect result. It was confirmed by placing straight rods down the transducer port in the manifold that the sound wave or pulse should not encounter a stationary object such as a pipe wall at the distances in question, so the result was very confusing. See Figure 35 below for the graph of an actual profile measurement. Note the dip in velocity or ‘null’ point just before 150 mm distance from the transducer.

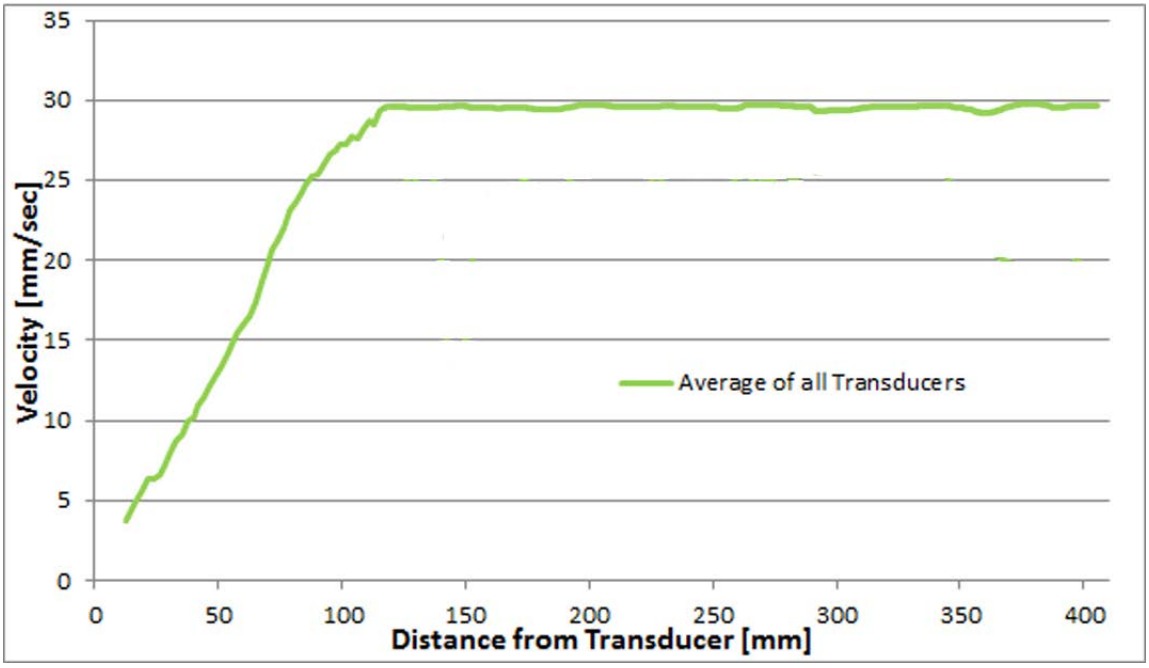


**Figure 34.** Expected Velocity Profile

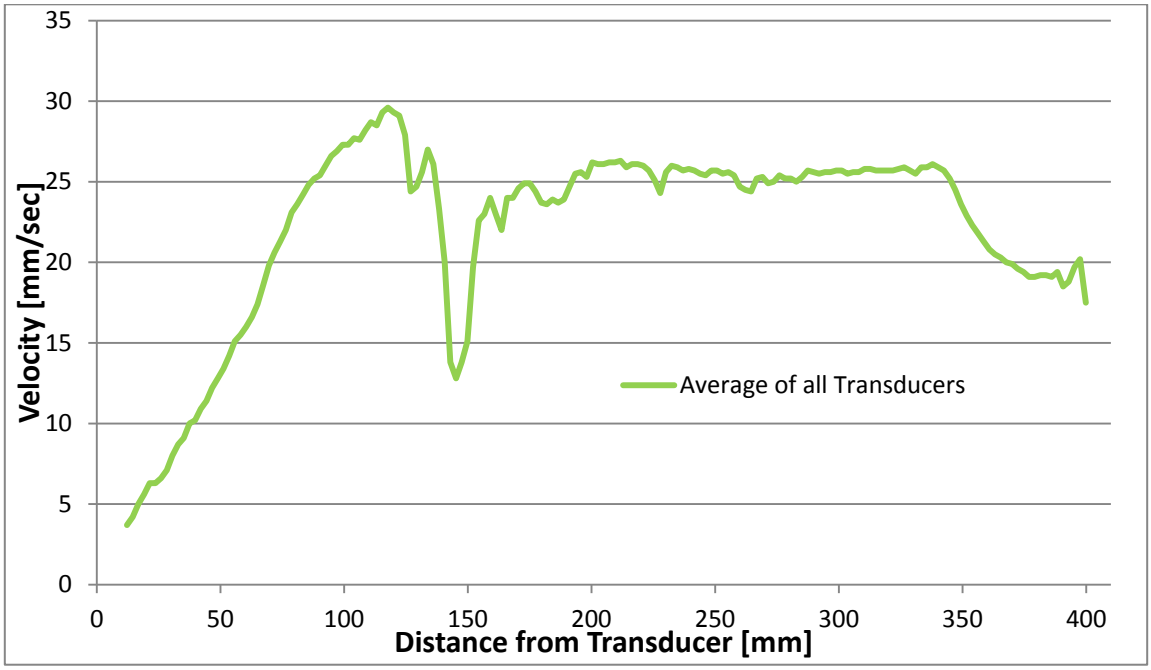


**Figure 35.** Actual Velocity Profile (average of 6 transducers)

In practice, it cannot be assumed beforehand that the flow is ‘fully developed’ as there is a varying heat flux profile across the steel riser just before the flow enters the 2” (50 mm) glass tube of the manifold. This can affect the development of the velocity profile. It is not likely, however, that this heating of the fluid explains the ‘null points’ in the profiles seen in Figure 35. It was initially thought that possible sources of error were the parameter settings of the UVP-DUO or geometric misalignments between the transducer, the glass riser tube, and the steel riser in the Cooling Panel. As will be seen in the next subsection, each editable parameter of the DUO system was adjusted in order to try and obtain a profile with a more expected shape, and in this process it was discovered that changing the ‘Max Distance’ parameter affected location of the ‘null’ point. An example of this phenomenon can be seen in Figure 36 on the next page.

This parameter directly alters the Pulse Repetition Frequency, which by definition alters the timing between the emissions of pulses. What is believed to be happening is that when the US pulse, which is a sound wave, is emitted it encounters the reflected wave of the previously emitted US pulse at some point in its path of travel. If the sound waves meet at a point in space where they are out of phase, then from wave theory they will cancel each other out. Changing the PRF would change the location of this point in space. As previously mentioned this is exactly what was observed, so there is not a point in the flow path where the fluid (i.e. the particles) slow down, it is in fact destructive interference from previously emitted pulses. Geometric issues and misalignments could be causing the signals to reflect back prematurely, but unfortunately there is no way to resolve those issues without making new glass manifolds with tighter tolerances.

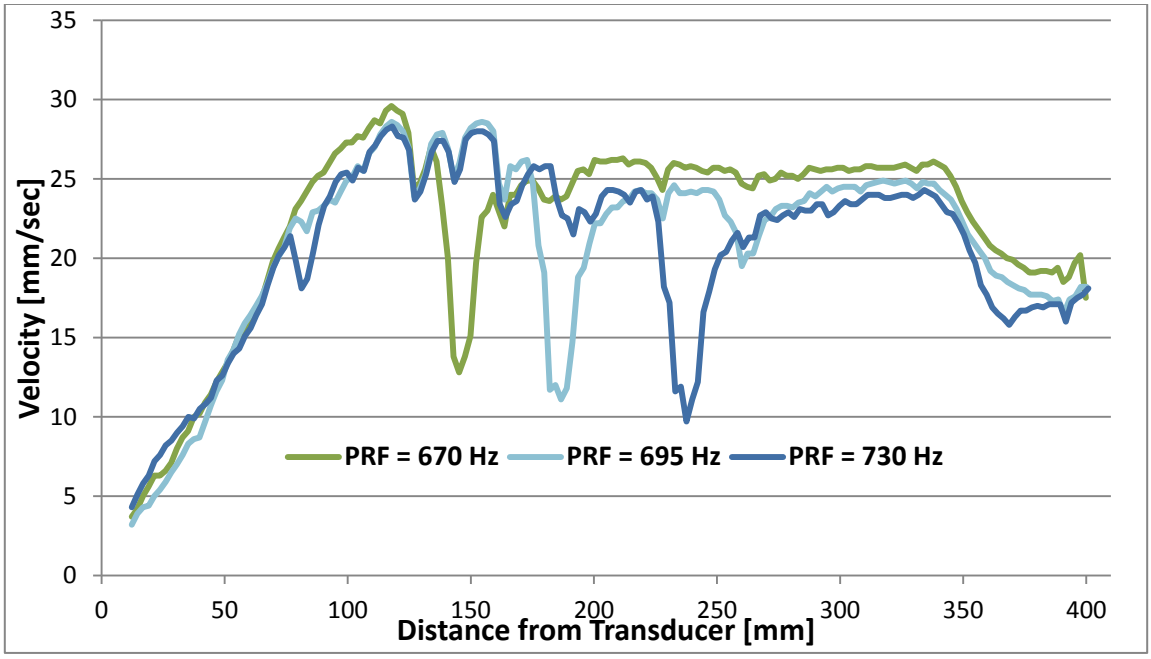


**Figure 36.** Movement of 'Null' Points with Alteration of PRF (Max Distance)

*III.1.2.2 UVP-DUO Parameter Optimization*

The UVP-DUO machine has several parameters to be optimized for a given application. These include:

1. Transducer Voltage
2. # of Cycles Emitted per Pulse (i.e Pulse Width)
3. # Repetitions per Profile
4. Channel Width and the Number of Channels
5. Start Gain and End Gain
6. Noise Filter
7. Maximum Distance (i.e. Pulse Repetition Frequency (PRF)
8. # of Profiles per Transducer per Measurement Cycle and # of Cycles

All settings used in the experiments and the rationale for them will be covered quickly in the following subsections.

#### III.1.2.2.1 Transducer Voltage

Transducer Voltage affects the amplitude or energy of the emitted wave. Because it is the previously emitted wave that is believed to cause the destructive interference, and wave amplitude decreases the longer it travels due to absorption of energy, it is logical to assume that if the initial wave has a lower amplitude then it may be too small to cause a significant interference effect with the current signal when they do meet. The DUO gives options for 30, 60, 90 and 150 volts. The 30 and 60 V cases did not have enough energy to work in the water at all; and there was not really much noticeable difference between the 90 and 150 V settings. Adhering to the logic above though, it was decided to stick with the minimum required so 90 V was selected for all experiments.

#### III.1.2.2.2 Start Gain and End Gain

In a similar manner, the gain can be adjusted to amplify the received echo signals. Altering these parameters had no significant positive effect on the shape of the resulting profiles, so they were left at default settings. This makes sense because if the previous echo and current arrive at the same point in space and cancel each other; it is this resultant signal that is picked up by the transducer, so it doesn't matter if it is amplified more or less.

#### III.1.2.2.3 Noise Filter

A noise filtering function is present on the DUO and is alterable from 1 to 9 with a default of 4. Noise, however, was apparently not the problem as altering this value had little effect on the results, so it was left at the default setting.

III.1.2.2.4 # of Cycles Emitted per Pulse (i.e. Pulse Width)

This parameter affects the Pulse Width; in typical SONAR or RADAR applications that is what this parameter would be referred to as. Increasing this parameter does two things: it puts more energy on target since more cycles of the wave are sent, which is typically desirable, but this is done at the expense of decreased spatial resolution. Spatial resolution, however, is not necessary in this application, so it was decided to increase it from the default value of 4 cycles/pulse to 16 cycles/pulse. It was also thought that a wider space would effectively cause some built in averaging or smoothing of the profile. Ultimately, however, changing this parameter did not significantly improve the shape of the profiles.

III.1.2.2.5 Channel Width and the # of Channels

The velocity profile is actually a series of cells or channels of finite width and regular spacing which are both selectable by the user (see Figure 37 for an illustration [11]). The Channel Width was set equal to the Pulse Width, and the distance to the start channel, the end channel, and the number of channels was selected so that the end of one channel was the beginning of another. This would ensure velocity information was obtained at all points in space in the profile, without any overlap.

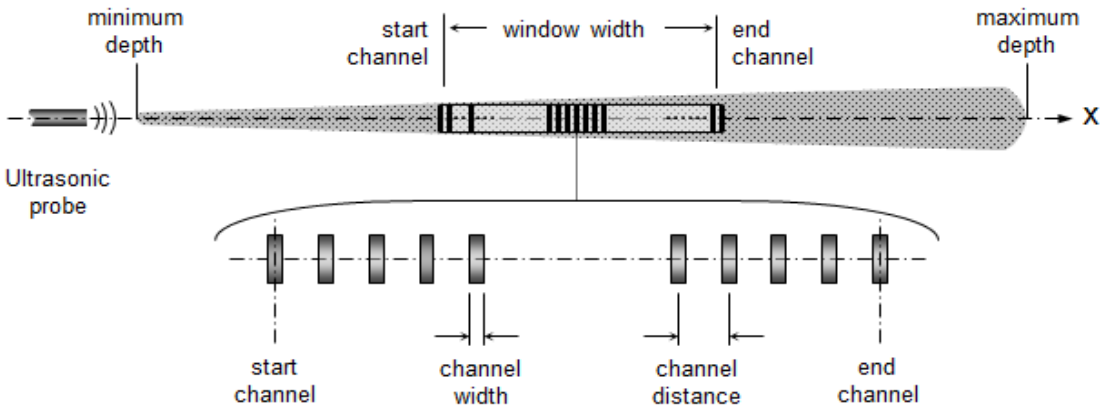


**Figure 37**. Illustration of Channel Settings for the UVP-DUO System [11]

III.1.2.2.6 # Repetitions per Profile (i.e. # of Pulses averaged to make a single profile)

Preliminary testing showed that this parameter has a strong effect on the Amplitude of the reported velocities at all points in the profile. In general, the more repetitions that were averaged higher velocities were reported across the entire profile. Changing it did not affect profile shape or the interference points however. See Figure 38 for a comparison of three different settings.

During this test, the reading of the system flowrate as read by the magmeter dropped out, but it is estimated based on the heater power level used that the flowrate was 28 LPM. At this volumetric flowrate, the combined average cross sectional velocity of the flow through each riser would have been 25.6 mm/sec. Analysis of the three profiles shown in Figure 38 show that the peak values of the signals are 21.9, 18.3 and 8.9 mm/sec corresponding to # Repetitions per Profile of 1024, 256, and 128, respectively. This strongly indicates that the data from the profiles with a higher # of repetitions would be more accurate and applicable for the purposes of this study. This parameter was ultimately set to 2048 Repetitions per Profile.

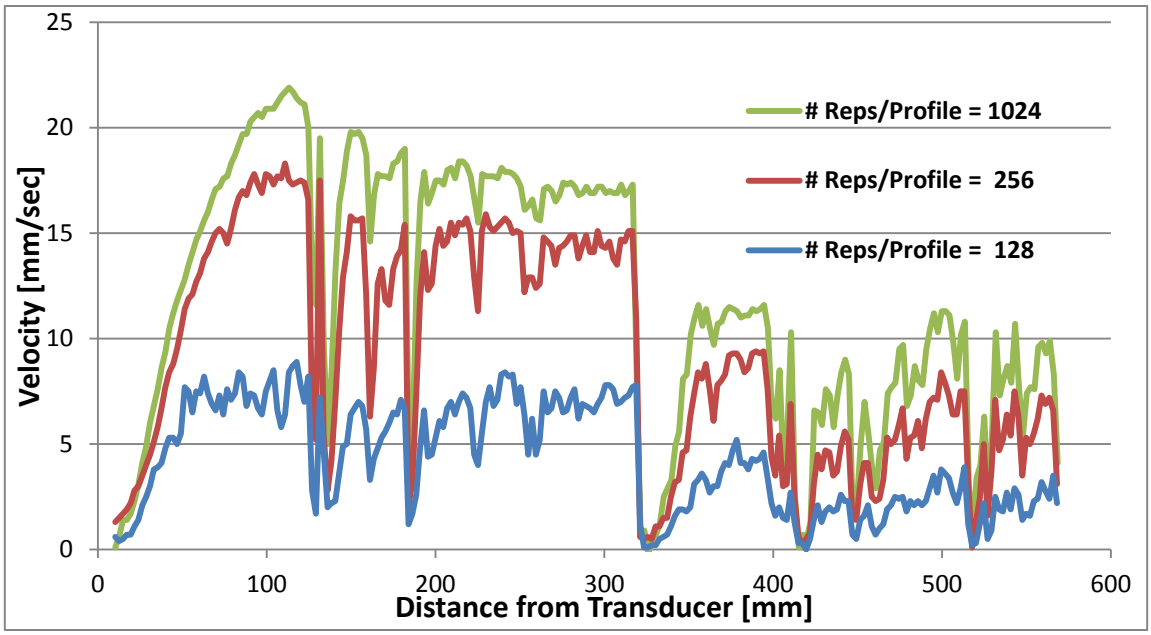


**Figure 38.** Effect of Varying the # Repetitions per Profile Parameter

The primary reason this parameter affects the magnitude is that a Doppler-shifted echo burst from a certain channel is generally much shorter than the time corresponding to the required frequency measurement. Therefore it is necessary to obtain the required information by analysis of several echoes resulting from several repeated US pulses.

Finally, increasing this parameter limits the maximum number of channels that can be processed, which is one reason that the Pulse Width and Channel Width were left at high values to limit the number of channels. When raised this high, it also affects the total length of time it take to process a profile, affecting the timing to go from one transducer to another. The DUO does not pulse each transducer simultaneously, rather it is a sequential operation and is affected by this dwell time.

III.1.2.2.7 Maximum Distance (i.e. Pulse Repetition Frequency (PRF))

Experiments were conducted on several separate occasions to find the PRF setting that most reduced or eliminated the interference effects observed, but no single setting was found that would eliminate them from the profile completely. The range of settings tested was from about 648 Hz to as high as 1.350 kHz, in increments as small as 25 Hz. It was observed that the lower frequencies gave higher reported velocities than the higher frequencies; the exact reason for this is unknown (see Figure 39). The PRF does affect the Velocity Resolution, or the smallest difference in velocity that can be read, but this does not explain the effect observed.

In the particular example shown in the figure, the Peak value of the 670 Hz profile was 29.6 mm/sec, which is only -2.4% below the average cross sectional velocity value for all pipes: 30.33 mm/sec. In contrast, the peak of the roughly harmonic signal at a PRF of 1350 Hz was only 25.7 mm/sec, which is -14.76% below the average cross sectional velocity at that time: 30.15 mm/sec. Thus, the lower PRFs were favored as candidates for the final setting. 675 Hz, or 1145 mm Maximum Depth, was used for all of the experiments because it produced profiles with velocities reported the closest to the expected range and had the least amount of inference patterns.

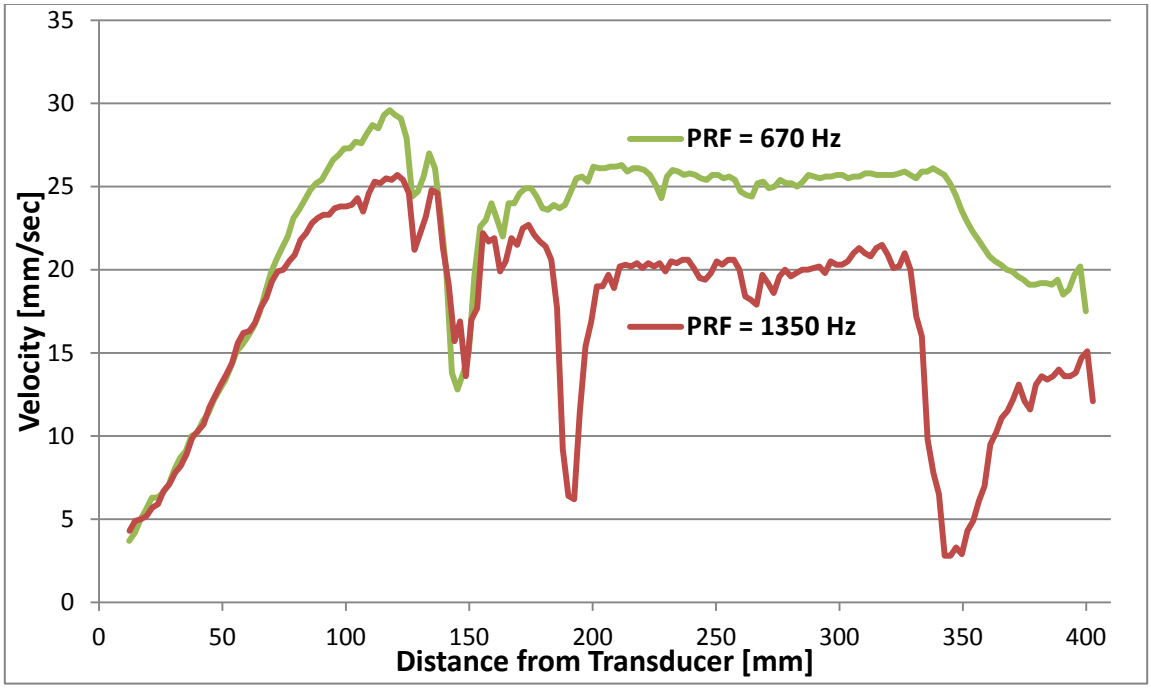


**Figure 39.** Effect of Varying the Maximum Distance (PRF) Parameter

III.1.2.2.8 # of Profiles per Transducer per Cycle / # of Cycles

All of the previous settings directly affect the profile generated by a single transducer. In order to measure the flow distribution however, the DUO would need to obtain profiles from 6 transducers. As mentioned previously, the DUO obtains a profile from 1 transducer at a time sequentially. The act of obtaining a single measurement from every transducer is referred to as a single measurement cycle. The Multiplexor parameters of the DUO allow the user to vary time delays between switching to the next transducer and the number of measurement cycles to perform in total. It was desired to obtain multiple profiles for each riser in case there were errors during any single measurement and to average results.

In addition, as will be seen in the next chapter, there is a sinusoidal oscillation in the system flow rate under most test conditions. It was desired that the entire measurement process occur over a multiple of this Oscillation Period, and that measurements be equally spaced among transducers so that any possible effects of the

oscillation could be cancelled out. For example, some profiles may be taken when the system flowrate is at a peak and others during a trough, so if multiple profiles are obtained at different points during the oscillation those effects can be averaged out.

For the 6 kW input power as used in most of the measurements, the system flowrate oscillation period was approximately 150 seconds. With the multiplexor set to take 1 profile per transducer per cycle and 8 cycles total, with no additional delays between transducers or cycles, it takes about 300 seconds to complete the entire measurement cycle. This corresponds to 2 complete flow oscillation periods, and these were the settings used for all experiments in this report. Please refer to Figure 40 for an illustration of how the 8 measurements were spaced for each transducer during a complete measurement cycle. The system flowrate is superimposed on the measurements for clarity of the concept just discussed. Please note that each and every measured velocity profile shown for a single riser after this point is actually the average of the 8 individual profiles taken during the entire measurement cycle.

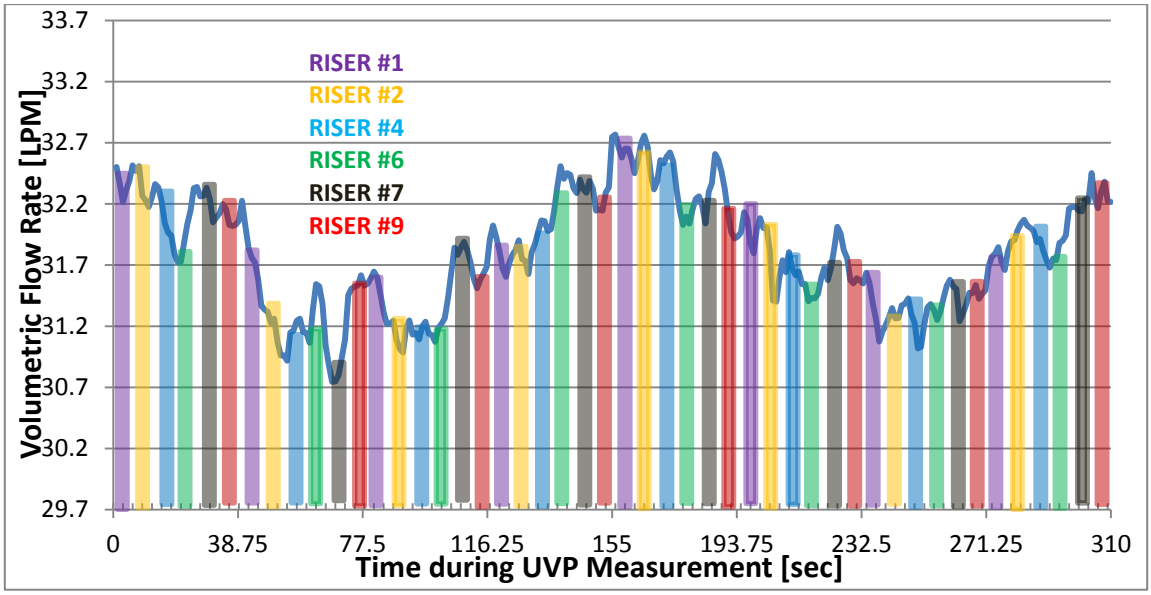


**Figure 40**. Timing of Individual UVP Profile Measurements during a complete Measurement Cycle – Superimposed on the System Flowrate

To summarize, the settings used for measurements are given in Table 1 and Table 2 below.

**Table 1**. UVP-DUO Settings for Individual Transducers

| Parameter | Setting | Units |
|---|---|---|
| Transducer Voltage | 90 | V |
| # of Cycles/Pulse<br>(Channel Width, *nominal*) | 16<br>(3) | <br>(mm) |
| # of Repetitions / Profile | 2048 | |
| # of Channels | 96 | |
| Window Start (*nominal*) | 12 | mm |
| Window End (*nominal*) | 300 | mm |
| Start Gain | 4 | |
| End Gain | 8 | |
| Noise Filter | 4 | |
| Maximum Depth (*nominal*) | 1145 | mm |

**Table 2.** UVP-DUO Multiplexor Parameters

| Parameter | Value | Units |
|---|---|---|
| # Profiles per Transducer Per Cycle | 1 | |
| Switching Delay within Cycle<br>(for all transducers) | 0 | msec |
| # of Cycles | 8 | |
| Delay between Cycles | 0 | msec |

In addition, the Speed of Sound was updated for each new set of measurements taken at the next temperature (typically every 5 °C). This was done manually by referencing a lookup table of speed of sound in water versus temperature.

*III.1.2.3 Determination of the 'Reference Velocity'*

As stated previously in this chapter, the plan was to compare the centerline flow velocities between risers in order to ascertain the flow distribution. To repeat, if it is assumed that there is a fully developed laminar flow profile in every riser, and that the US transducer is aligned with the axial centerline of the riser, then the velocity the DUO reads should be the maximum velocity in the riser. It further follows that the ratios of the maximum velocities in each riser should be the same as the ratios of the volumetric flowrates in each riser. Further, the average velocity would be 2/3 the maximum velocity, and of course the average velocities would yield the volumetric flowrates directly since the cross-sectional area is known.

There are several problems with this approach, however. The velocity profile cannot be assumed to fit the textbook shape since a face of the riser is being heated, so it is not an isothermal boundary. Secondly, due to geometric errors in the orthogonality of the transducer mounts and the glass risers, the US beam cannot be assumed to lie perfectly in the axial centerline. Finally, it has already been observed that the profile does not fit the expected shape, due to irregularities from wave interference effects. Still, it is necessary to determine a single metric with which to compare the flow magnitude in each riser from the information available in the velocity profiles.

Our solution comes from recalling in that the peak of the 670 Hz PRF velocity profile shown in Figure 39 had a value of 29.6 mm/sec. This is significant because the average system flowrate as read by the magmeter was 33.2 LPM during that time, which if divided by the total cross-sectional area of all 9 riser tubes yields an average riser flow velocity of 30.33 mm/sec, a difference of only 2.4%. Also note that the profile shown in Figure 39 was the average of the profiles from all six transducers in the panel at that time. *So it was observed that the average peak velocity recorded in the profile roughly corresponded to the average flow velocity in the Cooling Panel.*

We can observe that, in fact, in each individual riser profile there is typically a peak that occurs in this same general area; before the first major 'null' point caused by wave interference. Except for the first two risers closest to the inlet, this peak is distinct

and repeatable throughout all experiments. Since this peak seems to have a magnitude that corresponds to the expected average velocity in the riser and is typically distinct and repeatable, it was decided to utilize the maximum value of this peak before the first 'null' point (but still within the boundary of the 2" (50 mm) riser tube) as the metric that will be used to compare the flow distribution between risers. This metric will henceforth be referred to as the Reference Velocity for that profile.

In order to capture this peak value, the profiles were loaded into Microsoft Excel, and a search algorithm implemented to find the peak given within the limits of a search window. All search windows were set to a width of 25 mm, and were placed within each riser in order to provide the highest probability of capturing the peak within that riser. An illustration of a typical profile with the search window limits for each riser is shown in Figures 41 through 48 below. Recall the risers are numbered 1 to 9 from the inlet at the cold leg bottom manifold to the outlet at the hot leg upper manifold, and the 100 mm mark is the joint of the riser outlet to the 4" pipe of the upper manifold. All points past 100 mm are within the interior of the 2" (50 mm) glass riser tube of the upper manifold.

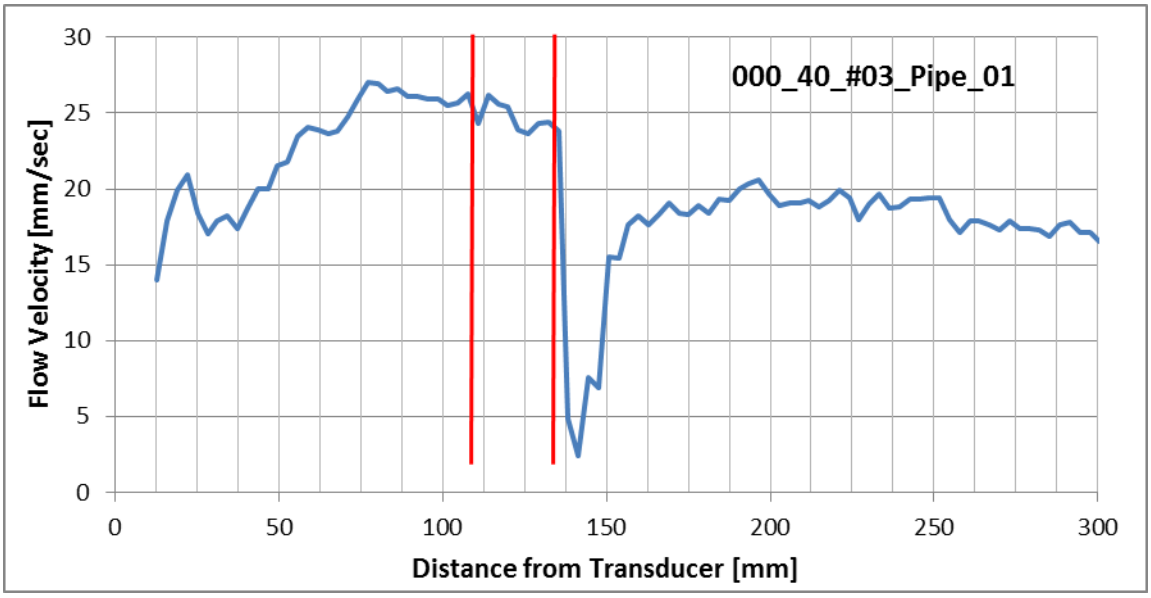


**Figure 41.** Typical Velocity Profile for Riser #1
with Search Window Limits for the Reference Velocity

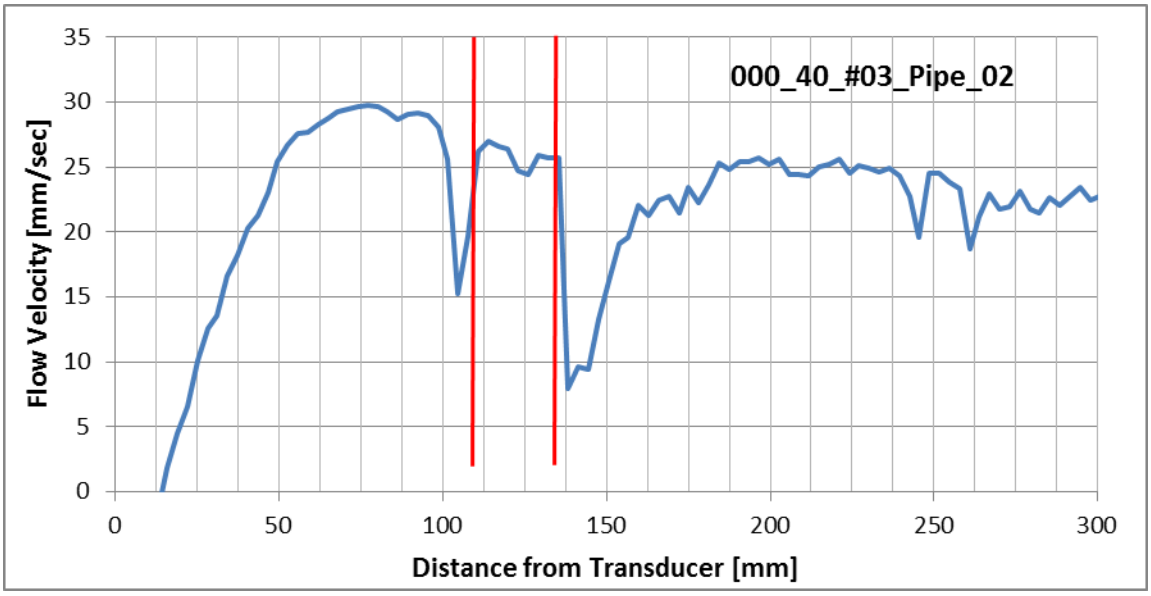


**Figure 42.** Typical Velocity Profile for Riser #2
with Search Window Limits for the Reference Velocity

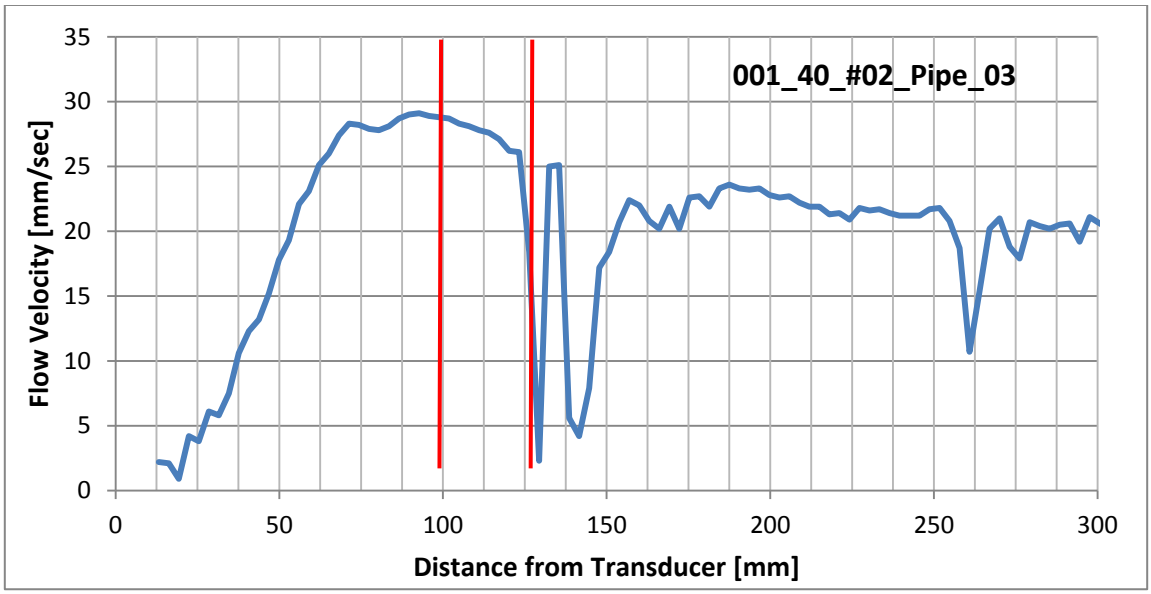


**Figure 43.** Typical Velocity Profile for Riser #3
with Search Window Limits for the Reference Velocity

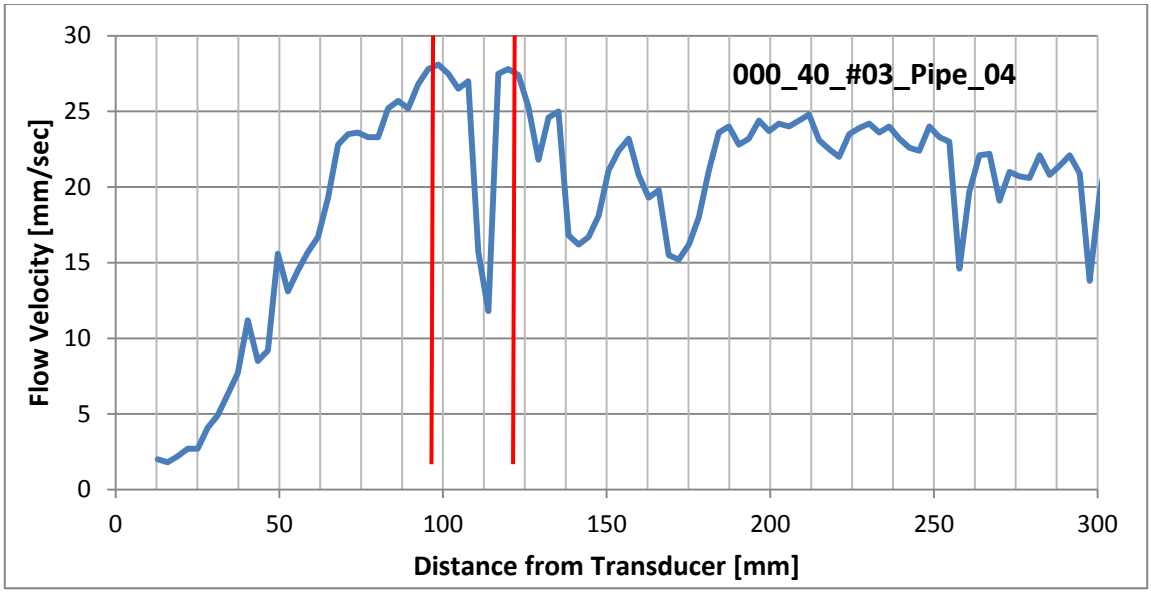


**Figure 44.** Typical Velocity Profile for Riser #4
with Search Window Limits for the Reference Velocity

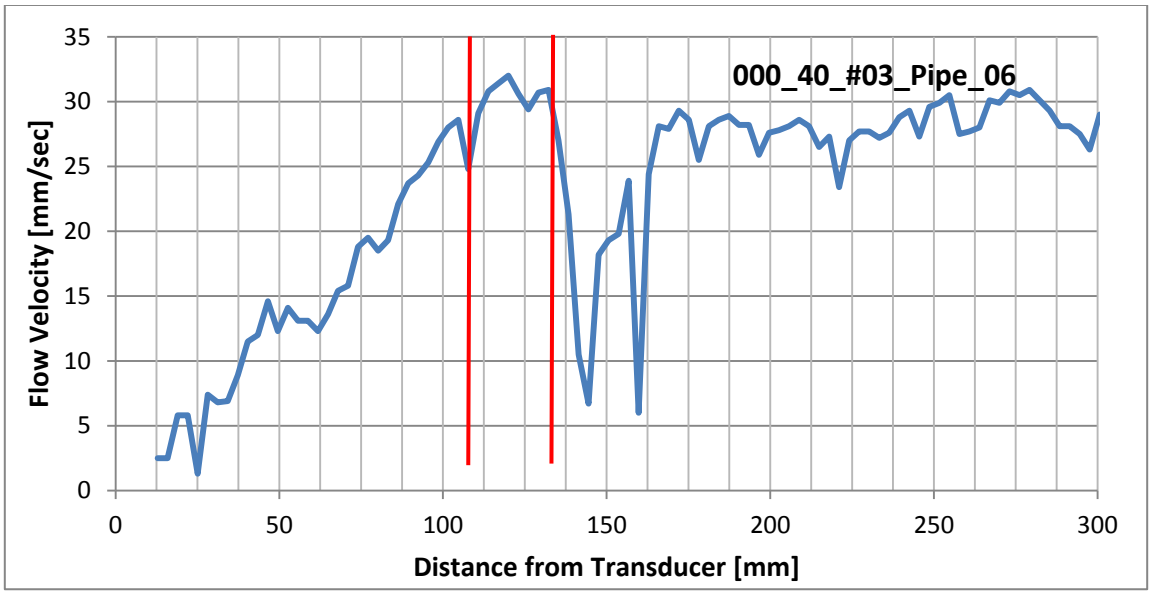


**Figure 45.** Typical Velocity Profile for Riser #6
with Search Window Limits for the Reference Velocity

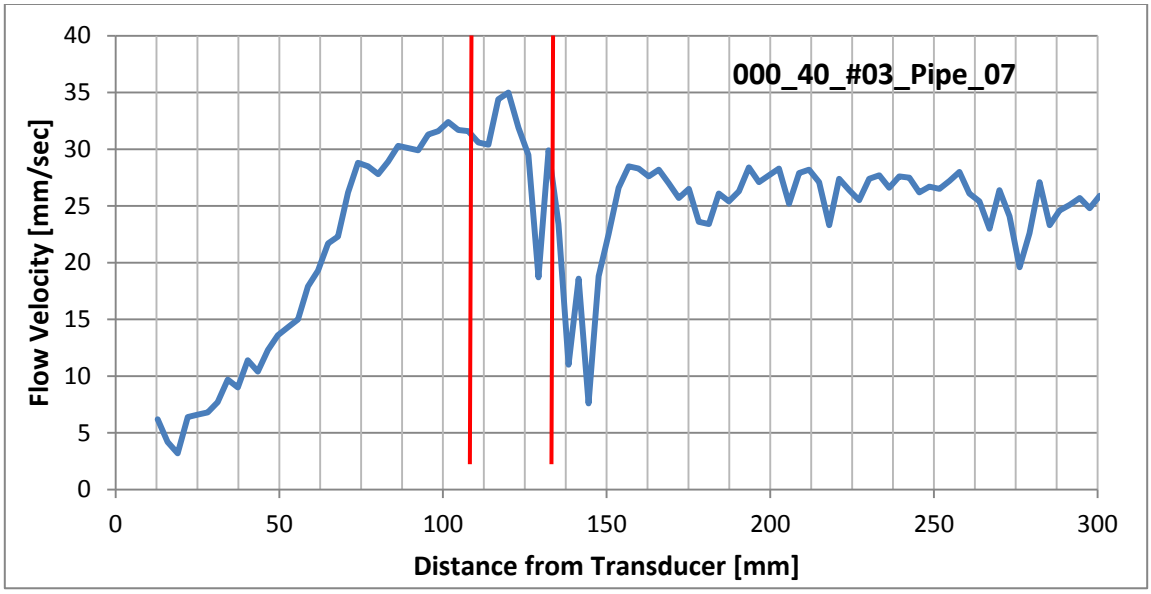


**Figure 46.** Typical Velocity Profile for Riser #7
with Search Window Limits for the Reference Velocity

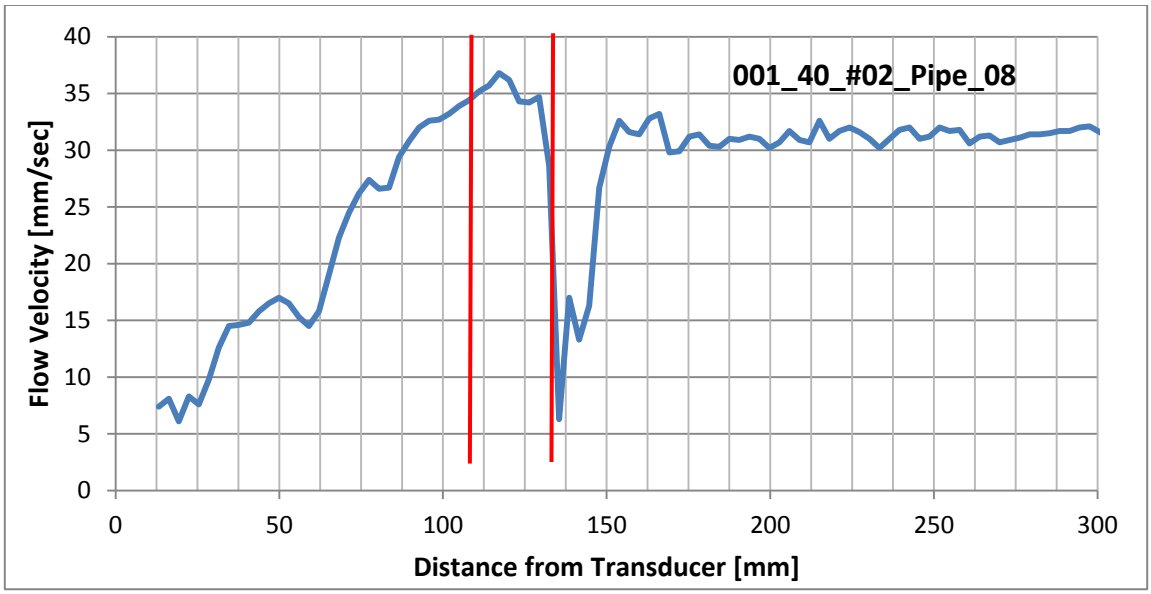


**Figure 47.** Typical Velocity Profile for Riser #8
with Search Window Limits for the Reference Velocity

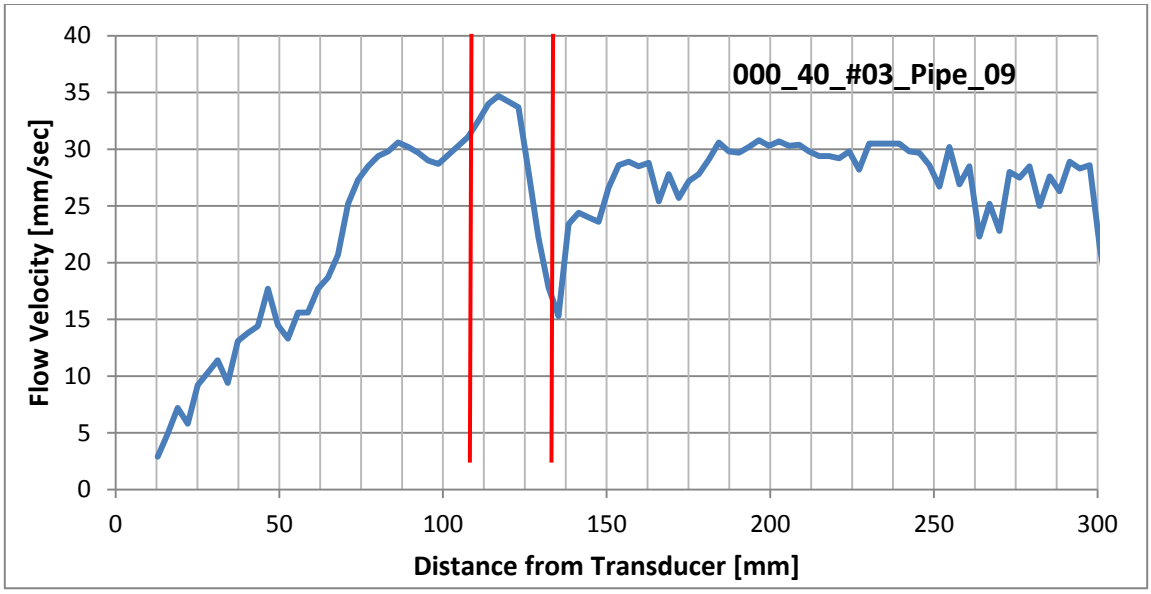


**Figure 48.** Typical Velocity Profile for Riser #9
with Search Window Limits for the Reference Velocity

A summary of all window limits is in Table 3 below.

**Table 3.** Reference Velocity Search Window Limits for each Riser

| | Low Limit | High Limit | Notes |
|---|---|---|---|
| Riser 1 | 110 | 135 | Peak is to the Left |
| Riser 2 | 110 | 135 | Peak is to the Left |
| Riser 3 | 100 | 125 | |
| Riser 4 | 95 | 120 | |
| Riser 5 | n/a | n/a | |
| Riser 6 | 110 | 135 | |
| Riser 7 | 110 | 135 | |
| Riser 8 | 110 | 135 | |
| Riser 9 | 110 | 135 | |

Note from the Table and the Figures that the limits for pipes 6, 7, 8 and 9 are all the same and adequately capture the velocity peaks. Risers 3 and 4 are observed to have the limits set to lower values, corresponding to the exit of the riser or slightly past it.

This is because their peaks seem to consistently occur a little earlier than for the outlet risers. The same is true for risers 1 and 2, but in this case the lower limit was set to the value used for risers 6 through 9 for two reasons: first the peak is sometimes well within the main body of flow of the 4" (100 mm) manifold, not even remotely within the riser itself; second the velocity values for 1 and 2 would sometimes be higher than in 3 or 4 if using the peak values from 100 to 110 mm (from the tail of the peak in the manifold). From visual observation and PIV studies this result is believed to be erroneous, so the lower limits were set to 110 mm in order to obtain more expected results.

#### *III.1.2.4 Acoustic Reflector Particles*

This subsection will discuss what type of reflective particles were used, how they were selected, determining the optimal concentration and detailing the method of introducing them into the system.

##### III.1.2.4.1 Particle Selection

In order to get a good reflection, the particles' diameter should be at least ¼ of the wavelength of the emitted US wave. The US transducers use a frequency of 4 MHz, meaning the particles should have a minimum diameter of 93 μm based on a sound speed of 1490 m/s. For the consideration of moving faithfully with the flow, the particles should have as little mass and therefore be as small as possible, so 93 μm was set as the target diameter. In addition, the density of the particles should match that of the water so that they neither settle out nor float out of the fluid due to buoyancy forces. Finally, reflected signal strength is also directly affected by the speed of sound through the material that the particles are made of, since this is a direct indicator of the material's acoustic impedance. If you have two materials with different sound propagation speeds then they will also have proportionally different acoustic impedances, and a reflection will be created at their interface if encountered by a wave. As compared to the water, a material with a relatively similar acoustic impedance will require a higher concentration

of particles to be dispersed in the coolant than a material than has a more dissimilar acoustic impedance.

Several candidates listed in the UVP-DUO manual [11] and used in previous similar research endeavors were considered, including:

- Sumimoto CL-2507
- Sekisui SBX-100
- Sekisui MBX-100
- Dow Chemical DOWEX™ 50WX4 (H+) 100-200 Mesh
- AkzoNobel Expancel 551 DU-40

Unfortunately none of these particles were sufficiently matched in density to meet the research requirements. This proved to the deciding factor, because in a natural convection system the flow velocities are so small there is plenty of time for the particles to float or settle out to the top or bottom of the pipe while traveling through horizontal sections. Buoyancy forces could also make them more likely to get trapped in the crevices around pipe junctions, and finally the readings would not be correct in the vertical riser section if they rise faster or slower than the fluid.

The solution came from the suggestion of a fellow lab worker, Saya Lee, in the form of polyethylene particles from Cospheric LLC in California. These particles can be ordered density matched to water at 20 °C and are available in a 100 um size. Additionally, the particles are fluorescent and can be readily used for PIV measurements (see Figure 49 below [12]). The next step was to conduct testing to determine the necessary concentration.

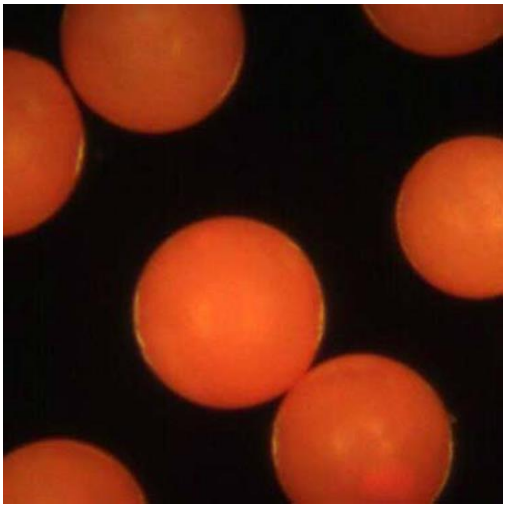

**Figure 49.** Closeup of Cospheric Microparticles (UVPMS-BO-1.00 90-106um) [12]

III.1.2.4.2 Optimization of Concentration

It was expected that as the particle concentration were increased the signal strength would rise, and accordingly the velocities would increase. It was also thought that this would occur until the concentration reached a saturation point; at which no further increase in concentration would yield increasing velocity measurements. An experiment was conducted to determine at what concentration this point would occur. This was done after the final determination for the DUO parameters was made, so the concentration is optimized for the settings listed in Table 1 and Table 2. After trying 5 different concentration levels, it was determined that 3 grams of particles in 400 liters of water or 7.5 [mg/L] was adequate to produce consistent results.

III.1.2.4.3 Injection into the System

This discussion would not be complete without mentioning the procedure by which the particles were introduced into the system. It was discovered upon first trying the Cospheric particles that they are in fact hydrophobic, and will merely float on the surface of the water when added dry. Upon calling the manufacturer, they advised that the particles must first be coated with a surfactant (soap) that will allow them to settle in

with the fluid. Accordingly, the particles were soaked in a pure solution of Simple Green, a common household/commercial detergent, before being added to the system.

As previously mentioned in subsection II.10.3, a port had been added to the SS elbow between the magmeter and Inlet Manifold wherein a small injection tube was placed in the centerline, opening facing the direction of flow. The Harvard Apparatus was used to simultaneously push on three 60 mL syringes that each had 1 gram of the Cospheric particles suspended in a solution of 10 mL of Simple Green and 50 mL of tap water, as depicted previously in Figure 30. The quantity of particles was adjusted during the experiments conducted with higher than normal tank levels in order to keep the concentration the same.

As previously mentioned in subsection II.10.3, it was decided that the best way to create an even concentration of particles in the coolant inventory was to inject the particles under flow, rather than simply dump them into the Coolant Storage Tank or similar alternatives. To that end, the particles would have to be injected at a rate that is constantly proportional to the flowrate in a manner that allows injection to cease at the same time the total coolant inventory has passed through the injection point.

Fortunately, as can be observed in Figure 50 below, the flow behavior of the system upon startup is that it very rapidly escalates to around 25 LPM shortly after the heaters are turned on, and stays close to this value for the first several minutes of operation. At this rate it would take about 16 min (400 L divided by 25 LPM) in order to turn over the entire system inventory once.

Just as fortunately, one of the injection speeds (gear #4) available on the Harvard Apparatus also takes about 16 minutes to complete, so as soon as flow at 25 LPM was read on the magmeter display, the injection device would be turned on. This procedure was modified slightly by selecting a different gear for the High Power (10 Series), Throttled (20/21 Series) and High Level (40 Series) experiments to accommodate the higher and lower flow rates seen immediately after startup and the alternate inventory levels.

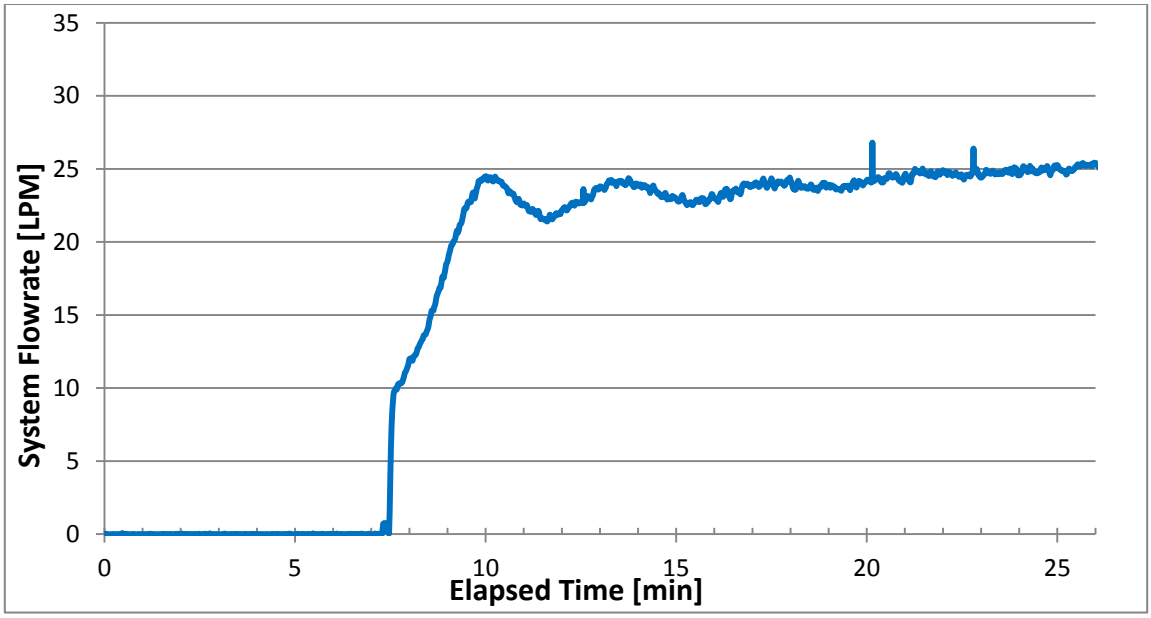

**Figure 50.** Typical System Flow Behavior during Particle Injection

At the end of each individual experiment, the entire system inventory was emptied through drain valves located at the system low points into nearby holding tanks. This was done to prevent the possibility of a LOCA occurring while no one was at the lab to clean it up. Not all of the particles drain out with the water, so the system was cleaned out by opening up one of the windows on the Storage Tank and the center port of the top manifold and a water hose was used to wash all the pipes down. The Cospheric particles are actually quite expensive, about $150 for 10 grams, so all water that was drained out of the system, both initially after experiment shutdown and during cleaning, was filtered using a #200 US Standard mesh SS sieve. During the last few experiments, collection rates approached 90%; so only 1 bottle of particles had to be used. After cleaning, the window and port cover were put back in place and testing could recommence the following day.

*III.1.2.5 Transducer Mounting Angle*

For completeness, one last source of error needs to be addressed: the mounting of the transducers. For the most part, any geometric misalignments in the system between the glass and steel risers and the transducer mounts are fixed. The holes bored in the upper manifold for the transducers to fit through, however, had been cut oversized, so there is a small amount of play in the pointing angle of the transducer. Since there is only an O-ring squeezed tightly against it that holds it in, the transducer can be pushed to one side or the other a small amount. Adjusting the angle of the transducer could potentially produce three separate effects of significance:

1. The reported profile velocities would change directly with the sine of the mounting angle. This effect would likely be insignificant however, since a 5° deviation only produces a 0.4% error when directly opposing the flow
2. The path of the US signal would hit the flow stream at a different point in its cross-sectional profile, therefore reading the a different velocity at that same distance (e.g. centerline velocity vs. at the wall)
3. The signal could hit the pipe wall at a different distance than before (if at all). This could alter the reflections produced in the riser and ultimately the wave interference patterns

During testing however, the amount of angular deviation that can be produced from pushing the transducer to one side or the other proved to be insignificant to the velocity profile results, so more intricate and repeatable ways to mount the transducer were not explored.

## III.2 Particle Image Velocimetry

### III.2.1 PIV Equipment Setup

The PIV test setup was as follows:

1. A high-definition digital camcorder was hung from a simple mount made of T-slot aluminum extrusion bars, placed far enough away such that the width of a single riser is in the camera's field of view. Camera settings did not seem to have significant effects, except the Low Light setting which was turned ON. It was setup to record in High Definition mode at 60 frames/second
2. Three 36" (91.5 cm) long blacklights, each with a single 25 W bulb, were laid adjacent to the upper manifold to provide illumination and induce fluorescence of the Cospheric particles. The illumination was continuous and was not spatially altered, such that it illuminated the entire volume of the riser tube.
3. A heavy, thick black cloth was hung around all six sides of the area around the upper manifold and camera in order to shield out all ambient light

### III.2.2 PIV Video Decomposition and Image Enhancements

Recordings were made sequentially, from riser to riser, and video was typically shot for about 30 seconds. From this, a continuous 25 second clip of film was selected that was free of camera shake for decomposing into an image sequence of .jpg files. This was done using a generic conversion program that was available free online. Curiously, it was noted that every other image was essentially identical to the previous image, such that the effective frame rate was only 30 frames per second. It appears that the 60 fps option is actually taking two images, or fields, every $1/30^{th}$ of a second, and the combination of the two fields creates a high fidelity image. Whatever the case, every other image was discarded, giving an effective frame rate of 30 frames per second. With 25 seconds of video, this yields 750 images per set for analysis.

The first step of post-processing for the images was to improve the visibility of the particles via the Autocontrast function of a program called XnView. From the enhanced image, the outer boundaries of the glass riser tubes were easier see, and the width of the image was cropped so that the left and rights boundaries of the image visually coincided with the boundaries of the riser. Since the outside tube diameter is 60 mm for each riser, this provided the conversion ratio necessary to later convert pixels to mm. The height of the image was then cropped so that the aspect ratio of the image would be 2:1, width to height.

After contrast and size adjustments, the images were converted to 8 bit greyscale and saved as .bmp files, also using XnView. From here, a program called ImageJ was used to take an average of each 750 image set, and this average image was subtracted from each image in the set in order to further improve the contrast. At this point the images were ready for PIV analysis using the ImageJ plugin, 'PIV' written by Dr. Quingzong Tseng and available for download online [13]. An example of the changes made to a single image as each of these steps is taken is shown in Figure 51 below.

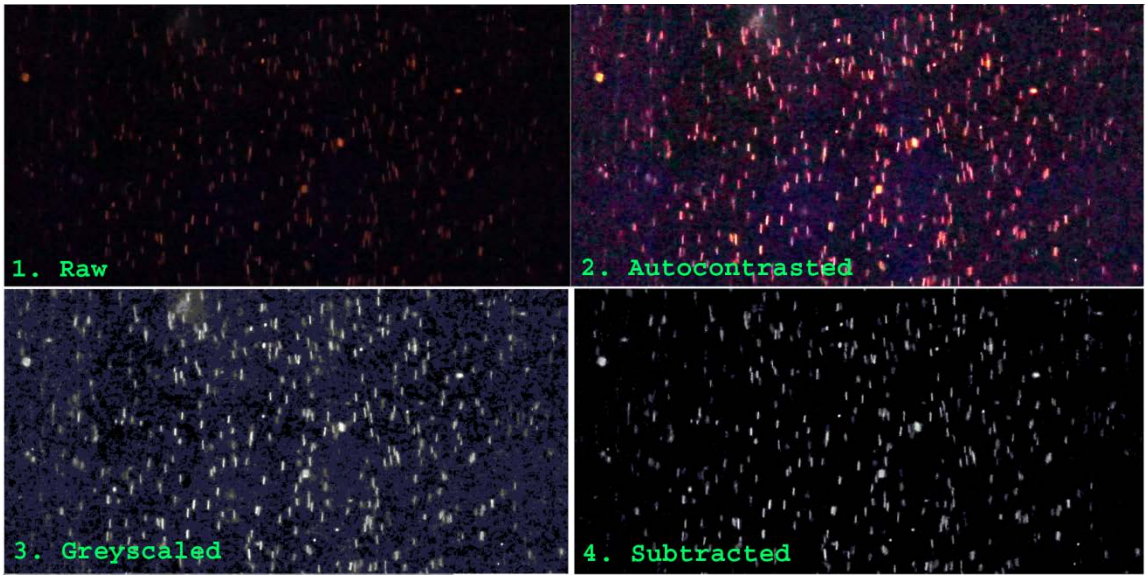


**Figure 51.** Each Stage of Image Processing for PIV Analysis

III.2.3 PIV Analysis

The PIV plugin, in the 'advanced' algorithm, uses a 3 stage iterative process that employs the template matching method using normalized correlation coefficient algorithm [13]. The relevant parameters that the user must set for each iteration are the Interrogation Window (IW) and Search Window (SW) sizes and the Vector Spacing, all in pixels. A rigorous optimization of these values was not undertaken for this preliminary study, so there may be room for improvement in the accuracy of the results to follow in the next chapter.

Typically, the 1st pass IW size was set to roughly ¼ the dimension of the image's minor axis, and was halved at each subsequent iteration. The SW size was set equal to the IW size for that pass, plus two times the expected maximum displacement of the particles, and the Vector Spacing was set to ½ the IW size for that pass. The Correlation Coefficient and additional options were left at the default values.

Normally, after a pair of images is processed there is the option within the plugin to do a Post-Processing operation of replacing questionable vectors with interpolated ones via the 'Normalized Median Test' (NMT) or the 'Dynamic Mean Test'. It was observed that when employing the NMT using default values that obviously erroneous vectors were replaced with reasonable looking results. Subsequently, it was desired to use this for each pair of images in the set (of which there are 749 pairs). Unfortunately, this option is unavailable when using the Batch processing mode. To remedy this, the source code for the plugin was downloaded from Dr. Tseng's Googleplus site [13] and was modified by the author to automatically perform the NMT after each set. Dr. Tseng graciously recompiled the code free of charge, and the modified plugin was used to produce all of the results seen in the next Chapter. A typical vector output is shown graphically in Figure 52 below.

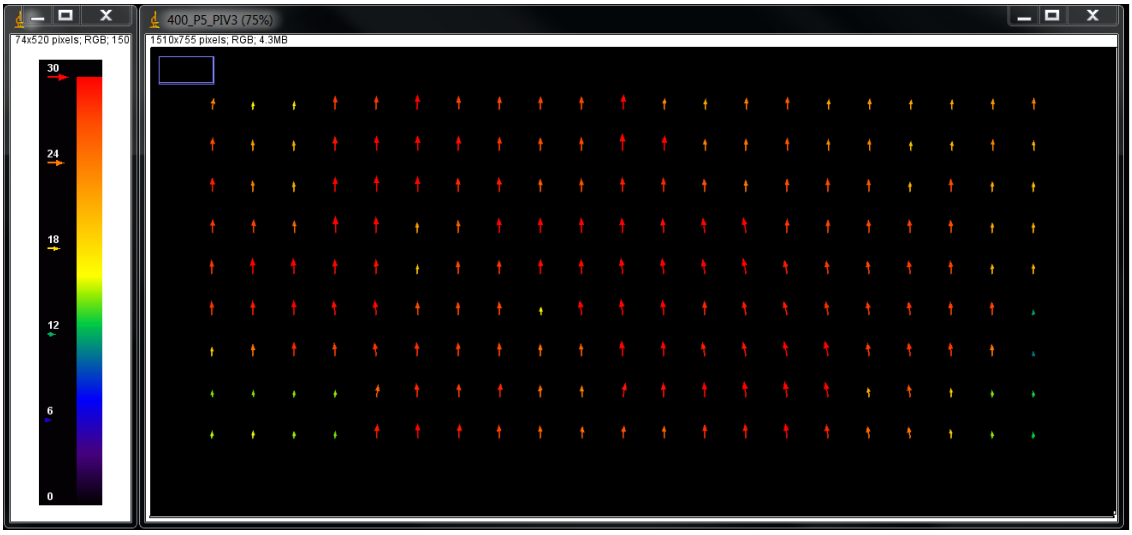

**Figure 52.** Typical Vector Field Output of the 'PIV' ImageJ plugin

III.2.4 Determination of the Reference Velocity via PIV

In order to provide a similar metric for comparison to the UVP derived Reference Velocity, the vertical components of all output vectors in each image pair were averaged together. This produced a single value representing the average flow velocity and may be referred to as the PIV Reference Velocity in this report. A more sophisticated analysis may require that the vectors be given different weighting factors across the horizontal axis during the averaging operation, but this was not done for the results presented in this report. Additionally, the output files were analyzed for consistency in the two following ways.

First, from the principle of continuity each horizontal line of vectors should have the same average velocity. The population standard deviation of each individual line in an image pair was calculated from the overall mean for that pair, and subsequently the RMS value of all 749 line-by-line standard deviations was taken to provide a single statistical figure representing the spatial variability of the overall average. Second, the standard deviation of each image's mean value from the overall average was calculated to capture the temporal deviation of the PIV Reference Velocity.

# CHAPTER IV
# SINGLE PHASE EXPERIMENTS AND RESULTS

## IV.1 Summary of Experimental Conditions

This chapter will summarize the flow behavior of the system as a whole and the local flow behavior in the Cooling Panel under different experimental conditions. These conditions are meant to explore the response of the system to different heat flux profiles, power levels, throttling, and coolant inventory levels. Experiments are numbered using the following 3 digit system where the first digit defines the element that was varied and the second digit signifies the degree of the variation (high, low, skewed inlet, outlet, etc.). The third digit arises from the fact that each experiment would need to be repeated at least 1 time under identical conditions since there are 8 risers ported to allow for UVP measurements, but only 6 transducers, so it allows each individual experiment to be identified. First digit identifier codes are as follows:

| | |
|---|---|
| 0 | Base or Scaled Prototype Case |
| 1 | Alternate Power Levels |
| 2 | Throttling |
| 3 | Non-uniform Heat Flux Profiles |
| 4 | Coolant Inventory Level |
| 5 | Saturation (Multi-Phase) |

The complete list of experimental conditions, including the dates the experiments were conducted, is contained in Table 4 on the next page.

**Table 4.** Summary of Experimental Conditions

| Series | Description | Power | Throttling | Coolant Inventory | Duration | Dates [mm/dd/yy] |
|---|---|---|---|---|---|---|
| 00 | Base | 6 kW total<br><br>Uniform | none | 402.2 L | to 70 °C<br><br>(8.75 hrs) | Exp. 000 – 08/07/14<br>Exp. 001 – 08/08/14 |
| 10 | High Power | 9.6 kW total<br><br>Uniform | none | 402.2 L | to 70 °C<br><br>(5 hrs) | Exp. 100 – 08/09/14<br>Exp. 101 – 08/10/14 |
| 11 | Low Power | 3.6 kW;<br><br>Uniform | none | 402.2 L | to 50 °C<br><br>(9.5 hrs) | Exp. 110 – 08/11/14<br>Exp. 111 – 08/12/14 |
| 20 | Partially Throttled | 6 kW;<br><br>Uniform | to attain a 6 °C ΔT in the Test Section | 402.2 L | to 60 °C<br><br>(6.5 hrs | Exp. 200 – 08/17/14<br>Exp. 201 – 08/18/14 |
| 21 | Fully Throttled | 6 kW;<br><br>Uniform | to attain a 10 °C ΔT in the Test Section | 402.2 L | to 60 °C<br><br>(7.5 hrs) | Exp. 210 – 08/19/14<br>Exp. 211 – 08/20/14 |
| 30 | Skewed Heat Flux - Inlet | 6 kW total<br>3.2 – 2 – 0.8<br>In…….. Out | none | 402.2 L | to 60 °C<br><br>(6.25 hrs) | Exp. 300 – 08/14/14<br>Exp. 301 – 08/16/14 |
| 31 | Skewed Heat Flux - Outlet | 6 kW total<br>0.8 – 2 – 3.2<br>In…….. Out | none | 402.2 L | to 60 °C<br><br>(6.25 hrs) | Exp. 310 – 08/13/14<br>Exp. 311 – 08/15/14 |
| 40 | High Water Inventory | 6 kW;<br><br>Uniform | none | 623.5 L | to 60 °C<br><br>(8.75 hrs) | Exp. 400 – 08/21/14<br>Exp. 401 – 08/22/14 |
| 50 | Saturation | 6 kW;<br><br>Uniform | none | 402.2 L | Saturation<br><br>(14.75 hrs) | Exp. 500 – 08/24/14 |

The first subsection will be devoted to characterizing system behavior for all experimental series except the Throttled series 20 and 21. This will include startup behavior, flow instabilities, the relationships between total heater power, power absorbed in the coolant, the temperature difference between the coolant at the inlet and outlet of the Test Section, system flowrate, and a first order estimation of the rate of heat loss from the coolant as it travels around the balance of the flow loop outside the Heated Cavity.

As a side note for clarity, the temperature difference referred to above will hereinafter be referred to as the ΔT; and the system flowrate may sometimes be referred to as the variable Q. Risers are numbered 1 through 9 from the inlet to the outlet of the Test Section. Please see Figure 53 for an illustration of the location of the thermocouples used to calculate ΔT, and the magmeter used to record Q and the riser order.

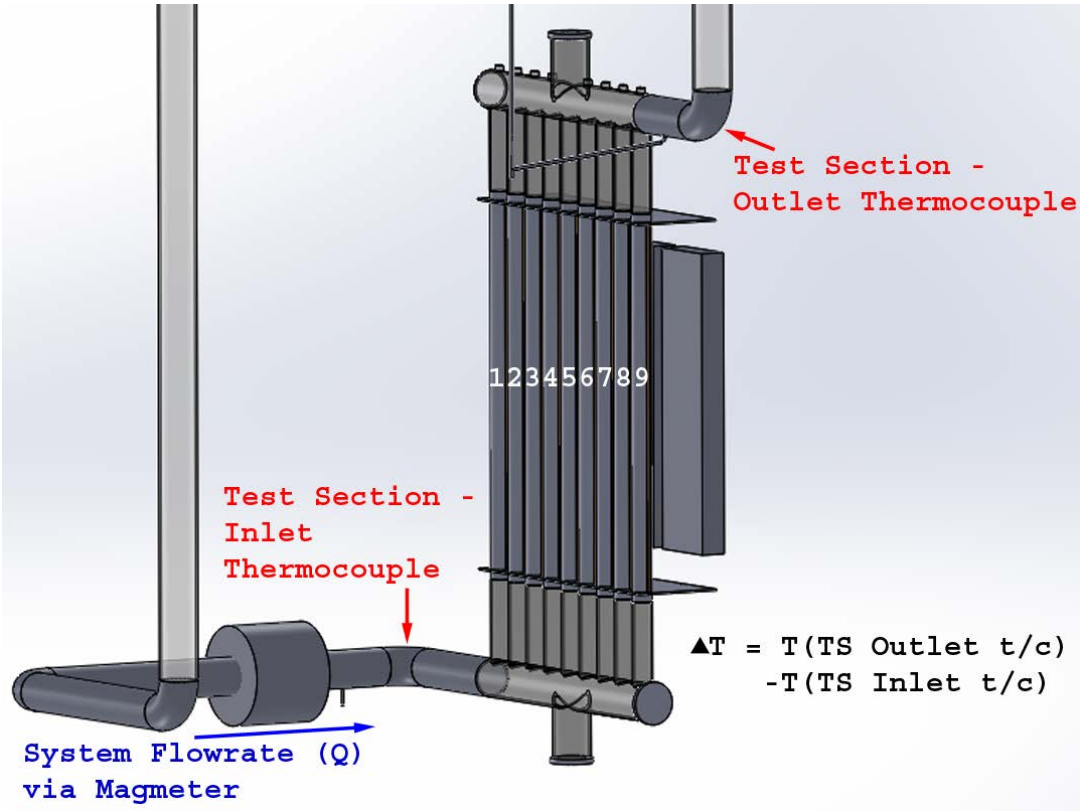


**Figure 53.** Illustration of Test Section ΔT and System Flowrate (Q)

A single representative example using the base level experiment will be used to show typical system behavior whenever there are no significant differences between experiments. A separate section will address results obtained when the system was throttled to incur a higher ΔT in the Test Section, as not as much data was available (the electromagnetic flowmeter was not able to read the flowrate due to the extremely low flow velocities in the throttled cases).

Results of the local behavior are in the next subsection and focus on the relative flow velocities between each riser in the Cooling Panel, via UVP and PIV measurement techniques. A few simple sanity checks are presented to show the validity of the measurements. These include comparing the total flow rate obtained by summing the flowrate from each riser via the UVP and PIV measurements to the magmeter readings, and comparing the energy absorption rates in a similar manner. This chapter will end with a summary comparison of the PIV measurements to the UVP.

## IV.2 System Level Results and Analysis

### IV.2.1 Non-Throttled Experiments (00, 10, 11, 30, 31, 40, 50 Series)

#### *IV.2.1.1 Startup Behavior*

Experiments began with a step power input applied to the heaters, causing the heater surface temperature to rise exponentially towards an asymptotic value. See Figure 54 below for a typical example from Experiment 000. None of the experiments used a time-varying power profile, so the behavior was similar for all other experiments conducted.

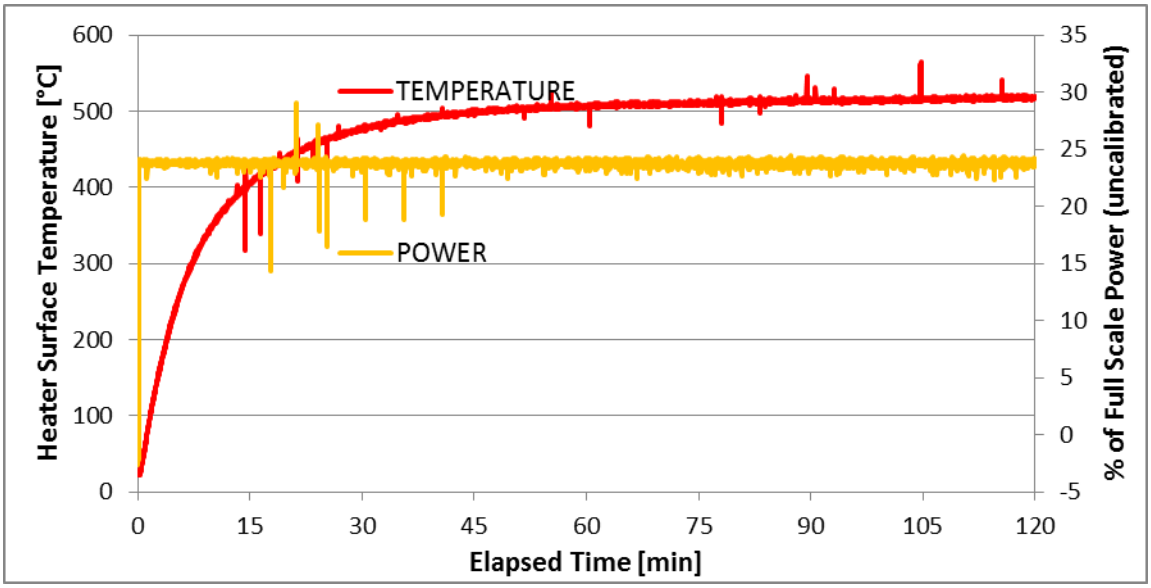


**Figure 54.** Typical Startup Behavior for Heater Power and Surface Temperature

As the heater surface temperature rose, a temperature difference developed in the water in the coolant panel and the rest of the system, giving rise to a sudden flow excursion as shown in Figure 55 below. This is also from Experiment 000.

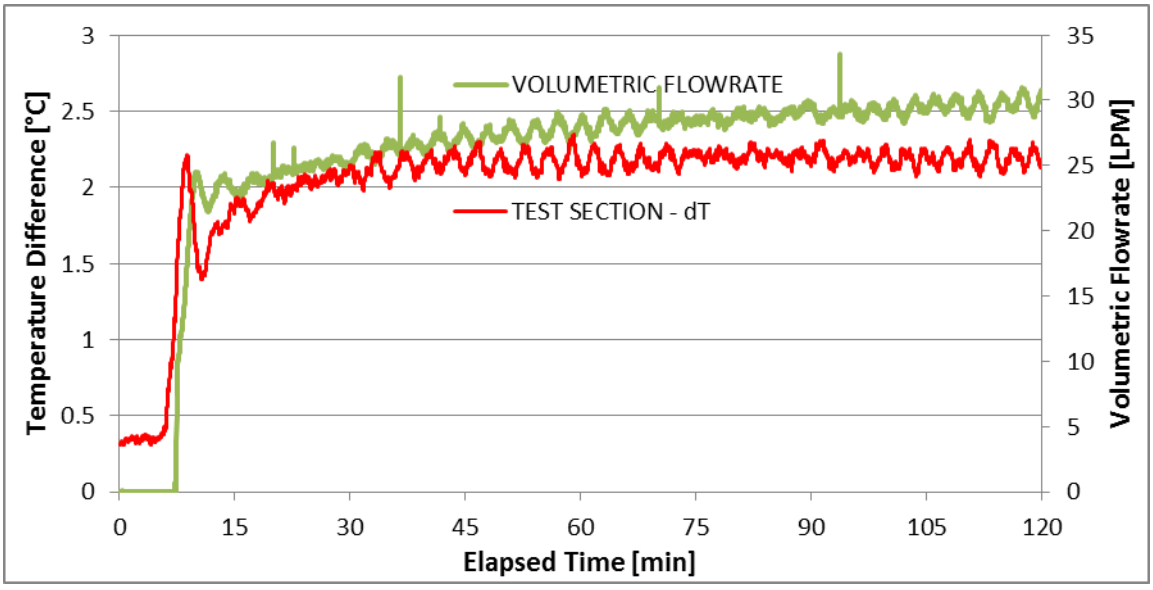


**Figure 55.** Typical Startup Behavior for Test Section ΔT and System Flowrate

It can be noted from the figure that after the water initially begins to flow there is a sudden drop in ΔT. This drop in ΔT likewise causes a drop in the flowrate since it is the driving force behind the flow. From this it is evident that there is a negative feedback effect between ΔT and the system flowrate. Since all experiments are ran without a secondary cooling loop this effect never goes away. It is observed in Figure 55 that a sinusoidal oscillation is present in both the flow and temperature difference plots, seemingly 180° out of phase. This will be analyzed at depth in a later subsection. Again, the behavior noted in the figure was similar for all experiments (except the Throttled Series, discussed later).

*IV.2.1.2 Quasi-Steady State Relationships between Heater Power, Heater Temperatures, Coolant Panel ΔT, System Flowrate (Q) and Power Absorption*

It is observed in the previous figures that the heater temperature approaches an asymptotic value over the long term. A summary slide showing the quasi-steady state heater temperatures vs applied electrical power for all experiments (shown by the average for the series) is in Figure 56 below. It is observed that the relationship is linear.

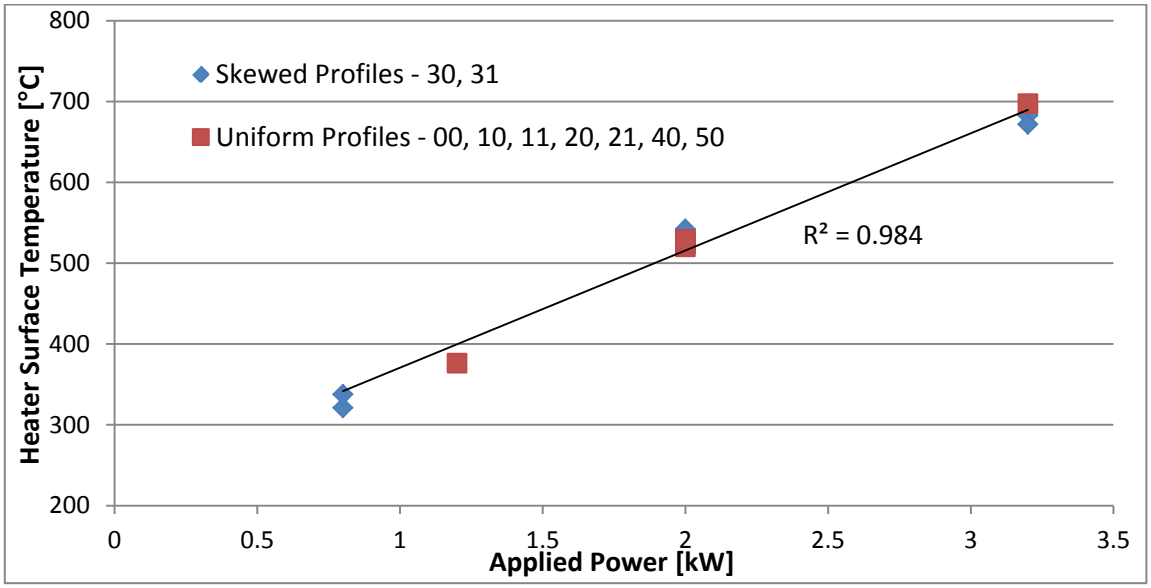


**Figure 56.** Relationship between Heater Power and Surface Temperature

Similarly, the ΔT induced by the heat from the heaters also quickly goes to a relatively stable value during long term operation. The relationship between the total power level and the resulting quasi-steady temperature difference across the Test Section is shown in Figure 57 below. The data points are from all individual experiments except those in the throttled series.

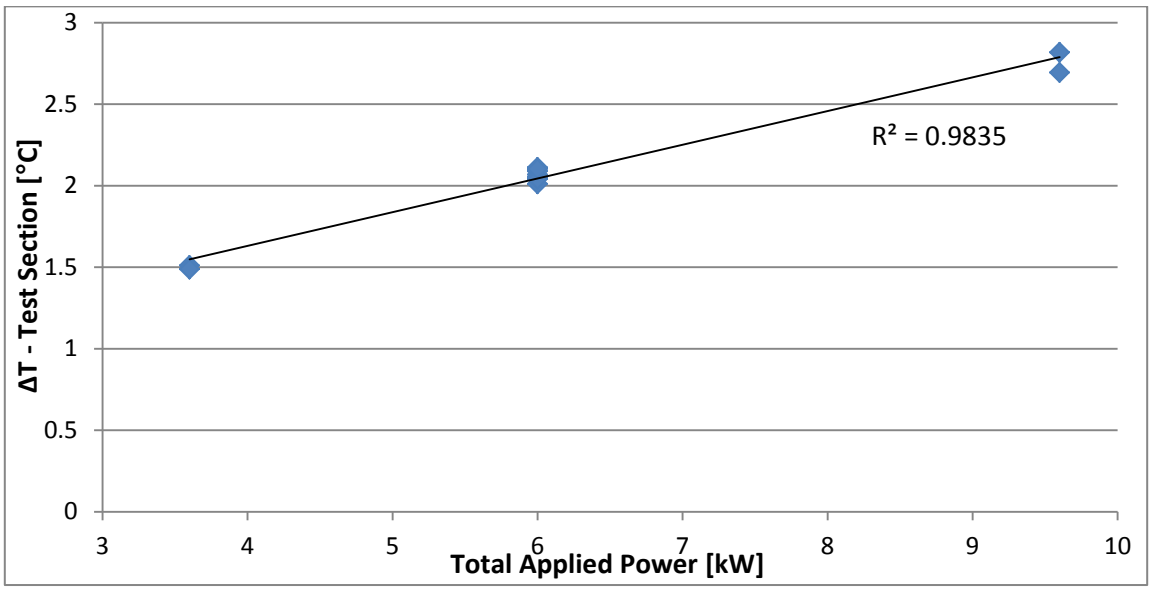


**Figure 57.** Relationship between Heater Power and Test Section ΔT

The system flowrate also tends to a relatively stable value shortly after startup, but there is some rise over time which is believed to be due to the fact that the specific volume is changing as the fluid rises in temperature. It is believed that the mass flowrate may in fact be steady, but this has not been verified at the time of writing this report. The relationships between the resulting quasi-steady system flowrate and Test Section ΔT is shown in Figure 58 below, using data from every individual experiment except those in the throttled series.

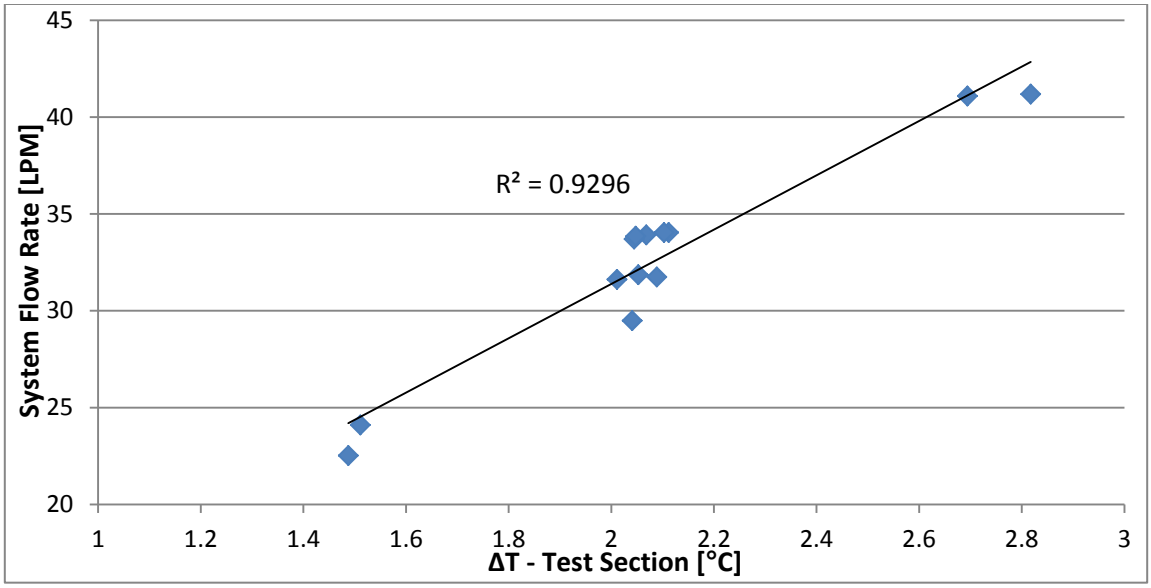


**Figure 58.** Relationship between Test Section ΔT and System Flowrate

Again it is observed that the temperature difference and flowrate responses are highly linear to each other, and by extension each is also linear with respect to applied power and to the average heater surface temperature in the cavity.

It is now noted that the fraction of the emitted power that is absorbed by the water flowing through the Cooling Panel can be determined from Equation 1 below, where $P_{abs}$ is the rate of energy absorption from the heaters, $\dot{m}$ is the mass flowrate, Q is the volumetric flowrate as read by the magmeter, ρ and $c_p$ are the temperature corrected density and specific heat capacity of the water, and ΔT is the bulk fluid temperature difference of the water entering and leaving the Test Section.

$$P_{abs} = \dot{m} c_p \Delta T = Q \rho c_p \Delta T \qquad \text{Equation 1}$$

Using Equation 1 above the quasi-steady relationship between applied and absorbed power was calculated for each experiment except the Throttled Series, results are in Figure 59 below. As seen previously, the relationship is highly linear. It is also noted that the fraction of power absorbed increases at higher power levels, approaching

81% for the high power (10 Series) experiments. This makes sense since the rate of heat transfer increases with higher temperature differences that come from higher power levels.

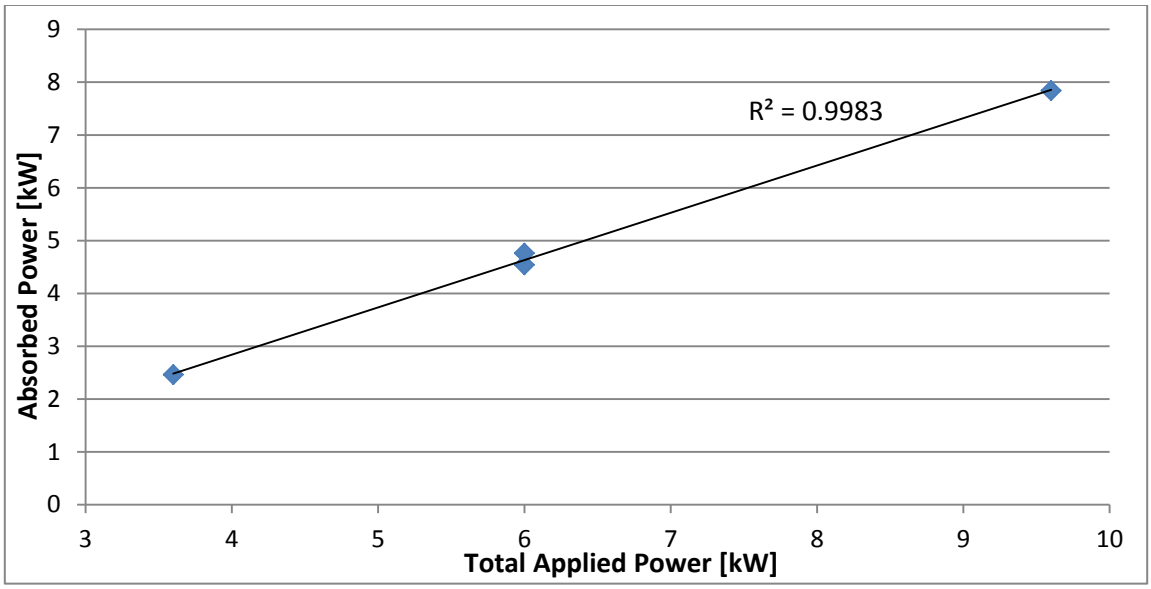


**Figure 59.** Relationship between Heater Power and Power Absorbed in the Coolant

*IV.2.1.3 Calculation of the Rate of Heat Loss to the Environment*

The power sent to the heaters that was not absorbed by the coolant is assumed to simply have entered the ambient environment via the back of the heaters and (less so) through the walls of the Heated Cavity. There is one other power/energy variable remaining to be calculated, however, and that is fraction of the power initially absorbed by the coolant that is lost to the environment as the coolant travels around the balance of the flow loop outside of the Heated Cavity. Again due to a lack of accurate flow data from the Throttled experiments this section will not have any results from those tests.

The heat loss rate will be affected by the temperature difference between the fluid and its surroundings, so in order to accurately compare results under similar circumstances the heat loss rate was calculated over the temperature range of 30 to 50 °C

as this was common to all tests. The estimation of the heat loss involves the following process:

1. The total amount of energy required to raise the temperature of the initial mass of water in the system is calculated according to Equation 2 below
2. The rate of heat absorption in the Cooling Panel, given by Equation 1, is numerically integrated over the time that the Test Section inlet temperature was 30 °C until it reaches 50°C. This gives the total amount of energy absorbed by the fluid (see Equation 3)
3. The difference in the energy calculated from Step 2 and Step 1 is divided by the time it took for the temperature to rise from 30 to 50 °C. This gives the average rate of heat loss over that time period (Equation 4)

$$E_{req} = V\rho_{itl}c_p\left(T\left(50°C\right) - T\left(30°C\right)\right) \quad \text{Equation 2}$$

$$E_{abs} = \int_{t(T_{in}=30°C)}^{t(T_{in}=50°C)} P_{abs}dt \quad \text{Equation 3}$$

$$P_{loss,avg} = \frac{E_{abs} - E_{req}}{t\left(T_{in} = 50°C\right) - t\left(T_{in} = 50°C\right)} \quad \text{Equation 4}$$

In order to practically implement Equation 4, the $E_{abs}$ will be numerically integrated via a summation, as shown in Equation 5 below.

$$P_{loss,avg} = \frac{\sum_{t(T_{in}=30°C)}^{t(T_{in}=50°C)} Q\rho c_p \Delta T \Delta t - V\rho_{itl}c_p\left(T\left(50°C\right) - T\left(30°C\right)\right)}{t\left(T_{in} = 50°C\right) - t\left(T_{in} = 50°C\right)} \quad \text{Equation 5}$$

In the above equations, V is the initial volume the system, ρ and $c_p$ are density and specific heat capacity appropriately averaged across the temperature range, Δt is the time difference between measurements (the inverse of the sampling frequency), $T_{in}$ is the bulk fluid temperature at the Test Section inlet, t is time. $\rho_{itl}$ is the density of the coolant

at the same initial temperature as the when the volume was calculated and is used to determine the initial mass of coolant in the system, which is assumed to remain constant during the heating process. For the 00, 10, 11, 30, 31, and 50 Series of Experiments, the initial coolant volume is 402.2 liters, and the energy required to raise the temperature from 30 to 50 °C is 33,353.7 kJ. For the High Coolant Inventory Series the initial volume is 623.5 L and the energy required is 51,705.7 kJ.

A comparison of the heat loss rates for the Base, High Power, and Low Power experiments is presented in Figure 60 below. Note total heater power levels and energy absorption rates of the coolant are also presented. Where the information is presented by Series the data is the average of the two experiments. This would have been done for the High Power (10 Series) experiments but the signal from the magmeter dropped out during part of the experiment.

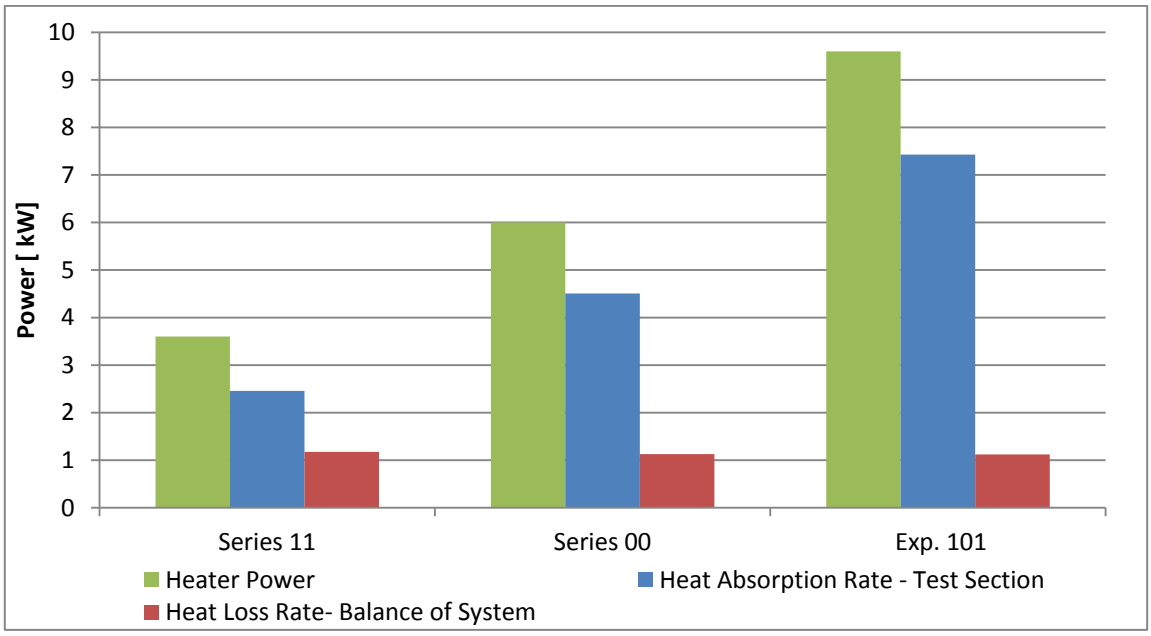


**Figure 60.** Coolant Heat Loss Rates by Heater Power Level

It is noted that the rate of heat loss was relatively constant at about 1.13 kW during all 5 experiments represented above. This result is to be expected because it is only the temperautre differneces between the fluid and the ambient environment that matter, the flow rate itself should not have an effect.

Similar results are seen for the 30 Series and Experiment 311 (again there is missing flow data for Experiment 310), except that the heat loss rates are about 10% higher. Please see Figure 61 for reference. One possible explanation is that the ambient tempeatures may have been lower on the days that the 30 and 31 Sereies experiments were done. This is possible because the building that the RCCS is in is a large warehouse, and the environment is subject to being influenced by outdoor temperaures and humidity despite the best efforts of the HVAC system there. Information on the environmental conditions was not kept, however, so this cannot be confirmed.

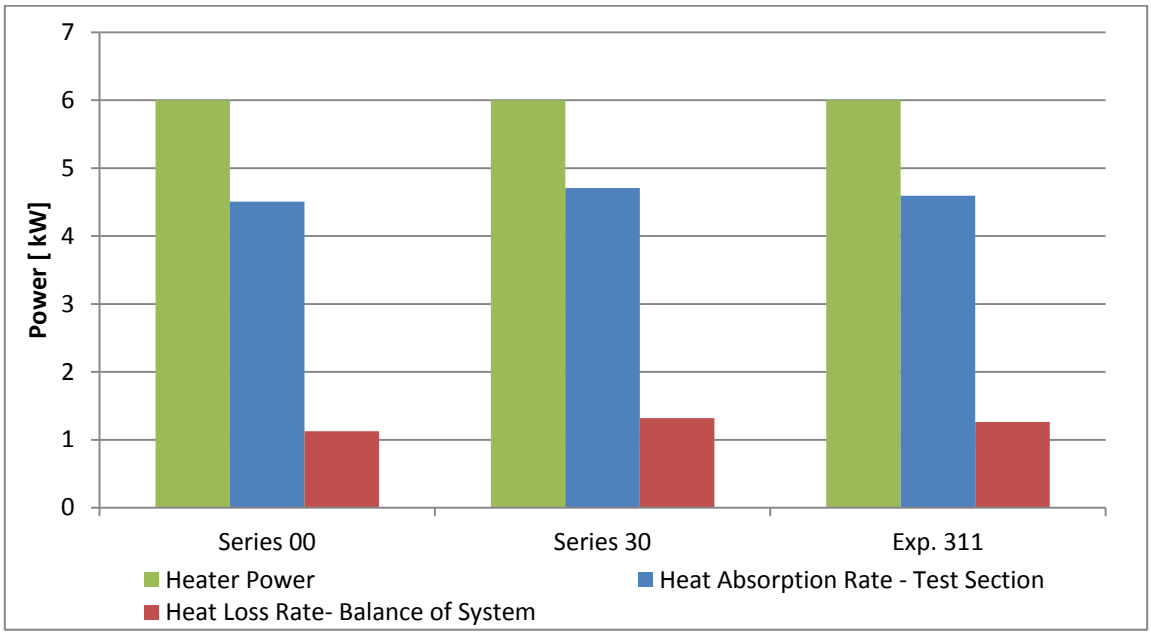


**Figure 61.** Coolant Heat Loss Rates by Heat Flux Distribution

Data for the High Coolant Level Series of experiments, 400 and 401, requires some explanaiton. It is observed from Figure 62 below that the heat loss rate for Experiment 400 is significantly higher and for 401 significantly lower than the 00, 10, 11, 30, and 31 Series of experiments.

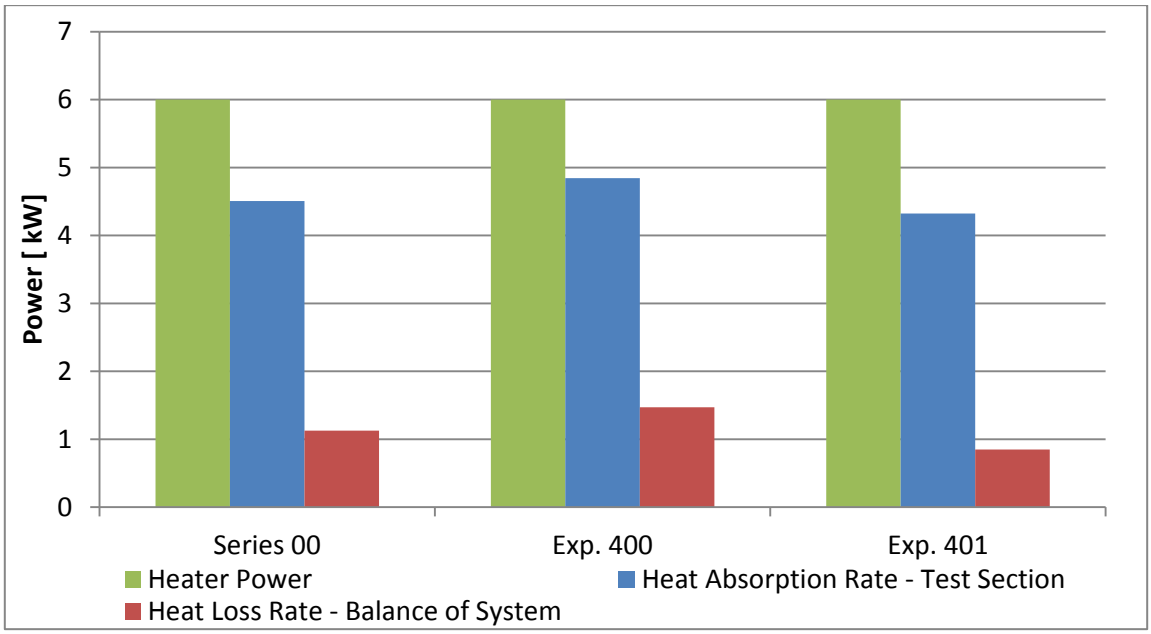


**Figure 62**. Coolant Heat Loss Rates by Coolant Level

It should be noted that the system flowrate was also unusually low in Exp. 401 at 29.5 LPM as compared to 34 LPM in Exp. 400, even though the experimental conditions were identical. The 34 LPM of Exp. 400 was also a little higher than seen in other experiments at the same total power level. Curiously, the ΔT for both expermients was about the same, indicating that the flowrates *should* have been the same as well. Furthermore, the time period required to go from 30 to 50 °C, however, was only 3% different, indicating that heat absorption and loss rates should have been about the same. Other unexplained anomalies will be seen between Exp. 400 and 401 in the Flow Instabilities section. It is suspected that the magmeter data may have bene skewed high

and then low for some unknown reason, but at the time of this writing this hypothesis has not been investigated.

It is worthy to note that the average of the two results for 400 and 401 yield numbers similar to those seem with the other 6 kW experiments, and that the time required to go from 30 to 50 °C is roughly 3/2 times the time required in the other 6 kW expeirments using 2/3 the inventory, which is to be expected.

For experiment 500, seen in Figure 63 below, the heat absorption rate for the coolant in the Test Section is similar to the base scenario, which is expected, but it is noted that the heat loss rate is lower. Here the result makes intuitive sense because all of the hot and cold leg piping and both upper and lower manifolds were completely insulated during the two phase test in order to bring the system to saturation as quickly as possible by minimizing heat losses. Compared to the base case, the extra insulation gave about a 18.7% reduction in heat loss.

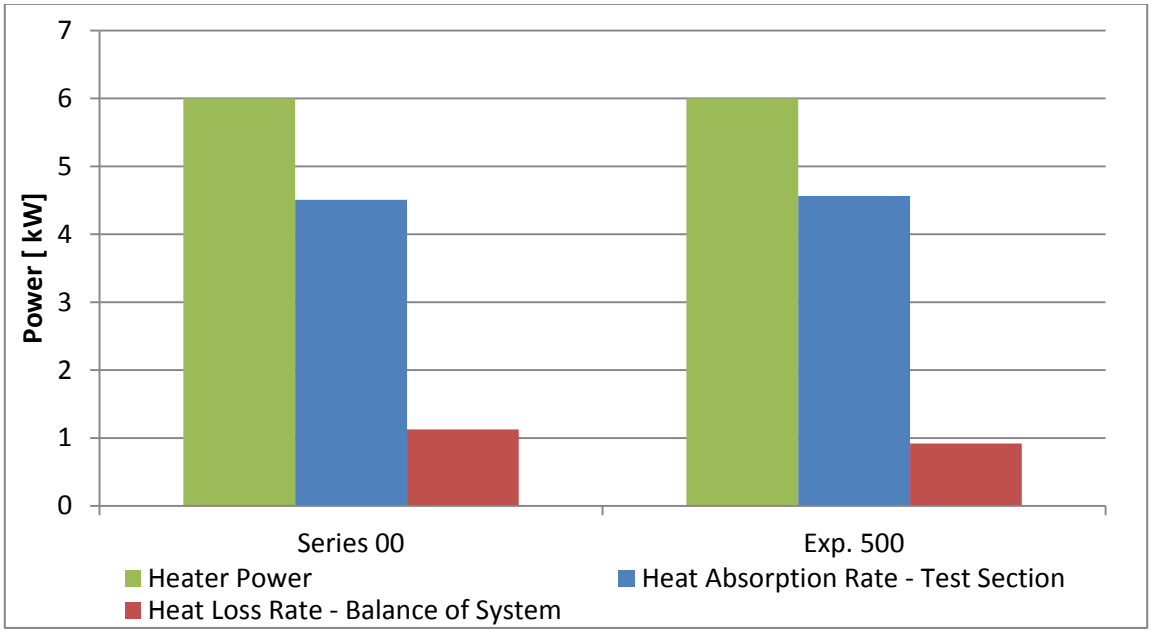


**Figure 63**. Coolant Heat Loss Rates by Loop Insulation

*IV.2.1.4 Flow Instabilities in the Non-Throttled Experimental Series*

Following is a frequency domain analysis of the sinusoidal oscillations previously noted in Figure 55.

IV.2.1.4.1 Frequency Analysis of ΔT and Q: Frequency and Phase Relationships

A Fast Fourier Transform (FFT) analysis was done on the last 50 minutes of data for the flowrate and ΔT for each test; except for the Throttled series as the restriction created by the butterfly valve prevented small scale oscillations from forming. Typical results of the frequency spectrum components are shown in Figure 64 below and are from Experiment 000.

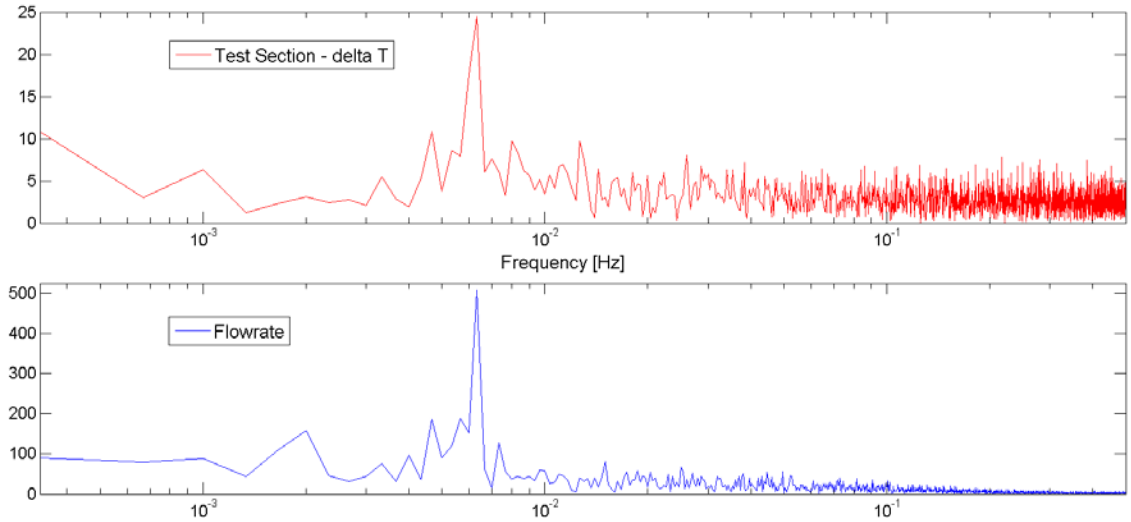


**Figure 64.** Spectral Analysis of the Sinusoidal Oscillations of Q and ΔT

The strongest harmonic is at the same frequency for both variables and occurs at 0.0063 Hz, corresponding to a period of 158.73 seconds. The phase angles of the 0.0063 Hz frequency components were 176.75° and 18.22° for the ΔT and Flowrate spectrums, respectively. This yields a phase difference of 158.53°.

It is expected from looking at the results in the time domain that the phase difference be 180°, and when the results for all the strongest frequency components are analyzed for all experiments the average phase difference is 179.6°. It is believed that the deviations from 180° for any individual experiment are due to a combination of noise in the signal and a lack of resolution since the sampling frequency is only 1 Hz, yielding a frequency domain resolution of ½ Hz from Nyquist sampling theorem. Indeed for some experiments, there appeared to be two adjacent frequencies that were comparable in height to each other. In these cases the results were averaged together to obtain the periods and phase differences.

IV.2.1.4.2 Relationship of Oscillation Period to Flowrate

It is worthy to note that the oscillation frequency and amplitude changed with power level (and from linearity, with ΔT, flowrate, and heater temperature as well). The most linear relationship between the Q & ΔT Oscillation Period and other variables was to the system flowrate. This relationship is shown in Figure 65 below for all experiments series. Note that the higher the flowrate, the higher the frequency of the oscillations. It is also noted that the values for experiments 400 and 401 did not trend well with the other experiments and are not included in the regression analysis shown in the figure. The magnitude of the oscillation changed as well with total power level but this was difficult to quantify, so that aspect of the analysis is not included in this report.

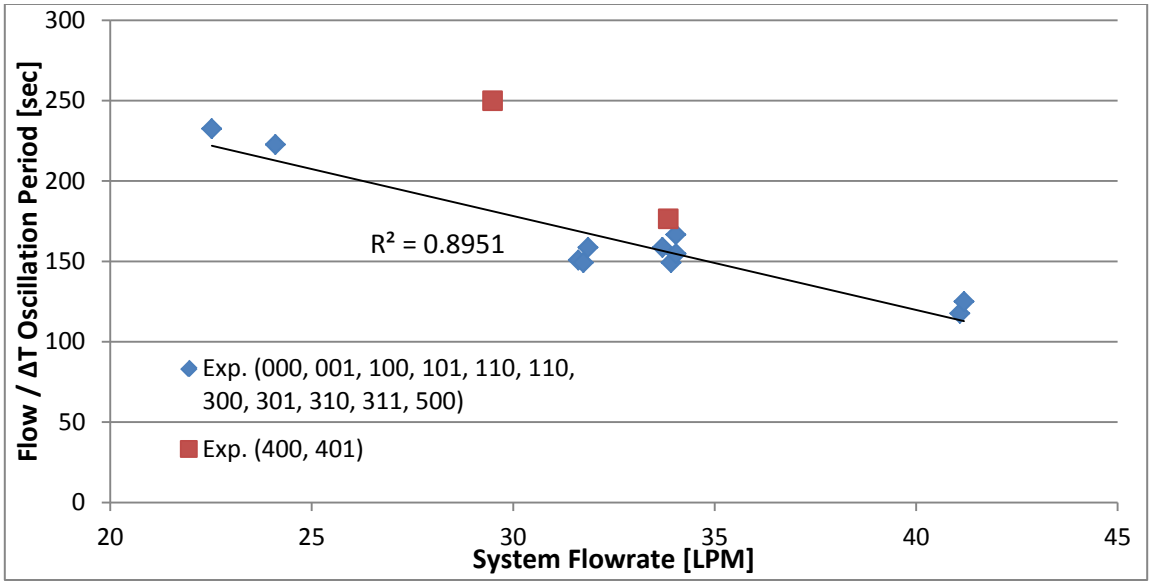


**Figure 65.** Relationship between Q and ΔT Oscillation Period and System Flowrate

IV.2.1.4.3 Detail of Oscillation Behavior of High Level / Inventory Experiments

Interestingly, the High Coolant Inventory or 40 Series of Experiments had strange oscillation phenomena compared to the other non-throttled series of experiments. First, the time domain data appeared unusually noisy, and the subsequent FFT analysis yielded several large peaks at various frequencies, making it difficult to ascertain which one represented the main flow oscillation frequency. In order to work around this, the data was smoothed by taking the rolling average of each point's 12 nearest neighbors on either side, and then plugged into the FFT via MATLAB. This did successfully provide a single dominant and matching peak for both the ΔT and Q waveforms, but they occurred at different frequencies between Experiment 400 and 401. See Figure 66 and Figure 67 below for a comparison.

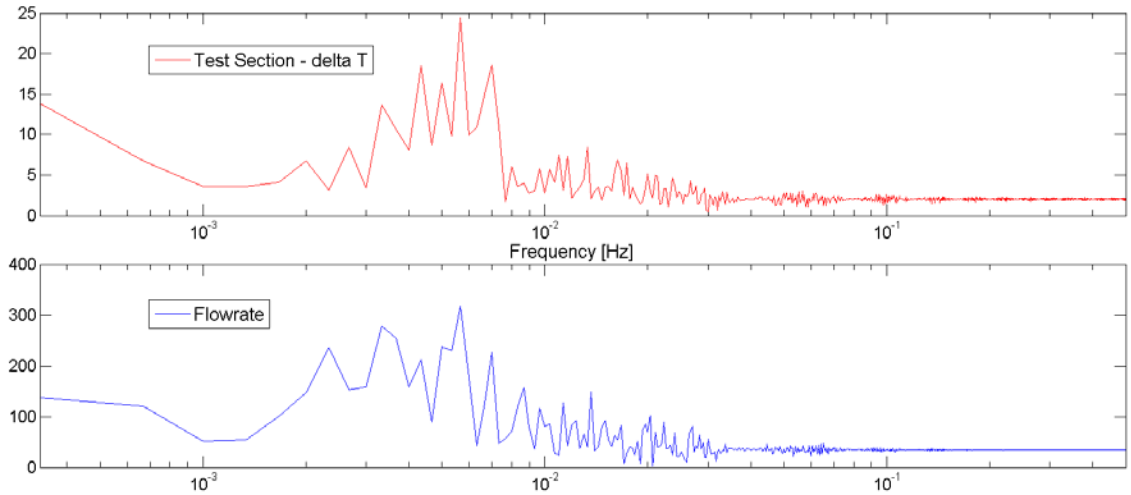


**Figure 66.** Experiment 400 Spectral Analysis: ΔT and Q

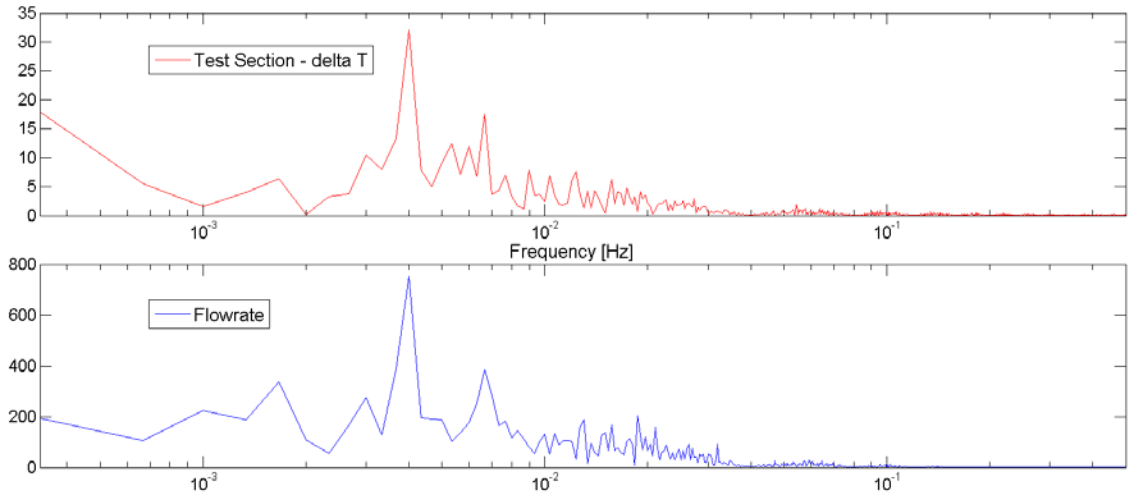


**Figure 67**. Experiment 401 Spectral Analysis: ΔT and Q

The period of oscillation for experiment 400 is 176 seconds, but 250 seconds for 401. The oscillation behavior could be related to the differing flowrates seen between the two experiments. From Figure 65 we know that increasing flowrate gives higher oscillation frequencies, and the flowrate during Experiment 400 was 34 LPM, giving an oscillation frequency of $5.56_{E\text{-}03}$ Hz. During Experiment 401 flowrate was 29.5 LPM, giving an oscillation frequency of $4.00_{E\text{-}03}$ Hz. Still, when compared with the other

values in Figure 65 the oscillation frequency does not change at the expected rate given the difference in flowrates. It is apparent that the higher tank level had some sort of effect on the instability.

It is the author's belief that it is either the effect of increased pressure at the Cooling Panel from the increased head, or the effect of the increased pressure at the outlet of the internal tank elbow in the Water Storage Tank that may be causing the changes observed. For an illustration of how the tank level is different for the 40 Series as compared to the others, please refer to Figure 68 below. This is an area that should be further researched.

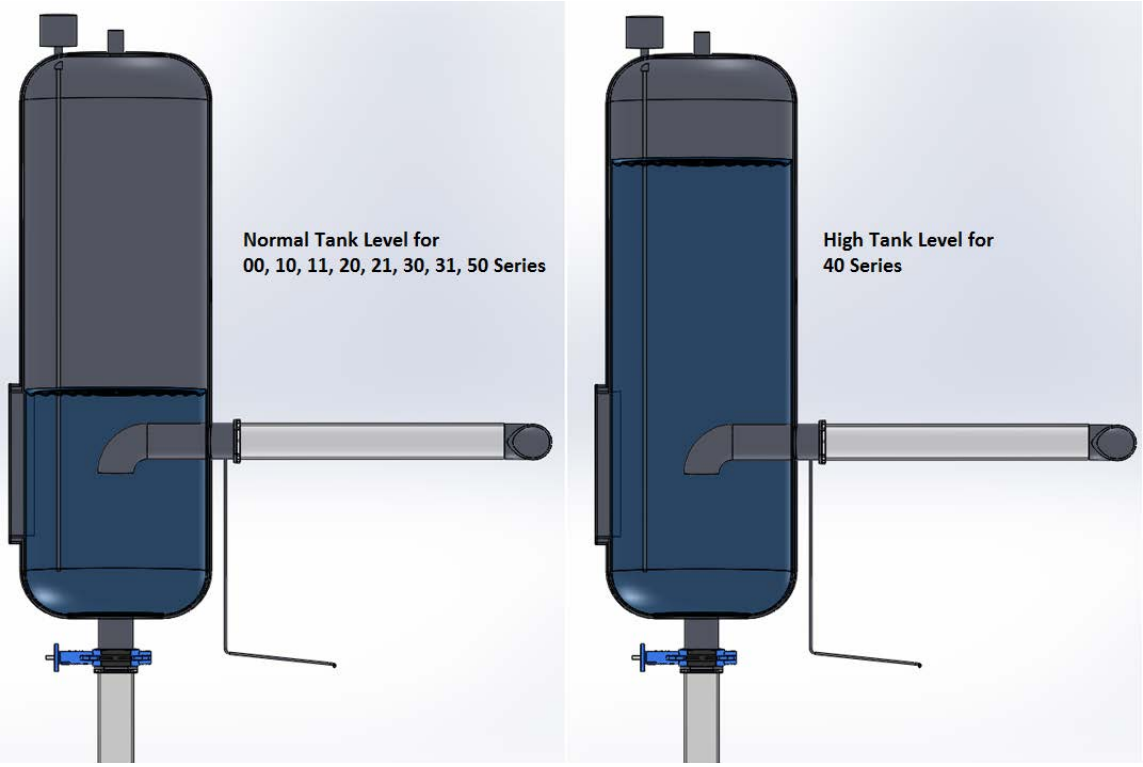


**Figure 68.** Coolant Levels for the 40 Series Experiments as Compared to All Others

## IV.2.2 System Level Analysis of the Throttled Experiments (20 and 21 Series)

### *IV.2.2.1 Purpose and Description of Experiments*

The purpose of the throttled experiments was two-fold. First, as mentioned previously, the scaling analysis developed by Argonne National Laboratory was based on a 10 °C differential over the Test Section, so it was desired to conduct at least one experiment at that temperature to observe system behavior. This was done in the 21 Series of experiments. Second, it would be interesting to see how the system would respond to a general situation of obstructed flow. To extend the range of conditions encountered, it was decided to also look at the intermediate point between the normal 2 °C ΔT and the 10 °C ΔT, so the 20 Series involved closing the butterfly valve below the Coolant Tank until a 6 °C difference was reached. The valve settings necessary to achieve these two values were found in earlier scoping tests. During Experiments 200, 201, 210, and 211 the valve was set to these points before testing began and was not moved during the test.

### *IV.2.2.2 Experimental Series 20*

Analysis of the throttled Series of experiments was hampered by the fact that the extremely low flow rates disabled normal operation of the magmeter. As noted in Figure 69 for Experiment 200, the flow readings only lasted for about 3 hours before the flow velocity slowed to a point that was too low to be read. At the same time as the flowrate was decreasing, the temperature difference across the Test Section was rising. This indicates that the Test Section ΔT increased due to the increased dwell time of the fluid in the Heated Cavity. During the experiment, no definitive flow oscillations were observed in the main flow rate. There might be oscillations present, but the magnitude is so damped by the obstruction that the instruments are not sensitive enough to read it through the noise.

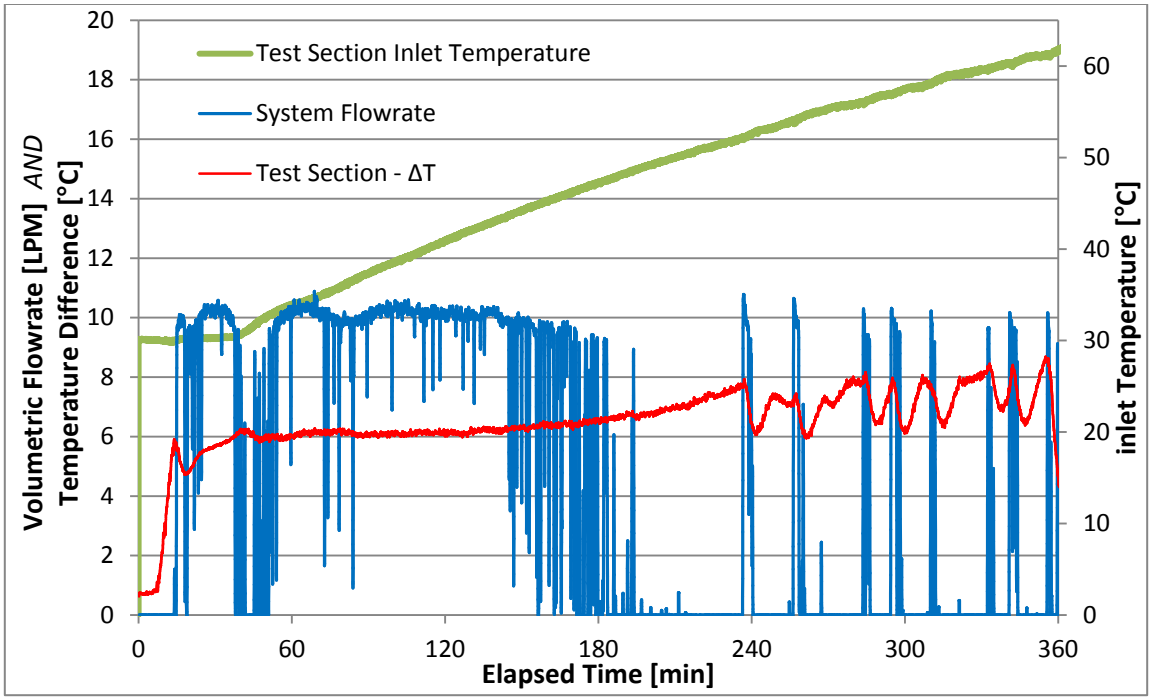


**Figure 69.** System Flowrate, ΔT, and Test Section Inlet Temperature for Exp. 200

The average steady flowrate during experiments 000 and 001 was 31.735 LPM, while the ΔT was 2.032 °C. During Experiment 200 the flowrate was 10.075 LPM and ΔT was 6.12 °C. This was during the 36 minute timespan that the flow and ΔT were nearly steady, before ΔT began to rise at 132 minutes elapsed time. It is apparent that the ratio of flowrates between the two experiments is very nearly the same as the inverse of the ratio of the ΔT's, differing by about 4.6%

It is also noted that 8 intermittent, short duration flow excursions were witnessed beginning at approximately 240 minutes until the experiment was stopped at around 360 minutes. Each excursion coincided with a sudden drop in the ΔT, again signifying the fresh influx of water from the cold leg coming into the Cooling Panel during the excursion.

The Inlet Temperature is relatively stable and smoothly increasing, so it is the outlet temperature that rises and falls to produce the ΔT waveform we observe in Figure 69 above. As noted previously, the outlet thermocouple is at the elbow that turns up into

the vertical 4” (100 mm) riser of the hot leg, denoted as the Chimney. There is also another thermocouple at the top of the Chimney before the SS elbow that turns the flow horizontal again, as pictured in Figure 70 below.

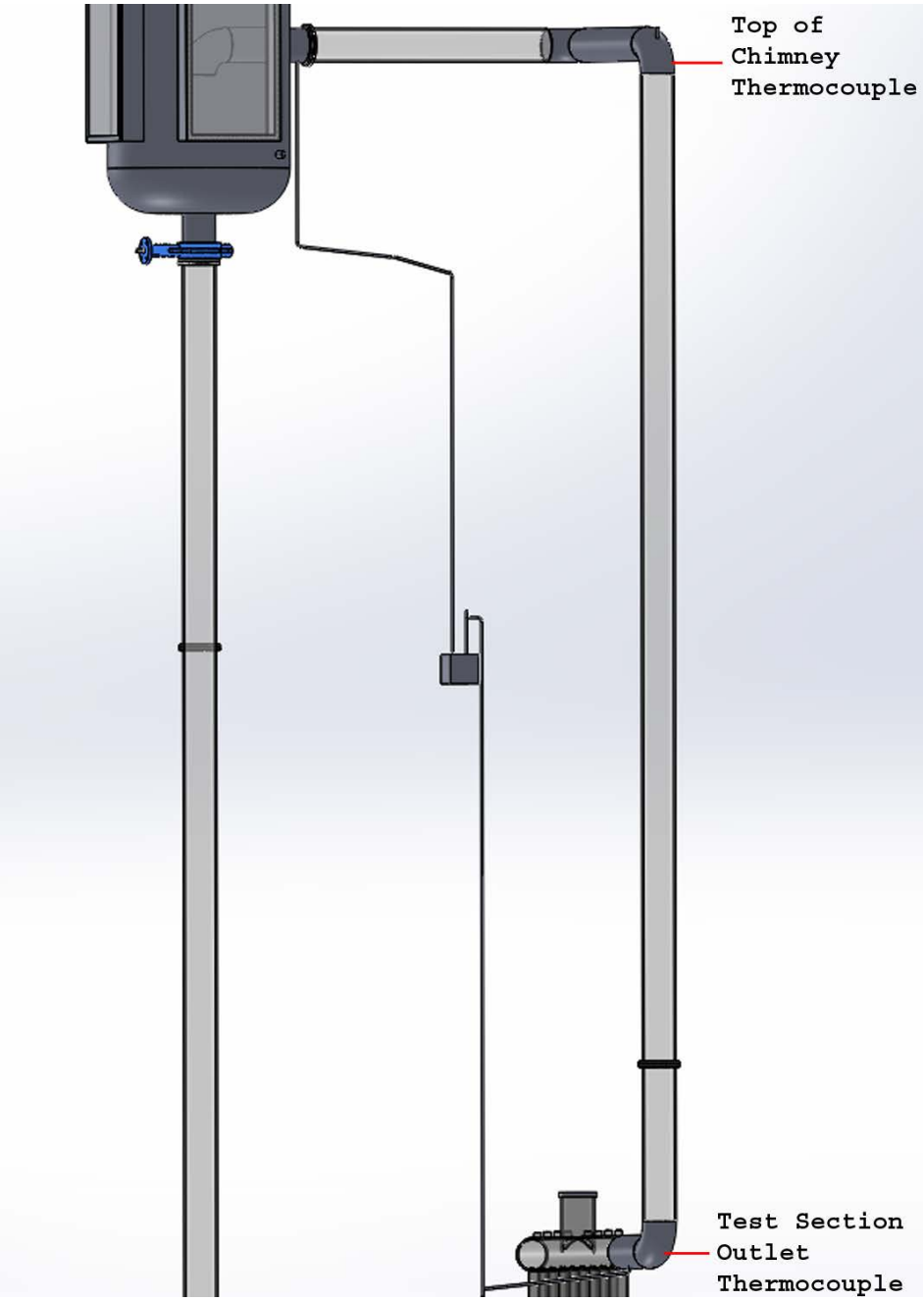


**Figure 70.** Relative Location of Thermocouples in the Chimney and Test Section Outlet

Noting that whatever temperature changes are seen by the Test Section Outlet thermocouple in the form of sudden spikes or dips should propagate up to the Chimney thermocouple with the same shape, it stands to reason that the average flow velocity during the time between the capturing of the event by the two thermocouples can be calculated by dividing the distance between the t/c's by that time difference and multiplying by the Chimney's cross-sectional area. The temperature curves for these two thermocouples are plotted in Figure 71 below.

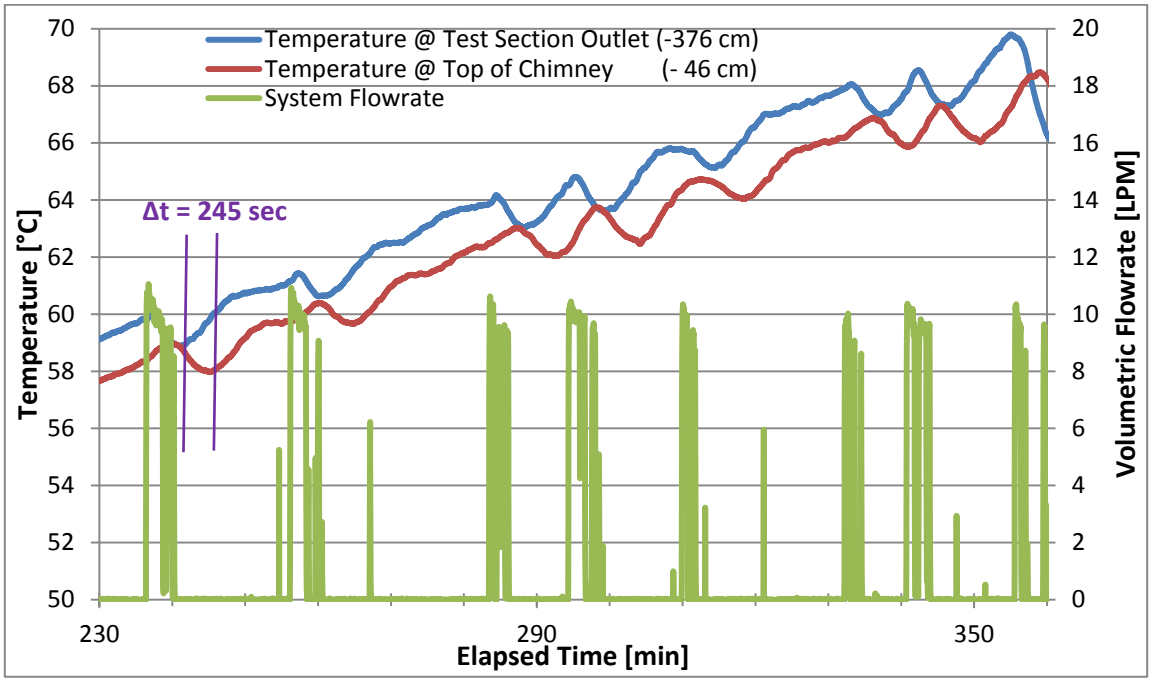


**Figure 71.** Flow Surges seen in the Partially Throttled – 20 Series of Experiments

Note that the low point seen during the first excursion by the outlet thermocouple is seen 245 seconds later by the thermocouple at the top of the Chimney. As the thermocouples are $-46-(-336)=330\,cm$ apart, the average flow velocity over these 4 minutes was 1.328 cm/sec. With these numbers the flowrate calculates out to 6.258 LPM. This value appears reasonable by noting the rate of decay of the flowrate as read

by the magmeter before the signal dropped out. Note that the -46 and -376 cm values are the depths of the thermocouples below the water line in the storage tank.

It is not currently known why the flow ebbs and surges in this manner with the butterfly valve partially closed. The way a butterfly valve works is it only allows flow around the outside edge of the pipe, so it could be that there is an accumulation of the Cospheric particles around this perimeter, slowing the flowrate until increased buoyancy forces created by the excess ΔT in the Test Section create enough force to purge them out.

Alternatively, it will be noted in Chapter 5 that over time, non-condensable gases diffuse out of the liquid water and accumulate in the horizontal section of piping that enters the storage tank on the hot leg side. This accumulation eventually blocks the flow of water, and it is possible that this was occurring on a small scale during the 20 Series experiments. The accumulation of gas in the horizontal leg was not under observation during the experiment so it is not known how much gas, if any, may have accumulated in the Tank Return Line.

*IV.2.2.3 Fully Throttled Experimental Results (21 Series)*

The effect of the flowrate slowing down over time and ΔT subsequently increasing was multiplied in the Series 21 experiments, as noted in the specific example of Experiment 210 in Figure 72 below. There is not any flow data from the magmeter during either test, but a few observations can still be made from the temperature data.

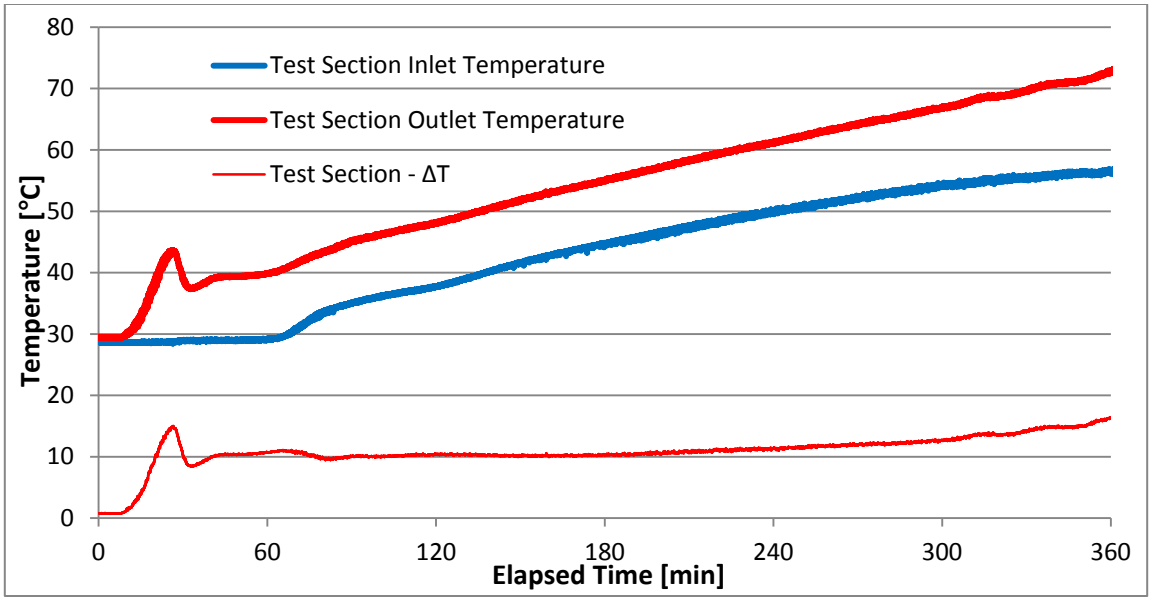


**Figure 72.** Test Section ΔT and Inlet Temperature for Experiment 210

In Figure 72, we can see that the ΔT has the familiar spike, fall, and subsequent settling to a steady value through the first 180 minutes that is observed in all the other experiments. It is believed that the flow is also following a similar behavior, and the following methodology can give us an estimate of the flowrate during the time from approximately 45 to 180 minutes elapsed time (E.T.).

Recall that the ratio of the flowrates was approximately equal to the ratio of the Test Section ΔT's between the 00 Series and 20 Series of experiments. Assuming this relationship continues with higher amounts of flow throttling, the flowrate after startup but before 180 minutes elapsed time should be approximately 6.3 LPM based on an average ΔT of 10.2 °C. After this time, a blockage of the flow begins to occur, likely for the same reasons as in the 20 Series experiments, and ΔT begins to rise. In both experiments of the 21 Series, however, the surging of flow is not seen, and the temperature difference simply keeps increasing. This is likely due to the fact that the butterfly valve had to be nearly completely closed in order to achieve the desired ΔT across the Test Section.

As such, any future experiments looking specifically to achieve an alternate ΔT across the Heated Cavity (while keeping the Total Heater Power level the same) will need to determine an alternative method of introducing a minor loss in the flowpath that still allows for flow to continue through the system.

## IV.3 Analysis of the Flow Distribution in the Cooling Panel

### IV.3.1 Description of the Experimental Procedure

As mentioned previously, there are 9 risers in the Cooling Panel, and ports and transducer mounts were installed on 8 of them (all except the center). Since only 6 high temperature transducers were on loan from the University of Idaho, it was decided to repeat each experiment once, moving 2 of the transducers in the process to obtain measurements for the missing spots. Data for Riser #5 would be unobtainable via UVP. It was decided to permanently keep transducers at Risers #1, 4, 6, and 9, and to have one transducer on either Riser #2 or 3 and one at Riser #7 or 8 at all times for symmetry.

After startup and particle injection, 3 consecutive sets of velocity profiles were taken every time the Test Section Inlet Temperature increased an additional 5 °C, starting at 30°C. The Reference Velocity was then processed from each profile. The methodology of determining the Reference Velocities from the velocity profiles for use in comparing the flow distributions in the Cooling Panel is described in Chapter III. Therefore, after both experiments in the series were finished there were six Reference Velocities obtained for risers #1, 4, 6 and 9, and three Reference Velocities for risers #2, 3, 7, and 8, at each inlet temperature. An example of the results obtained for a single inlet temperature for a single experimental series is illustrated in Figure 73 below.

After all the reference velocities for the series were obtained, the results (such as those seen in Figure 73) were averaged together to give a single Average Reference Velocity for each riser at each inlet temperature sampled. The relative values of the Average Reference Velocities define the flow distribution for the purposes of this thesis.

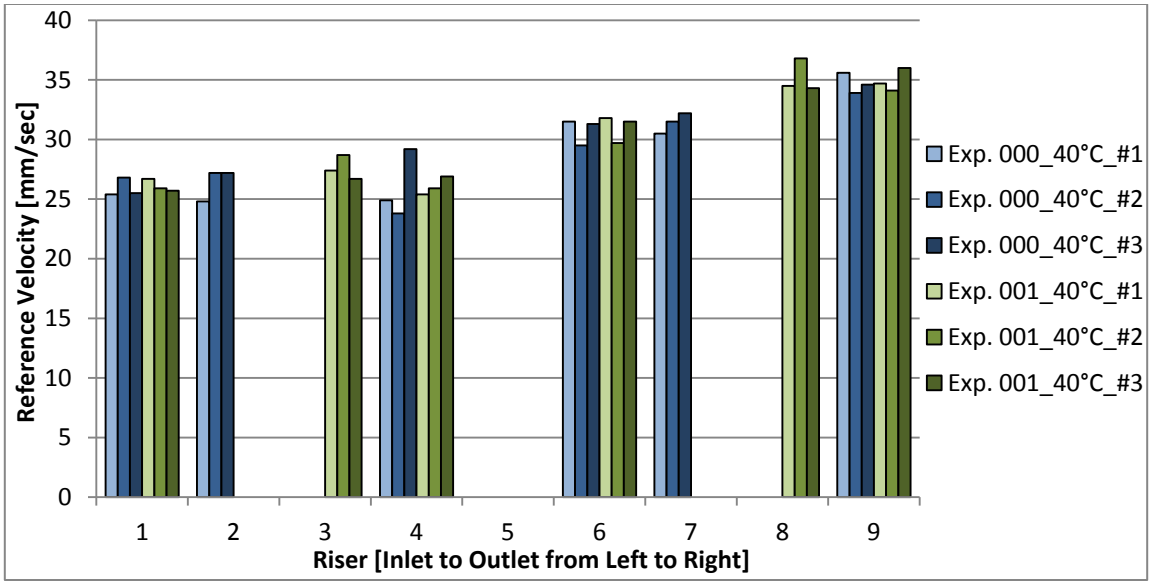


**Figure 73.** Example of Reference Velocity Measurements at a single Inlet Temperature for both Experiments in an experimental Series

It can be seen from Figure 73 that the Reference Velocities were very consistent, with only the third measurement made on Riser #3 during Experiment 000 looking out of place relative to the others for its riser. To quantify the degree of consistency, the percent deviation of each individual measurement from the average of the remaining measurements for that riser and temperature was calculated for all Reference Velocities taken for the series. Statistics showing the number of measurements in a series that deviate less than 10% from the remaining average will be provided along with the total number of measurements for each series. In total, 444 measurement sets were taken over 17 days of testing; with 6 transducers in each set a total of 2664 Reference Velocities were processed. All measurements were used for calculating the Average Reference Velocities which provide the flow distributions, except where noted.

IV.3.2 Reference Case (Series 00) Experimental Results

The total heater power level used in the reference case was 6 kW, which was derived from theoretical prototype reactor via the scaling laws developed by ANL [3]. The power was split evenly among the 3 heaters, the coolant level was to the top of the visualization window as seen on the left side of Figure 68, yielding a total system inventory of approximately 402.2 liters, and the flow was unrestricted. Velocity profiles were taken every 5 °C from 30 to 70 °C; the resulting flow distributions are condensed into Figure 74 below. 324 individual readings were taken over the course of both experiments; 314 (96.9%) of which were within 10% of the average of their fellow readings.

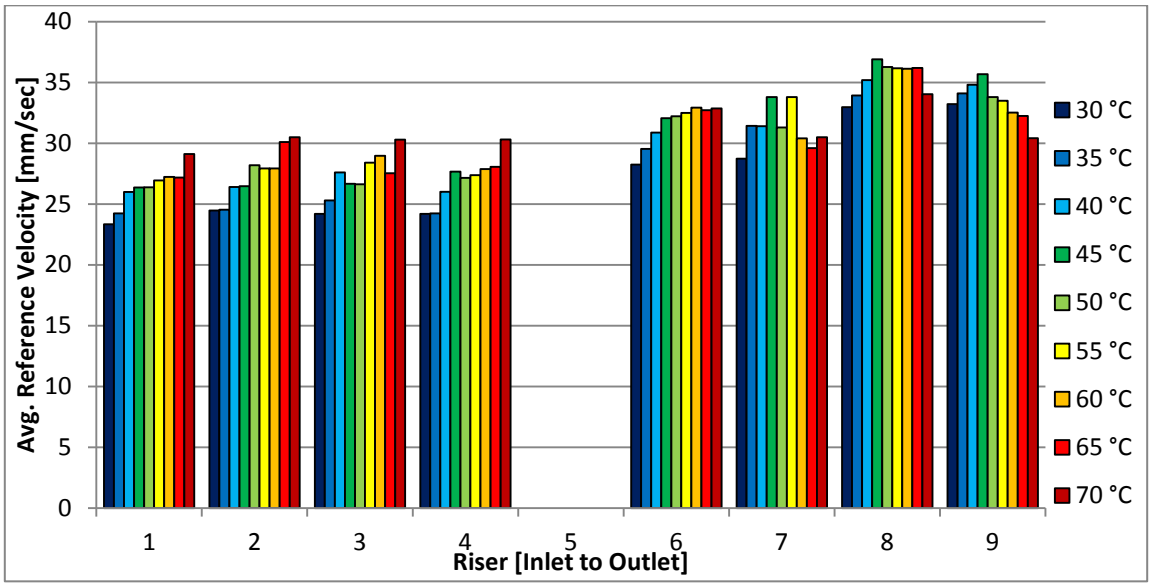


**Figure 74.** Flow Distribution across the Cooling Panel for the Reference Case (00 Series)

It is noted that the relative values between risers at any one temperature appear to be consistent. It also appears that the fluid's momentum carries more of the flow to the latter half of the manifold which is towards the outlet side. This result was expected from visual observation of the particles flowing in the pipe while the test was being

conducted. Finally, as the temperature increases the flow velocities generally increase as well (except Riser #9). This follows from the increasing volumetric flowrate as read by the magmeter over the course of the experiment. The UVP results can be compared directly to the magmeter by making two assumptions:

1. The Average Reference Velocity for the Riser represents the average cross-sectional flow velocity through the Riser
2. The Average Reference Velocity for Riser #5 is the simple average of the values for Riser #4 and Riser #6

With these two assumptions, it is a trivial matter to multiply each flow velocity by the riser's cross-sectional area and then sum the results to obtain the system flowrate. Results for Series 00 are presented against the magmeter readings for both experiments in Figure 75 below.

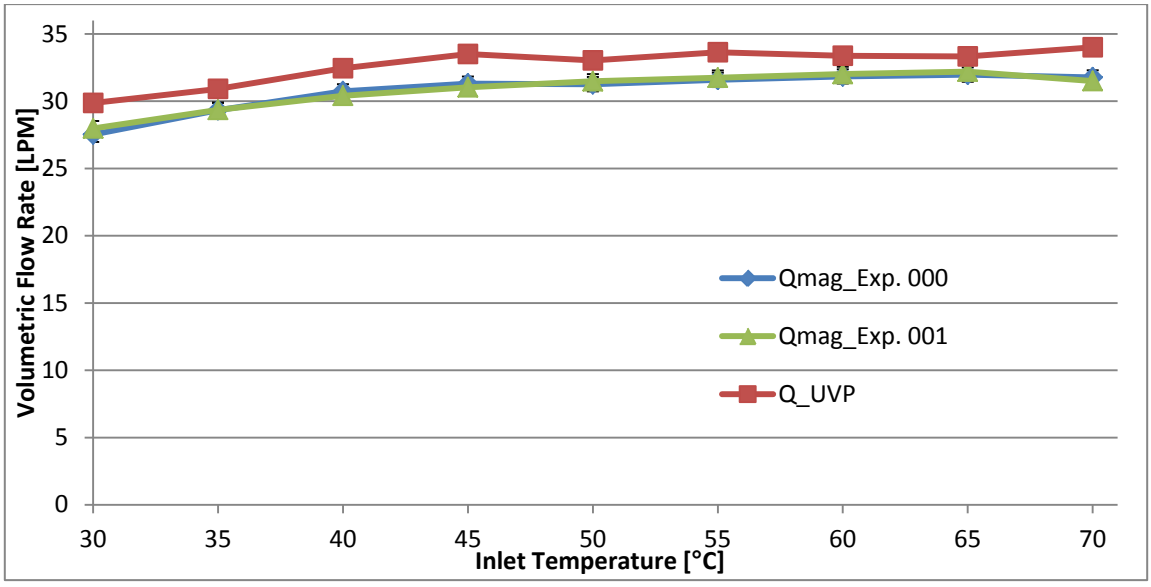


**Figure 75.** System Flow Balance for the Reference Case (00 Series) – UVP and Magmeter

It is noted that the system flowrates obtained via UVP are within 7.6% of the average of the two magmeter readings at each temperature. The trend of UVP derived results also follows the same increasing pattern as the magmeter. Both observations indicate that the assumptions made are generally valid.

A second type of 'sanity check' can be made in a similar manner by looking at the total power absorbed in the Cooling Panel by summing the power absorbed in each individual riser tube, and comparing the total to the absorbed power level as determined earlier using the data from the magmeter and Test Section inlet and outlet thermocouples. This would use an equation of the same form as Equation 1 earlier, but modified slightly to redefine certain nomenclature as in Equation 6 below.

$$P_{abs} = \sum_{i=1}^{9} Q_{UVP}^{i} \rho c_p \Delta T_{R5-R1}^{i} \qquad \text{Equation 6}$$

Here, $Q_{UVP}$ is the flowrate for the individual riser tube using the two assumptions mentioned earlier, and $\Delta T_{R5\text{-}R1}$ is the temperature difference between the thermocouple embedded at the top of the riser, designated as Row 5, and the thermocouple at the entrance of the Riser, designated as Row 1. $\Delta T_R$ shall be used to designate the temperature difference for an individual riser, retaining $\Delta T$ with no subscripts to mean the across the Test Section as a whole. For reference, the $\Delta T_R$ distribution across each of the nine risers for the 00 Series of experiments is given in Figure 76 below.

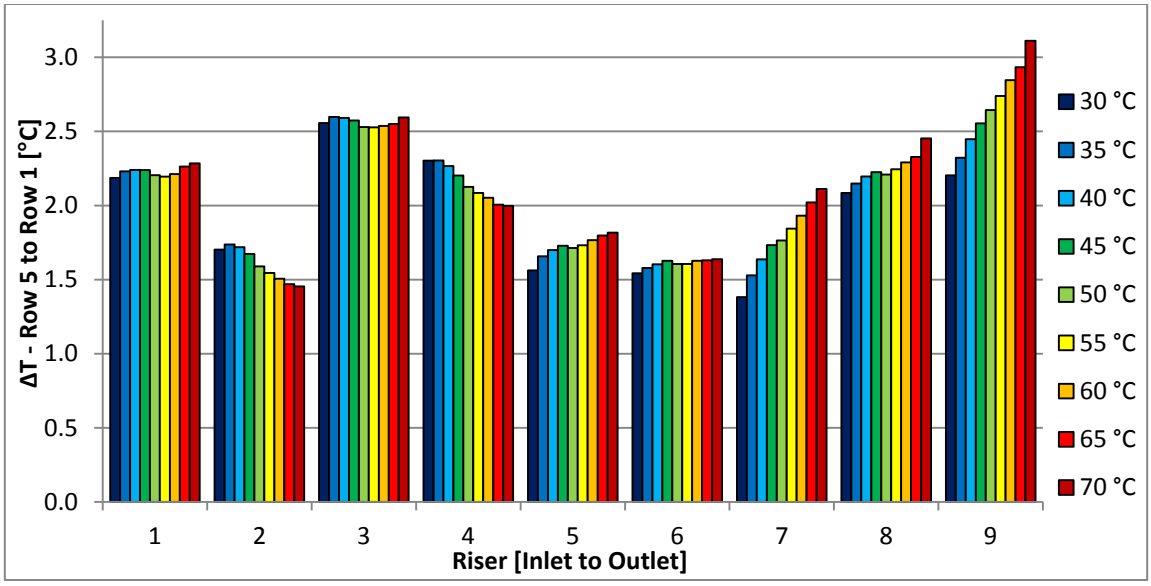


**Figure 76.** $\Delta T_R$ Distribution across the Cooling Panel for the Reference Case (00 Series)

It is apparent that for channels 2, 4, 5, 7, 8, 9 that the $\Delta T_R$ changes significantly over time. The exact reasons for this are unknown, and the author believes that knowledge of the Cooling Panel surface temperature distribution would be required to investigate further. It could be that it is simply drift in the Data Acquisition system. In any case the resulting power absorption rate in each individual riser tube is presented in Figure 77 below for reference.

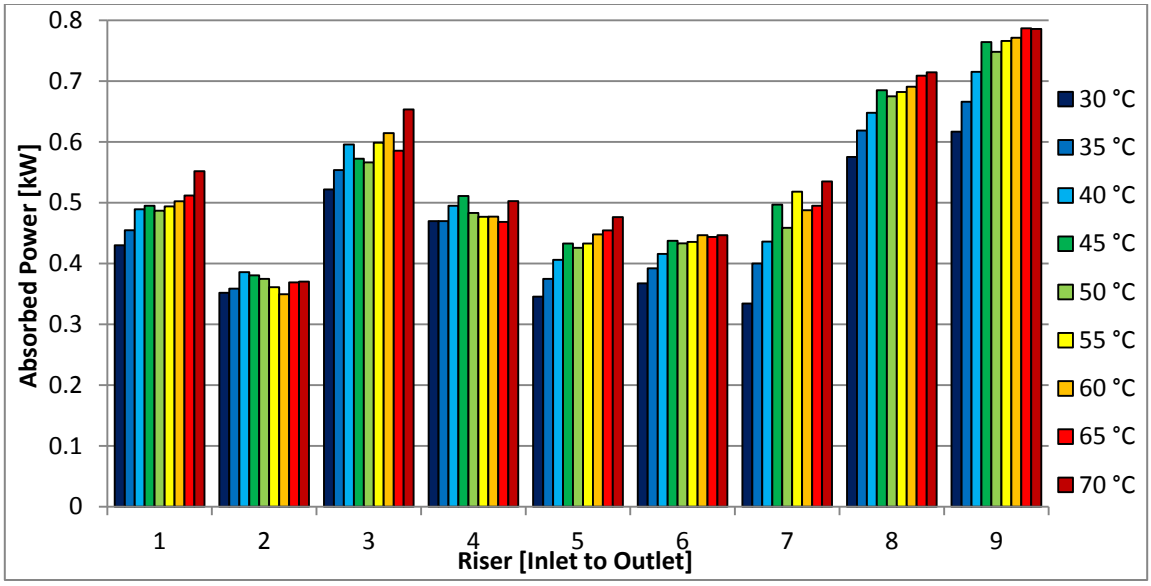


**Figure 77.** Distribution of the Power Absorption across the Cooling Panel for the Reference Case (00 Series)

It is noted in Figure 77 that the $\Delta T_R$ distribution from Figure 76 dominates the power absorption distribution, as opposed to the flow distribution seen in Figure 74. Again at this point it would be most desirable to have the surface temperature data to further analyze why the distribution is this way, especially considering that the same amount of electrical power is being sent to each heater in the cavity. In any event, after summing up the values at each riser using Equation 6, and using Equation 1 to calculate comparison values using the magmeter and Test Section thermocouples, the results are in Figure 78 below for each inlet temperature sampled.

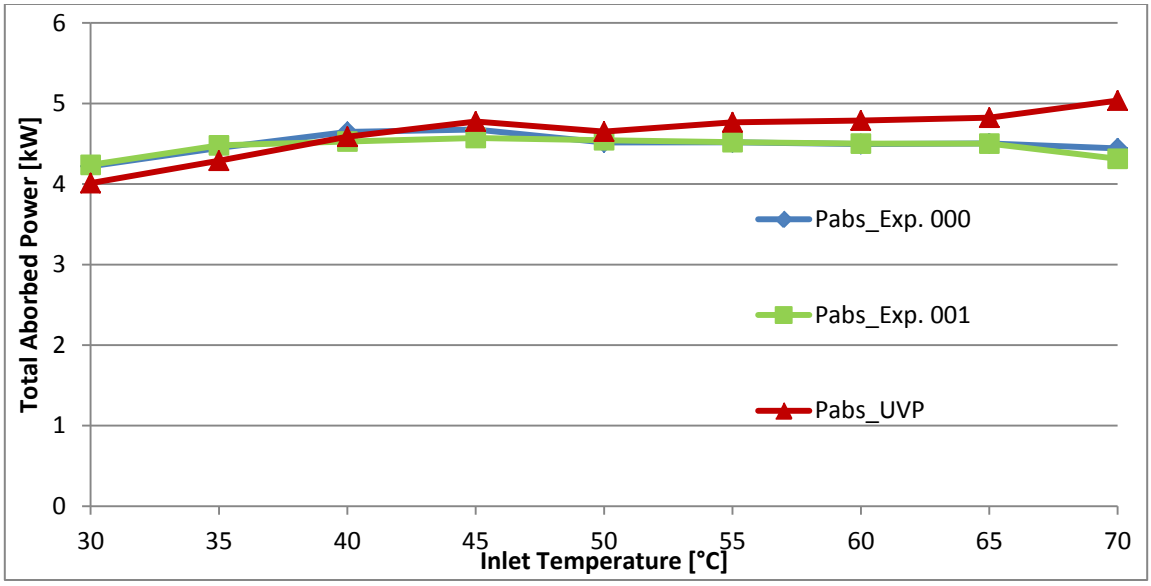


**Figure 78.** Balance of the Total Absorbed Power in the Cooling Panel for the Reference Series – Sum of Individual Risers to Test Section

The percent difference between the values calculated by the UVP and the averages of the mag-derived values is less than 7.1% for all points, except at 70 °C where it is +15%. This level of consistency is exceptional given the fact that the flowrate is being calculated via two different measurement technologies, and multiple different thermocouple sets were used to measure temperature differences that are in fact smaller in magnitude than the published accuracy of a Type-K thermocouple.

This completes the range of analysis completed for the 00 Series. The rest of this chapter will present similar figures showing the same types of results as seen here for the remaining experimental series (with the addition of PIV results which were not performed for the 00 Series). Where appropriate, a summary of the effects of varying the power level, heat flux profile, flow throttling and level variations will be made as well.

IV.3.3 High Power Case (10 Series) Experimental Results

This test was run with the total heater power level close to the maximum allowed by the temperature limits of the heaters, which from private correspondence with the heater supplier is 760 °C. At 9.6 kW this represents a 60% increase in power from the 00 Series. The power was split evenly among the 3 heaters; all other parameters were the same as the Reference Case. Velocity profiles were taken every 5 °C from 30 to 70 °C; the resulting flow distributions are condensed into Figure 79 below. 324 individual readings were taken over the course of both experiments; 320 (98.8%) of which were within 10% of the average of their fellow readings.

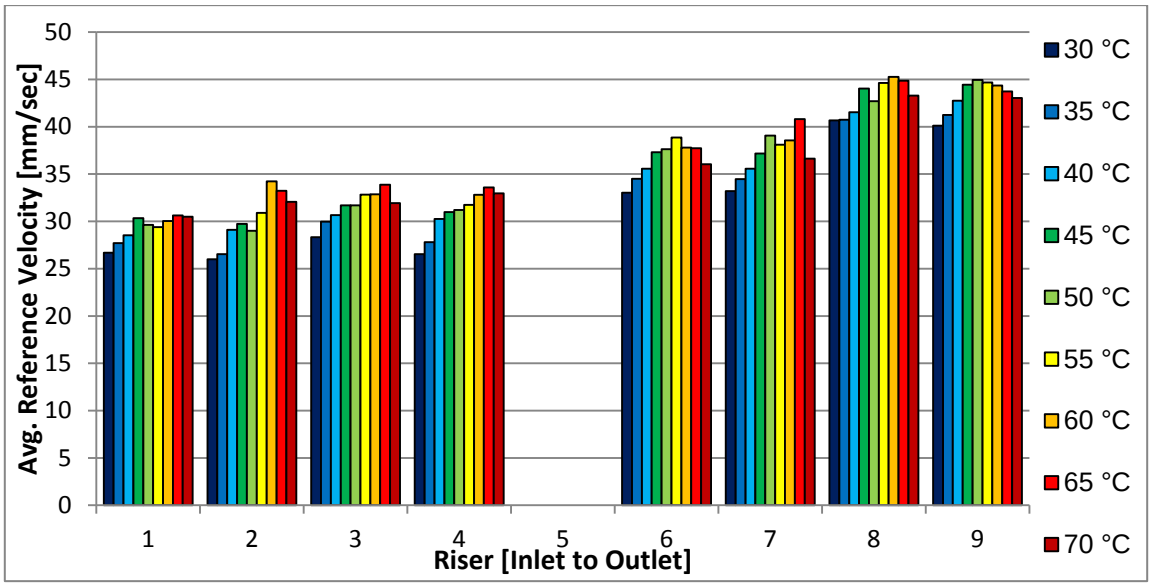


**Figure 79.** Flow Distribution in the Cooling Panel for the High Power Case (10 Series)

Again it is noted that the relative values between risers at any one temperature appear to be consistent. There is also an even larger percentage of the total flow going to the Outlet side of the panel, presumably because the flowrate is 30% higher so there is more momentum to force the liquid to that side. This result was expected from visual observation of the particles flowing in the pipe. Again, the velocities generally increase

with temperature, which is reflecting that over time the volumetric flowrate of the system is increasing as well.

PIV measurements at Risers 1 through 8 were acquired during Experiment 100 just before the 55 °C UVP measurement set was taken and are present in Figure 80 below. As compared to the UVP measurements, the Reference Velocities at Risers 1, 2, 3, and 6 are comparable; but the readings at #4 and #7 are significantly higher, and #8 lower. The accuracy of the measurement at Riser #8 is most questionable since it breaks from the general trend observed via the UVP. Perhaps most interesting is that the result for Riser #5 is closer in value to Riser #6 than to a simple average between # 4 and 6.

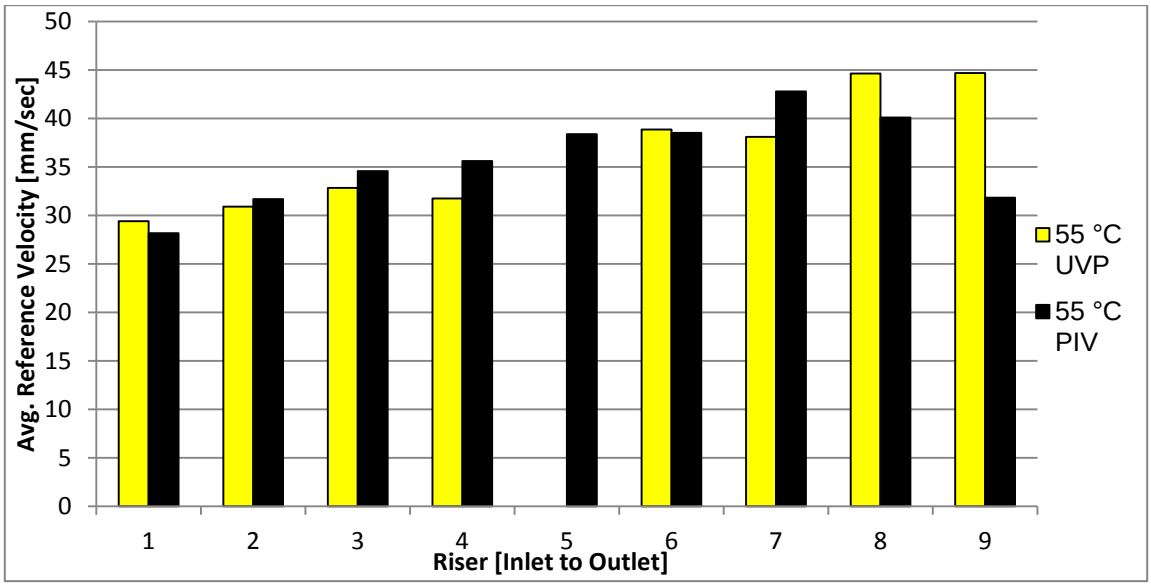


**Figure 80.** Comparison of PIV to UVP derived Reference Velocities for the High Power Case (10 Series)

A summary of the PIV results and statistics are in Table 5 below.

**Table 5.** Statistics for the PIV Analysis of the High Power / 10 Series

| Riser # | Average Velocity [mm/sec] | Combined Line-to-Line Standard Deviation [mm/sec] | Temporal Standard Deviation [mm/sec] | % Difference to UVP Reference Velocity |
|---|---|---|---|---|
| 1 | 28.17 | 2.96 | 2.07 | -4.18 |
| 2 | 31.68 | 3.41 | 1.73 | 2.51 |
| 3 | 34.57 | 2.30 | 1.34 | 5.29 |
| 4 | 35.61 | 2.18 | 1.13 | 12.16 |
| 5 | 38.38 | 2.39 | 1.37 | n/a |
| 6 | 38.51 | 3.36 | 1.75 | -0.92 |
| 7 | 42.79 | 3.32 | 1.67 | 12.31 |
| 8 | 40.10 | 5.96 | 2.37 | -10.16 |
| 9 | n/a | n/a | n/a | n/a |

It is noted in Table 5 that the Spatial and Temporal standard deviations of the analysis of Riser #8 are significantly higher than those from the other riser tubes. This is a further indicator that the data and/or the post-processing did not accurately capture the flow phenomena.

A volumetric comparison of the PIV results to the magmeter cannot be made since data was not obtained for Riser #9. UVP based volumetric flowrate results are compared to magmeter readings for both experiments in Figure 81 below, using the same methodology as described earlier for the 00 Series.

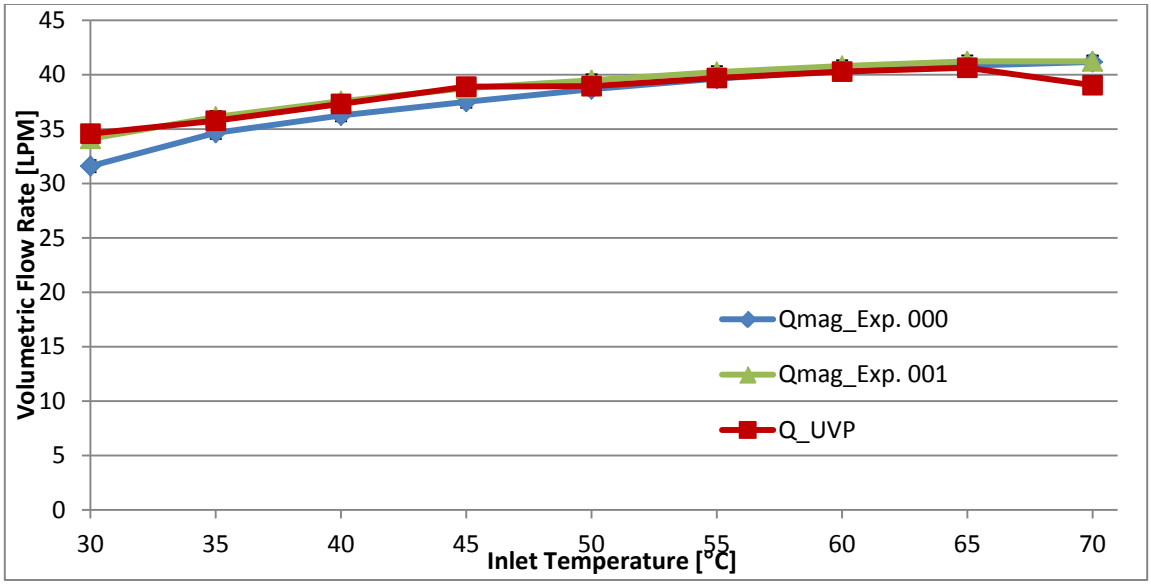


**Figure 81.** System Flow Balance for the High Power Case (10 Series) – UVP and Magmeter

It is noted that the system flowrates obtained via UVP are within 5.3% of the average of the two magmeter readings at each temperature. The trend of UVP derived results also follows the same increasing pattern as the magmeter. Both observations indicate that the results are generally valid. The $\Delta T_R$ distribution is given in Figure 82 below.


**Figure 82.** $\Delta T_R$ Distribution across the Cooling Panel for the High Power Case (10 Series)

As in the results for the 00 Series, it is apparent that in some channels the $\Delta T_R$ changes significantly over time, though not exactly the same ones. The resulting energy absorption rate in each riser tube is presented in Figure 83 below.

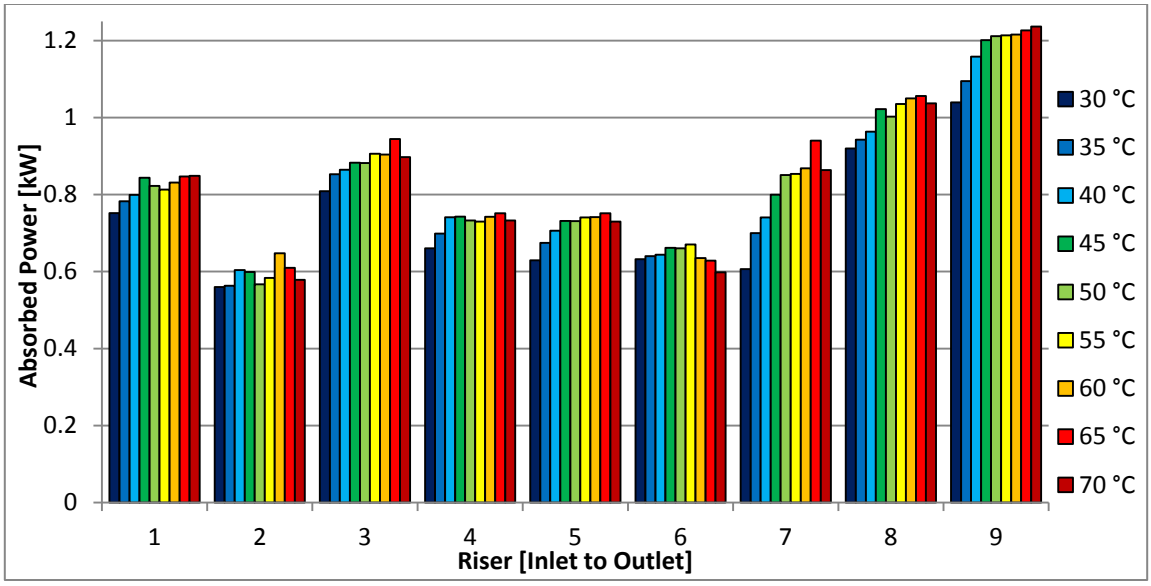


**Figure 83.** Distribution of the Power Absorption across the Cooling Panel for the High Power Case (10 Series)

Again, it is noted that the $\Delta T_R$ distribution dominates the power absorption distribution, as opposed to the flow differences. The comparison of the total absorbed power between the results derived from individual risers and the Test Section as a whole is in Figure 84 below.

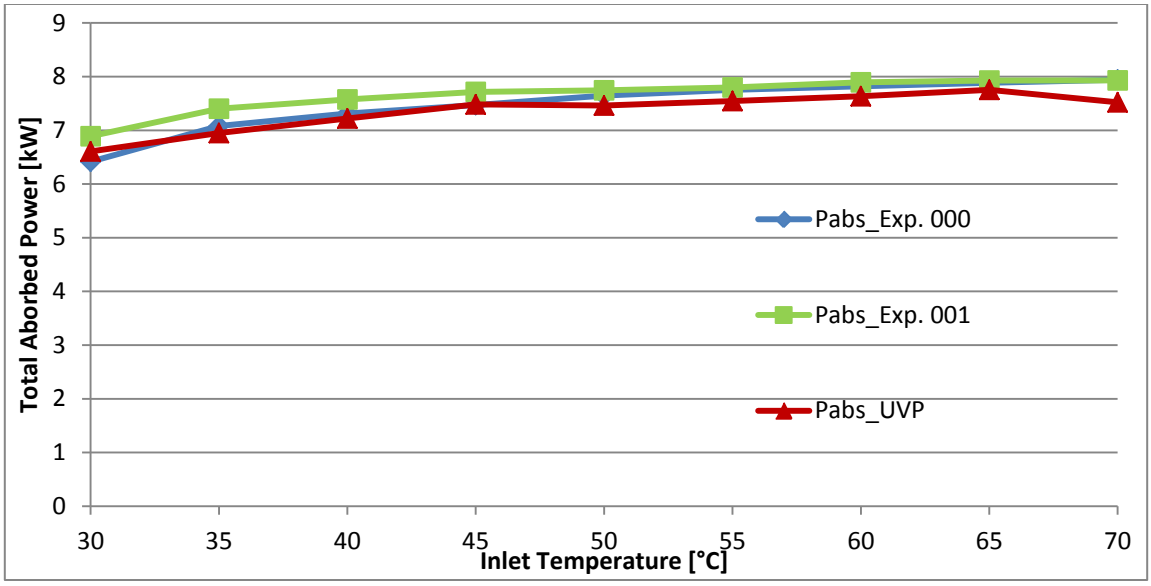


**Figure 84.** Balance of the Total Absorbed Power in the Cooling Panel for the High Power Series – Sum of Individual Risers to Test Section

The percent difference between the values calculated from summing the individual risers and the average of the magmeter derived values is less than 5.2% for all points. The level of consistency for the volumetric flowrate and absorbed power balances is slightly better overall in the 10 Series than the 00 Series.

IV.3.4 Low Power Case (11 Series) Experimental Results

The power level for the low power test was chosen somewhat arbitrarily at 3.6 kW. This represents a 40% decrease in power from the 00 Series. The power was split evenly among the 3 heaters; all other parameters were the same as the Reference Case. Data was taken every 5 °C from 30 to 50 °C; the resulting flow distributions are condensed into Figure 85. The experiments were stopped at 50 °C because the rate at which the water temperature was rising became very small and it was not desired to extend the amount of time to run the experiments. 180 individual readings were taken over the course of both experiments; 178 (98.9%) were within 10% of the average of their fellow readings.

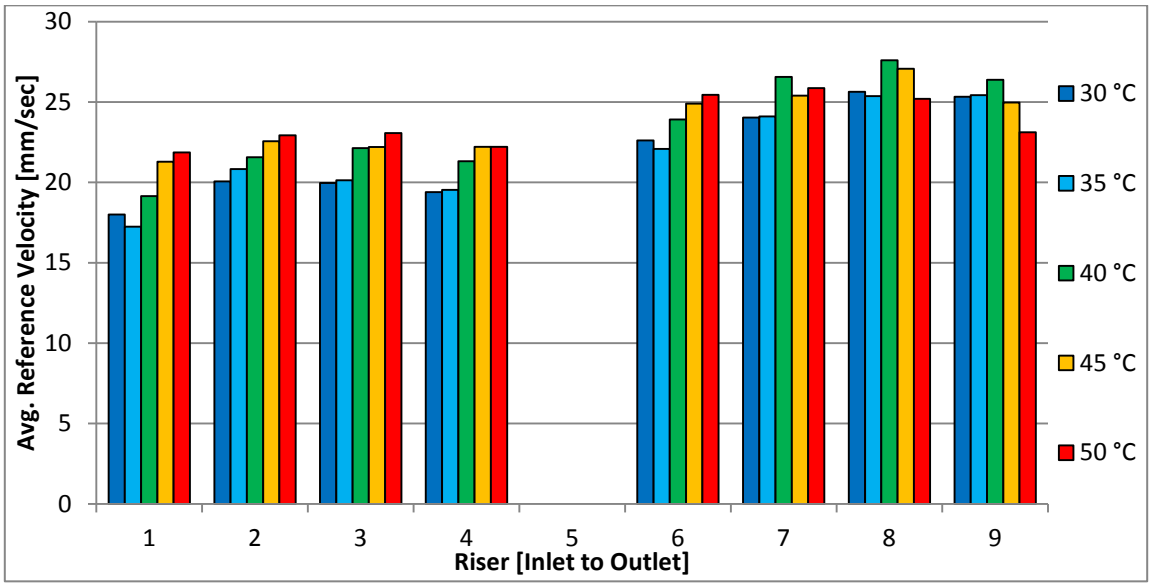


**Figure 85.** Flow Distribution in the Cooling Panel for the Low Power Case (11 Series)

Again it is noted that the relative values between pipes at any one temperature appear to be consistent. The flow distribution is slightly more even than during the 00 Series, the opposite effect as noted in the High Power – 10 Series. This was not unexpected given the lower system flowrate. Changes in flow velocities over

temperature and time appear to reflect the changes in overall flowrate. Overall, the results appear consistent with visual observations of the particles made during the experiment.

PIV measurements at all Risers were acquired during Experiment 111 while the 40 °C UVP measurement set was taken and are presented in Figure 86 below. All measurements are within 7.9% of the UVP values and appear to follow the same general distribution. Again the result for Riser #5 is closer in value to Riser #6 than to a simple average between # 4 and 6.

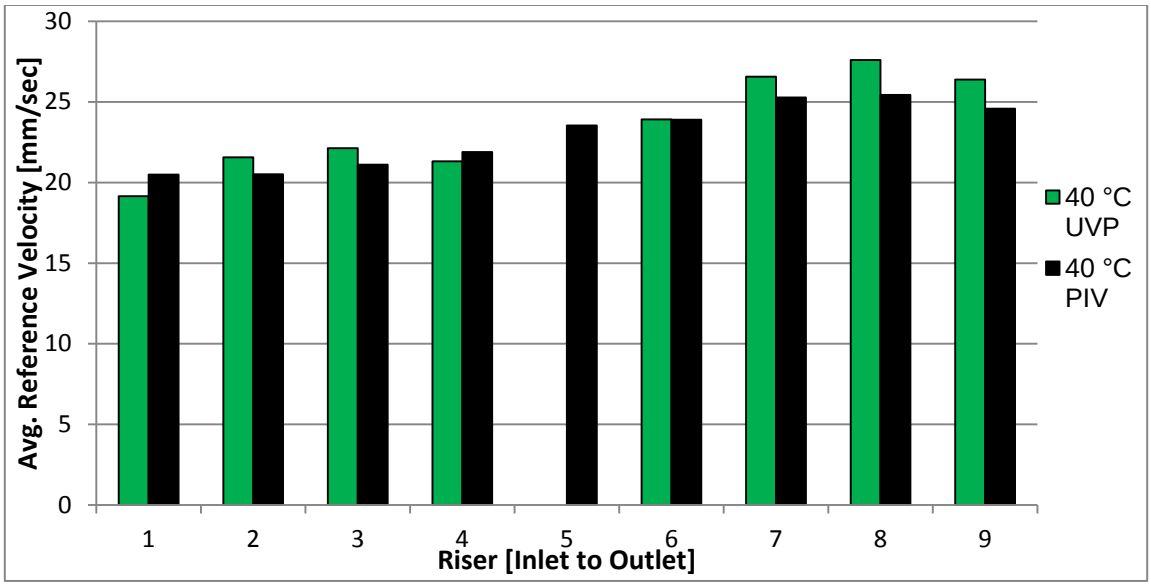


**Figure 86.** Comparison of PIV to UVP derived Reference Velocities for the Low Power Case (11 Series)

A summary of the PIV results and statistics are in Table 6 below.

**Table 6.** Statistics for the PIV Analysis of the Low Power / 11 Series

| Riser # | Average Velocity [mm/sec] | Combined Line-to-Line Standard Deviation [mm/sec] | Temporal Standard Deviation [mm/sec] | % Difference to UVP Reference Velocity |
|---|---|---|---|---|
| 1 | 20.49 | 1.26 | 0.76 | 7.02 |
| 2 | 20.51 | 1.49 | 0.87 | -4.90 |
| 3 | 21.11 | 1.29 | 0.8 | -4.61 |
| 4 | 21.90 | 1.32 | 0.72 | 2.72 |
| 5 | 23.54 | 1.50 | 0.74 | n/a |
| 6 | 23.89 | 0.99 | 0.66 | -0.10 |
| 7 | 25.27 | 1.54 | 0.71 | -4.86 |
| 8 | 25.43 | 1.84 | 0.90 | -7.86 |
| 9 | 24.58 | 2.33 | 1.40 | -6.82 |

A volumetric comparison of the PIV results to the magmeter shows that the PIV reading was within 7.8% of the magmeter's reading during Experiment 111. UVP and PIV based volumetric flowrate results for the 11 Series are presented against the magmeter readings for both experiments in Figure 87 below.

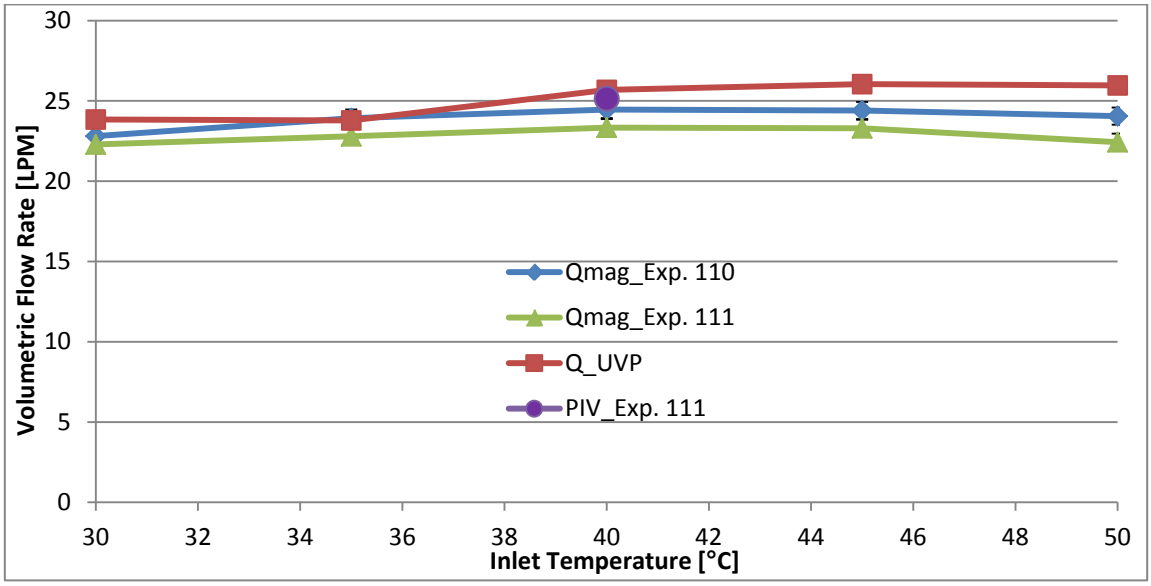


**Figure 87.** System Flow Balance for the Low Power Case (11 Series) – UVP, PIV and Magmeter

It is noted that the system flowrates obtained via UVP are within 11.75% of the average of the two magmeter readings at each temperature. The trend of UVP derived results also follows the same increasing pattern as the magmeter. Both observations indicate that the results are generally valid. The $\Delta T_R$ distribution is given in Figure 88 below.

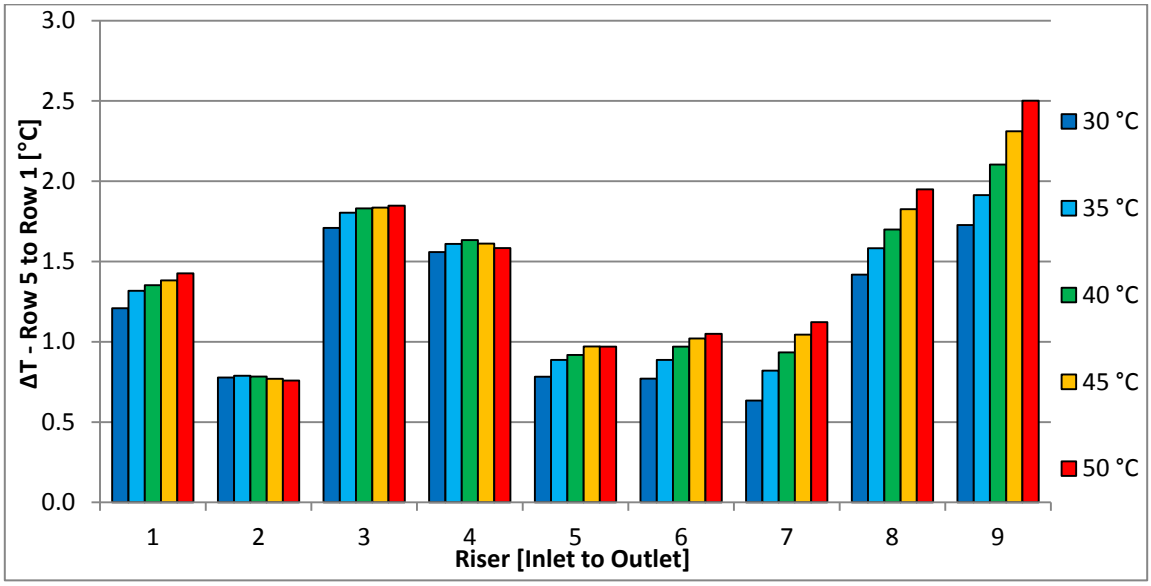


**Figure 88.** $\Delta T_R$ Distribution across the Cooling Panel for the Low Power Case (11 Series)

Temperature drifts are seen at several risers, and again it is the outlet risers, especially riser #9, that have the greatest changes over time. The resulting heat transfer rate in each riser tube is presented in Figure 89 below.

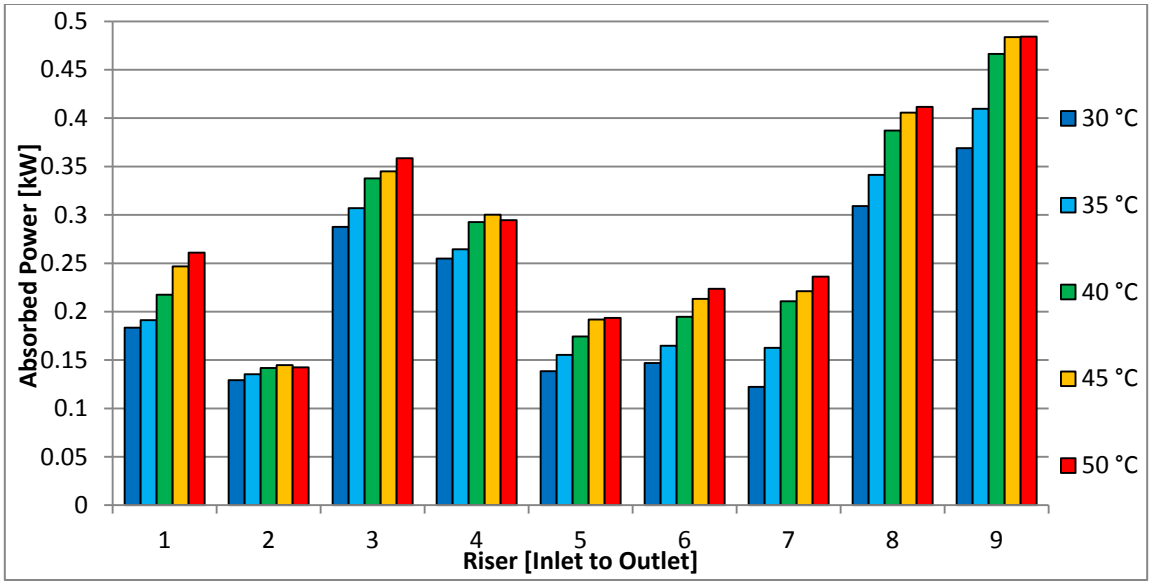


**Figure 89.** Distribution of the Power Absorption across the Cooling Panel for the Low Power Case (11 Series)

Again, it is noted that the $\Delta T_R$ distribution dominates the power absorption distribution. The comparison of the total absorbed power between the results derived from individual risers and the Test Section as a whole is in Figure 90 below.

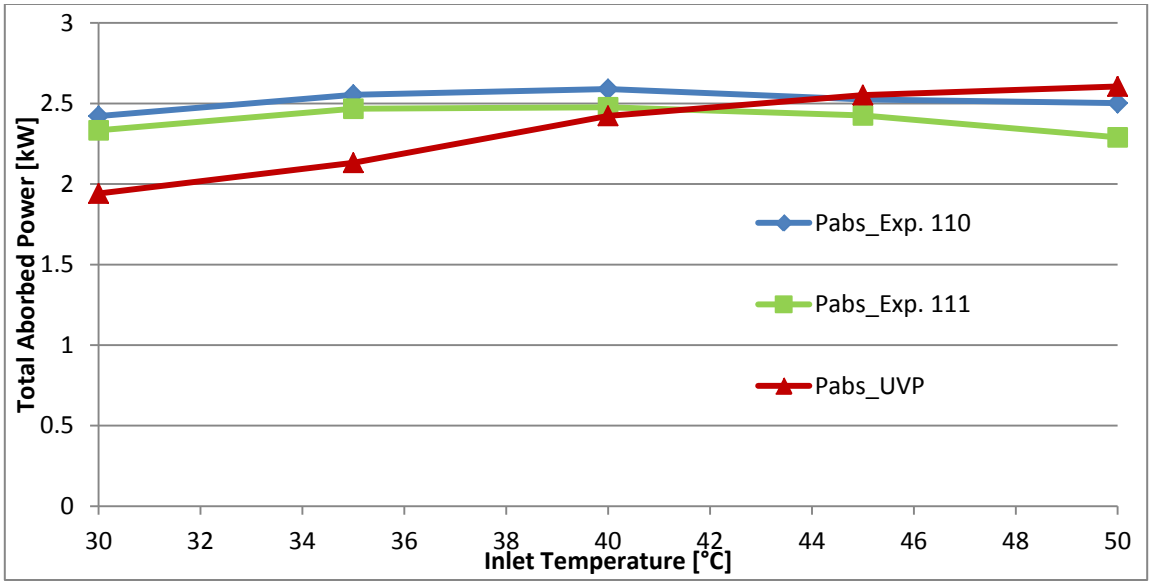


**Figure 90.** Balance of the Total Absorbed Power in the Cooling Panel for the Low Power Series – Sum of Individual Risers to Test Section

The percent difference between the value calculated from summing the individual risers and the average of the magmeter derived values is between -18.4 to 8.9% for all points, reaching as close as 2.3%. The level of consistency for the volumetric flowrate and absorbed power balances is worse for this series than for the 00 and 10 Series. One possible reason for this is the simple fact that the flowrates and temperature differences are so much lower in this series than the others, driving the signal to noise levels down for all instruments involved. This completes the range of analysis completed for the 10 Series.

IV.3.5 Survey of Effect of Power Level on the Flow Distribution

To give a general understanding of the effect of changing power levels on the flow distribution, the Reference Velocities for the 00, 10, and 11 Series of experiments are shown at the common Coolant Temperature of 50 °C in Figure 91 below. The general shape is similar, except a larger percentage of the flow goes to the outlet side of the Cooling Panel as the total power level increases. Higher power levels coincide with higher system volumetric flowrates, so it is believed to be the effect of increased fluid momentum that causes the flow distribution to skew towards the outlet side.

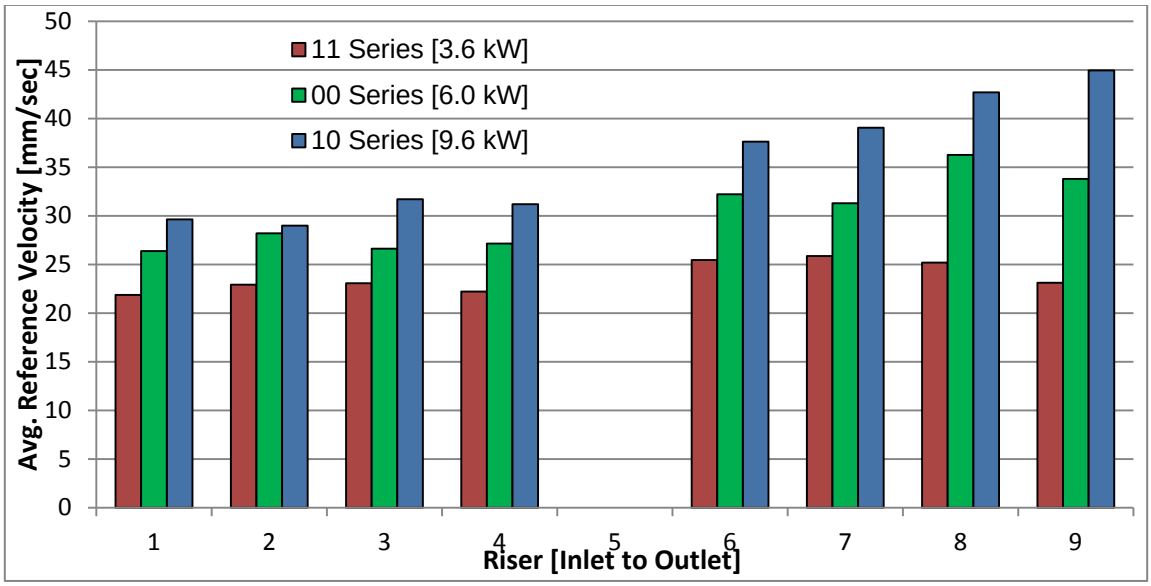


**Figure 91.** Effect of Total Heater Power Level on the Flow Distribution

IV.3.6 Inlet Skewed Power Profile (Series 30) Experimental Results

The total power level for this series was the same as the reference case, but instead of uniformly distributing it at 2 kW per heater, the heater closest to the inlet of the Test Section received 60% increase in power to 3.2 kW, and the heater closest to the outlet received a 60% drop in power to bring it down to 0.8 kW; all other parameters were the same as the Reference Case. Data was taken every 5°C from 30 to 60 °C; the resulting flow distributions are condensed into Figure 92 below. 252 individual readings were taken over the course of both experiments; 250 (99.2%) of which were within 10% of the average of their fellow readings.

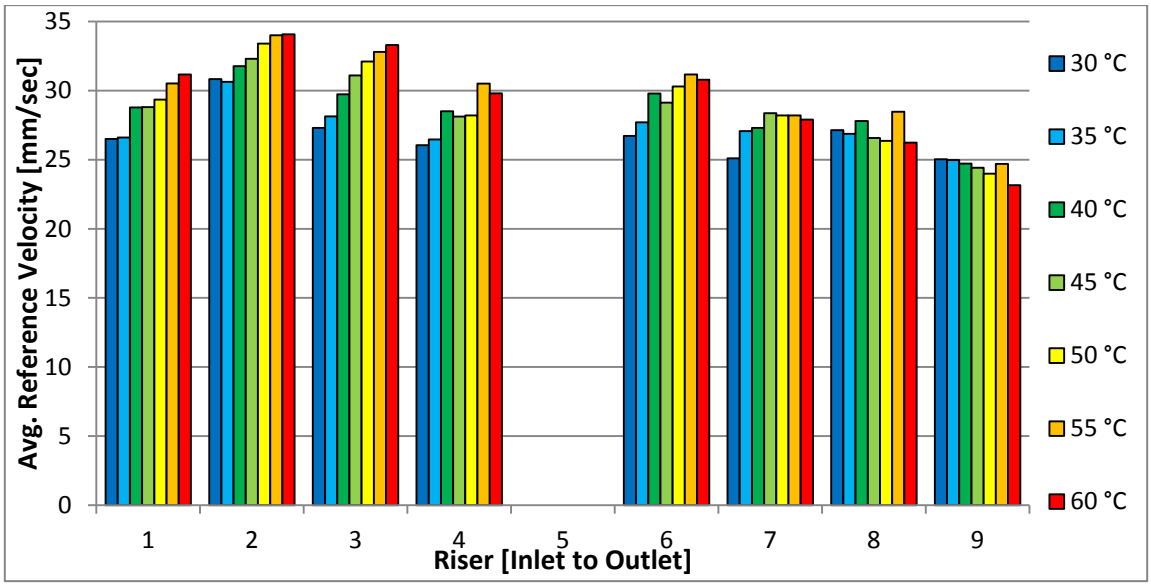


**Figure 92.** Flow Distribution across the Cooling Panel for the Inlet Skewed Power Profile (30 Series)

Again it is noted that the relative values between pipes at any one temperature appear to be consistent. The flow distribution is skewed toward the inlet relative to the 00 Series, in the same manner as the power, which was the expected result. Changes in flow velocities over temperature / time appear to reflect the changes in system flowrate.

Overall, the results appear consistent with visual observations of the particles made during the experiment

PIV measurements at all Risers were acquired during Experiment 300 while the 40 °C UVP measurement set was taken and are presented in Figure 93 below. All measurements are within 9.7% of the UVP values and appear to follow the same general distribution. Again the PIV result for Riser #5 is closer in value to the PIV result of Riser #6 than to a simple average between #4 and 6.

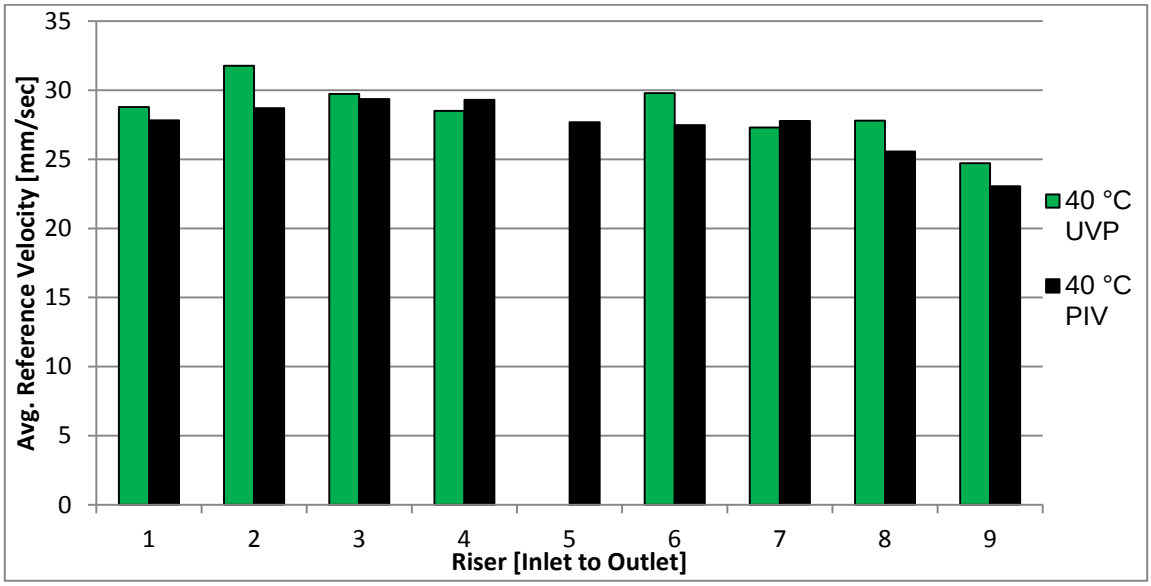


**Figure 93.** Comparison of PIV to UVP derived Reference Velocities for the Inlet Skewed Power Profile (30 Series)

A summary of the PIV results and statistics are in Table 7 below.

**Table 7.** Statistics for the PIV Analysis of the Inlet Skewed / 30 Series

| Riser # | Average Velocity [mm/sec] | Combined Line-to-Line Standard Deviation [mm/sec] | Temporal Standard Deviation [mm/sec] | % Difference to UVP Reference Velocity |
|---|---|---|---|---|
| 1 | 27.82 | 1.91 | 1.21 | -3.34 |
| 2 | 28.70 | 2.24 | 1.71 | -9.64 |
| 3 | 29.36 | 1.83 | 0.96 | -1.24 |
| 4 | 29.30 | 1.93 | 0.94 | 2.79 |
| 5 | 27.68 | 1.85 | 1.57 | n/a |
| 6 | 27.48 | 1.75 | 1.30 | -7.75 |
| 7 | 27.77 | 1.68 | 0.92 | 1.73 |
| 8 | 25.56 | 1.70 | 1.07 | -8.06 |
| 9 | 23.05 | 2.17 | 1.20 | -6.73 |

A volumetric comparison of the PIV results to the magmeter shows that the PIV reading was within 6.1% of the magmeter's reading during Experiment 300. UVP and PIV based volumetric flowrate results for the 30 Series are presented against the magmeter readings for both experiments in Figure 94 below.

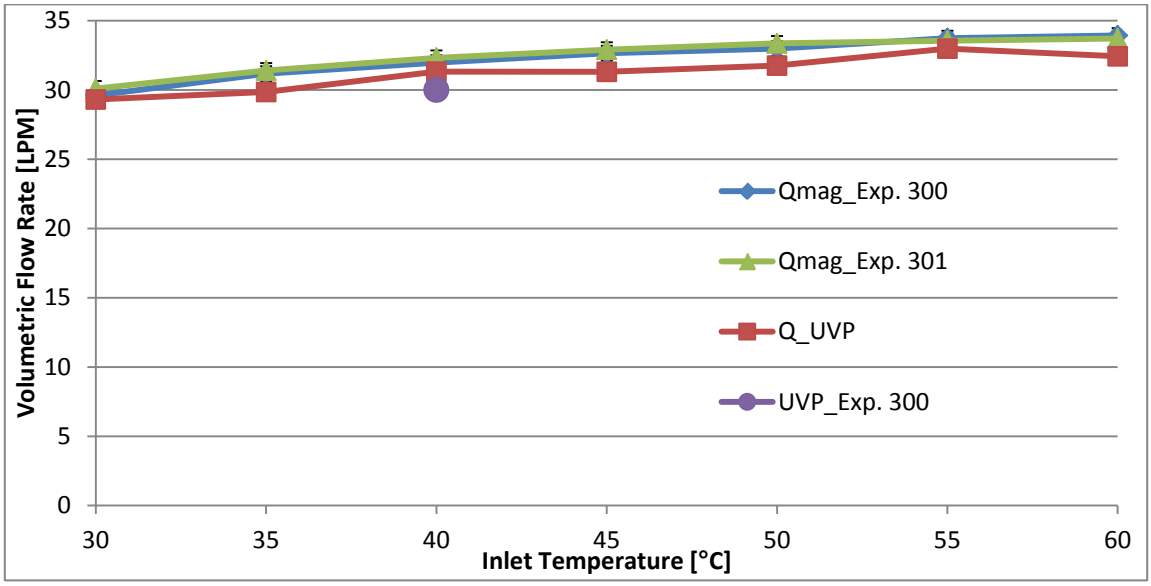


**Figure 94.** System Flow Balance for the Inlet Skewed Power Profile (30 Series) – UVP, PIV and Magmeter

It is noted that the system flowrates obtained via UVP are within 4.6% of the average of the two magmeter readings at each temperature. The trend of UVP derived results also follows the same increasing pattern as the magmeter. Both observations indicate that the results are generally valid. The $\Delta T_R$ distribution is given in Figure 95 below.

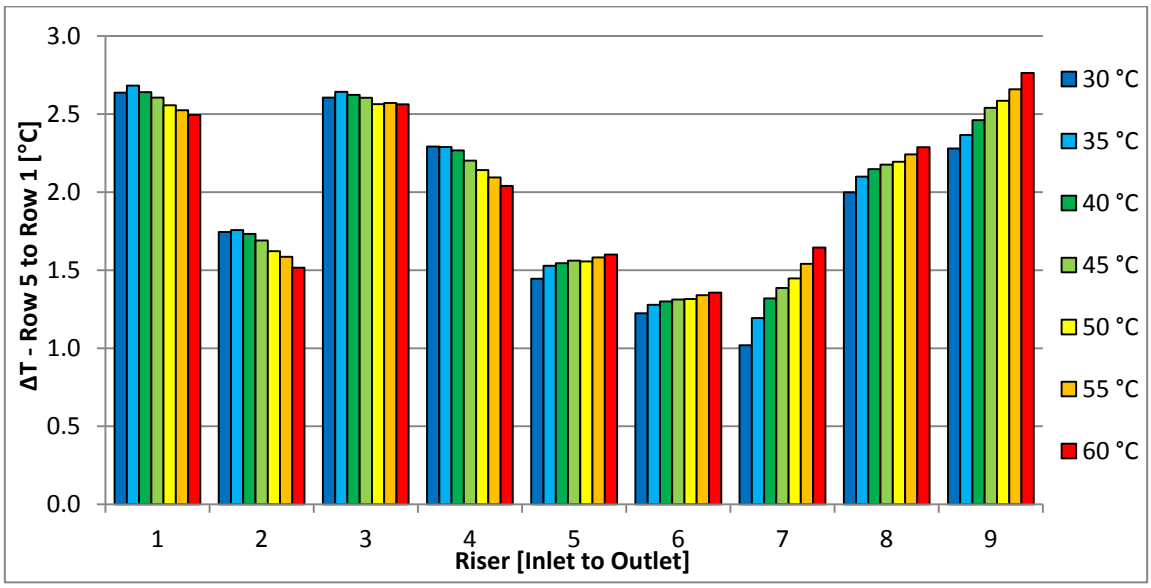


**Figure 95.** $\Delta T_R$ Distribution across the Cooling Panel for the Inlet Skewed Power Profile (30 Series)

Temperature drifts are seen at essentially all risers, decreasing over time/temperature for the first 4 risers and increasing at the rest. The resulting heat transfer rate in each riser tube is presented in Figure 96 below.

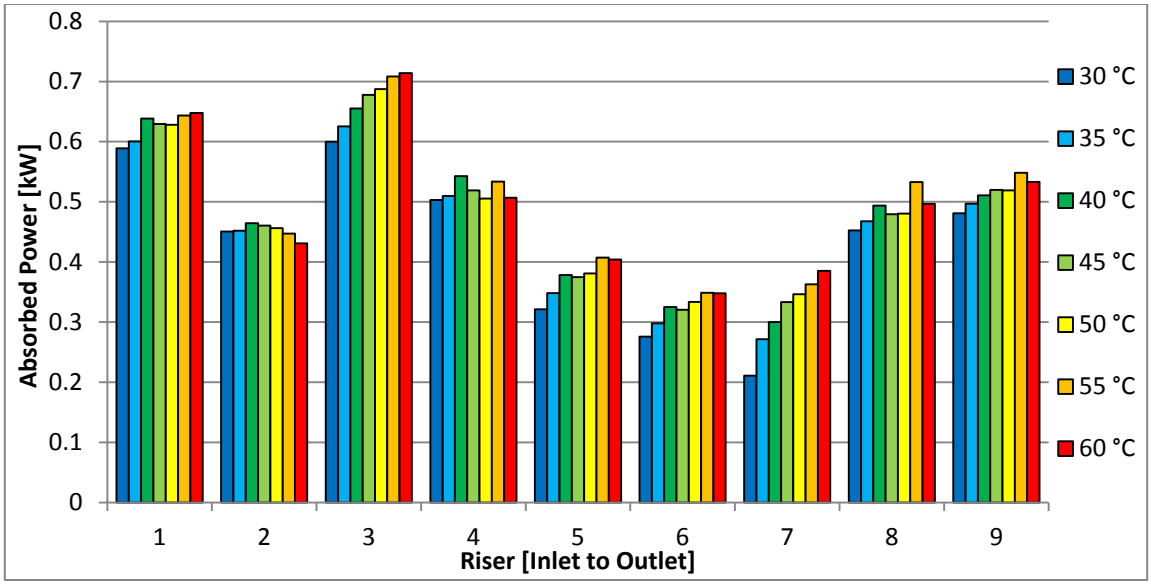


**Figure 96.** Distribution of the Power Absorption across the Cooling Panel for the Inlet Skewed Power Profile (30 Series)

Again, it is noted that the shape of the $\Delta T_R$ distribution essentially defines the shape of the power absorption distribution. The effect of the flow distribution in this case is to scale the values down at the outlet and higher at the inlet. The comparison of the total absorbed power between the results derived from individual risers and the Test Section as a whole is in Figure 97 below.

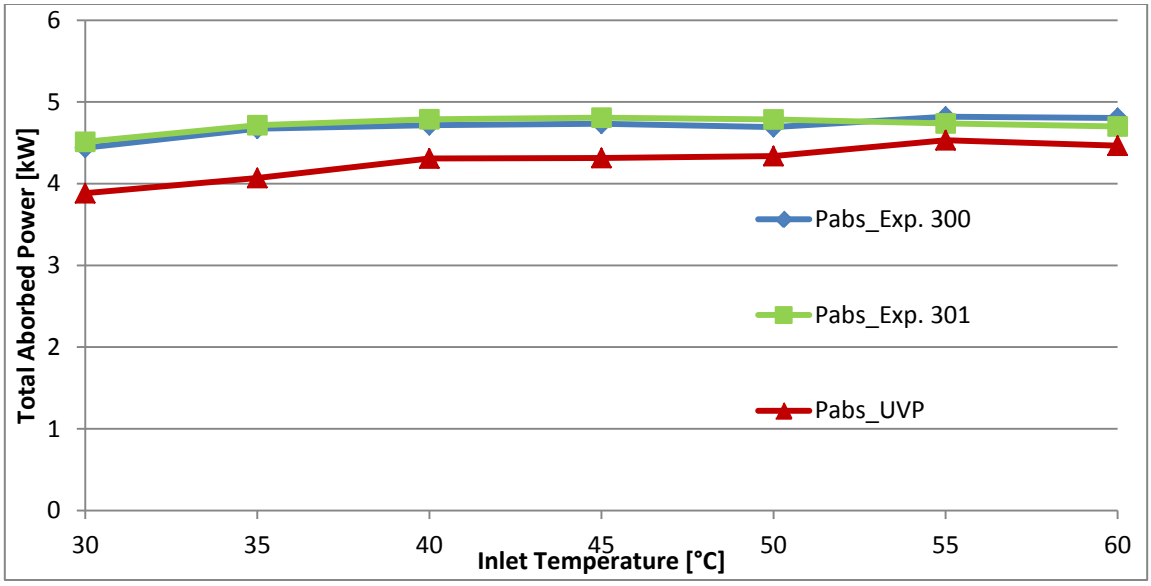


**Figure 97.** Balance of the Total Absorbed Power in the Cooling Panel for the Inlet Skewed Power Profile – Sum of Individual Risers to Test Section

The percent difference between the value calculated from summing the individual risers and the average of the magmeter derived values is between -13.3 to -5.15% for all points. The sum of individual riser results trend in the same manner as those for the Test Section, but they are consistently lower in magnitude. This makes sense since the UVP derived flowrate was also consistently low as compared to the magmeter for both experiments. This completes the range of analysis completed for the 30 Series.

IV.3.7 Outlet Skewed Power Profile (Series 31) Experimental Results

The total power level for this series was the same as the reference case, but instead of uniformly distributing it at 2 kW per heater, the heater closest to the outlet of the Test Section received 60% increase in power to 3.2 kW, and the heater closest to the inlet received a 60% drop in power to bring it down to 0.8 kW (the exact opposite of the 30 Series); all other parameters were the same as the Reference Case. Data was taken every 5°C from 30 to 60 °C; the resulting flow distributions are condensed into Figure 98 below. 252 individual readings were taken over the course of both experiments; 250 (99.2%) of which were within 10% of the average of their fellow readings.

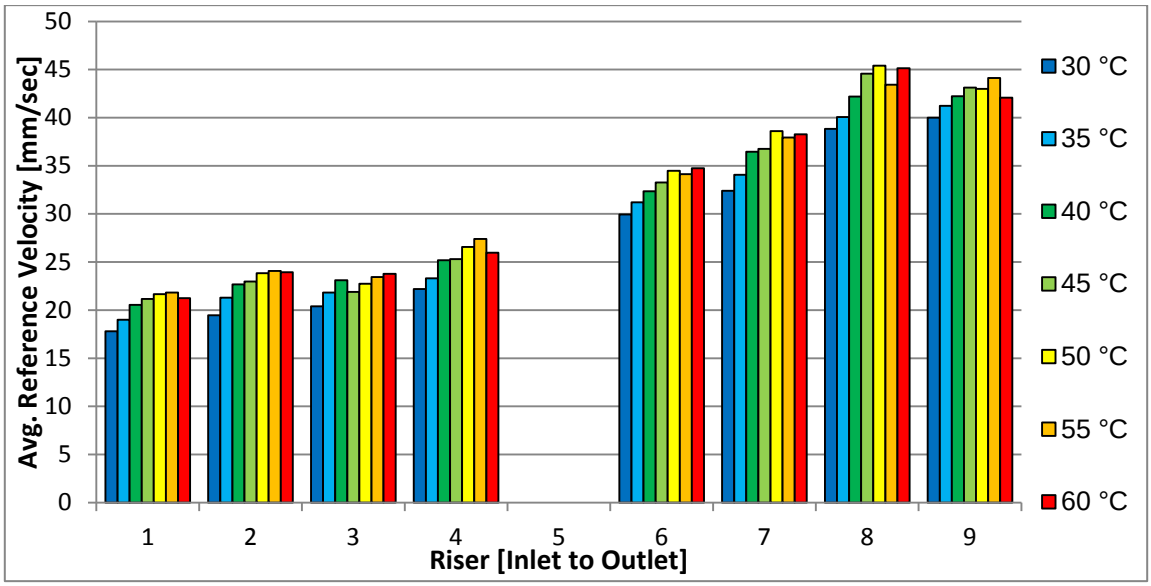


**Figure 98.** Flow Distribution across the Cooling Panel for the Outlet Skewed Power Profile (31 Series)

Again it is noted that the relative values between risers at any one temperature appear to be consistent. The flow distribution is skewed toward the outlet relative to the 00 Series, in the same manner as the heater power, which was the expected result. In fact, the unevenness of the flow distribution is greatest in the 31 Series of experiments. Changes in flow velocities over temperature / time appear to reflect the changes in

system flowrate. Overall, the results appear consistent with visual observations of the particles made during the experiment.

PIV measurements at all Risers were acquired during Experiment 310 while the 40 °C UVP measurement set was taken and are presented in Figure 99 below.

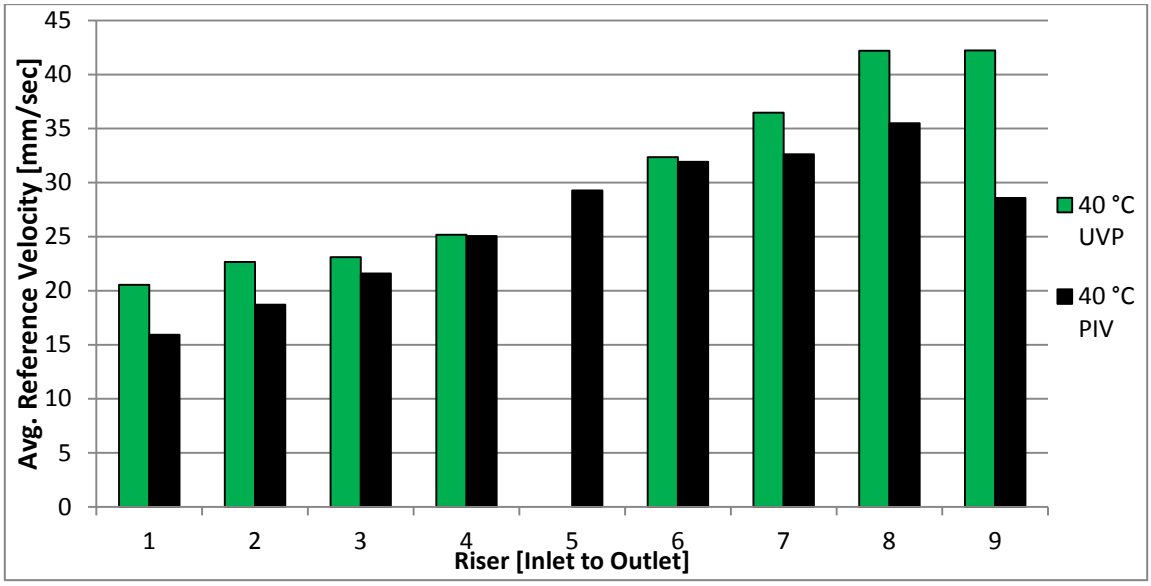


**Figure 99.** Comparison of PIV to UVP derived Reference Velocities for the Outlet Skewed Power Profile (31 Series)

Measurements for Risers # 3, 4, and 6 measurements are within 6.5% of the UVP values. All the other measurements, however, are between 10.5 to 32.3% different from the UVP values. This indicates there may be have a problem during the PIV or the UVP setup and/or post-processing of the data. The shape of the PIV distribution is similar to the UVP, however, except for Riser #9. A summary of the PIV results and statistics is in Table 8 below.

**Table 8.** Statistics for the PIV Analysis of the Outlet Skewed / 31 Series

| Riser # | Average Velocity [mm/sec] | Combined Line-to-Line Standard Deviation [mm/sec] | Temporal Standard Deviation [mm/sec] | % Difference to UVP Reference Velocity |
|---|---|---|---|---|
| 1 | 15.93 | 1.46 | 0.80 | -22.51 |
| 2 | 18.71 | 1.35 | 0.79 | -17.46 |
| 3 | 21.59 | 1.50 | 0.82 | -6.52 |
| 4 | 25.06 | 1.61 | 1.01 | 0.49 |
| 5 | 29.28 | 1.49 | 0.90 | n/a |
| 6 | 31.92 | 1.91 | 0.95 | -1.33 |
| 7 | 32.62 | 3.10 | 2.03 | -10.55 |
| 8 | 35.49 | 6.42 | 6.93 | -15.89 |
| 9 | 28.58 | 5.91 | 4.24 | -32.33 |

It is noted in Table 8 that the Spatial and Temporal standard deviations of the analysis for Risers #7, 8, and 9 are significantly higher than those from the other riser tubes. This is a further indicator that the data and/or the post-processing did not accurately capture the flow phenomena. This does not explain the large discrepancy between the UVP and PIV derived results for Riser #1 and #2, however.

A volumetric comparison of the PIV results to the magmeter shows that the PIV reading had a 9.5% deviation from the magmeter's reading during Experiment 310. UVP and PIV based volumetric flowrate results for the 31 Series are presented against the magmeter readings for both experiments in Figure 100 below.

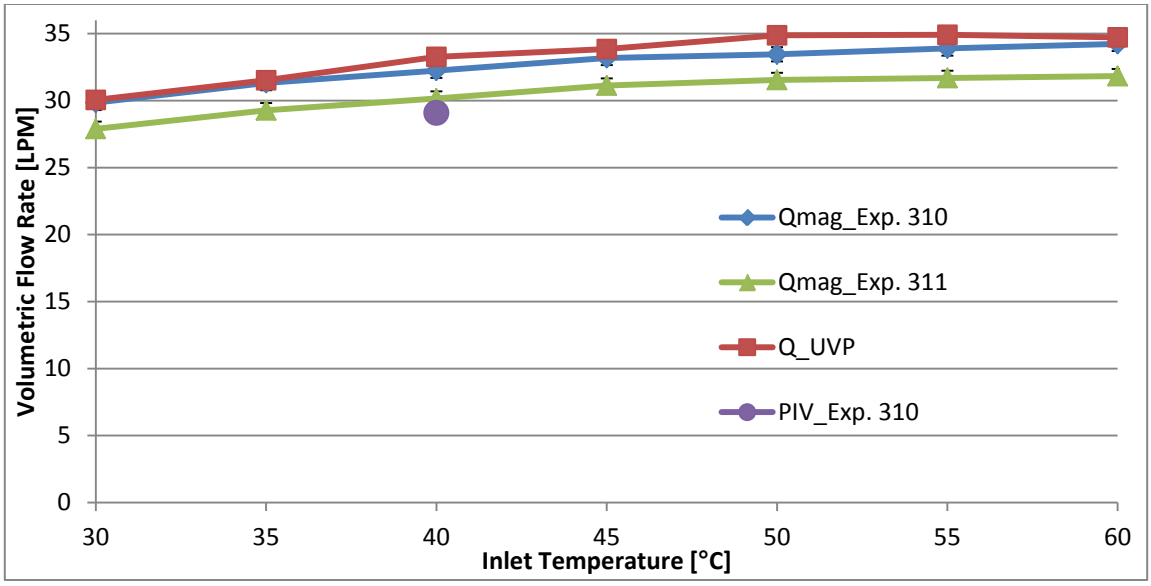


**Figure 100.** System Flow Balance for the Outlet Skewed Power Profile (31 Series) – UVP, PIV and Magmeter

It is noted that the system flowrates obtained via UVP are within 7.3% of the average of the two magmeter readings at each temperature. The trend of UVP derived results also follows the same increasing pattern as the magmeter. Both observations indicate that the results are generally valid. The $\Delta T_R$ distribution is given in Figure 101 below.

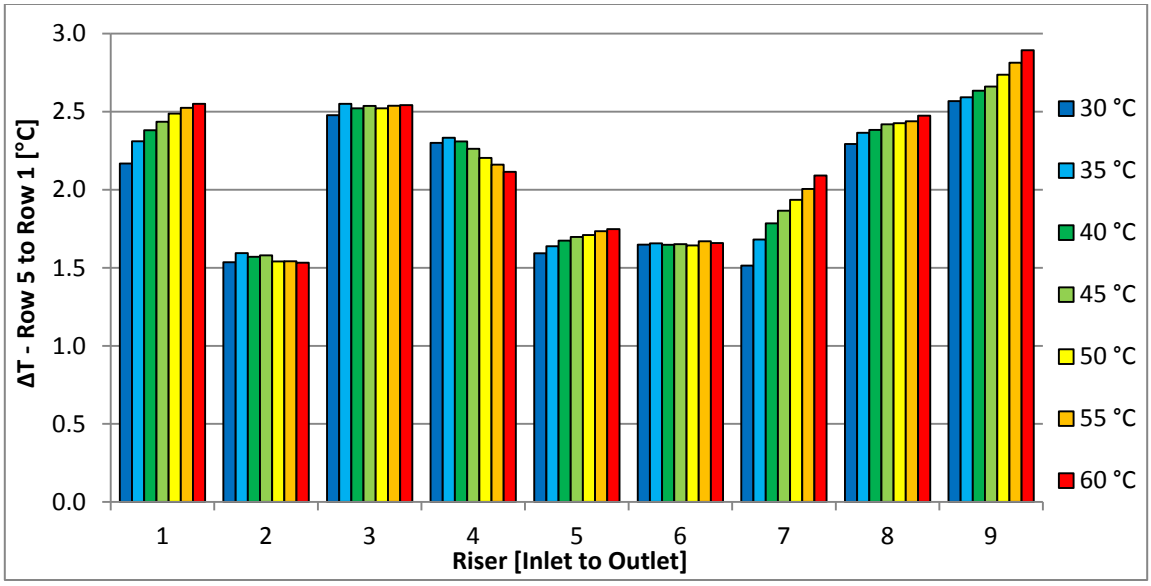


**Figure 101.** $\Delta T_R$ Distribution across the Cooling Panel for the Outlet Skewed Power Profile (31 Series)

Temperature drifts over time/temperature are seen at Risers #1, 4, 5, 7, 8, and 9. The shape of the $\Delta T_R$ distribution is remarkably similar to that seen in the 30 Series even though the power profile is reversed. The resulting heat transfer rate in each riser tube is presented in Figure 102 below.

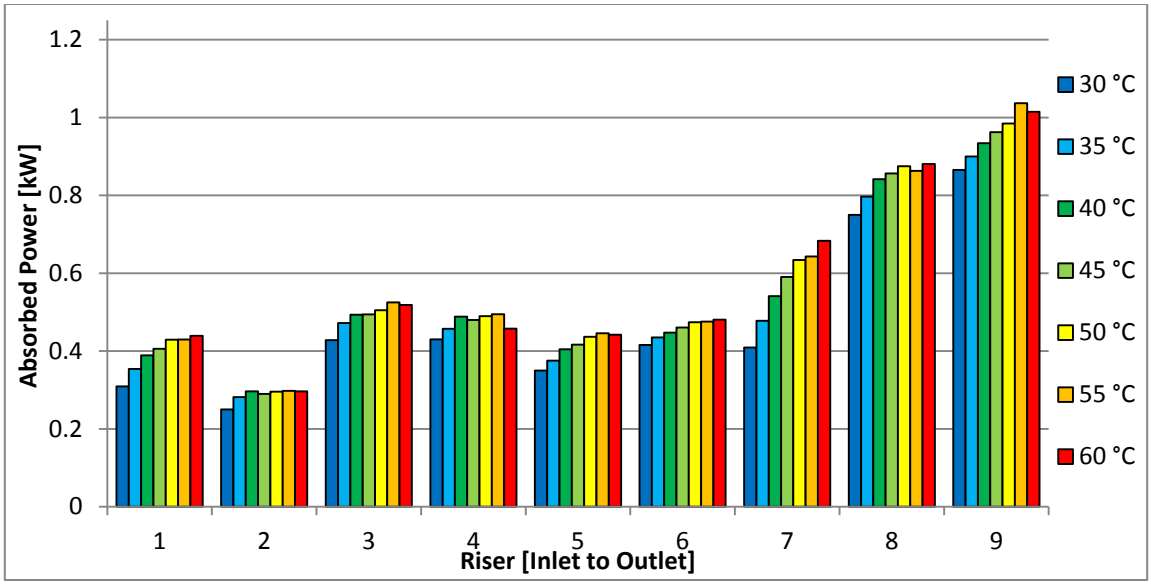


**Figure 102.** Distribution of the Power Absorption across the Cooling Panel for the Outlet Skewed Power Profile (31 Series)

In this Series, the flow distribution appears to exhibit a strong effect on the absorbed power distribution, negating the effect of the high temperature differences at the risers close to the inlet and accentuating those at the outlet. The comparison of the total absorbed power between the summation of the values for the individual risers and the Test Section as a whole is in Figure 103 below.

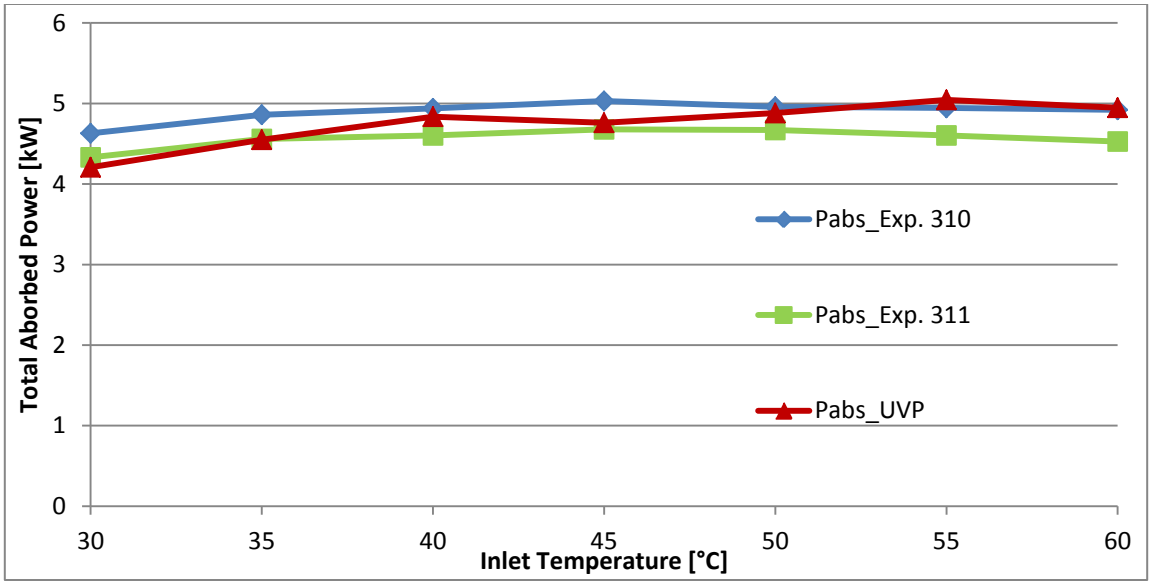


**Figure 103.** Balance of the Total Absorbed Power in the Cooling Panel for the Outlet Skewed Power Profile – Sum of Individual Risers to Test Section

The percent difference between the value calculated from summing the individual risers and the average of the magmeter derived values is less than 6.1% for all points, giving this Series one of the highest levels of agreement between methods of all experiments conducted. This completes the range of analysis completed for the 31 Series.

IV.3.8 Effects of Skewed Power Profiles

To give a general understanding of the effect of changing the distribution of power to the heaters on the flow distribution, the Reference velocities for the 30, 00, and 31 Series of experiments are shown at the common Coolant Temperature of 40 °C in Figure 104 below. It is observed that the changes to the general shape of the flow distribution follow the changes to the power profile, which was the expected result.

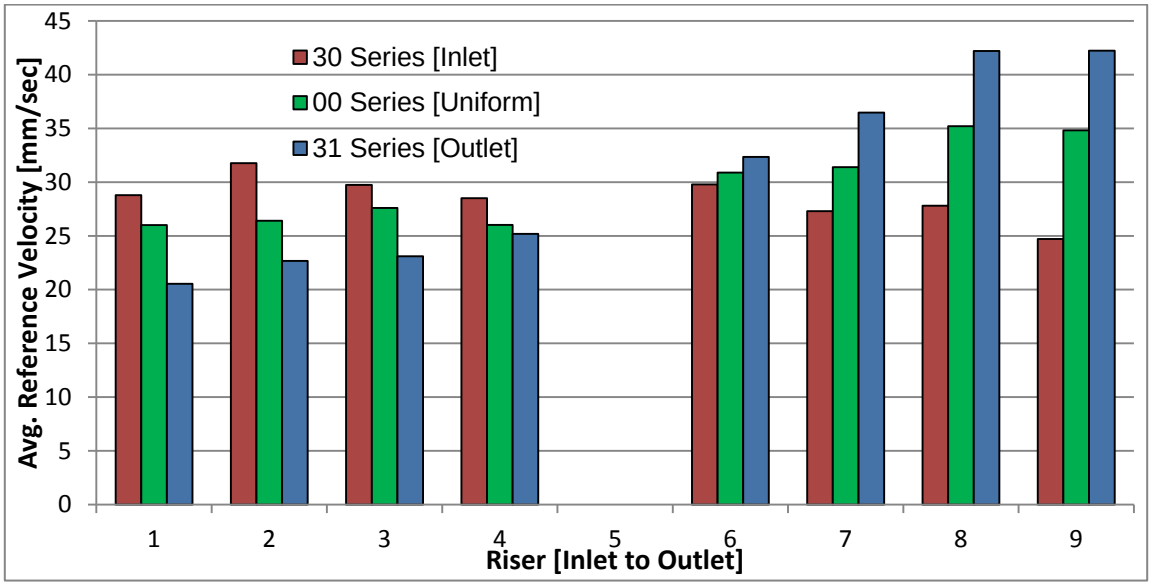


**Figure 104.** Effect of Heater Power Profiling on the Flow Distribution

IV.3.9 High Coolant Inventory (Series 40) Experimental Results

For this experimental series the volume of coolant was increased such that the tank was nearly completely full, yielding a coolant volume of 623.5 L. This put an additional 75 cm of head on the standard water level as shown in Figure 68 earlier. All other parameters were the same as the Reference Case. Data was taken every 5°C from 30 to 60 °C; the resulting flow distributions are condensed into Figure 105 below. 252 individual readings were taken over the course of both experiments; 244 (96.8%) of which were within 10% of the average of their fellow readings.

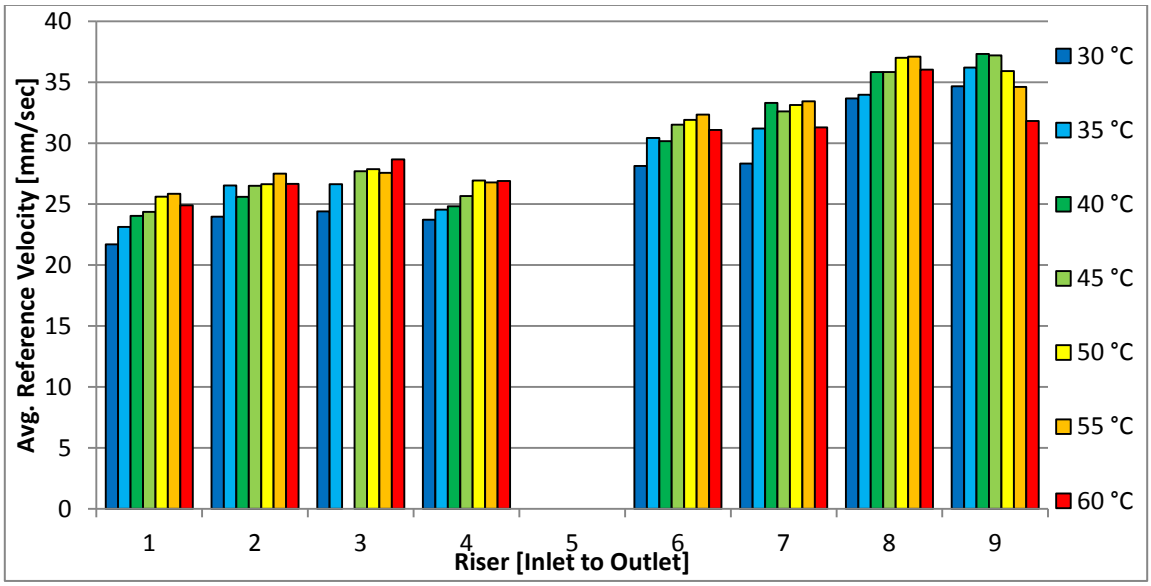


**Figure 105.** Flow Distribution across the Cooling Panel for the High Coolant Inventory Case (40 Series)

Again it is noted that the relative values between risers at any one temperature appear to be consistent. The flow distribution is similar to the 00 Series, except the values for Riser #9 are a little higher. Changes in flow velocities over temperature / time appear to reflect the changes in system flowrate. Overall, the results appear consistent with visual observations of the particles made during the experiment. The reader may

note that the measurement for Riser #3 at 40 °C is not present as the UVP-DUO experienced a malfunction at that channel during testing (Experiment #401).

PIV measurements at all Risers were acquired during Experiment 400 while the 40 °C UVP measurement set was taken, and are presented in Figure 106 below.

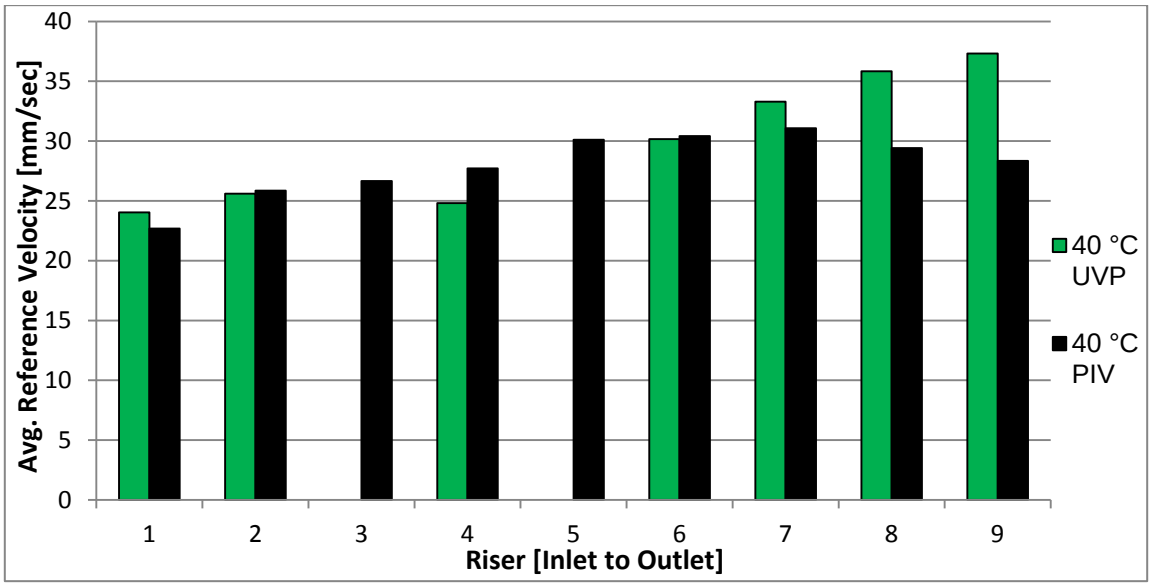


**Figure 106.** Comparison of PIV to UVP derived Reference Velocities for the High Coolant Inventory Case (40 Series)

Measurements for Risers # 1, 2, 6, and 7 measurements are within 6.7% of the UVP values. All the other measurements, however, are between 11.7 to 24% different from the UVP values. This indicates there may be have a problem during the PIV or the UVP setup and/or post-processing of the data. The shape of the distribution is similar to the UVP, however, except at Risers #8 and 9. A summary of the PIV results and statistics is in Table 9 below.

**Table 9.** Statistics for the PIV Analysis of the High Coolant Level / 40 Series

| Riser # | Average Velocity [mm/sec] | Combined Line-to-Line Standard Deviation [mm/sec] | Temporal Standard Deviation [mm/sec] | % Difference to UVP Reference Velocity |
|---|---|---|---|---|
| 1 | 22.69 | 1.70 | 0.89 | -5.61 |
| 2 | 25.85 | 1.80 | 1.01 | 0.99 |
| 3 | 26.65 | 1.60 | 0.82 | n/a |
| 4 | 27.71 | 1.78 | 0.97 | 11.67 |
| 5 | 30.11 | 1.78 | 0.99 | n/a |
| 6 | 30.42 | 2.18 | 1.06 | 0.86 |
| 7 | 31.07 | 2.67 | 1.53 | -6.70 |
| 8 | 29.41 | 3.38 | 2.15 | -17.92 |
| 9 | 28.35 | 4.05 | 3.14 | -24.03 |

It is noted in Table 9 that the Spatial and Temporal standard deviations of the analysis for Risers #7, 8, and 9 are significantly higher than those from the other riser tubes. This is a further indicator that the data and/or the post-processing did not accurately capture the flow phenomena. Riser #4 appears to have solid data, however, so this does not explain the large discrepancy between the UVP and PIV results at that riser. The reader may note that the UVP Reference Velocity for Riser #4 is consistently low as compared to adjacent risers, and it is believed by the author that the mounting of the UVP transducer is such that it is aimed off center in the riser, at least more so than in the mounting of the other transducers. Here, as in the 10 and 31 Series, it appears that better experimental technique is in order for future PIV measurements on the water cooled RCCS.

A volumetric comparison of the PIV results to the magmeter shows that the PIV reading had a 6.25% deviation from the magmeter's reading during Experiment 400. UVP and PIV based volumetric flowrate results for the 40 Series are presented against the magmeter readings for both experiments in Figure 107 below. Please note that in addition to assuming Riser #5's UVP derived velocity to be the average of its neighbors,

the same was done for Riser #3 at 40 °C since the data is missing. This data point is colored orange in the figure.

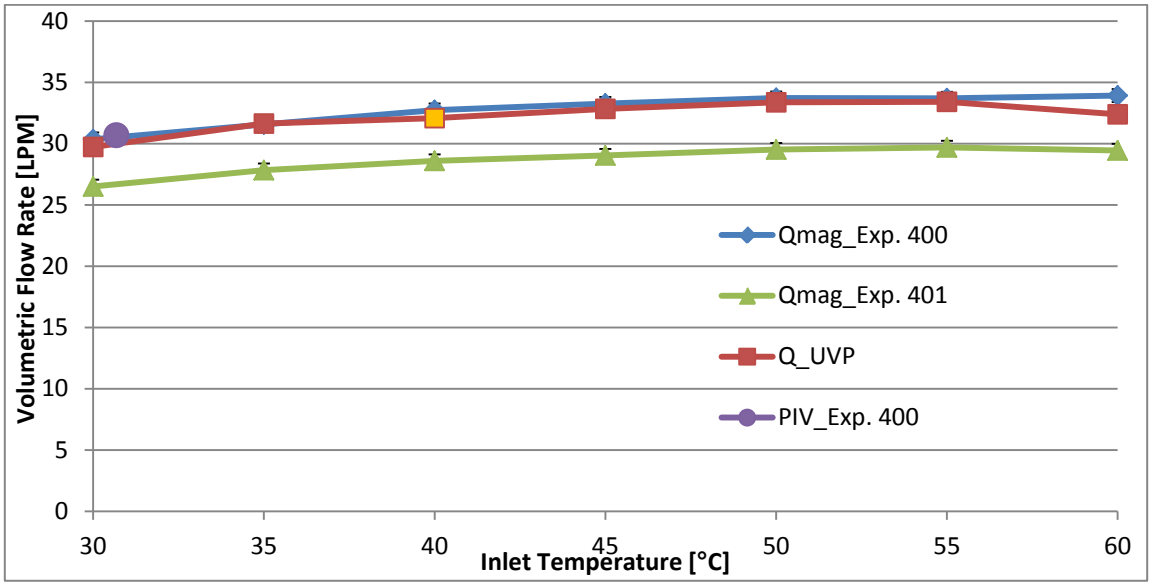


**Figure 107.** System Flow Balance for the High Coolant Inventory Case (40 Series) – UVP, PIV and Magmeter

It is noted that the system flowrates obtained via UVP are within 6.5% of the average of the two magmeter readings at each temperature. The trend of UVP derived results also follows the same increasing pattern as the magmeter. Both observations indicate that the results are generally valid. The $\Delta T_R$ distribution is given in Figure 108 below.

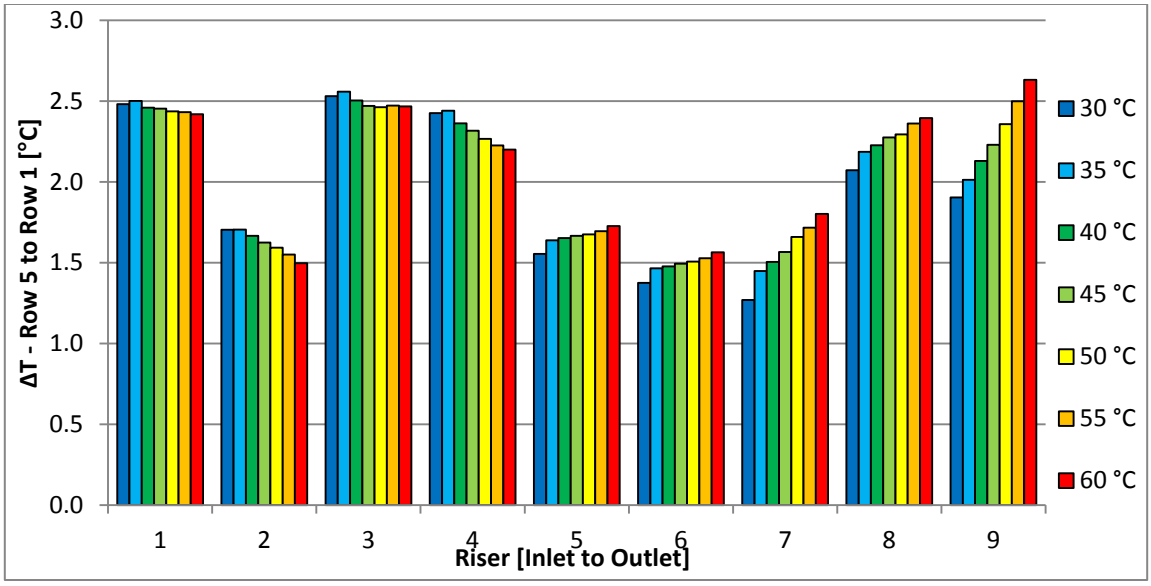


**Figure 108.** $\Delta T_R$ Distribution across the Cooling Panel for the High Coolant Inventory Case (40 Series)

Temperature drifts over time/temperature are seen at all risers. The resulting heat transfer rate in each riser tube is presented in Figure 109 below.

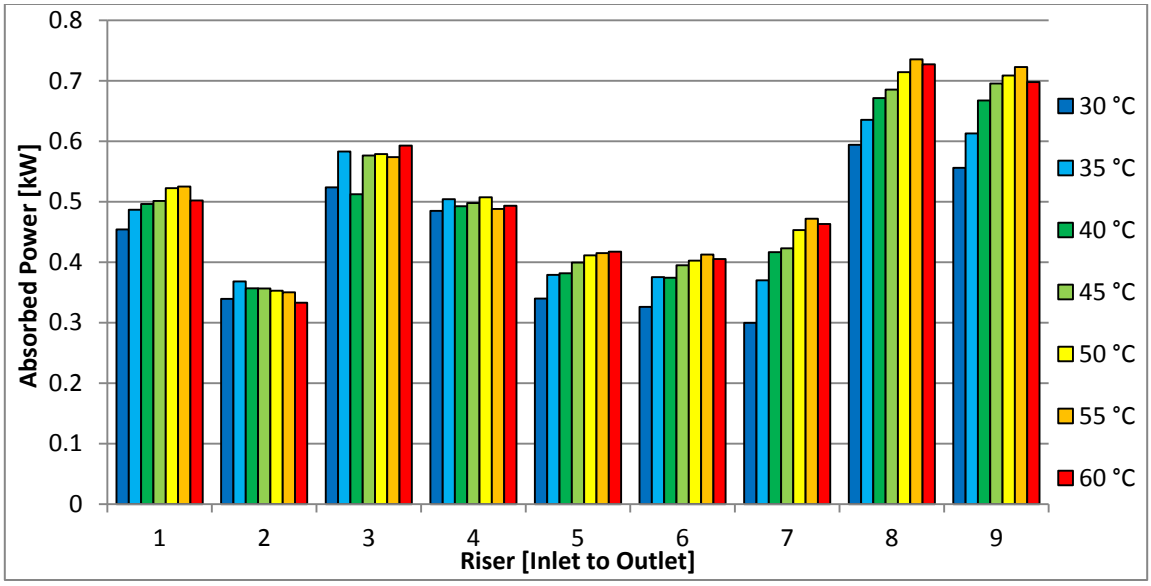


**Figure 109.** Distribution of the Power Absorption across the Cooling Panel for the High Coolant Inventory Case (40 Series)

As in the 00 Series, the $\Delta T_R$ distribution dominates the power absorption distribution. The comparison of the total absorbed power between the summation of the values for the individual risers and the Test Section as a whole is in Figure 110 below.

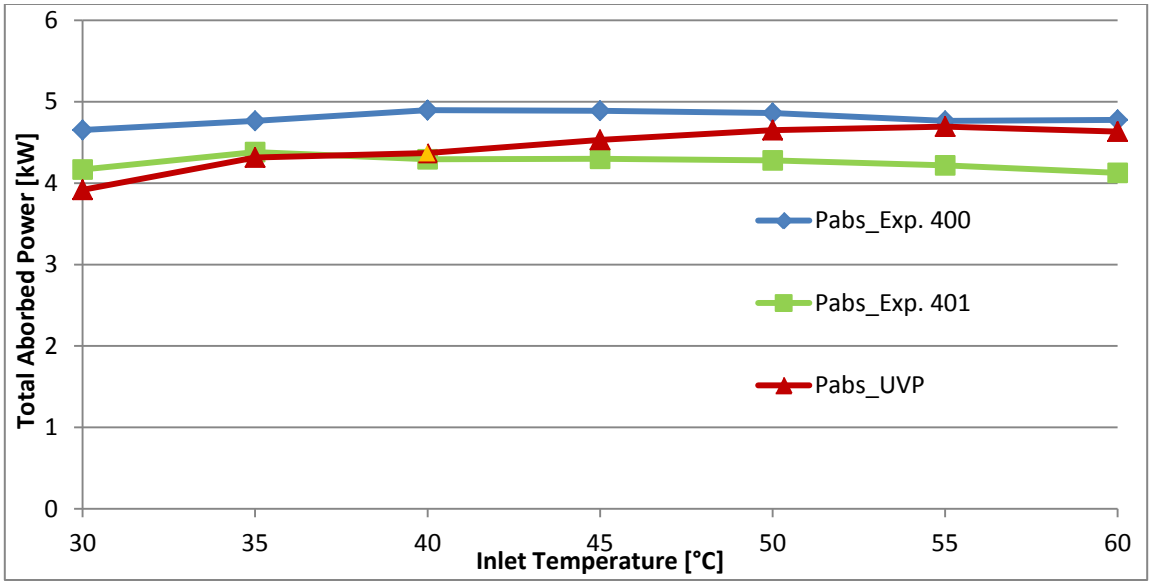


**Figure 110.** Balance of the Total Absorbed Power in the Cooling Panel for the High Coolant Inventory Case – Sum of Individual Risers to Test Section

The percent difference between the values calculated via UVP and the average of the magmeter derived values is less than 5.7% for all points, except at 30°C where the difference is 11.2%. The level of consistency for the flowrate and absorbed power results is comparable to the 00 Series. This completes the range of analysis completed for the 40 Series.

IV.3.10 Effect of Increased Coolant Volume / Tank Level

To give a general understanding of the effect of changing the coolant inventory and tank level on the flow distribution, the Reference velocities for the 00 and 40 Series of experiments are shown at the common Coolant Temperature of 45 °C in Figure 111 below. The flow distribution is similar and it does not appear that the increased pressure from the increased head had any significant effect.

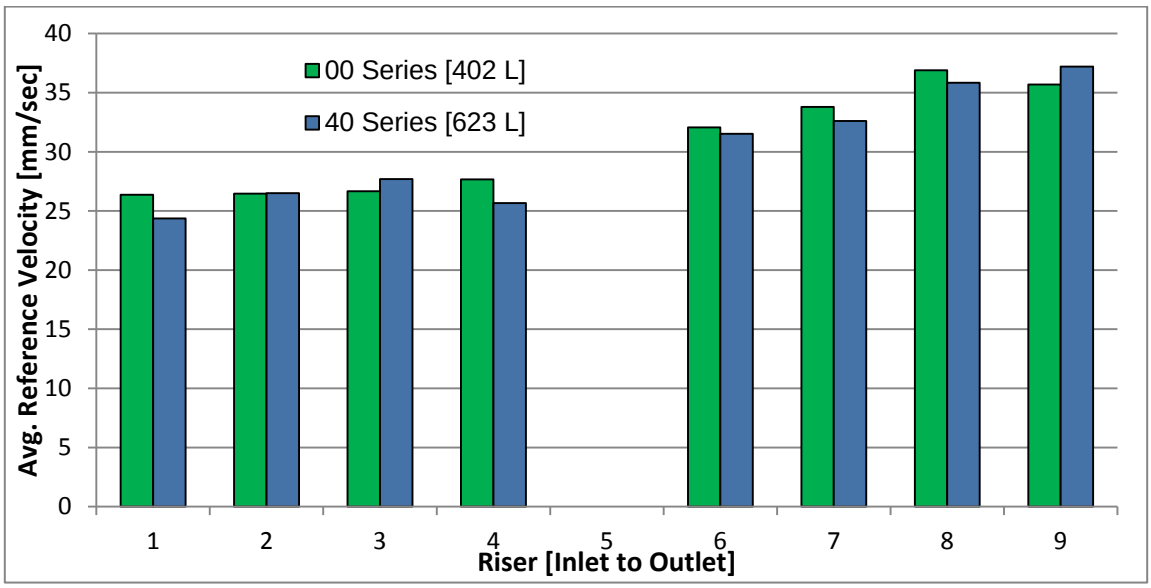


**Figure 111.** Effect of High Coolant Level on the Flow Distribution

IV.3.11 Partially Throttled Case (Series 20) Experimental Results (ΔT = 6 °C)

For this experimental series, the flow was restricted by the butterfly valve located below the storage tank to the extent required to generate a 6 °C temperature difference across the thermocouples at the inlet and outlet of the Test Section. All other parameters were the same as the Reference Case. Data was taken every 5°C from 35 to 60 °C; the initial coolant temperature was already high that day so the 30° readings are omitted. The resulting flow distributions are condensed into Figure 112 below. 216 individual readings were taken over the course of both experiments, but only 130 (60.2%) of which were within 10% of the average of their fellow readings. A lot of variability was seen in the results and it will be noted ahead that UVP seemed to not function well in this Series or in the 21 Series either.

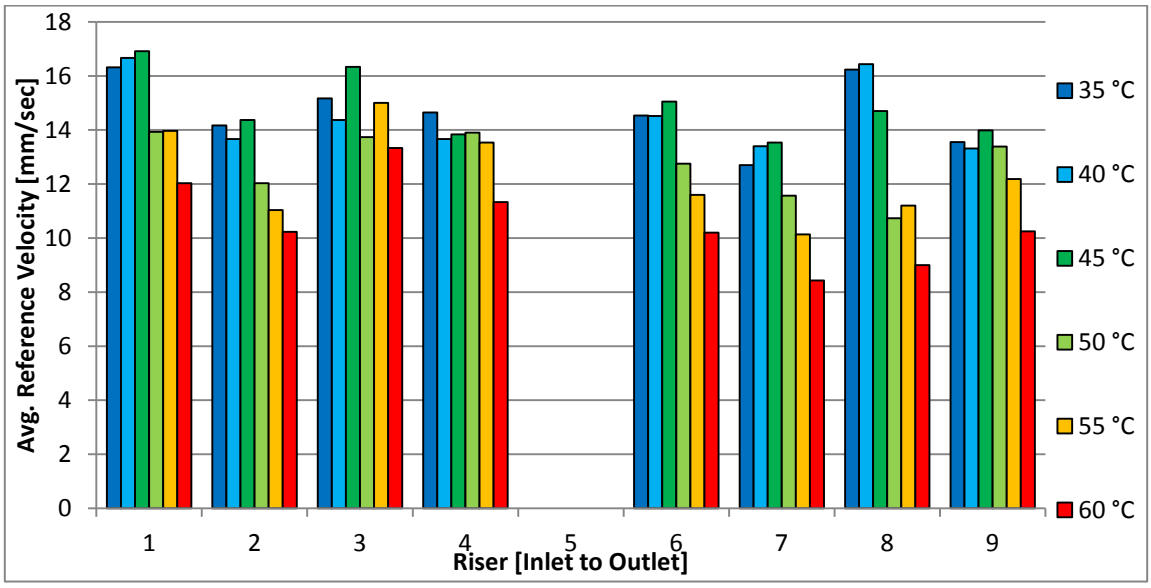


**Figure 112.** Flow Distribution across the Cooling Panel for the Partially Throttled Case (20 Series)

Results show a high degree of variation over temperature/time. There is a generally decreasing trend at all transducers over time, which is consistent with the observed changes to the system flowrate in Figure 69 from earlier. The distribution

appears to be very uniform, with slightly higher flow velocities at the Risers closest to the inlet. This is consistent with having the greatly reduced momentum of coolant at the inlet from the restriction. Overall, the results appear consistent with visual observations of the particles made during the experiment.

PIV measurements at all Risers were acquired during Experiment 200 while the 40 °C UVP measurement set was taken, and are presented in Figure 113 below.

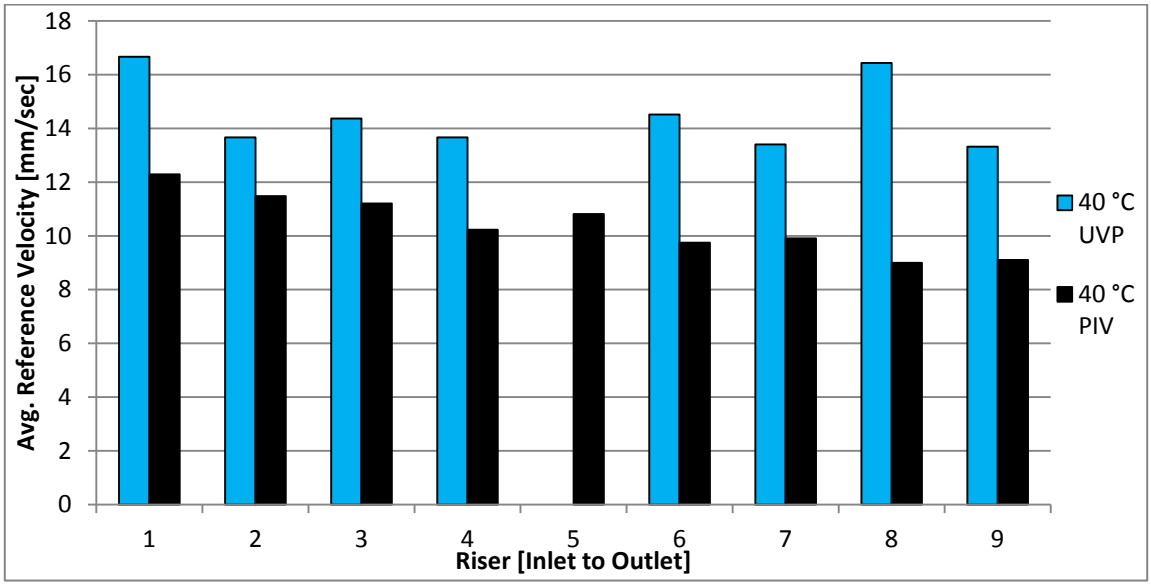


**Figure 113.** Comparison of PIV to UVP derived Reference Velocities for the Partially Throttled Case (20 Series)

The shape of the PIV derived results more closely fit observations made by eye during the experiment than the UVP results. It also makes more intuitive sense, as there is no logical reason for Riser 8 to have a significantly higher flow velocity than its neighbors as indicated by the UVP. With the exception of the UVP result for Riser #8, the trends of the two methods are generally similar, however. A summary of the PIV results and statistics are in Table 10 below.

**Table 10.** Statistics for the PIV Analysis of the Partially Throttled / 20 Series

| Riser # | Average Velocity [mm/sec] | Combined Line-to-Line Standard Deviation [mm/sec] | Temporal Standard Deviation [mm/sec] | % Difference to UVP Reference Velocity |
|---|---|---|---|---|
| 1 | 12.29 | 0.99 | 0.53 | -26.28 |
| 2 | 11.48 | 1.03 | 0.49 | -16.00 |
| 3 | 11.21 | 0.94 | 0.42 | -22.00 |
| 4 | 10.23 | 1.16 | 0.62 | -25.17 |
| 5 | 10.81 | 0.83 | 0.33 | n/a |
| 6 | 9.75 | 1.15 | 0.59 | -32.86 |
| 7 | 9.91 | 0.88 | 1.05 | -26.07 |
| 8 | 9.00 | 1.18 | 0.77 | -45.26 |
| 9 | 9.11 | 1.17 | 0.76 | -31.62 |

Statistical deviations in the PIV data are consistent from riser to riser, and are lower than in the all of the non-throttled series. A volumetric comparison of the PIV results to the magmeter shows that the PIV reading was within 13.78% of the magmeter's reading during Experiment 200, which is when the PIV measurement was performed. It should be noted that the magmeter's readings can be ±0.5 LPM from the true flowrate at that value, and the PIV result only differs from the magmeter by 1.4 LPM.

UVP and PIV based volumetric flowrate results for the 20 Series are presented against the magmeter readings for both experiments in Figure 114 below. Please note that flowrate data from the magmeter was not available after the time of the 45 °C inlet temperature measurement (recall the data shown in Figure 69), but the decreasing flowrate indicated by the UVP is consistent with the author's expectations. For the 20 Series experiment, it is readily observed that the PIV measurements were much more accurate than the UVP, which deviated from the magmeter readings by 54 to over 100%.

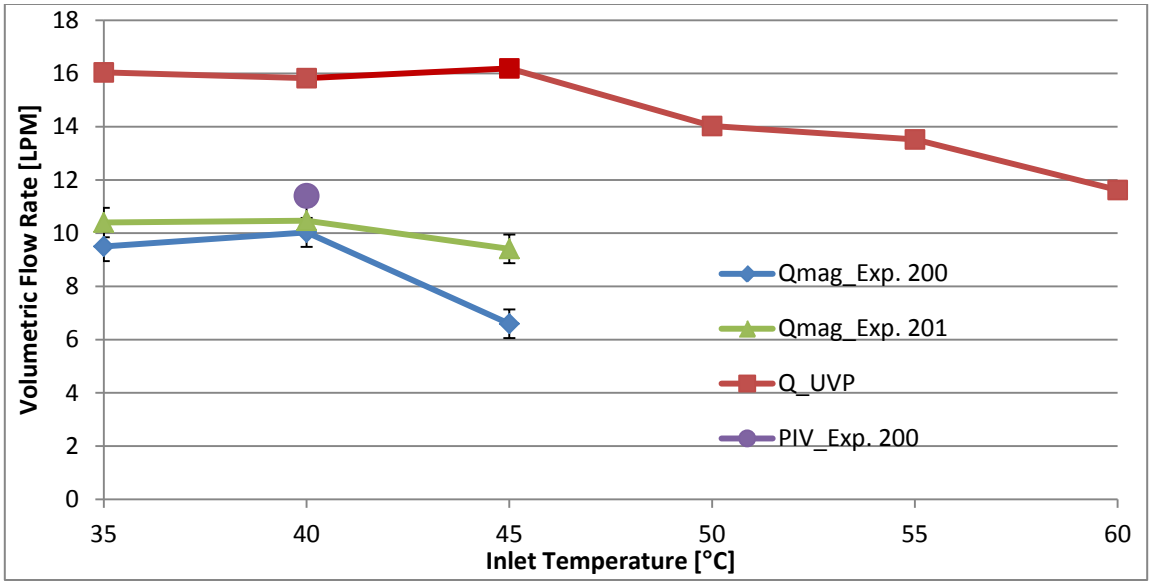


**Figure 114.** System Flow Balance for the Partially Throttled Case (20 Series) – UVP, PIV and Magmeter

The $\Delta T_R$ distribution is given in Figure 115 below.

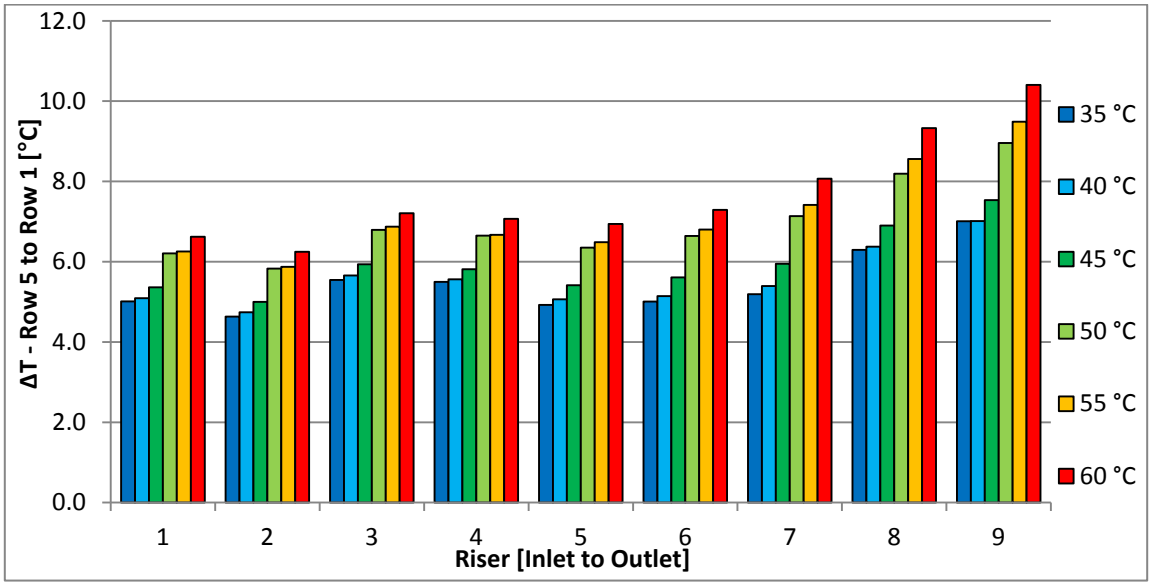


**Figure 115.** $\Delta T_R$ Distribution across the Cooling Panel for the Partially Throttled Case (20 Series)

It is noted that the $\Delta T_R$ distribution is relatively uniform for the first 6 risers from the Test Section inlet, and then steadily increase in magnitude. This shape is essentially the mirror image of the flow distribution, which is what was expected but not seen in the other experimental series. Temperature drifts over time/temperature are seen at all risers, which is to be expected in this case because the volumetric flowrate is decreasing over time, allowing more time for heating in the cavity.

An analysis of the absorbed power at each individual riser in the Cooling Panel will not be presented in this thesis for the 20 Series experiments due to a lack of reliable flow data. In any case, it is likely that the $P_{abs}$ distribution is relatively flat based on the relative shapes of the flow and $\Delta T_R$ distributions. This completes the analysis for the 20 Series.

IV.3.12 Fully Throttled Case (Series 21) Experimental Results: ΔT = 10 °C

For this experimental series, the flow was restricted by the butterfly valve located below the storage tank to the extent required to generate a 10 °C temperature difference across the thermocouples at the inlet and outlet of the Test Section. All other parameters were the same as the Reference Case. Data was taken every 5°C from 30 to 60 °C; the initial coolant temperature was already high that day so the 30° readings are omitted. The resulting flow distributions are condensed into Figure 116 below. 228 individual readings were taken over the course of both experiments, but only 96 (42.1%) of which were within 10% of the average of their fellow readings. Even more variability in the UVP readings was seen here than in the 20 Series.

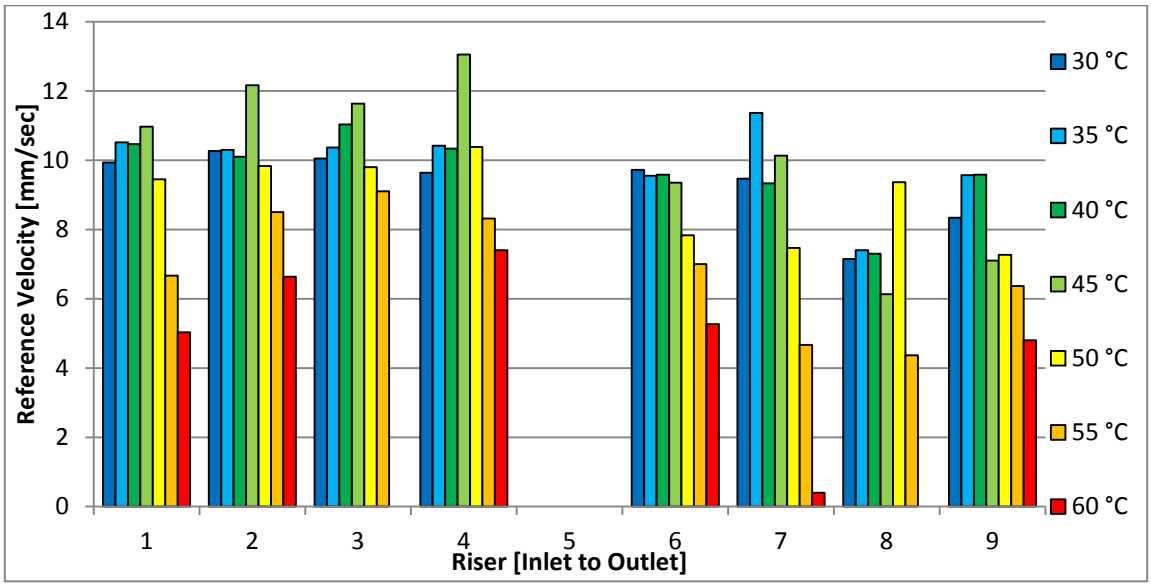


**Figure 116.** Flow Distribution across the Cooling Panel for the Fully Throttled Case (21 Series)

Results show a high degree of variation from over temperature/time. There is a generally decreasing trend at all risers over time, which is consistent with the observed changes to the Test Section ΔT seen previously in Figure 72. The distribution decreases steadily from inlet to outlet, similar to Series 20 but to a greater extent, and likely for the

same reasons. Overall, the results appear consistent with visual observations of the particles made during the experiment.

PIV measurements at all Risers were acquired during Experiment 210 while the 40 °C UVP measurement set was taken, and are presented in Figure 117 below.

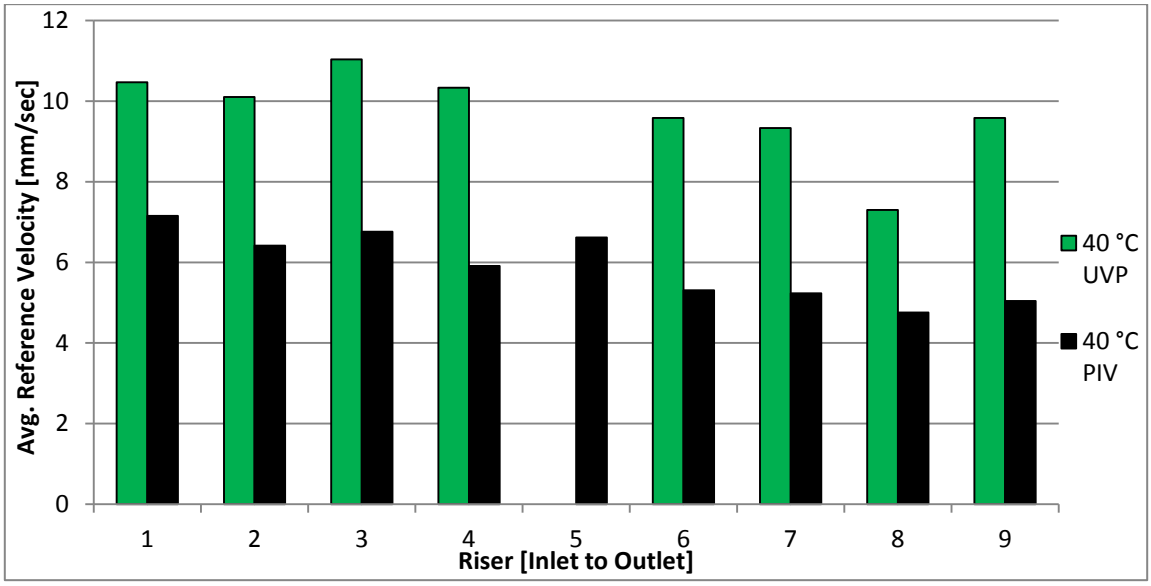


**Figure 117.** Comparison of PIV to UVP derived Reference Velocities for the Fully Throttled Case (21 Series)

As in the 20 Series, the shape of the PIV derived results more closely fit observations made by eye during the experiment than the UVP results. It also makes more intuitive sense, as there is no logical reason for Riser 8 to have a significantly lower flow velocity than its neighbors as indicated by the UVP. With the exception of the UVP result for Riser #8, the trends of the two methods are generally similar. A summary of the PIV results and statistics are in Table 11 below.

**Table 11.** Statistics for the PIV Analysis of the Fully Throttled / 21 Series

| Riser # | Average Velocity [mm/sec] | Combined Line-to-Line Standard Deviation [mm/sec] | Temporal Standard Deviation [mm/sec] | % Difference to UVP Reference Velocity |
|---|---|---|---|---|
| 1 | 7.15 | 1.00 | 0.71 | -31.67 |
| 2 | 6.41 | 0.91 | 0.39 | -36.49 |
| 3 | 6.76 | 1.01 | 0.54 | -38.72 |
| 4 | 5.91 | 1.02 | 0.45 | -42.81 |
| 5 | 6.62 | 0.94 | 0.53 | n/a |
| 6 | 5.31 | 0.93 | 0.82 | -44.62 |
| 7 | 5.23 | 1.00 | 0.66 | -43.93 |
| 8 | 4.76 | 1.64 | 1.95 | -34.83 |
| 9 | 5.04 | 1.25 | 1.46 | -47.38 |

Statistical deviations in the PIV data are consistent from riser to riser except for Risers 8 and 9, but the results still make intuitive sense and the statistical deviations are not as large as some of those seen for certain risers in the 10, 31, and 40 Series of experiments. It should be noted that statistical deviations for both throttled series of experiments were lower than any for the non-throttled ones.

A volumetric comparison of the PIV results to the magmeter was not possible due to there being no data from the mag, but the reader may recall that the volumetric flowrate was predicted to be about 6.3 LPM with a 10.2 °C ΔT across the Test Section. To recap, this is based on the observation of the ratio of system flowrates between the non-throttled and partially throttled experiments being the inverse of the ratio of the ΔT's over the Test Section. In reference to Figure 72, the PIV measurements were made during the elapsed time of 137 to 146 minutes, while the average ΔT was 10.22 °C. This is about 5 times the ΔT seen during the 00 Series, which was 2.03 °C. The average system flowrate for the 00 Series was 31.73 LPM, dividing this by 5.03 yields 6.31 LPM. By comparison, multiplying the reference velocities in Table 11 by the risers' cross-sectional area and summing them up the results yields a volumetric flowrate of 6.47 LPM, a difference of only 2.7%!

UVP and PIV based volumetric flowrate results for the 21 Series are presented in Figure 118 below. The extrapolated data point is also presented for reference. The matching PIV and extrapolated data strongly indicate that PIV is the superior measurement technique for the throttled series. The deviation of the UVP based results from the PIV and extrapolated values at an inlet temperature of 40 °C is nearly 70%.

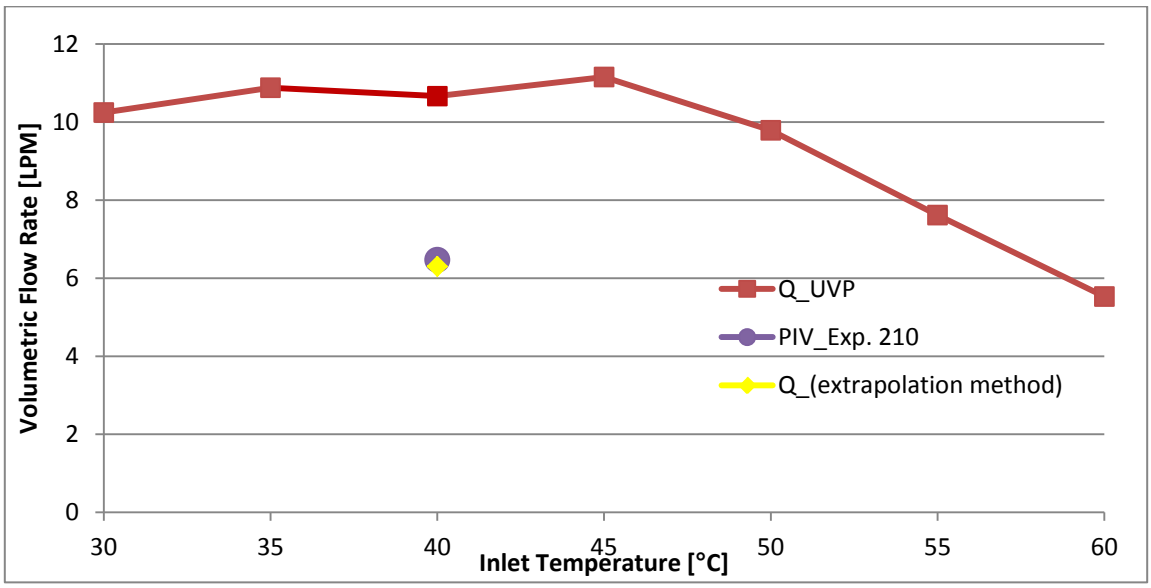


**Figure 118.** System Flow Balance for the Fully Throttled Case (21 Series) – UVP, PIV and Extrapolated Values

The $\Delta T_R$ distribution is given in Figure 119 below. Results are similar to what was seen in the 20 Series and for the same reasons. Temperature drifts over time/temperature are seen at all risers, and are quite dramatic at the 55 and 60 °C data points. This is indicative of a near complete blockage of the flow, and it is for this reason that the experiment was aborted at that point.

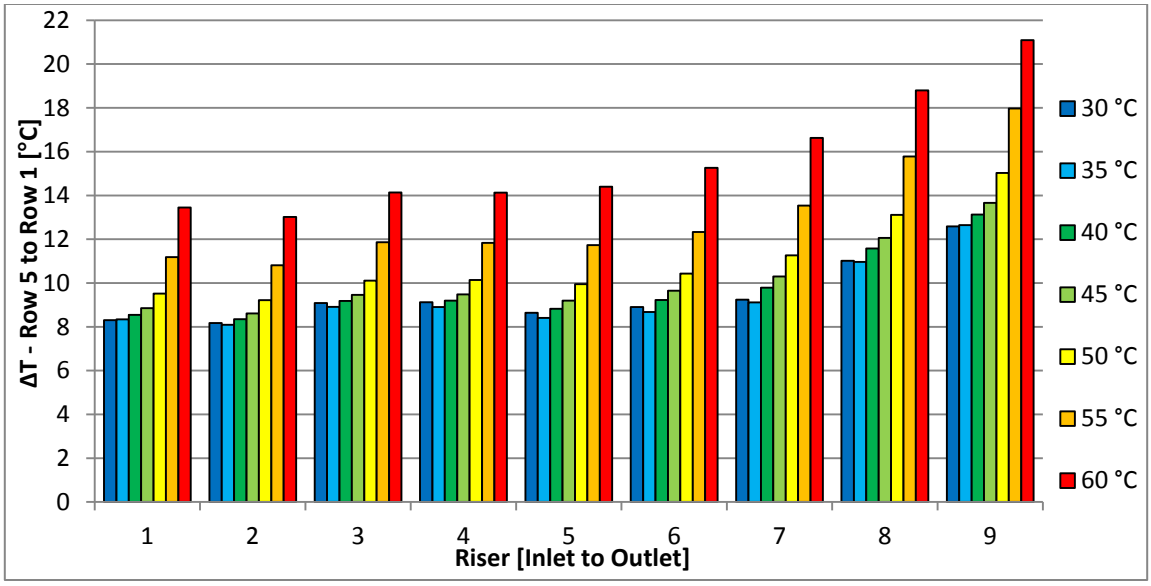


**Figure 119.** $\Delta T_R$ Distribution across the Cooling Panel for the Fully Throttled Case (21 Series)

An analysis of the absorbed power at each individual riser in the Cooling Panel will not be presented in this thesis for the 21 Series of experiments due to a lack of reliable flow data, though reasonable answers could probably be arrived at by assuming the distribution is as shown by the PIV for the 40 °C case. The absorbed power distribution would likely be uniform in the same manner as estimated for the 20 Series and for the same reasons of the flow distribution being the mirror image of the $\Delta T_R$ distribution. For example, the ratio of PIV Reference Velocities from inlet to outlet is 1.42, and the ratio of $\Delta T_R$ from outlet to inlet is about 1.53. Based on these ratios and others any value in the $P_{abs}$ distribution would likely be within 10% of the average. This completes the range of analysis completed for the 21 Series.

IV.3.13 Effect of Flow Throttling on the Flow Distribution

Figure 120 below shows the differences in terms of the degree of throttling, indicated by the ΔT produced in the Test Section. As mentioned previously, it is believed that the lower momentum of the liquid coolant coming into the lower manifold due to the lower volumetric flowrate is the reason for the shape of the flow distribution in the Cooling Panel becoming more uniform.

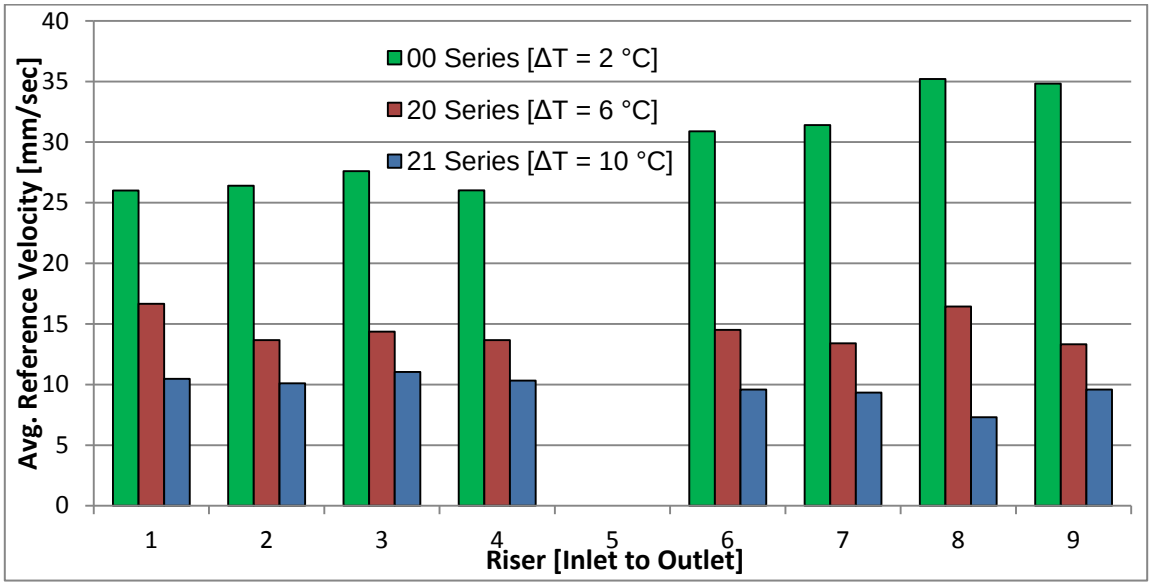


**Figure 120.** Effect of Flow Throttling on the Flow Distribution

IV.3.14 Saturation Case (50 Series) Experimental Results

Conditions for the Saturation Experiment were the same as the Reference Case (00 Series), except that instead of stopping at 70 °C the coolant was heated until it reached saturation. The only difference during the subcooled phase of the experiment was that all of the pipes and manifolds were completely insulated to hasten the approach to $T_{sat}$, and it was decided to take data via UVP to see if the presence of insulation outside the Heated Cavity had any significant effect on the results. Data was taken every 5 °C from 30 to 80 °C, the results are condensed into Figure 121 below. Data was not taken with the UVP-DUO after 80 °C because it had become apparent by that time that the results were erroneous and there was no point in taking further measurements.

Unlike the other experimental series, only one single experiment was done for the 50 Series as it was a scoping test. 198 individual readings were taken over the temperature range from 30° to 80 °C experiments, and of these 160 (80.8%) were within 10% of the average of their fellow readings. It should be noted that data taken after 65 °C was severely degraded in quality, as 97.2% of the 144 measurements taken up to and including 65 °C were within 10% of the average of their fellow readings.

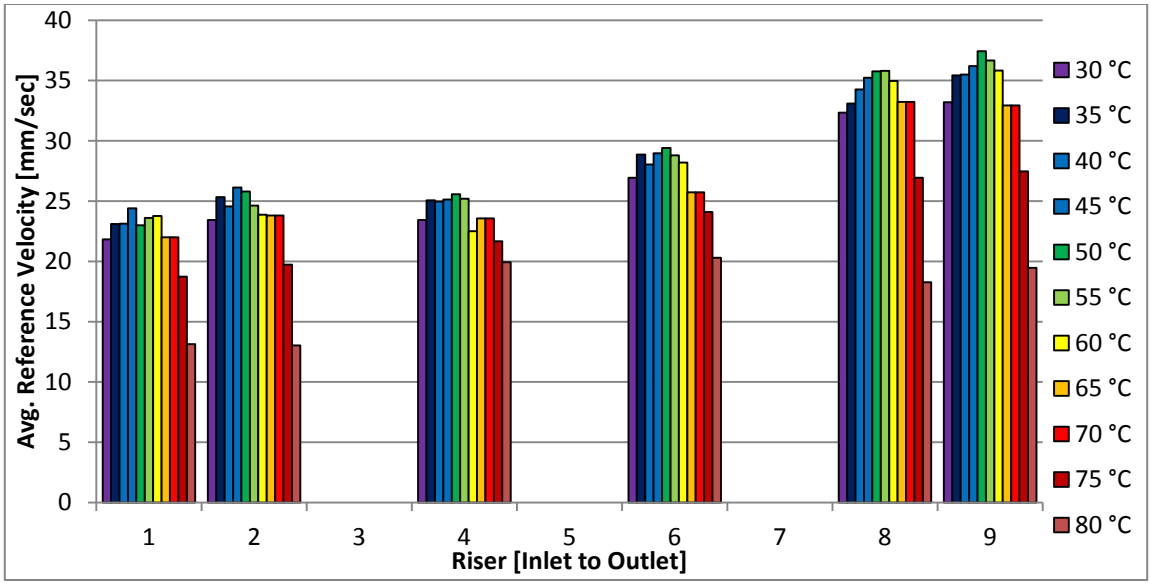


**Figure 121.** Flow Distribution across the Cooling Panel for the Two-Phase Scoping Experiment (50 Series)

Again it is noted that the relative values between risers at any one temperature appear to be consistent. The overall distribution is the same as for the 40 Series, which itself is the same as the 00 Series except the values for Riser #9 are a little higher. The author cannot remember exactly, but the mount may have been reset for Riser #9 in between the 00 and 40/50 Series of experiments. Changes in flow velocities over temperature / time appear to reflect the changes in overall flowrate, except that it is noted there are large consecutive drops in magnitude from 70°C to 75°C and then to 80 °C. Visual observations of the flow were not made during this experiment. PIV measurement results were not taken as the pipe insulation prevented this procedure. Volumetric UVP Results for Series 11 are presented against magmeter readings in Figure 122 below.

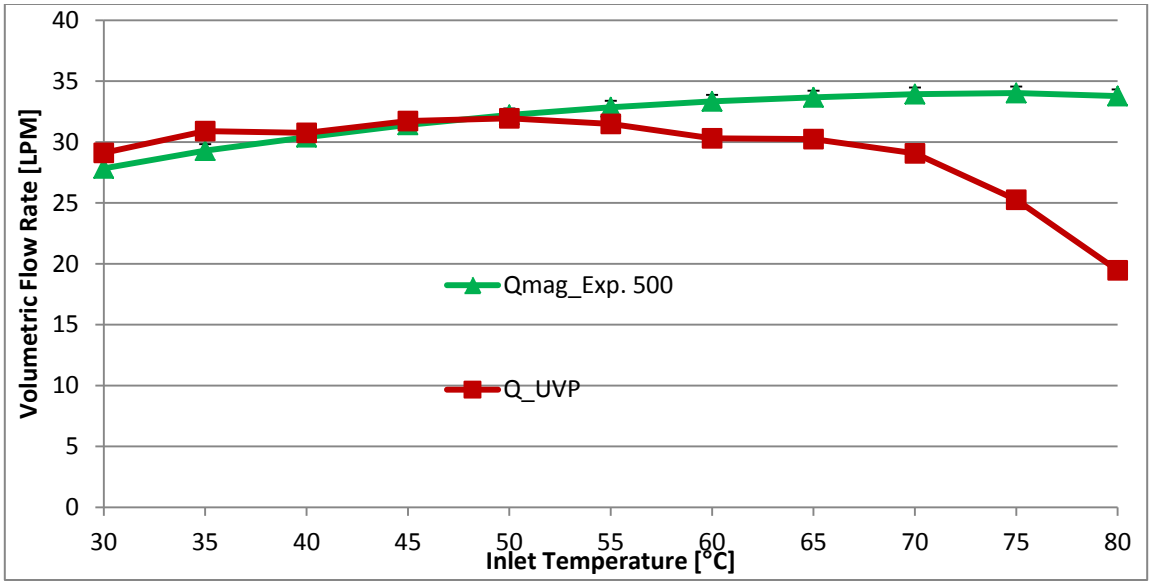


**Figure 122.** System Flow Balance for the Two-Phase Scoping Experiment (50 Series) – UVP and Magmeter

It is noted that the system flowrates obtained via UVP are within 5.5% of the magmeter readings at each temperature up to and including 55°C. After this, the error drops to around 10%, increasing to 42% for the 80°C case. Previous experiments (the 00 and 10 Series) did not have significant issues running up to 70°C.

The acquisition channel of the UVP-DUO for Riser #2 failed during the 3rd measurement set taken at 70°C. It was moved to a different channel before the 75 °C acquisition. It was thought that perhaps density changes had caused a significant number of particles to 'float out' of the water and rest at the top of the water line in the storage tank, and/or a significant number had adhered to the pipe walls throughout the system, leading to a reduced signal. An additional 3.0 g of Cospheric particles were injected after the75 °C measurement, but this did not help the results. The $\Delta T_R$ distribution is given in Figure 123 below.

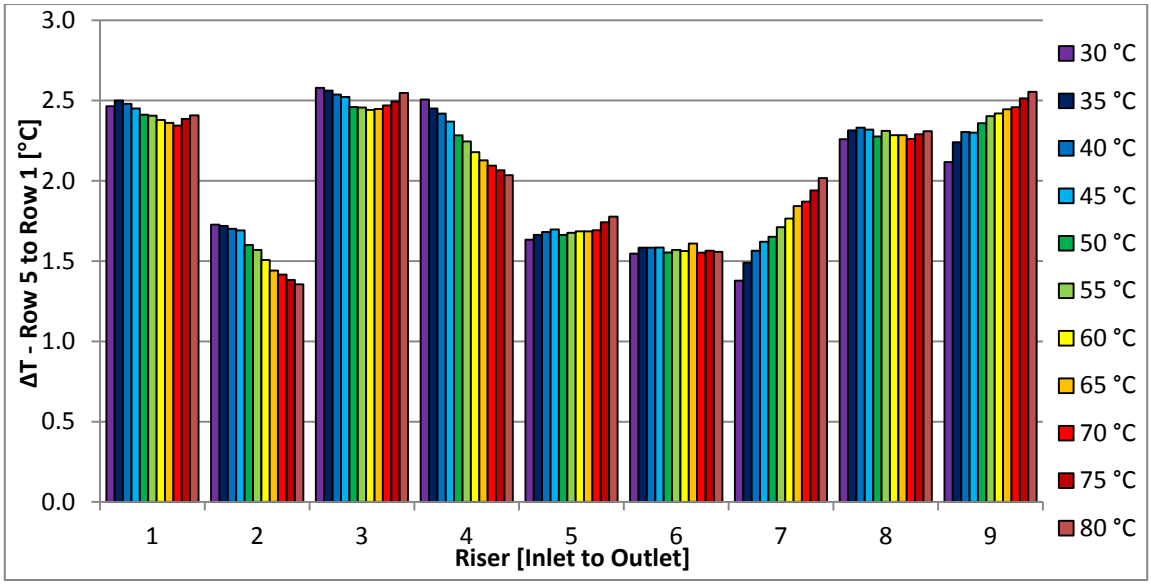


**Figure 123.** $\Delta T_R$ Distribution across the Cooling Panel for the Two-Phase Scoping Experiment (50 Series)

Temperature drifts over time/temperature are seen at all Risers except #5, 6, and 8. Again, the $\Delta T_R$ distribution is similar to previous experiments. The resulting heat transfer rate in each riser tube is presented in Figure 124 below.

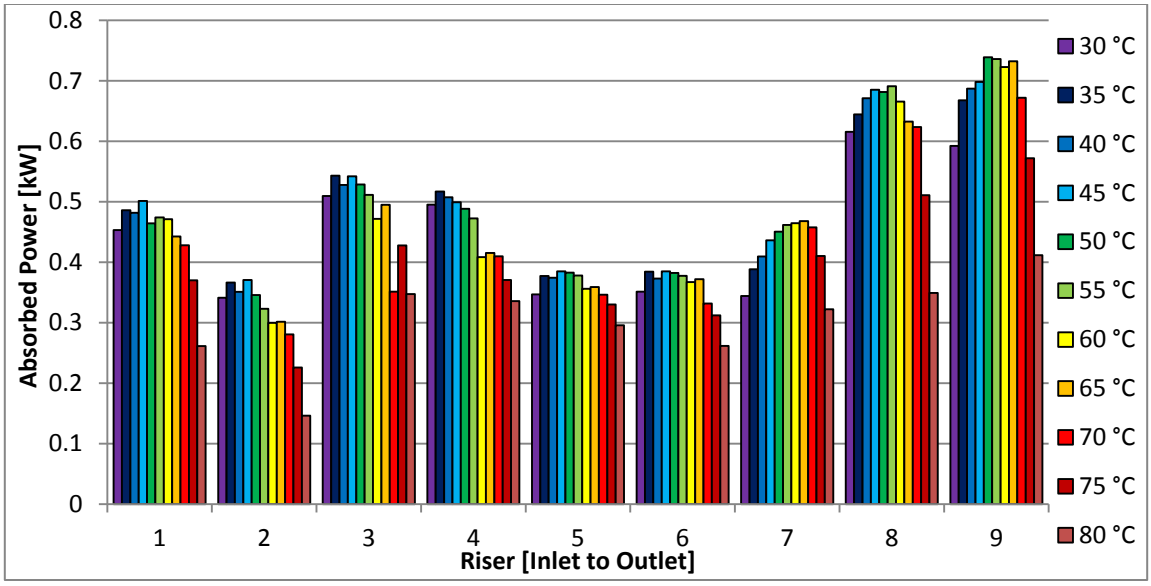


**Figure 124.** Distribution of the Power Absorption across the Cooling Panel for the Two-Phase Scoping Experiment (50 Series)

The absorbed power distribution is similar to previous results, and is dominated by the $\Delta T_R$ distribution, somewhat augmented at risers 8 and 9 by the high percentage of the flow distribution there. The comparison of the total absorbed power between the summation of the values for the individual risers and the Test Section as a whole is in Figure 125 below.

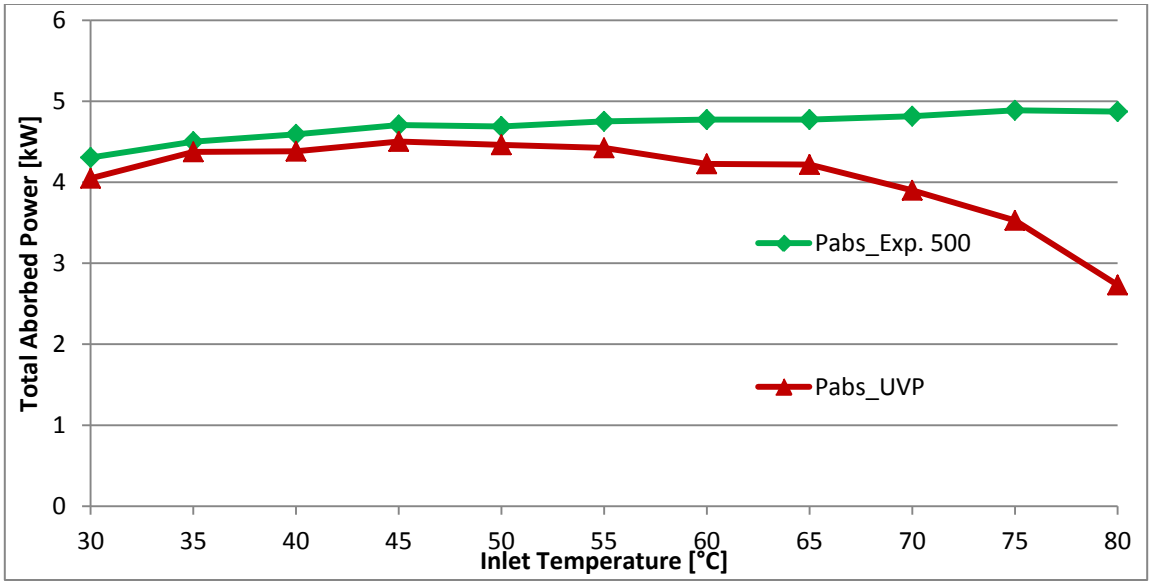


**Figure 125.** Balance of the Total Absorbed Power in the Cooling Panel for the Two-Phase Scoping Test – Sum of Individual Risers to Test Section

The percent difference between the values calculated via UVP and the average of the magmeter derived values less than 6.9% for all points below 60°C. The difference then jumps up greatly, in a similar manner seen with the system flowrate in Figure 122. The level of consistency for the flow and power distributions is comparable to the 00 Series for the lower temperatures, but it is much worse for the higher temperatures. This completes the range of analysis completed for the 50 Series.

IV.3.15 Effects of Pipe Insulation on the Flow Distribution

To give a general understanding of the effect of additional pipe insulation outside of the Heated Cavity on the flow distribution, the Reference velocities for the 00 and 50 Series of experiments are shown at the common Coolant Temperature of 45 °C in Figure 126 below. Differences are less than 10% at each riser and therefore are not felt to be statistically significant.

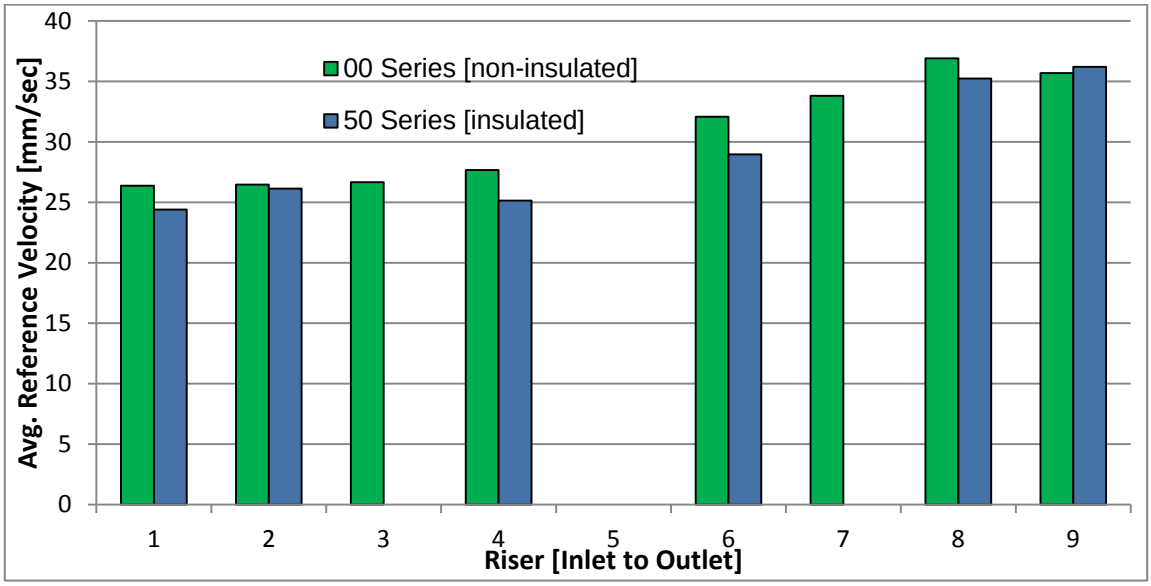


**Figure 126.** Effect of Pipe Insulation on the Flow Distribution

IV.3.16 General Comparison of UVP to PIV Measurements

For both of the throttled series of experiments, 20 and 21, the PIV derived results clearly show better agreement with the system flowrate as read by the magmeter, and the distribution itself has a more expected shape. Also, for both sets of series, the statistical deviations of the data about the overall mean were generally consistent from riser to riser, indicating good integrity of the data and experimental technique.

The PIV results for the Low Power and Inlet Skewed experiments (the 11 and 30 Series) also showed excellent agreement with the magmeter and with the UVP

measurements as well. The temporal and spatial standard deviations of the results about the mean or average value for each riser were also low and consistent with each other for these two experiments, again indicating good integrity of the data and experimental technique

The results for the 10, 31, and 40 Series of experiments, however, had significant deviations from the UVP results for several risers, most consistently with risers 7, 8 and 9. In addition, the temporal and spatial standard deviations for these risers were typically much higher as well, indicating that there was a problem with either the images or the post-processing parameters. Problems with image quality are believed to stem from two main sources. First the illumination was inconsistent; the risers in the middle were more evenly illuminated than those at the ends. Second, due to the way the camera was mounted, it was not possible to capture video for Riser #9 from the same orthogonal angle and distance as for the other risers. For the 31 Series in particular there were also large deviations from the UVP at the inlet risers, #1 and 2, which did not accompany large deviations in the PIV data.

This and other anomalies are not fully explained, but nevertheless it is the opinion of the author that PIV type measurements will be of greater usefulness for determining the flow behavior of the system than UVP in the future. Estimates of the total volumetric flowrate using very elementary PIV techniques were less than 10% different from the magmeter's reading in all cases (including the 20 Series if the range of possible values given by the mag's uncertainty is taken into account). Again it must be re-iterated that the PIV was of secondary importance in this work, and with better equipment, experimental technique, and post-processing it is believed that extremely accurate results will be possible.

# CHAPTER V

# TWO-PHASE SCOPING EXPERIMENT AND OBSERVATIONS

It was desired to conduct at least one experiment to see what would happen as the system reached saturation, and subsequently to observe any two-phase flow phenomena which may then occur as the water begins to boil. The system was insulated in order to hasten its journey to saturation, and it was planned to remove various insulation panels located at various points in the flowloop in order to observe any behavior of interest, and record it using a High Definition camcorder. This chapter will catalog the events seen during the journey to saturation.

## V.1 System Flow Behavior to Saturation

The system flowrate versus time is plotted in Figure 127 below. The temperature of the coolant entering the inlet to the Test Section is superimposed for reference.

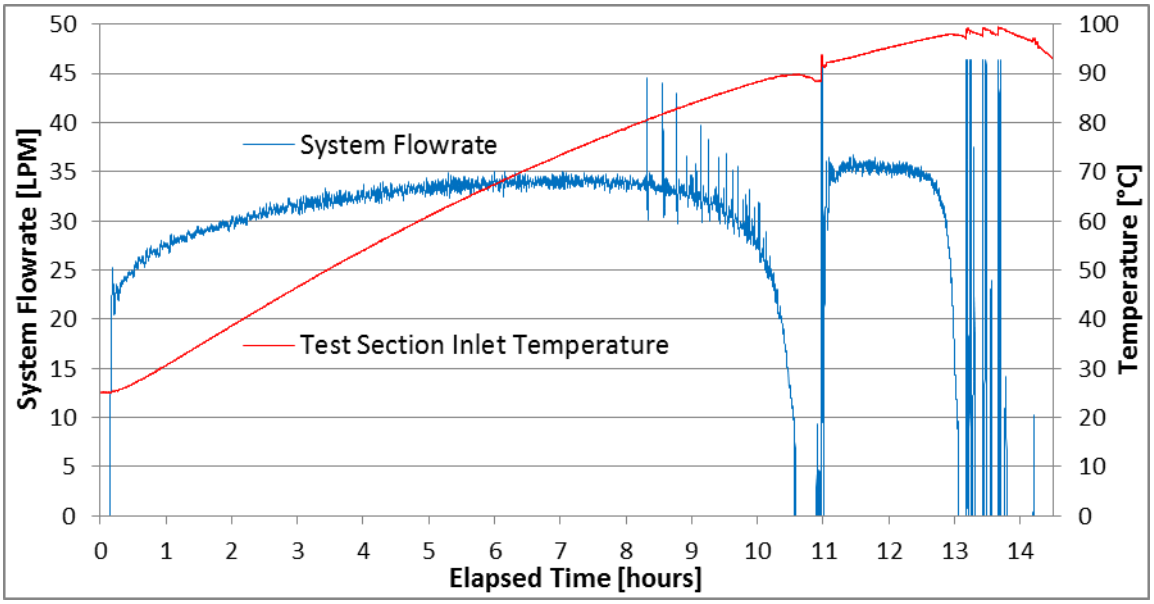


**Figure 127.** System Flow Behavior during the Two-Phase Scoping Experiment

It is noted that the flowrate peaks at about 35 LPM around 7 hours after the heaters were turned on, corresponding to a Test Section inlet temperature of 74 °C. At this point, the flowrate steadily decreased until its rate was below the sensitivity of the magmeter and the reading dropped out. It is noted that the inlet temperature began to drop at this point, indicating that the coolant was moving slow enough to lose heat from conduction to the environment faster than higher temperature water was convecting in. Then there is a sudden flow excursion that is off the scale of the magmeter's 4 – 20 mA output, followed by the resumption of normal flow.

The flow continues as normal for almost 2 hours, then the flow suddenly stops again, and the flow excursion is repeated 3 more times. The experiment was stopped after the 3$^{rd}$ excursion of the series. The flow excursions will hereinafter be referred to as geysering due to the similarity to a natural geyser's behavior, thus there were 4 geyser events captured before the heaters were shut off and the experiment aborted.

The Test Section $\Delta T$ is plotted with the flowrate in Figure 128 below. Here it is noted that the temperature difference across the Test Section climbs to as high as 20 °C just before the 1$^{st}$ geyser event, then to around 10°C for each of the subsequent 3 flow excursions that happen a little more than 2 hours later.

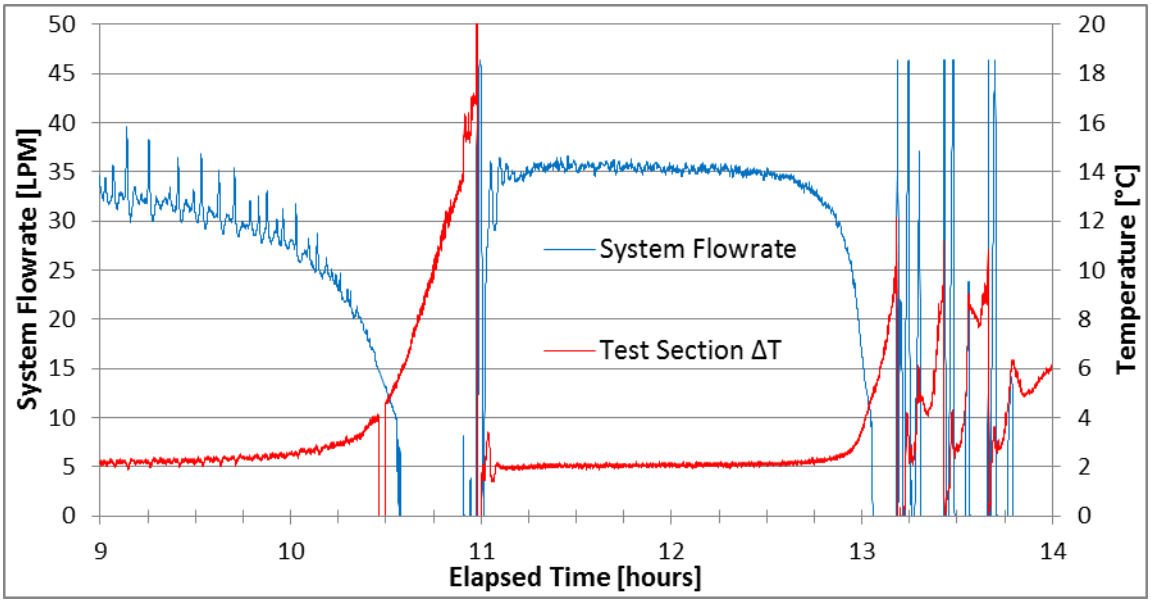


**Figure 128.** ΔT and Q during the 4 Flow Excursions

The analysis in the next subsection will begin by investigating the causes of the stop of flow and subsequent rise in ΔT that ended with the 1st Geyser Event at 11 hours E.T., and end with a detailed characterization of the geyser event itself. The following 3 Geyser Events between 13 and 14 hours E.T. will be characterized as a group.

## V.2 Characterization of the First Geyser Event

### V.2.1 Causes

It had been previously observed during other experiments that the system begins outgassing when the coolant temperature reaches around 60 °C. The phenomenon of outgassing is the release of non-condensable gases, typically air, from a liquid as it is heated. This occurs because almost all water obtained from the tap has some air entrained and dissolved in it. This is mainly due to running through pumps; and also because gas (air) will naturally permeate a liquid to some degree even when still. The dissolved air will be referred to as non-condensable gas (NCG) to differentiate it from steam, which can also be produced via phase change of the liquid water itself.

A large number of bubbles were observed traveling up the Chimney during Experiment 500, prior to the 1st geyser event. Note the image sequence of Figure 129 showing how the non-condensable gas begins to fill up the horizontal section of the hot leg immediately adjacent to the Coolant Storage Tank inlet, aka the Tank Return Line.

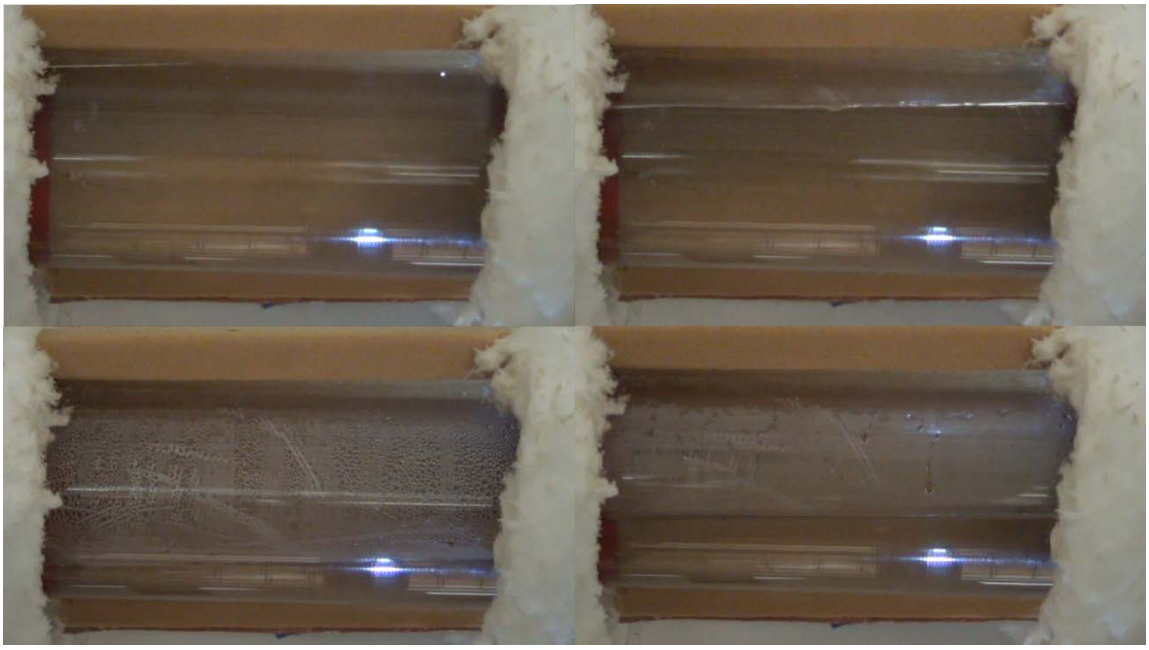

**Figure 129.** NC Gas Progressively Filling up the Tank Return Line
(Clockwise from Upper Left)

The gas was trapped in the Tank Return Line because when the pipe enters the Coolant Storage Tank it terminates into a 90° elbow that faces down towards the bottom of the tank, as seen in Figure 130 below. Note that the water line is above the elbow, trapping the gas inside.

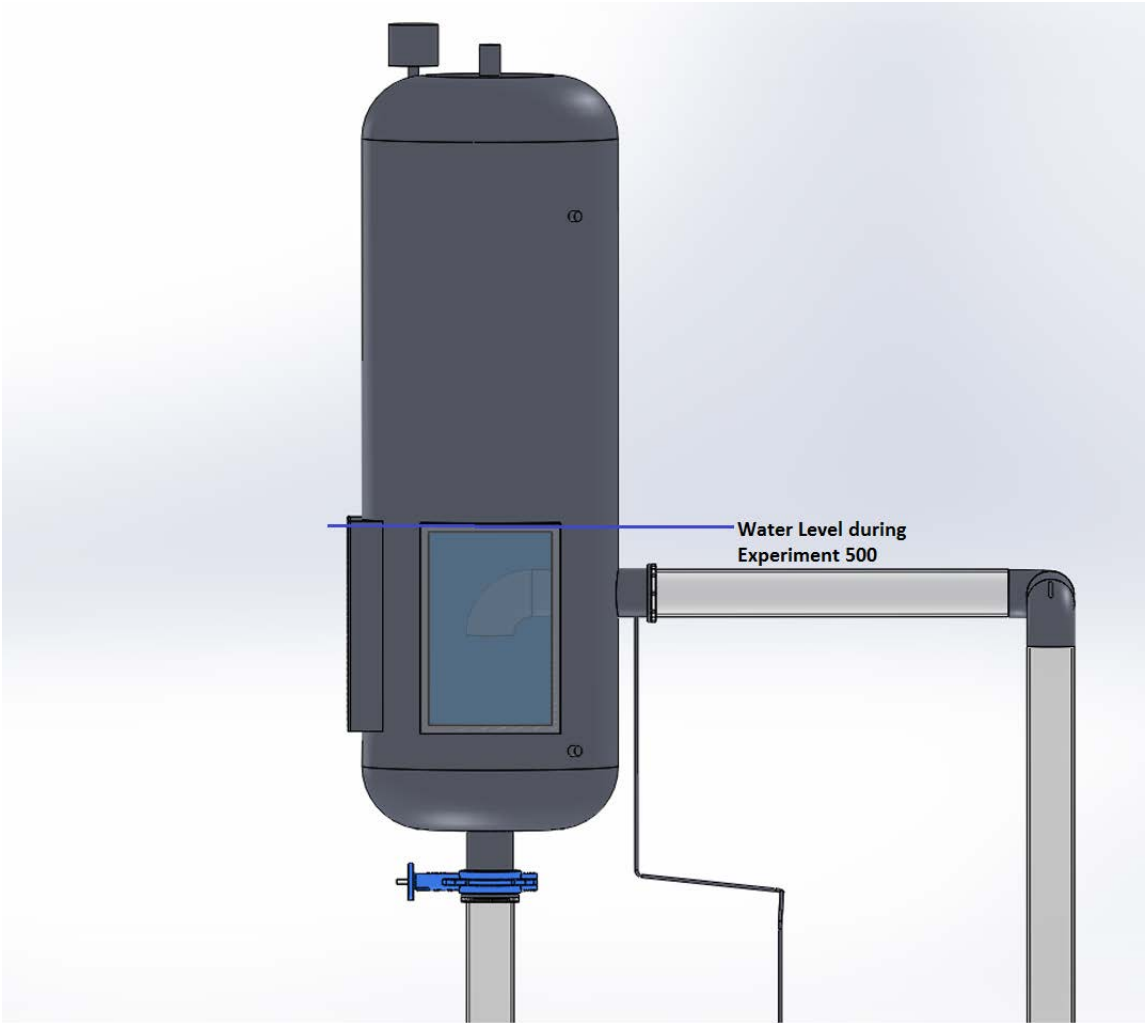


**Figure 130.** Downward Facing 90° Elbow inside the Coolant Storage Tank

Thus, it is the accumulation of NC gas that blocks the flow and causes ΔT to rise. It is noted in Figure 131 below that the water temperature at the outlet of the Test Section reaches 109 °C right as the flow excursion occurs. This particular thermocouple is located 376 cm below the water line, and at that depth the additional pressure from the water raises the saturation temperature to approximately 108.7 °C.

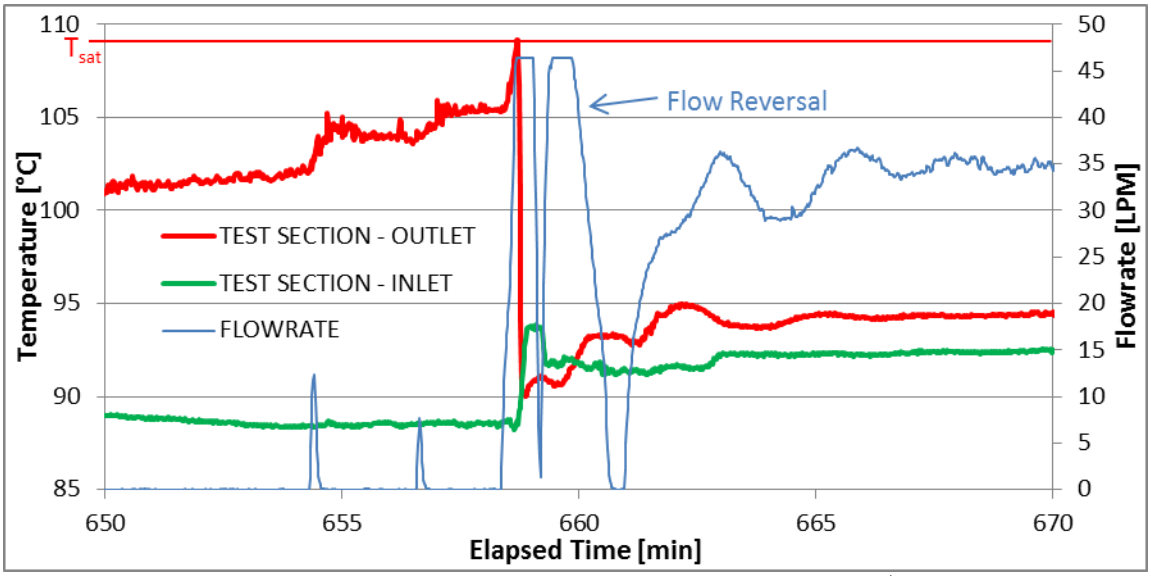


**Figure 131.** Test Section Inlet and Outlet Temperatures during the 1st Geyser Event

It is highly probably that once some of the liquid water in the Cooling Panel reached saturation temperature, this saturated liquid continued to rise up the Chimney since the flow was not completely stopped. The fact that the flow never completely stopped was confirmed by watching the flow in the Tank Return Line. As the saturated liquid rose up the Chimney, the saturation temperature dropped due to less head (i.e. lower pressure at the shallower depth), and the liquid flashed into steam. It only takes a small amount of liquid to flash into steam to create an intense flow excursion since water expands to approximately 1600 times its original volume when it undergoes this phase change.

It is also possible but not as likely that the water becomes steam because of a true boiling action occurring in the Cooling Panel. This would require the water to absorb an amount of energy equal to the heat of vaporization after it reaches saturation. Note the amount of energy required to vaporize a liquid at constant pressure is much higher than what is required to cause changes in temperature, and even if the liquid travelling through the panel reaches saturation it likely exits the Heated Cavity before it has enough time to absorb the amount of energy necessary to vaporize at constant pressure.

This cannot be determined, however, from the data shown in Figure 131 as neither thermocouple is actually located in the Cooling Panel itself.

It does appear that the liquid in the panel is higher in temperature than what is read at the Test Section Outlet. In Figure 131 above, note that there are two small flow excursions at 654 minutes, 15 seconds E.T. and 657 minutes E.T., and that the temperature spikes suddenly each time. This is because higher temperature water from within the panel has suddenly been forced out and passed by the thermocouple at the Test Section outlet. Thus it is possible that some boiling could have occurred in the panel. To gain more insight into what may have happened, the coolant temperatures at the top row (Row 5) of the Cooling Panel in the few minutes before the 1st geyser event are presented in Figure 132 below.

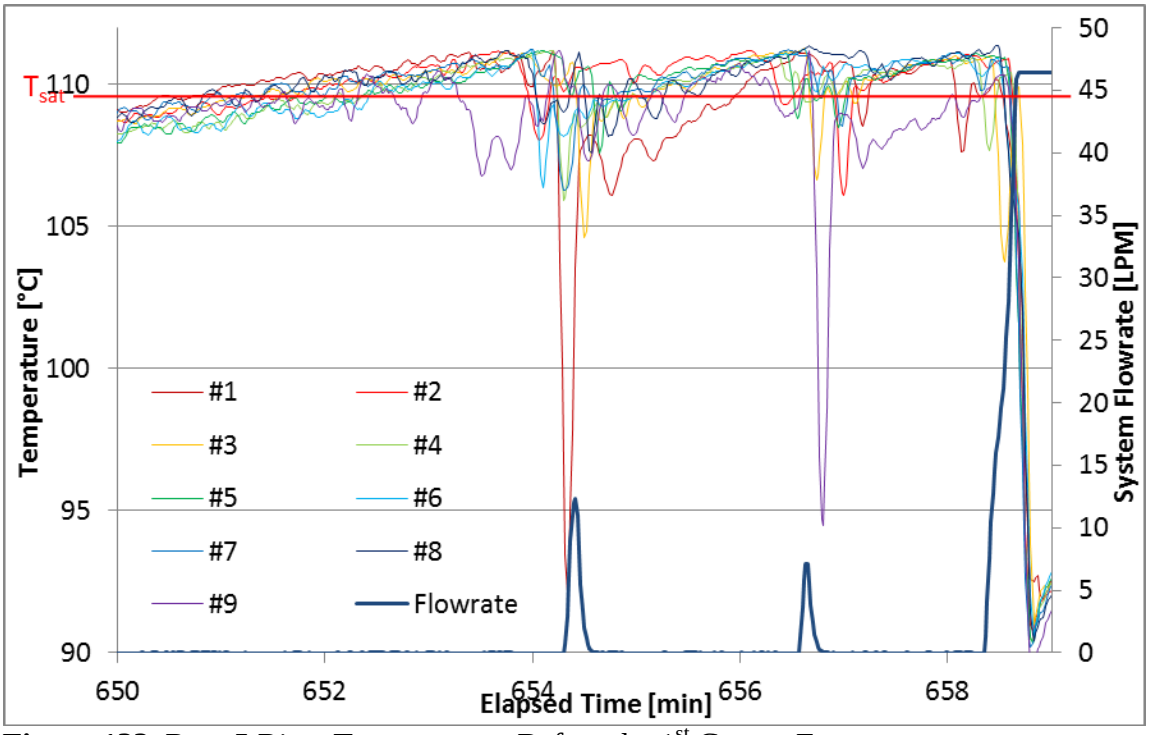


**Figure 132.** Row 5 Riser Temperatures Before the 1st Geyser Event

Note that at this depth the saturation temperature should theoretically be about 109.7 °C. Coolant temperatures reach this point in most risers by about 652 minutes E.T. and continue to rise. This of course means that the temperatures have not actually yet reached saturation. It is possible that the system is slightly pressurized more than is assumed at this location (and it would only require slightly more than 5 kPa to raise $T_{sat}$ 1 additional degree Celsius), or the thermocouple readings are simply inaccurate (recall the accuracy of a Type K thermocouple is only 2.2 °C).

It does appear, however, that the riser temperatures do plateau slightly above 111 °C at around 654 minutes E.T. At this point a small magnitude flow excursion promptly occurs, which causes riser temperatures to fall. This coincides with the sudden increase in temperature seen at the Test Section outlet in Figure 131. One more small flow excursion occurs before the geyser event at 656m 45s E.T. It can be noted that after all three times the temperature reaches 111 °C a flow excursion of some sort occurs shortly thereafter, which lends further evidence to the theory that the water flashes after it reaches saturation as it probably does not have enough time to boil at constant pressure.

### V.2.2 Video Capture of the 1st Geyser Event

The 1st geyser event began at approximately 658 minutes E.T. and was captured on video at the Tank Return Line. Recall that the piping there is made of clear polycarbonate and the insulation had been partially removed from this area prior to filming. Please see Figure 133 for an illustration denoting this location. The video itself was also submitted to the TAMU Thesis Office as a supplemental video file in .mp4 format.

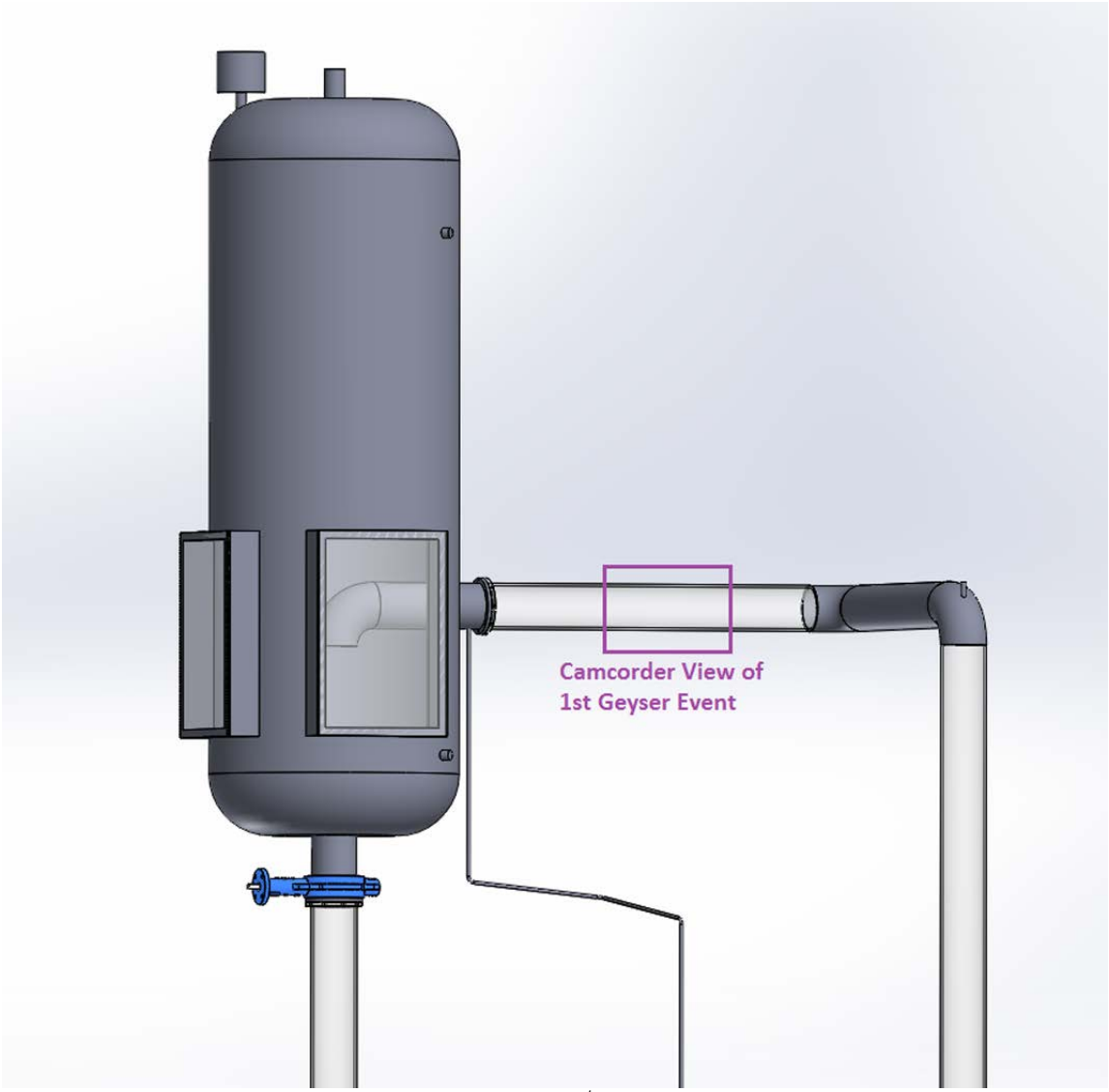


**Figure 133.** Location of Video Recording of 1st Geyser Event

While the geyser event must be seen on video to be fully appreciated, some selected still images of this recording are presented in Figure 134 below. These images move chronologically in each row from left to right, beginning with the top row. The time between each pair of images is not uniform.

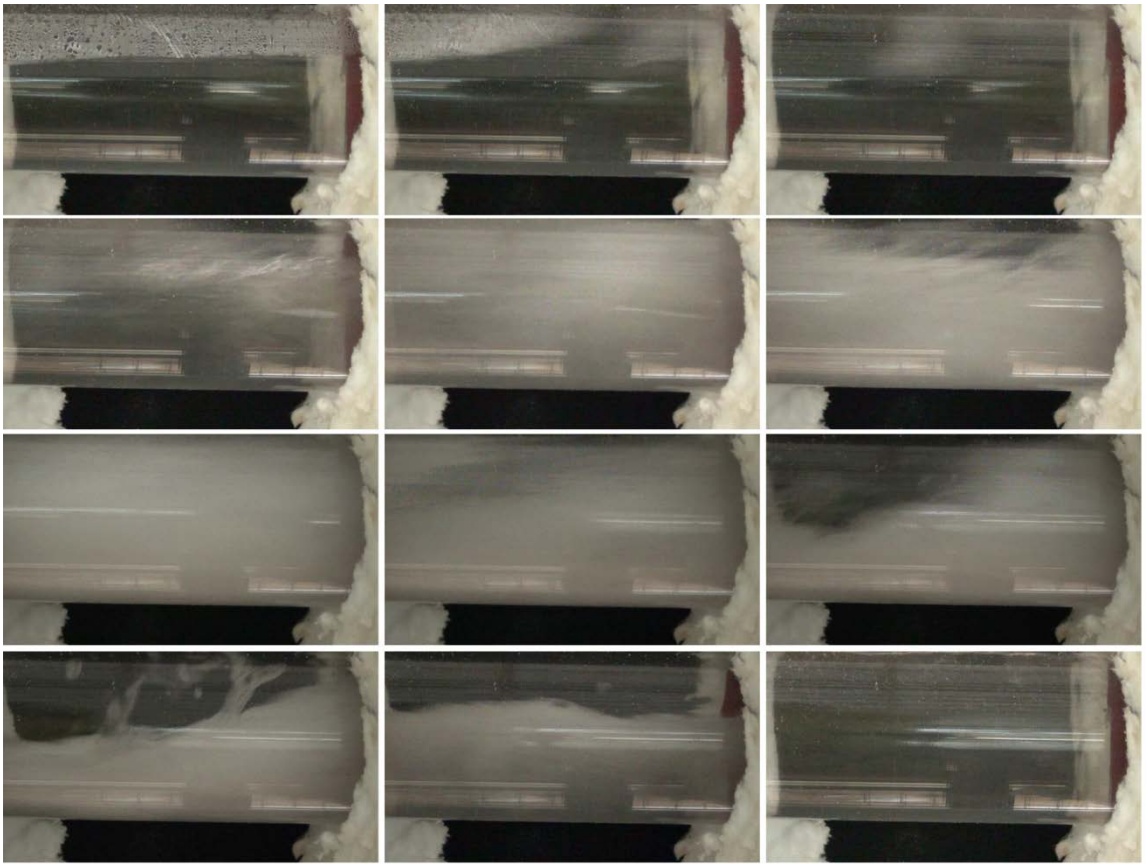

**Figure 134.** Select Video Stills from Geyser Event #1

The last image in the lower right corner of Figure 134 shows that all of the non-condensable gas was flushed from the Tank Return Line at the end of the geyser event, and the piping is again completely full of liquid water. At this time the Test Section Inlet and Outlet temperatures return to a normal ΔT of approximately 2 °C. It can be noted in Figure 131 previously that after the initial geyser event, the flowrate goes back to zero and then at about 659 min 11 sec E.T. it shoots back up off of the scale. This second flow excursion is not a geyser event but is actually a complete flow reversal throughout the entire system. The magmeter does read flow in both directions but requires an additional binary output to be wired up so the polarity can be distinguished. The reversed flow slows down and goes back to zero at 660 min 41 sec E.T., and then resumes normal operation.

V.2.3 Riser Temperatures during the 1st Geyser Event

It is also interesting to note the Coolant Temperatures at the top of each individual riser (in Row 5) in the few seconds before and during the geyser event. Though it is difficult to show in a small chart, Figure 135 has all nine temperatures with the system flowrate superimposed.

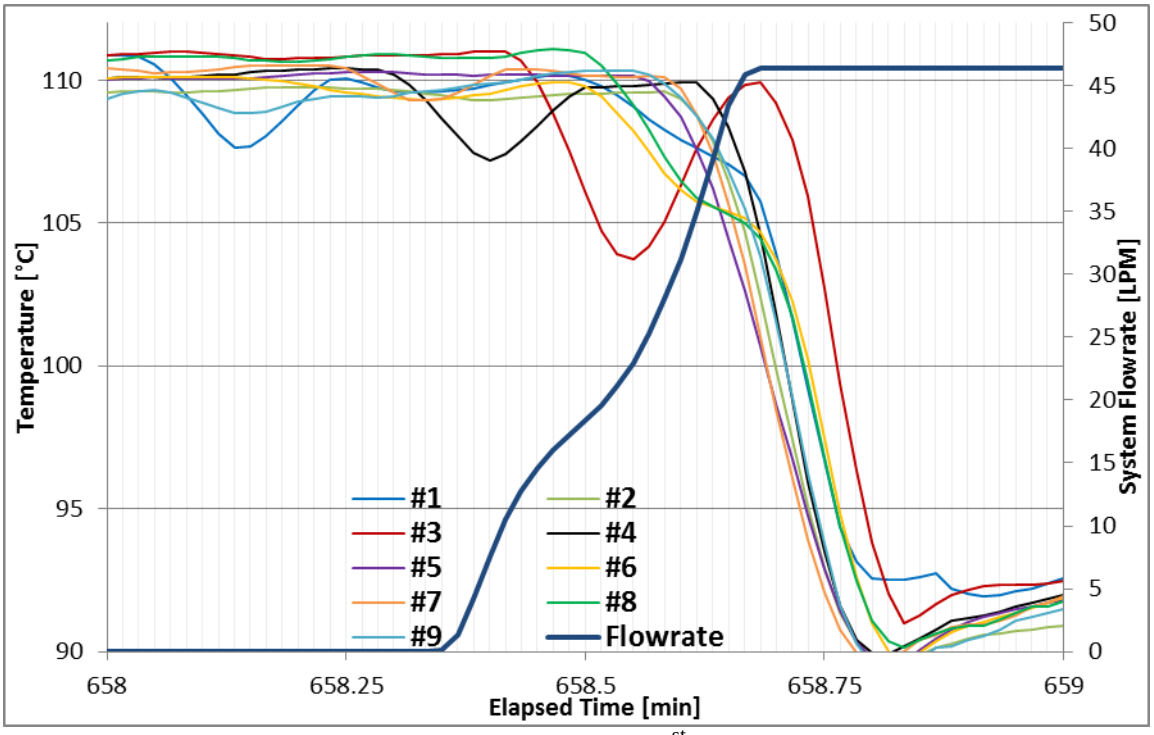


**Figure 135.** Row 5 Riser Temperatures during the 1st Geyser Event

It is noted in the figure above that the sudden drops in Riser Temperatures are not synchronized with each other in time, and that there are some sporadic smaller dips and fluctuations before the Geyser Event begins and as it progresses. This is an area of research worth further study, to try and understand the phenomena occurring in the Cooling Panel immediately before the geysering, and why the order of temperature drops (representing rapid, sudden flow in the riser) is as shown. It will be noted in the next section that the order of riser temperature drops is not the same in each geyser event.

### V.3 Summary of Geyser Events #2, #3, and #4

It is observed in Figure 136 below that the once the 2nd Geyser Event occurs, they continue to occur about once every 15 minutes. Between geyser events normal flow does not resume, and the exact reason why is uncertain. The level measurements (not shown in this thesis) indicate that the tank level returns to the value at startup after each geyser event (before each event there is some 'swell' in the coolant level due to the water being displaced by the non-condensable gases, and during the geyser event the coolant level as indicated by the capacitive level transmitter rises more than 10 cm). This indicates that the system is not losing a significant amount of inventory during geyser events. It should be noted, however, that after the last geyser event at approximately 820 minutes E.T. that the Tank Return Line did not fill back up completely with liquid water.

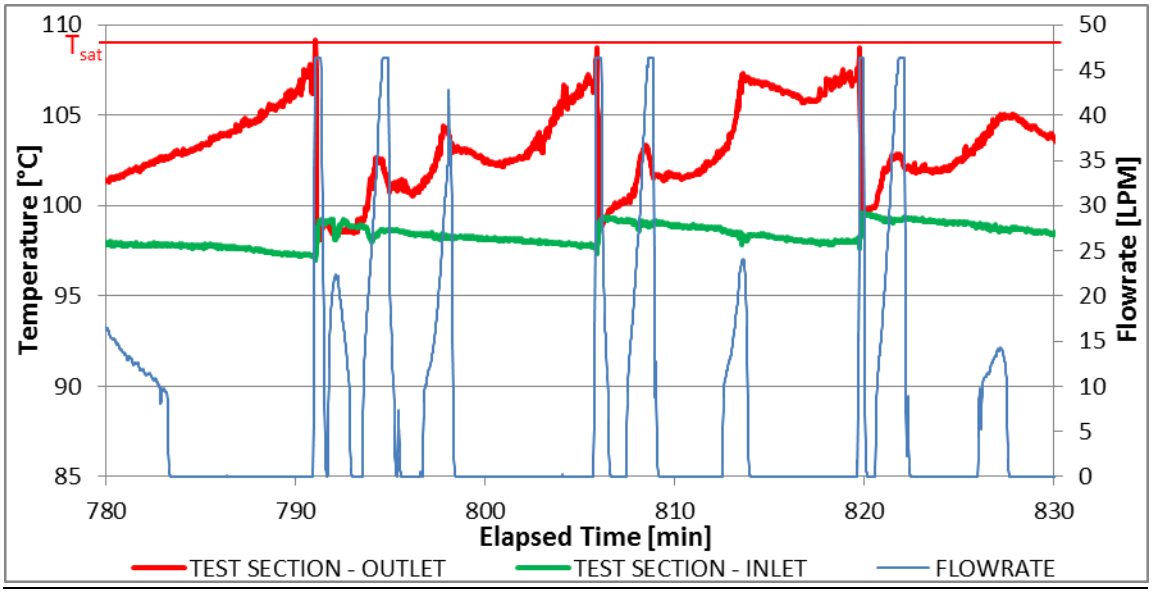


**Figure 136.** Test Section Inlet and Outlet Temperatures during the later Geyser Events

The 2nd and 3rd geyser events where not captured on video, but the 4th one was. It was actually captured at two separate locations simultaneously using 2 camcorders. A set of video stills from both camcorders, similar to what was shown for the 1st geyser event, is available for view in the Appendix. The video itself was also submitted to the TAMU Thesis Office as a supplemental video file in .mp4 format.

Finally, the temperatures at the top of each riser (Row 5) around the time of the each geyser event are shown in Figure 137, Figure 138 and Figure 139 below. As alluded to earlier, it can be noted that the order in which the temperature drops, which indicates flow through the riser, is not the same for each event. The time scales are also different for each figure.

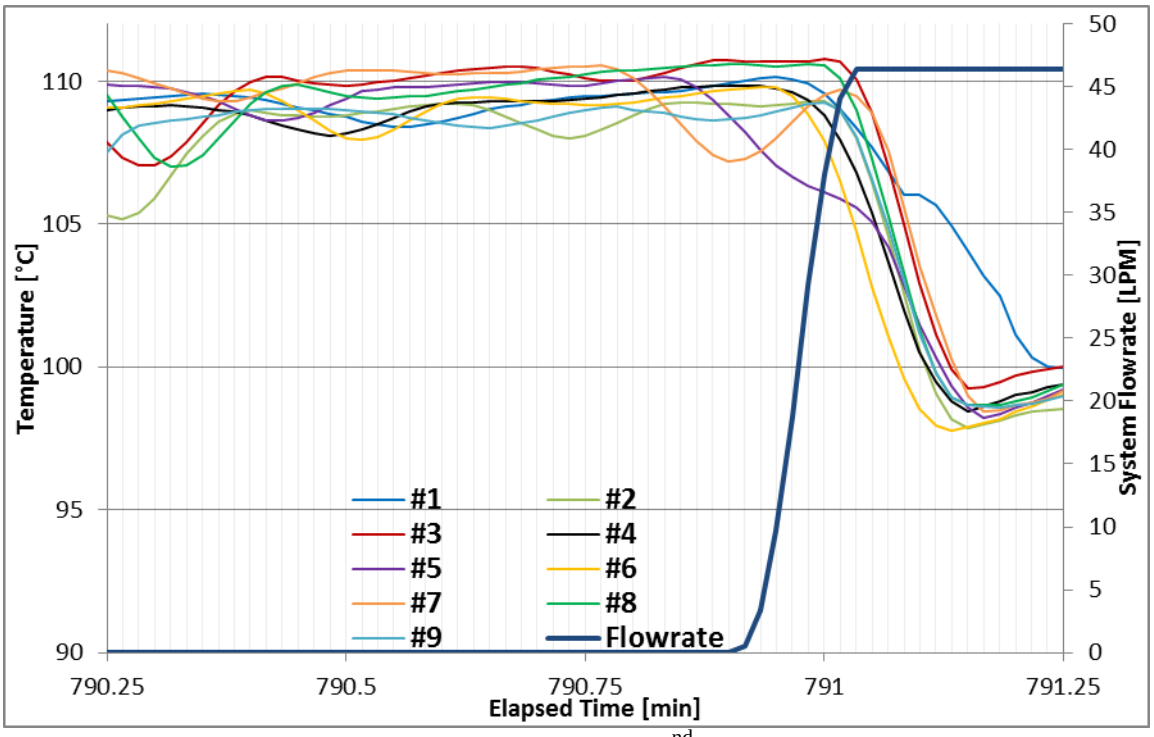


**Figure 137.** Row 5 Riser Temperatures during the 2nd Geyser Event

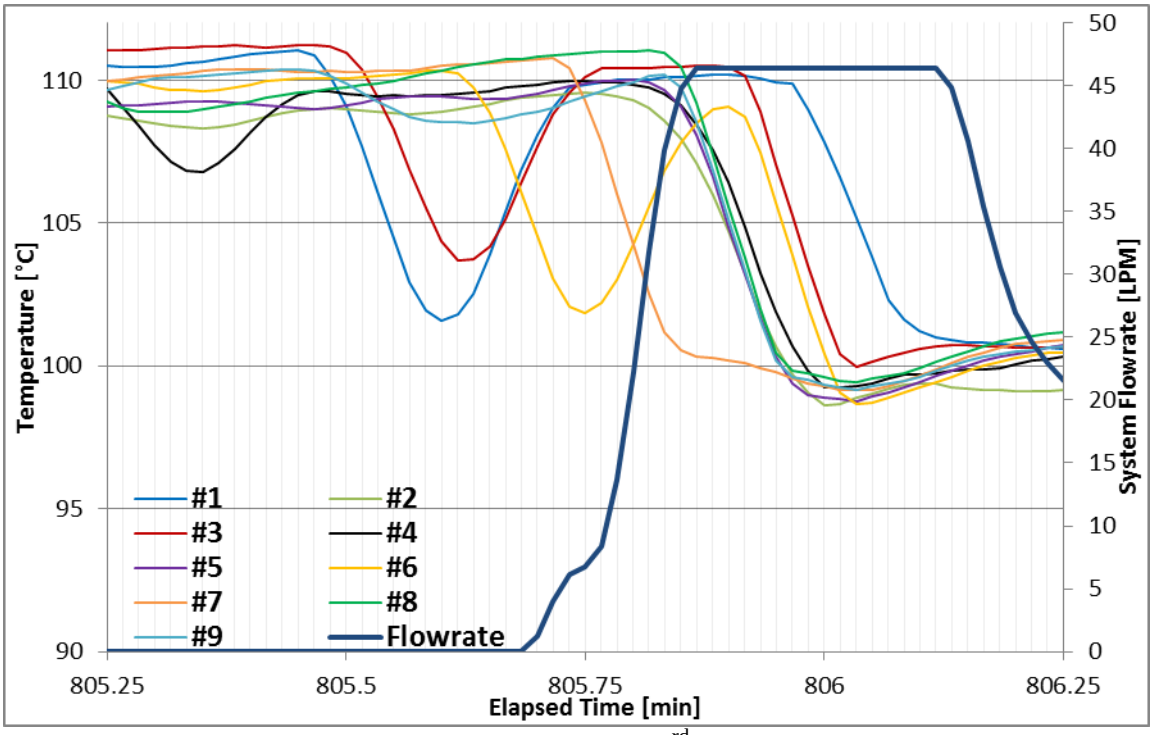


**Figure 138.** Row 5 Riser Temperatures during the 3rd Geyser Event

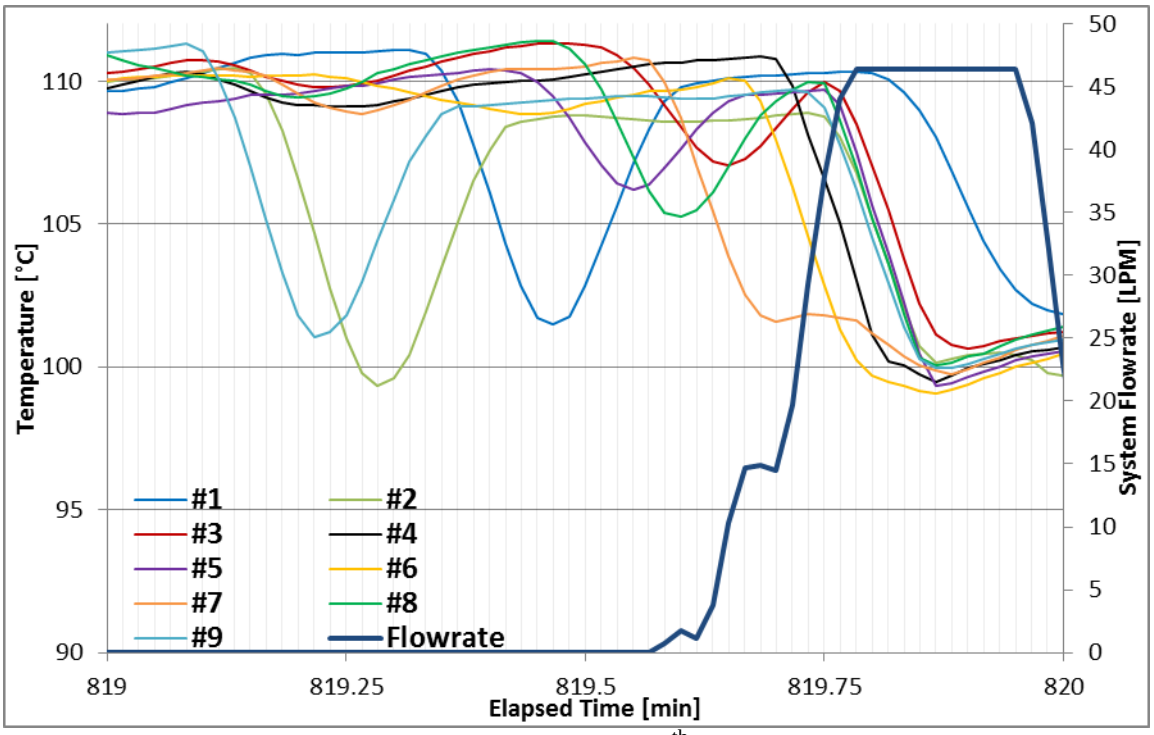


**Figure 139.** Row 5 Riser Temperatures during the 4th Geyser Event

It is noted in the third and fourth geyser events that there are large temperature drops and recoveries in some of the risers immediately before the flow excursion. The possibility of flow reversals within the Cooling Panel cannot be discounted and should be confirmed in future research.

# CHAPTER VI
# CONCLUSIONS

In regards to the NUEP Project #09-202 objectives, the single phase behavior of the RCCS was characterized in a manner consistent with previous work done at the University of Wisconsin's water cooled RCCS, in terms of both system-wide and local flow variables and coolant temperatures, using similar methods. The major caveat in any comparison in the UW and TAMU systems is that UW study in [5] focused on true steady-state behavior at single-phase, combined with extensive operation with saturated liquid and steam at two-phase conditions. Characterization of single-phase behavior over the course of the temperature rise from 30 °C to saturation was not published in the UW study, which in contrast is what makes up the bulk of the TAMU analysis presented here. As such, the study in this thesis can be characterized as single phase, quasi-steady as the coolant temperature was constantly rising over the course of each experiment due to lack of a secondary heat exchanger.

In spite of the differences in the studies, linearity between the system flowrate and the total power supplied by the heaters was confirmed in the TAMU-RCCS system as it was in the UW-RCCS. In addition, the TAMU study confirmed linearity between other system variables, including the $\Delta T$ of the Test Section, heater power, heater temperature, and absorbed power under non-throttled conditions.

There is a lack of a study of flow oscillations during the UW experiments while the coolant was subcooled. It may be that oscillations at the UW system were not present as they may have died out as the secondary cooling loop stabilized system temperatures at 30 °C, whereas in the TAMU system flow instabilities developed and continued to persist do to the ever increasing coolant temperatures. It was found that the oscillation frequency is roughly proportional to the system volumetric flowrate, and that the level of head in the tank above the top of the flowloop may have a destabilizing effect on this relationship. Magnitude was not explicitly calculated, but it does appear to positively correlate with power level when looking at the results by eye.

At the time of this writing, direct comparison of results between the TAMU and UW systems in an attempt to verify the scaling laws derived at Argonne National Laboratory has not been performed, and it still remains a question of whether an attempt at verification of such laws would be valid due to the fact that the flow loop geometries outside of the Cooling Panel are different and the scaling laws do not take this into account.

The use of UVP to measure the flow distribution in the Cooling Panel was thoroughly investigated, and the results obtained via this method are believed to be sufficiently valid to determine relative change in distribution under a variety of experimental conditions. It is the author's opinion, however, that a more accurate assessment of the exact flowrates through each riser can be determined via PIV analysis in future experiments, if so desired. The PIV results were comparable to those derived via UVP whenever statistically sound data was obtained, and demonstrated more accuracy than UVP for the all experiments that involved flow throttling.

Using UVP, it was shown that the flow distribution under power levels imposed by the ANL scaling laws to a prototype 600 $MW_{th}$ reactor was not uniform, but favored the side of the Cooling Panel closer to the Test Section outlet. This effect was in proportion to the volumetric flowrate of the system, higher flowrates giving more skew of the distribution to the outlet side and lower flowrates giving less skew to the outlet side. This effect was the same whether the flowrate change was due to a change in overall power level to the heaters or from flow throttling. The distribution would also shift with changes in heat flux profile at constant total power, and in each case a proportionally higher percentage of flow would go to the side of the Cooling Panel with the higher heat flux (which is assumed to be the side in front of the heater with the higher percentage of overall power being applied to it). This matched behavior observed at the UW system under similar asymmetric heating conditions. Finally, the flow distribution was unaffected by changes to water level in the storage tank or insulation conditions of the flow loop piping outside of the Heated Cavity.

Extended operation of the TAMU_H2O-RCCS system was marked by the Tank Return Line filling up with non-condensable gases do to outgassing of air from the coolant. The presence of these gases created a flow restriction that eventually led to the gases being violently purged out by a rapidly expanding volume of steam. The creation of steam from the coolant was likely induced by flashing as saturated coolant rose in the vertical section of the hot leg and was suddenly subject to a lower pressure and hence saturation temperature due to the decreased head. Geysering phenomena was also observed at the UW_H2O-RCCS, but was due to entirely different causes as there are significant differences in loop geometry at the water storage tank. A method of purging the TAMU_RCCS facility of air while the coolant is still heating up to saturation would likely allow for extensive two-phase testing as was done at the UW facility and would be a suitable starting point for future research.

# CHAPTER VII
# RECOMMENDATIONS FOR FUTURE RESEARCH

At the time of this writing, it is expected that funding for further experiments utilizing the water cooled RCCS at Texas A&M will be procured in the future. In anticipation of this possibility, the author has compiled a list of system upgrades, revisions to test procedures, and possible topics for future research recommended to allow for more accurate measurements and further investigation into select phenomena of interest. A couple of items will benefit the quality of data for all types of experiments at relatively low cost and effort, but for most the decision to invest will depend on the test scenarios of interest and will require a cost benefit analysis on part of the principle investigators before implementation.

The electromagnetic flowmeter should be upgraded by doing the following items. First, rewire the magmeter using coaxial or double-shielded, large gauge wire in order to get absolute highest sensitivity possible from the instrument; this could be Signal Cable B – type BTS 300 and Field Current Cable C – 14 AWG as noted in the user manual [14]. Then, rescale the 4-20 mA output to allow for higher flow velocities in order to fully capture the geyser events seen at saturation, and wire up the binary Status Output to the DAQ and set it to switch on Reverse Flow. This will allow the capturing of flow reversals after geyser events.

It would be pertinent to investigate effects of the ambient environment on system behavior. As such, the ambient temperature, barometric pressure, and humidity at USB during experiments should be recorded in order to see if there is any effect on heat loss rate, system flowrate, anomalies, etc. These variables would not need continuous monitoring and recording, just a note of the initial value on the gauges.

In order to obtain more accurate flow distribution measurements, one could rig a more sophisticated PIV setup using a laser, light sheet, high speed camera, and precision mounting apparatuses for these devices, and use dedicated PIV analysis software to calculate the results.

In order to determine the heat flux profile at the outer surface of the Cooling Panel[2], the thermocouples should be 'welded' into the Cooling Panel. This information will help the researcher calculate separate effects of radiation & convection heat transfer modes, calculate power absorption into the coolant, and calculate the thermal and mechanical stresses over the panel.

A new range of experimental conditions could be investigated by devising a new way to throttle the flow without creating as abrupt a restriction as imposed by a nearly closed butterfly valve; perhaps using a venturi of some sort. In addition, one could repeat the experiments with the RPV Simulator in place to determine its effects on system behavior, if any. Furthermore, experiments could be repeated with the heaters laid horizontal in the cavity, as depicted in left hand side of Figure 19 to determine the effects of a heat flux profile in elevation. Finally, experiments could be conducted with time-varying power profiles applied to the heaters to more accurately model plant behavior in emergency and otherwise transient scenarios.

As noted previously, the flow instabilities at high Storage Tank level conditions are worthy of further investigation. Repeat the High Tank Level experiments, looking specifically at the consistency of the system volumetric flowrate during separate but identical experiments and the relationship between system flowrate and Test Section $\Delta T$ oscillation frequency.

Further investigation of two-phase experimental conditions presents the need or possibility for several upgrades and changes. To collect more data during geyser events, record the following locations using a camcorder when this phenomenon occurs: Coolant Storage Tank via the 2 Visualization Windows, the Upper Manifold, and the Lower Manifold. In order to rid the coolant of non-condensable gases, install a vent valve at the inlet to the Coolant Storage Tank (in close proximity to the Tank Inlet thermocouple). In order to more accurately calculate the saturation temperature at different depths, install a pressure gauge at the bottom of the system (at the same level as the Particle Injection Port). In order to investigate the effects of isolating the system from atmosphere,

[2] Contact Paul Brooks at the University of Wisconsin for more information: brooks@engr.wisc.edu

pressurizing the system as was done in previous experiments at UW [5], install a butterfly valve at the Tank Atmospheric Outlet and install a pressure gauge on the top of the Coolant Storage Tank. A possible safety issue exists in that doing so may over-pressurize the system during geyser events, leading to physical failure of joints between system piping. One precaution, which should be done even if pressurized system experiments are not conducted, is to glass weld the UVP transducer mounts to the Upper Manifold in order to permanently end the potential for leaks at these connections. Doing so harbors the risk of cracking the manifold but it may turn out to be necessary for reasons pointed out in section II.10.2 of this thesis.

Finally, the opportunity exists to verify relationships and data produced from external sources. Specifically, experiments could be performed to verify the ANL scaling laws [3], which will require coordination with UW or other facilities that have an RCCS built to a different scale but using the same methodology, and various computational models of this and similar systems could be verified via simulations using RELAP5-3D and STAR-CCM or other programs.

# REFERENCES


[1] U.S. Department of Energy. “Next Generation Nuclear Plant: A Report to Congress”. http://www.energy.gov/ne/downloads/next-generation-nuclear-plant-report-congress. Washington, D.C. Retrieved on 03/26/2015.

[2] IAEA. “Heat Transport and Afterheat Removal for Gas Cooled Reactors under Accident Conditions, IAEA-TECDOC-1163”. Vienna, Austria. 2000.

[3] C.P. Tzanos, M. Farmer. “Feasibility Study for Use of the Natural Convection Shutdown Heat Removal Test Facility NSTF for Initial VHTR Water-Cooled RCCS Shutdown, ANL-GenIV-079”. Nuclear Engineering Division, Argonne National Laboratory. Chicago, IL. 2006.

[4] L.J. Lommers, F. Shahrokhi, J.A. Mayer III, F.H. Southworth. “AREVA HTR concept for near-term deployment”. Nuclear Engineering and Design, vol. 251 p. 292-296. Elsevier. Amsterdam, Netherlands. 2012.

[5] D. Lisowski. “Thermal Hydraulic Analysis of an Experimental Reactor Cavity Cooling System with Water: Performance and Stability”. University of Wisconsin. Madison, WI. 2013.

[6] R. Vaghetto. “Experimental and Computational Study of a Scaled Reactor Cavity Cooling System”. Texas A&M University. College Station, TX. 2013.

[7] U.S. Department of Energy. “Nuclear Energy University Program”. http://www.energy.gov/ne/nuclear-reactor-technologies/nuclear-energy-university-program. Washington, D.C. Retrieved on 03/26/2015.

[8] M. Corradini. “Nuclear Energy University Programs – Experimental Studies of NGNP Reactor Cavity Cooling System with Water – Project #09-202”. University of Wisconsin. Madison, WI. 2009.

[9] SCHOTT North America, Inc. “KIMAX® Laboratory Glass Drain and Vent Systems Catalog, 2014 Catalogue”. Elmsford, NY. 2014.

[10] Heater Controls and Sensors LTD. “FBA Model Radiant Heaters, Product Datasheet”. London, Ontario. 2010.

[11] Met-Flow SA. “UVP Monitor Model UVP-DUO with Software Version 3, Users Guide, Release 5”. Lausanne, Switzerland. 2002.

[12] Cospheric, LLC.http://www.cospheric.com/UVPMSBO_fluorescent_orange_spheres_density100.htm. Santa Barbara, CA. Retrieved on 05/18/2015.

[13] Q. Tseng. “PIV --- ImageJ plugin”. https://sites.google.com/site/qingzongtseng/piv. Taipei City, Taiwan. Retrieved on 03/29/2015.

[14] Krohne GmbH. “IFC 300 Handbook - Electronic Revision 3.3.xx”. Duisburg, Germany. 2010.

APPENDIX A

VIDEO STILLS FROM THE 4TH GEYSER EVENT

As mentioned in Chapter V, the 4th and final geyser event was actually captured at two separate locations simultaneously using 2 camcorders. Filming locations are shown in Figure 140 below.

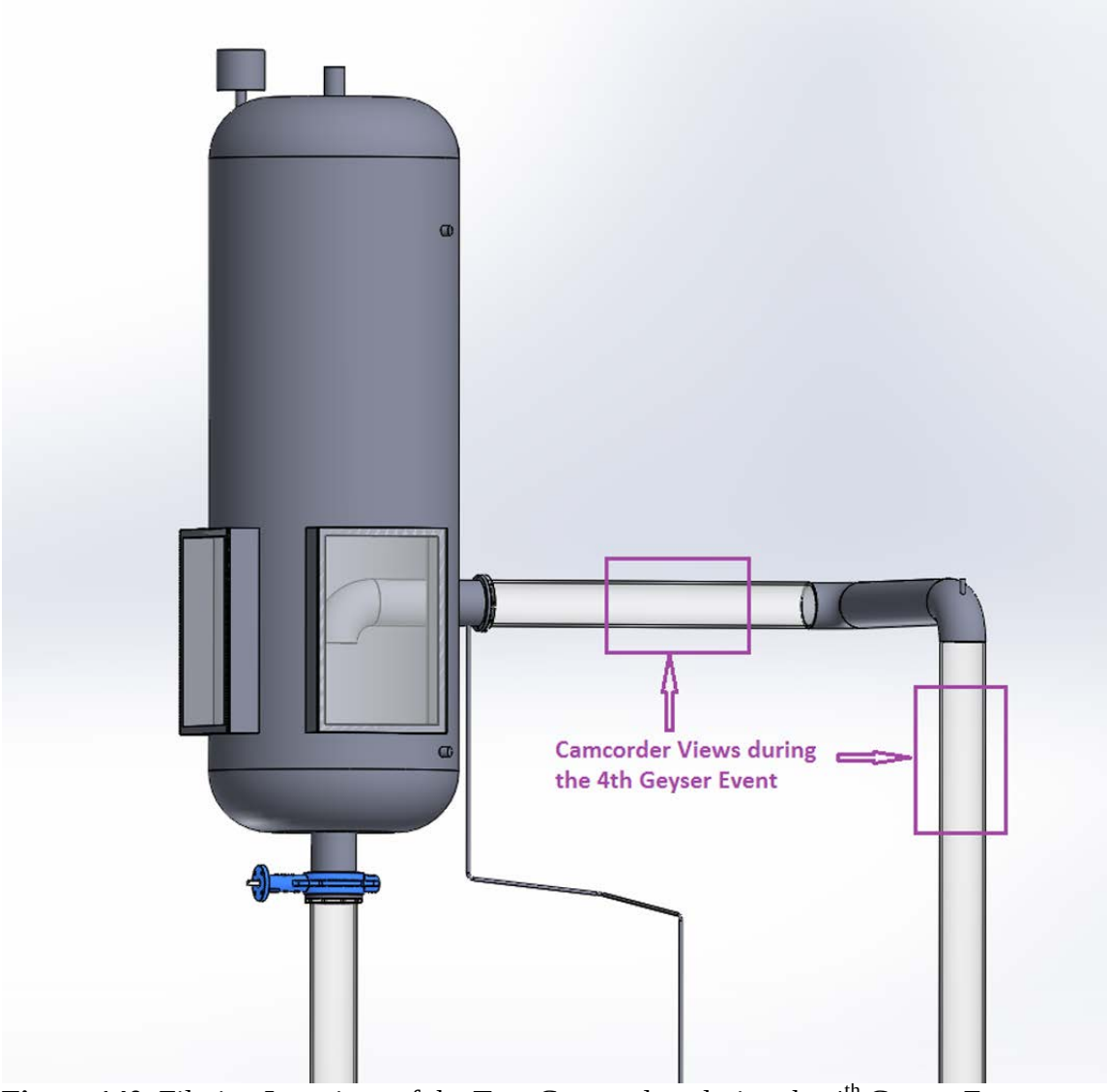


**Figure 140.** Filming Locations of the Two Camcorders during the 4th Geyser Event

Following are a few selected still frames from the video, in chronological order but not necessarily evenly spaced in time. To make the stills more intuitive, the images from the 2 videos are placed relative to each other on paper in the same manner as they are physically located in space at the system. A still photograph of the two consecutive out-of-plane elbows is also placed in its relative space for continuity. The lower left corner is blank. As a final note, the 2 videos were synchronized in time before being decomposed into image sets, so the progression of the geyser event as it rises up the Chimney and turns through two out of plane elbows before becoming visible again in the Tank Return Line was captured.

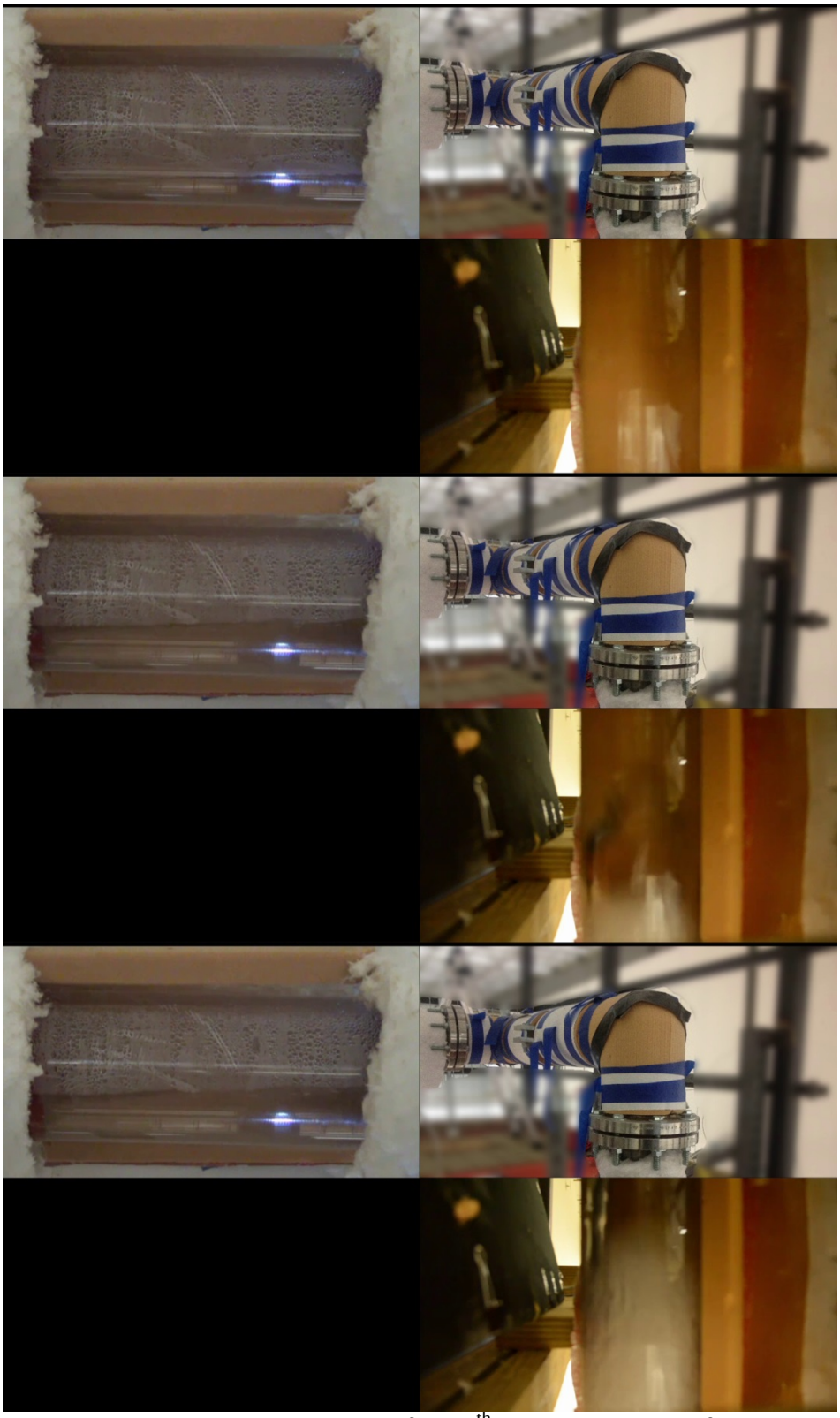

**Figure 141.** Selected Video Stills of the 4th Geyser Event (1 of 5)

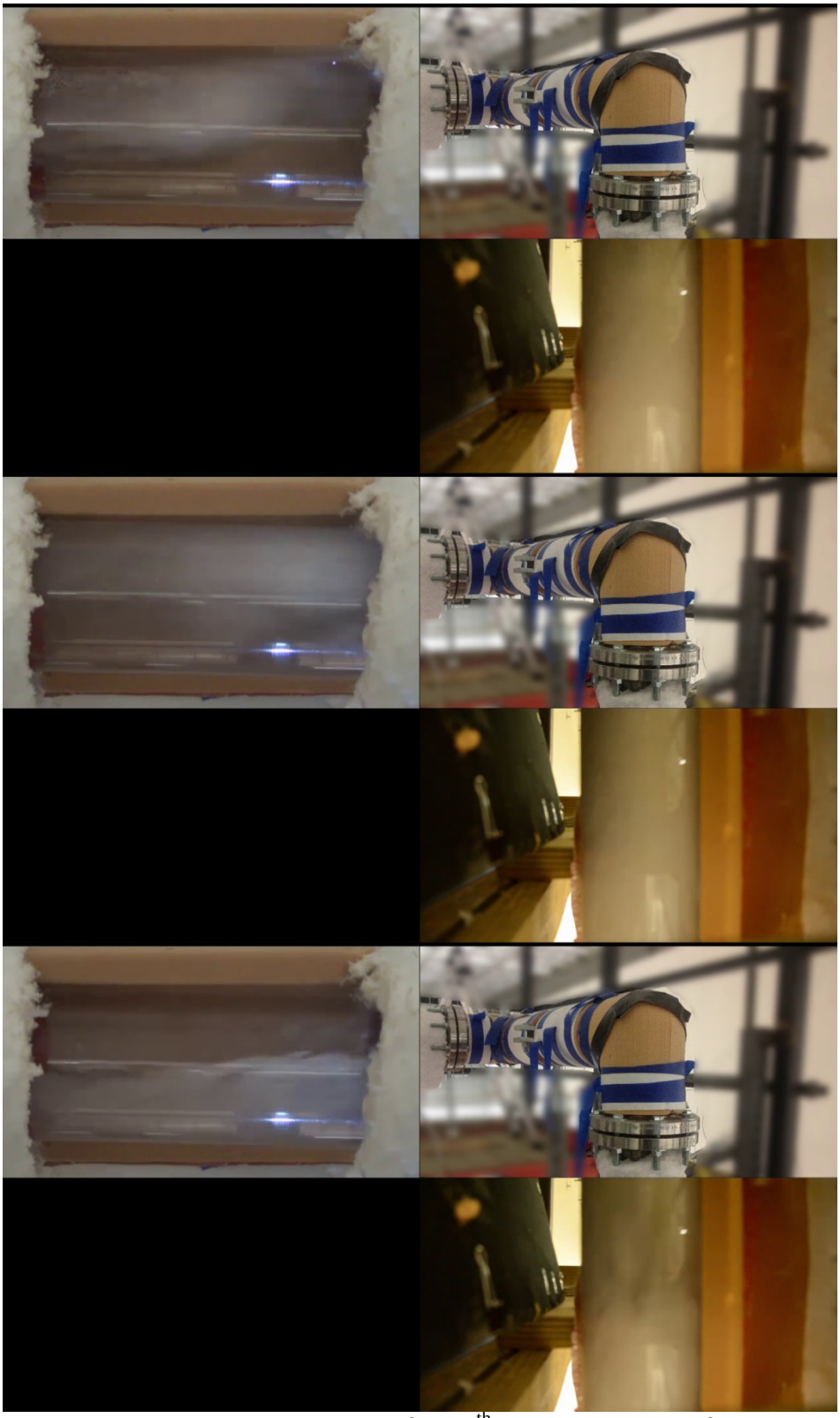

**Figure 142.** Selected Video Stills of the 4th Geyser Event (2 of 5)

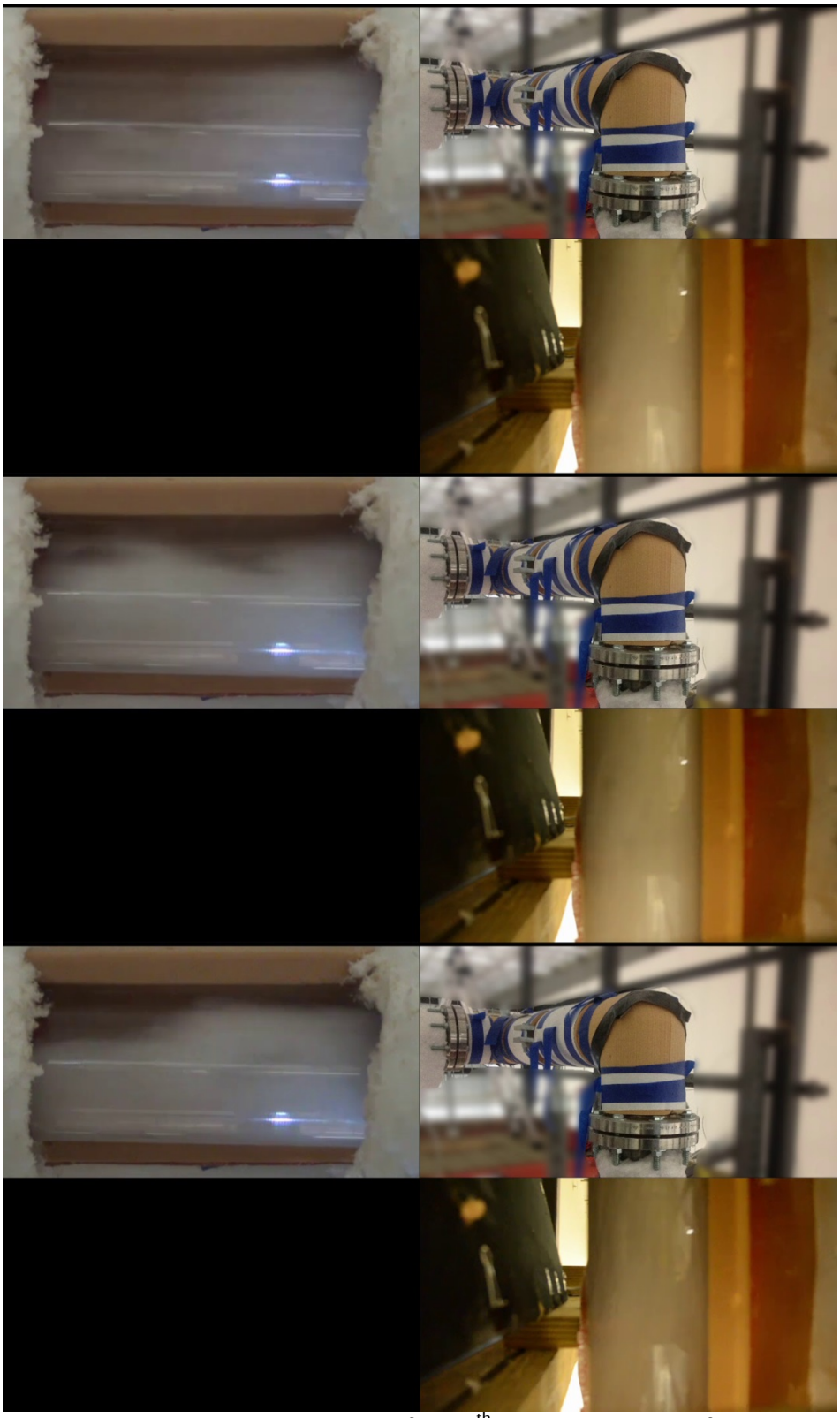

**Figure 143.** Selected Video Stills of the 4th Geyser Event (3 of 5)

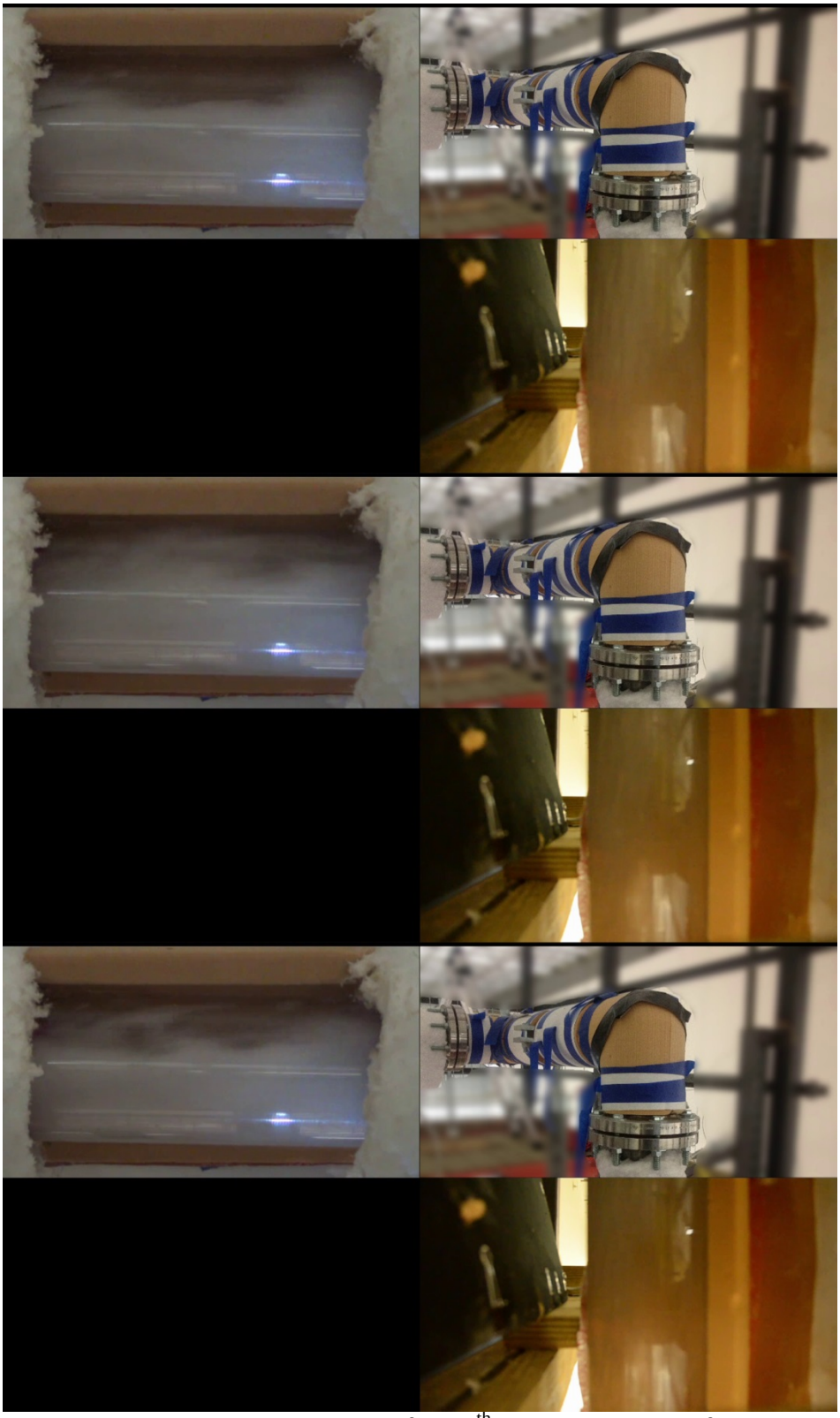

**Figure 144.** Selected Video Stills of the 4th Geyser Event (4 of 5)

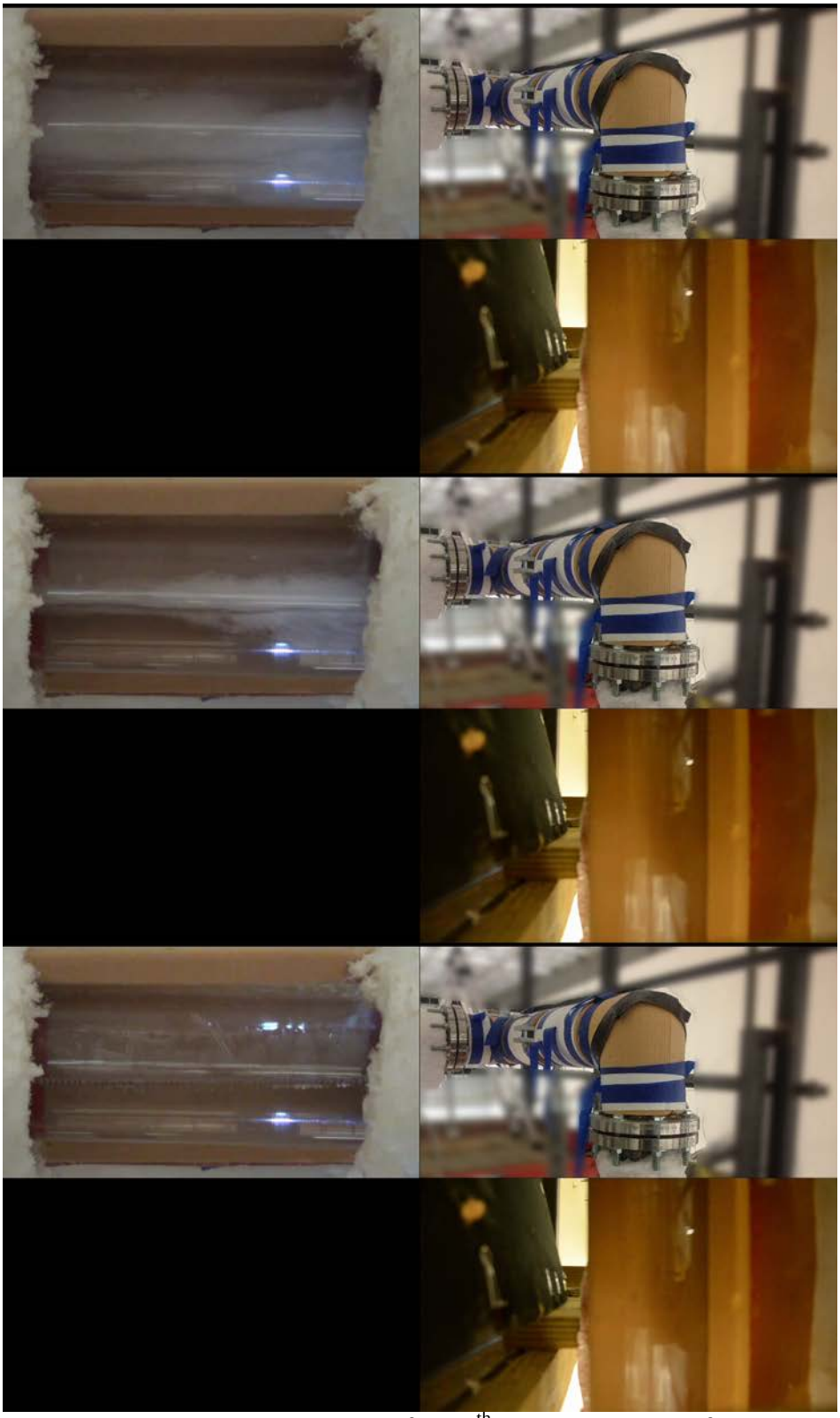

**Figure 145.** Selected Video Stills of the 4th Geyser Event (5 of 5)

# APPENDIX B

# THERMOCOUPLE DEPTHS AND CALCULATED WATER BOILING POINTS THROUGHOUT THE FLOW LOOP

For the majority of experiments the normal water level was flush with the top of the visualization windows at the side of the tank as shown previously in Figure 68 and Figure 130. From this reference the thermocouple depths and consequently the saturation temperatures are as follows:

**Table 12.** Saturation Temperature of Coolant at Each Thermocouple Depth

| Location | Depth (approx.) | Gauge Pressure | $H_2O$ Boiling Point |
|---|---|---|---|
| Tank - In | 19.0 cm | 5.19 mbar | 100.1 °C |
| Top of Chimney | 46.0 cm | 31.67 mbar | 100.9 °C |
| Tank - Out | 89.0 cm | 73.84 mbar | 102.0 °C |
| Test Section - Out | 376.0 cm | 355.29 mbar | 108.7 °C |
| Row 5 | 420.0 cm | 398.44 mbar | 109.7 °C |
| Row 4 | 446.3 cm | 424.18 mbar | 110.2 °C |
| Row 3 | 472.5 cm | 449.92 mbar | 110.7 °C |
| Row 2 | 498.8 cm | 475.67 mbar | 111.3 °C |
| Row 1 | 525.0 cm | 501.41 mbar | 111.8 °C |
| Test Section - In | 569.0 cm | 544.56 mbar | 112.6 °C |

The Clausius-Clapeyron equation was used to calculate change in Boiling Point. Atmospheric Pressure has to be added to the Gauge Pressure in order to determine the absolute pressure used to calculate $T_{sat}$. To determine the Atmospheric pressure, the Standard Atmospheric Pressure of 1013.25 mbar was adjusted by the elevation of College Station, TX which is 112 meters above sea level. This results in an elevation adjusted atmospheric pressure of 999.8 mbar. Please refer to Figure 146 below for a visualization of where these thermocouples are physically located in the system.

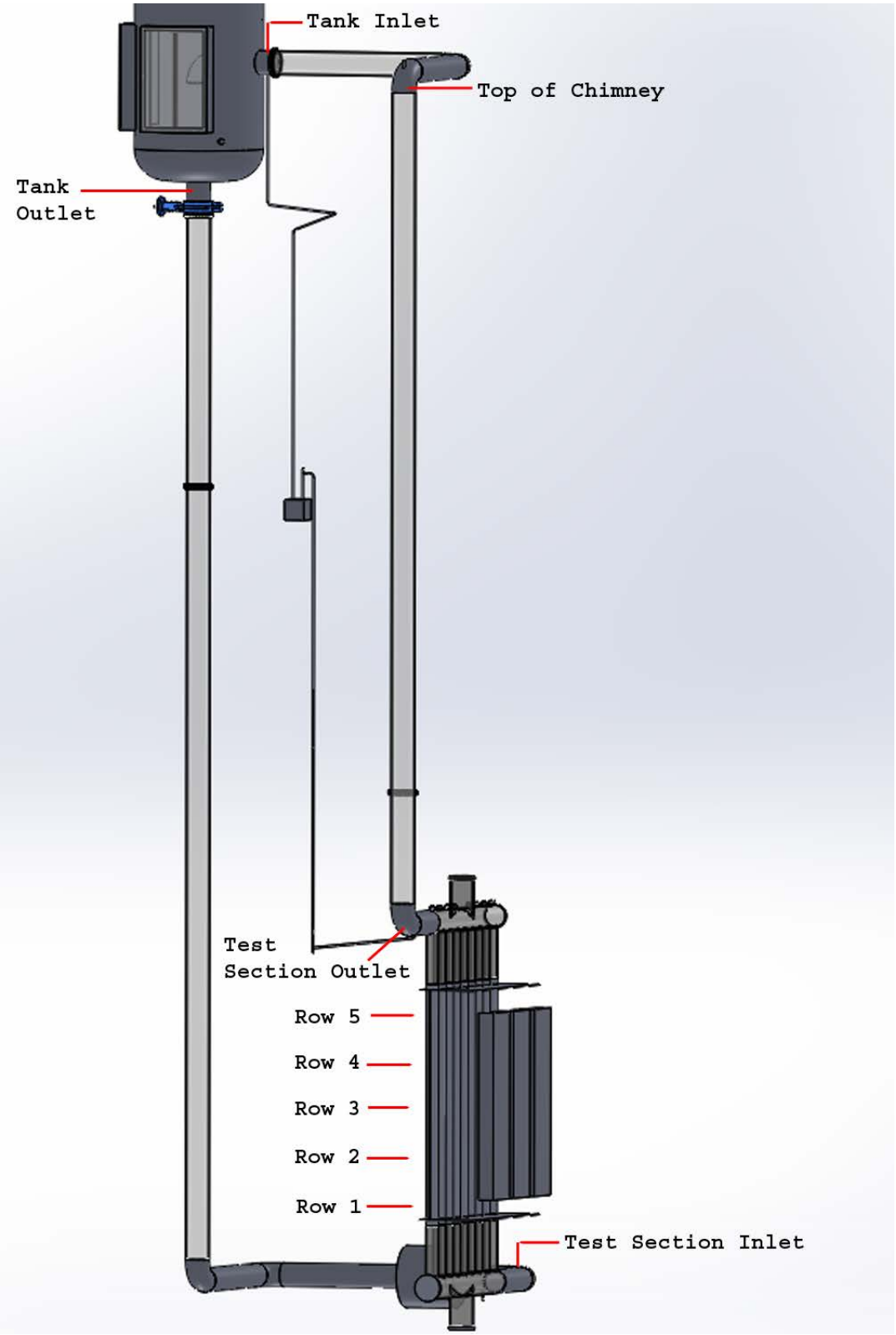


**Figure 146.** Thermocouple Locations in the TAMU-RCCS